An assessment of the relationship between the water vapour permeability and hydraulicity of lime based mortars with particular reference to building conservation materials science

By

Alan M. Forster BSc (Hon)

A thesis submitted to Heriot-Watt University, Edinburgh in accordance with the requirements for the degree of Doctor of Philosophy in the School of the Built Environment

November 2002

Abstract

The subject of this thesis is an assessment of the relationship between the water vapour permeability and hydraulicity of lime based mortars with particular reference to building conservation material science.

This work was borne from the fact that it is well understood that lime mortars and renders allow historic buildings to breathe, a particularly important requirement in northern climates, and that repairs done with cement-based materials have caused considerable damage due to their impermeability. However, what constitutes *"breathing"* has never been objectively defined with the result that it has become too nebulous a concept for rational use by professionals involved in the selection of materials for conservation.

A dense Portland cement mortar has a high resistance to the passage of water vapour whereas a feebly hydraulic lime mortar has low resistance. Portland cement brings about binding through the growth of a dense micro-crystalline network of calcium silicate hydrate which fills the voids left by free water in the mix, leaving a very fine pore size distribution. Hardened non-hydraulic limes have a much coarser pore size distribution. Just as in cement, the hydraulic components of an eminently hydraulic lime are formed from the interaction of clay impurities during the firing process and it is reasonable to expect that greater hydraulicity results from a larger proportion of the cement-like components and in consequence low permeability might be expected from more hydraulic limes.

This thesis has set out to investigate those factors that constitute hydraulicity and water vapour permeability through several experiments such as conduction calorimetry, thermal studies and environmental scanning electron microscopy (ESEM).

The findings have been discussed and explanations for the development and performance of the materials have been undertaken, including an assessment of 'breathing'. Finally, the conclusions of this work and proposals for further research have been set down.

Acknowledgements

I would like to express my sincerely appreciated thanks to the following people:

Professor P.F.G. Banfil for his support, guidance and input throughout my PhD years at Heriot-Watt University. Thanks for being so understanding and patient, I really appreciate everything that you have done for me.

Dr J. S. Stirling for inspiration, encouragement and friendship. If it were not for you I would not have been introduced to one of my greatest passions, namely, building conservation.

All my colleagues at the Scottish Lime Centre trust for being so understanding and accommodating during the write-up and submission of this thesis.

Finally, to my friends and family for putting up with me in over the latter few years. I will never forget the support and encouragement you have given me.

Table of Contents

Chapter One: Introduction

1.1 Historical background of lime for building **P1**

1.2 Specification of cementitious materials based upon strength **P3**

1.3 Implications of lime research within a building conservation context **P4**

1.4 Technological differences between traditional and modern construction **P7**

1.5 'Breathing' of traditional buildings **P8**

1.6 Deterioration of historic building fabric as a consequence adopting insensitive materials **P9**

1.6.1 Decay mechanisms caused by insensitive repair techniques **P9**

1.6.2 Moisture entrapment and frost attack **P11**

1.7 Development of a defensible hypothesis **P12**

Chapter Two: Literature Review

2.1 General Introduction **P14**

2.2 Historical development of hydraulic limes and artificial cements and the properties they impart **P14**

2.3 Traditional hydration theory and its historical development **P18**

2.4 Modern Hydration Theory **P19**

2.4.1 Hydration of Portland cement **P20**

2.4.2 General hydration of hydraulic lime **P26**

2.4.3 Hydrates relating to hydraulic lime and OPC **P32**

2.4.3.1 Calcium Hydroxide (CH) - Portlandite [$Ca(OH)_2$] **P32**

2.4.3.2 Calcium Silicate Hydrates (C-S-H) **P33**

2.4.3.3 Di-Calcium Silicate - Belite (C_2S) **P38**

2.4.3.3.1 High reactivity Belite cements - (C_2S) **P42**

2.4.3.4 Tri-Calcium Silicate - Alite (C_3S) **P48**

2.4.3.5 Tri-Calcium Aluminate (C_3A) **P63**

2.4.3.6 Hydration of the Ferrite phases **P64**

2.5 Calculation of Hydraulic Index and Cementing Index **P65**

2.5.1 Conduction calorimetry **P71**

2.6 Non-hydraulic lime hydration **P78**

2.7 Calcination considerations of non-hydraulic and hydraulic limes **P80**

2.7.1 Particle size of hydraulic materials P81
2.8 Pore structure development and characteristics P82
2.9 Current testing and terms for water vapour permeability P89
2.9.1 General water vapour permeability and moisture transfer mechanisms in porous media P94
2.10 A general introduction to breathability P106
2.11 Historic development of the Environmental Scanning Electron microscope (E.S.E.M.) and X-Ray diffraction imaging P108
2.11.1 Operation and application of SEM / ESEM P108
2.11.2 Existing research pertaining SEM / ESEM high resolution imaging, EDX analysis upon hydraulic and non hydraulic binders P110
2.12 Conclusion P118

Chapter Three: Experimental Procedure

3.1 General Introduction P120
3.2 Materials P120
3.2.1 Lime binders P120
3.2.2 Water ratios P121
3.2.3 Aggregates and moisture contents P122
3.3 Hydraulicity / hydration experimentation P123
3.3.1 Test procedure and manufacture of samples P124
3.3.1.1 Calorimeter operation P124
3.3.1.2 Data Input and calorimeter interface commands P127
3.3.1.3 Test duration and associated factors P128
3.4 Water vapour permeability sample manufacture & curing P128
3.4.1 Water vapour permeability experiments P129
3.4.2 Water vapour permeability results P133
3.5 Environmental Scanning Electron Microscope (ESEM) P134
3.5.1 Test procedure P135
3.5.2 Energy Dispersive X-ray (EDX) analysis P136

Chapter Four: Results

4.1 General Introduction P138
4.2 Hydraulicity Results P138
4.2.1 Natural Hydraulic lime 2 (NHL2) samples P138

4.2.2 Natural hydraulic lime 3.5 (NHL3.5) samples P139
4.2.3 Natural Hydraulic lime 5 (NHL5) samples P141
4.2.4 Natural Hydraulic lime: Jura-Kalk samples P142
4.2.5 Ordinary Portland cement samples P143
4.2.6 Average values of 72 hour conduction calorimetry test P144
2.4.7 Longer-term conduction calorimetry tests (720 hours) P145
4.3 Water Vapour Permeability Results P147
4.3.1 Initial data collection and calculations P147
4.3.2 Results P148
4.3.2.1 Plaster Board Samples P148
4.3.2.2 Non-Hydraulic lime, hydraulic lime and Portland cement samples P148
4.3.2.3 Summary of water vapour permeability results P150
4.4 Environmental Scanning Electron Microscope (ESEM) Results P154
4.4.1 Shap non hydraulic lime mortar sample P154
4.4.2 Blair Athol Non Hydraulic Lime mortar sample P156
4.4.3 Isle of Man non hydraulic lime mortar sample P158
4.4.4 Natural Hydraulic Lime 2 (NHL2) mortar sample P161
4.4.5 Natural Hydraulic Lime 3.5 (NHL3.5) mortar sample P163
4.4.6 Natural Hydraulic Lime 5 (NHL5) mortar sample P166
4.4.7 Natural Hydraulic Lime Jura-Kalk (NHL5) mortar sample P169
4.4.8 Ordinary Portland cement binary mortar sample P171
4.4.9 Shap non-hydraulic lime and NHL2 gauged sample P174
4.4.10 Shap non-hydraulic lime and NHL3.5 gauged sample P176
4.4.11 Shap non-hydraulic lime and NHL5 ternary gauged mortar sample P179
4.4.12 Shap non-hydraulic lime and Jura-Kalk ternary gauged mortar sample P181
4.4.13 Shap non-hydraulic lime and OPC gauged mortar sample P183
4.5 Concluding comments P185

Chapter 5: Discussion

5.1 General hydration theory of binders P186
5.2 Conduction calorimetry P190
5.3 Individual analysis of conduction calorimeter results and correlation P196

5.3.1 Natural hydraulic lime NHL2 classification 2 P196
5.3.2 Natural hydraulic lime NHL classification 3.5 P199
5.3.3 Natural hydraulic lime NHL classification 5 P201
5.3.4 Natural hydraulic lime, Jura-Kalk (NHL5) P202
5.3.5 Portland cement Samples P203
5.4 Summary of hydration P205
5.5 General water vapour permeability P208
5.5.1 Binary Jura-Kalk (NHL5) lime mortar samples P209
5.5.2 Binary Shap non-hydraulic lime mortar samples P209
5.5.3 Binary Isle of Man non-hydraulic lime mortar samples P210
5.5.4 Binary NHL2 lime mortar samples P210
5.5.5 Binary Blair-Athol non-hydraulic lime mortar samples P211
5.5.6 Binary NHL3.5 lime mortar samples P211
5.5.7 Binary NHL5 lime mortar samples P212
5.5.8 Binary O.P.C. mortar samples P212
5.5.9 Ternary Shap non-hydraulic lime & NHL5 mortar samples P213
5.5.10 Ternary Shap non-hydraulic lime & NHL3.5 mortar samples P213
5.5.11 Ternary Shap non-hydraulic lime & OPC mortar samples P214
5.5.12 Ternary Shap non-hydraulic lime & NHL2 mortar samples P215
5.5.13 Ternary Shap non-hydraulic lime & Jura-Kalk mortar samples P215
5.6 Summary of water vapour permeability P215
5.7 General ESEM Analysis P219
5.7.1 Binary Shap Non hydraulic lime mortar samples P220
5.7.2 Binary Blair-Athol non-hydraulic lime mortar samples P220
5.7.3 Binary Isle of Man non-hydraulic lime mortar samples P221
5.7.4 Binary NHL2 lime mortar samples P221
5.7.5 Binary NHL3.5 lime mortar samples P223
5.7.6 Binary NHL5 lime mortar samples P224
5.7.7 Binary Jura-Kalk (NHL5) lime mortar samples P224
5.7.8 Binary O.P.C. mortar samples P225
5.7.9 Ternary Shap non-hydraulic lime & NHL2 mortar samples P226
5.7.10 Ternary Shap non-hydraulic lime & NHL3.5 mortar samples P227
5.7.11 Ternary Shap non-hydraulic lime & NHL5 mortar samples P228
5.7.12 Ternary Shap non-hydraulic lime & Jura-Kalk mortar samples P228
5.7.13 Ternary Shap non-hydraulic lime & OPC mortar samples P229

5.8 Summary of ESEM **P229**

5.8.1 Binary mortar samples **P229**

5.8.2 Ternary mortar samples **P231**

5.9 General discussion **P232**

Chapter 6: Conclusions

6.1 Binary mortars **P233**

6.2 Ternary Mortars **P235**

6.3 General comments **P236**

Chapter 7: Recommendations for further research

P239

References

P241

List of Figures

Chapter one

Figure 1: Differences between traditional and modern construction P8

Figure 2: Hypothetical hydraulicity / permeability scale P9

Figure 3: A comparison of the technology of Portland cement and lime based harl coats P11

Chapter Two

Figure 4: Structure of single layer of $Ca(OH)_2$ P32

Figure 5: Binary phase system $CaO\text{-}SiO_2$ P34

Figure 6: Single layers of tobermorite (*bc*- and *ac*- projections) and jenite *(ac*-projection) P35

Figure 7: Polymorphs of Belite C_2S P40

Figure 8: Crystal structures of C_2S polymorphs P41

Figure 9: Concept of C_3S consumption as a function of time P50

Figure 10: Electrical double layer theory in C_3S P57

Figure 11: C-S-H primary and secondary formation, indicating effect of electrical double layer theory P58

Figure 12: Idealised representation of dissolution-precipitation process in C_3S P59

Figure 13: Dissolution of C_3S to form a silica-rich layer P60

Figure 14: Hydration of C_3A in the absence of $Ca(OH)_2$ P63

Figure 15: Characterisation of heat evolution in O.P.C P71

Figure 16:Heat of hydration in early, middle and late phases P73

Figure 17: Schematic representation of changes taking place in C_3S-water systems (w/s ratio < 1.0) P73

Figure 18: Effect of admixtures upon conduction calorimetry plots P75

Figure 19: heat of hydration curves adopting 0.375 w/c ratio P76

Figure 20: heat of hydration curves adopting 0.440 w/c ratio P76

Figure 21: Schematic representation of cement hydration P77

Figure 22: Relationship between cement water ratios and permeability P83

Figure 23: Decreasing permeability with age P85

Figure 24: Idealised segmented and interconnected pore system in cement pastes P85

Figure 25 : The relationship between porosity and water/cement ratios P86

Figure 26: The relationship between hydration and the fraction of interconnected pores P87

Figure 27 : Theoretical 'Duplex film' formation P88

Figure 28 : Water vapour diffusion coefficients for common building materials P91

Figure 29 : Moisture flow in a diffusion experiment P93

Figure 30 : Non steady state vapour diffusion P94

Figure 31 : Effect of contact angle P97

Figure 32: Surface tension forces within water P100

Figure 33 : Water distribution in a porous hydrophilic body P101

Figure 34 : Progress of moisture sorption in an idealised pore P104

Figure 35 : Different kinds of moisture flow through porous materials P104

Figure 36: The various effects of electron-specimen interaction P109

Chapter Three

Figure 37 : Conduction calorimeter (schematic) P125

Figure 38 : Calorimeter details P126

Figure 39 : JAF Conduction Calorimeter full system P127

Figure 40 : A typical experimental calorimeter trace including the calibration data P128

Figure 41 : General arrangement of permeability apparatus P131

Figure 42 : Weight change with time P132

Figure 43 : Typical results (schematic) P134

Figure 44 : A typical set of data for a lime mortar P134

Chapter Four

Figure 45 : Rate of heat for NHL 2 sample (72 hours) P139

Figure 46 : Total and rate of heat for NHL 2 sample (72 hours) P139

Figure 47 : Rate of heat for NHL 3.5 sample (72 hours) P140

Figure 48 : Total and rate of heat for NHL 3.5 sample (72 hours) P140

Figure 49 : Rate of heat for NHL 5 sample (72 hours) P141

Figure 50 : Total and rate of heat for NHL 5 sample (72 hours) P142

Figure 51 : Rate of heat for Jura Kalk sample (72 hours) P142

Figure 52 : Total and rate of heat for Jura Kalk sample (72 hours) P143

Figure 53 : Rate of heat for Portland cement sample (72 hours) **P144**

Figure 54 : Total and rate of heat for Portland cement **P144**

Figure 55 : Rate of heat for NHL3.5 (720 hours) **P146**

Figure 56 : Total heat for NHL3.5 (720 hours) **P146**

Figure 57 : Raw data from a permeability experiment **P147**

Figure 58 : Water vapour permeability adopting sodium nitrite as a desiccant **P151**

Figure 59 : Water vapour permeability adopting sodium chloride as a desiccant **P151**

Figure 60 : Water vapour permeability adopting potassium chloride as a desiccant **P152**

Figure 61 : Average water vapour permeability: binary samples range **P153**

Figure 62 : Average water vapour permeability: ternary sample range **P153**

Figure 63: EDX plot indicating chemical elements and concentration for the binary Shap non-hydraulic lime mortar samples **P155**

Figure 64: EDX plot indicating chemical elements and concentration for the binary Blair-Athol non-hydraulic lime mortar samples **P158**

Figure 65: EDX plot indicating chemical elements and concentration for the binary Isle of Man non-hydraulic lime mortar samples **P159**

Figure 66: EDX plot indicating chemical elements and concentration for the binary NHL2 mortar samples **P160**

Figure 67: EDX plot indicating chemical elements and concentration for the binary NHL3.5 mortar samples **P164**

Figure 68: EDX plot indicating chemical elements and concentration for the binary NHL5 mortar samples **P164**

Figure 69: EDX plot indicating chemical elements and concentration for the binary Jura-Kalk mortar samples **P170**

Figure 70: EDX plot indicating chemical elements and concentration for the binary Ordinary Portland Cement mortar samples **P172**

Figure 71: EDX plot indicating chemical elements and concentration for the ternary NHL 2 & Shap non-hydraulic lime mortar samples **P175**

Figure 72: EDX plot indicating chemical elements and concentration for the ternary NHL 3.5 & Shap non-hydraulic lime mortar samples **P178**

Figure 73: EDX plot indicating chemical elements and concentration for the ternary NHL 5 & Shap non-hydraulic lime mortar samples **P180**

Figure 74: EDX plot indicating chemical elements and concentration for the ternary Jura-Kalk & Shap non-hydraulic lime mortar samples P182

Figure 75: EDX plot indicating chemical elements and concentration for the ternary OPC & Shap non-hydraulic lime mortar samples P184

Chapter Five

Figure 76: Idealised conduction calorimetry hydration graphs or 'Foot prints' P191

Figure 77: β-C_2S and C_3S crushing strength P194

Figure 78: Schematic interpretation of the rate of heat development in St Astier NHL2 pastes P197

Figure 79: Hydration of C_3S grain indicating engulfing of $Ca(OH)_2$ crystals P198

Figure 80: Schematic interpretation of the rate of heat development in St Astier NHL3.5 pastes P199

Figure 81: Schematic interpretation of the rate of heat development in St Astier NHL5 pastes P201

Figure 82: Schematic interpretation of the rate of heat development in Jura-Kalk pastes P202

Figure 83: Schematic interpretation of the rate of heat development in O.P.C pastes P204

Figure 84: Theoretical hydration plot for Portland cement P205

Figure 85: Theoretical idealised pore structure condensation P216

Chapter Six

Figure 86: Relationship between water vapour permeability and hydraulicity P236

List of Plates

Chapter One

Plate 1: Deterioration of sandstone masonry due to dense impermeable Portland Cement mortar P5

Plate 2: Stained (Portland cement) harling on the south west tower of Brodie Castle P6

Plate 3. Delaminating impermeable Portland cement from permeable substrate: Livingstone Place, Edinburgh P10

Plate 4: Paye House, Cromarty. Portland cement harl-coat sheet failure P10

Plate 5: Much harder cementitious pointing has contributed to the excessive decay of the brickwork P12

Chapter Two

Plate 6: Pantheon (section), Rome P15

Plate 7: Durham Cathedral dominating the Durham City skyline P16

Plate 8: C-S-H formation P37

Plate 9: SEM micrographs of C_3S hydration in early stages of reaction P53

Plate 10: Hydration products in C_3A P64

Plate 11: Hydrophilic and hydrophobic material surfaces in quartz and illite P98

Plate 12: Hydrophilic and hydrophobic material surfaces in illite P99

Plate 13: Spherical and dome shaped water drops P99

Chapter Three

Plate 14: The Wexham isothermal conduction calorimeter P125

Plate 15 : The ESEM set up at Heriot-Watt University P135

Plate 16 : Samples placed upon universal stage in ESEM chamber P136

Chapter Four

Plate 17 : Gowrie sharp sand and Shap non-hydraulic lime P154

Plate 18 : Gowrie sharp sand and Shap non-hydraulic lime P156

Plate 19 : Gowrie sharp sand and Blair Athol non-hydraulic lime P157

Plate 20 : Gowrie sharp sand and Blair Athol non-hydraulic lime P158

Plate 21 : Gowrie sharp sand and Isle of Man non-hydraulic lime P160

Plate 22 : Gowrie sharp sand and Isle of Man non hydraulic lime P160

Plate 23 : Gowrie sharp sand and NHL2 hydraulic lime P161

Plate 24 : Gowrie sharp sand and NHL2 hydraulic lime P163

Plate 25 : Gowrie sharp sand and NHL3.5 hydraulic lime P164

Plate 26 : Gowrie sharp sand and NHL3.5 hydraulic lime P165

Plate 27 : Gowrie sharp sand and NHL3.5 hydraulic lime P166

Plate 28 : Gowrie sharp sand and NHL5 hydraulic lime P166

Plate 29 : Gowrie sharp sand and NHL5 hydraulic lime P168

Plate 30 : Gowrie sharp sand and NHL5 hydraulic lime P168

Plate 31 : Gowrie sharp sand and Jura-Kalk hydraulic lime P169

Plate 32 : Gowrie sharp sand and Jura-Kalk hydraulic lime P171

Plate 33 : Gowrie sharp sand and Jura-Kalk hydraulic lime binary mortar sample P171

Plate 34 : Gowrie sharp sand and ordinary Portland cement binary mortar sample P172

Plate 35 : Gowrie sharp sand and ordinary Portland cement binary mortar sample P173

Plate 36 : Gowrie sharp sand and ordinary Portland cement binary mortar sample P173

Plate 37 : Gowrie sharp sand and blended Shap non-hydraulic lime and NHL2 P174

Plate 38 : Gowrie sharp sand and blended Shap non-hydraulic lime and NHL2 P175

Plate 39 : Gowrie sharp sand and blended Shap non-hydraulic lime and NHL2 P176

Plate 40 : Gowrie sharp sand and blended Shap non-hydraulic lime and NHL3.5 P177

Plate 41 : Gowrie sharp sand and blended Shap non-hydraulic lime and NHL3.5 P178

Plate 42 : Gowrie sharp sand, Shap non-hydraulic lime and NHL3.5 ternary gauged mortar P179

Plate 43 : Gowrie sharp sand, Shap non-hydraulic lime and NHL5 ternary gauged mortar P179

Plate 44: Gowrie sharp sand, Shap non-hydraulic lime and NHL5 ternary gauged mortar P181

Plate 45 : Shap non-hydraulic lime and Jura-Kalk ternary gauged mortar P182

Plate 46:Shap non-hydraulic lime and Jura-Kalk ternary hybrid mortar P183

Plate 47: Shap non-hydraulic lime and O.P.C ternary hybrid mortar P183

Plate 48: Shap non-hydraulic lime and O.P.C ternary gauged mortar P185

List of Tables

Chapter Two

Table 1: Results of statistical analysis of heat of hydration of cement (21°C) **P22**

Table 2: The setting rates of both C_2S and C_3S, determined by strength development (Kg/cm^2) of pure compounds **P29**

Table 3: The $Ca(OH)_2$ concentration in common hydraulic limes **P33**

Table 4: Compressive strength (MPa) of cement paste cubes formed from belite - rich clinkers **P44**

Table 5: Phase composition of low -lime clinker cooled at high and normal rates **P45**

Table 6: Theories for onset and termination of stage II : the induction period **P54**

Table 7: Classification of C-S-H morphologies **P55**

Table 8: Theories on the mechanisms of C_3S hydration **P56**

Table 9 : Conflicting classification and hydraulic indices for limes **P68**

Table 10: Cementitious Index for various types of limes **P68**

Table 11 : Analytical calculated compound composition and physical properties of natural hydraulic limes **P70**

Table 12: Sequence of hydration of C_3S **P74**

Table 13: Meaning of basic hydration reactions in OPC **P78**

Table 14: Reversible reaction of non-hydraulic limes, $CaO \leftrightarrow Ca(OH)_2$ **P79**

Table 15: Particle size in hydraulic limes **P80**

Table 16: Blaine, Volume fraction and surface area of primary hydration products **P81**

Table 17: Properties of hydration products **P82**

Table 18: Pores in cement paste **P84**

Table 19 : Differences in data collection and test procedure **P89**

Table 20 : Wetness classifications **P97**

Table 21: Factors effecting moisture flow in cementitious materials **P105**

Chapter Three

Table 22 : Binders **P121**

Table 23 : Water lime / ratios **P121**

Table 24 : Summary of mortar mixes **P122**

Chapter Four

Table 25 : Max rate of heat and total heat values **P145**

Table 26 : Summary of max rate of heat and total heat values **P145**

Table 27 : Samples and water vapour permeability and resistivity values **P148**

Table 28 : Water vapour permeability **P149**

Table 29 : Water vapour permeability of NHL2 samples **P149**

Table 30 : Water vapour permeability of NHL3.5 samples **P149**

Table 31 : Water vapour permeability of NHL5 samples **P150**

Table 32 : Water vapour permeability of Jura-Kalk samples **P150**

Table 33 : Water vapour permeability of Portland cement samples **P150**

Chapter Five

Table 34: Classifications according to different systems **P187**

Table 35: Hydration products in OPC and hydraulic limes **P188**

Table 36: Percentage of combined silica in binders and its relationship to setting time and compressive strength **P189**

Table 37 : Setting times in natural hydraulic limes **P189**

Table 38: Assessment of hydration adopting heat of hydration graphs (72 hours) **P190**

Table 39: Setting rates of C_2S and C_3S **P193**

Table 40: Chemical and consequent mineralogical components found in St Astier natural hydraulic limes **P193**

Table 41: Free lime concentration in St Astier NHLs **P195**

Table 42 :Rank order of water demand **P198**

Table 43: Characteristics and significance of the main constituents of cement **P205**

Table 44 : Conduction calorimetry results for hydraulic lime and cement pastes (72hours) **P206**

Table 45 : Results of statistical analysis of heat of hydration of cement (21°C) **P207**

Table 46 : Water vapour permeability values **P208**

Table 47 : Permeability of plasterboard **P208**

Table 48 : Binary Mortar samples **P215**

Table 49 : Ternary Mortar samples **P219**

Chapter Six

Table 50 : Hydraulicity / Water vapour permeability of binary mortar types

P234

Table 51 : Hydraulicity / Water vapour permeability of ternary mortar types

P235

List of Equations

Equation 1: Avrami's equation **P51**

Equation 2: Jander's equation **P52**

Equation 3: Hydraulicity Index (Eckels) **P66**

Equation 4: Boynton's cementitious index (C.I.) **P67**

Chapter One: Introduction

This opening chapter sets out the background to this research and introduces the use of lime for building both in its historical context and as a suitable conservative repair material for historic buildings.

1.1 Historical background of lime for building

Lime has been used for building by many civilisations for over 10,000 years, and is still evident in structures from as early as the Epipaleolithic period [1]. The early Egyptians, Greeks and Romans [2] all adopted lime as a primary building material and this empirical knowledge was passed on from generation to generation through these civilisations. However, in isolated civilisations, the development of lime as a building material may have been derived by serendipitous means but we may never conclusively understand how lime and its derivatives were actually discovered, as documentary evidence of its origin is unknown.

It was the Romans who first documented and experimented with lime mortars, concretes and pozzolans. Vitruvius in his *'Ten books on architecture'* [3] lists suitable building materials of which lime was categorically included. In addition he believed that lime was an excellent building material with various qualities and fortunately he documented them in his writings.

As a consequence of his observations many great engineering works were constructed within the period of the Roman Republic and the subsequent Empire. However, after the fall of the Roman Empire scientific documentation and experimentation of lime stopped and did not resurgence for almost 1000 years with the start of the renaissance.

During the mid 15th Century, Alberti documented lime mortars and reinforced Vitruvious's belief stating that 'nothing in nature can be imagined more serviceable for all manner of uses' [4]. Unfortunately, some of his scientific understanding was limited as can be seen when he discusses damage caused to kilns (attributed to unknown creatures) during the calcination of lime, stating *'Once the fire in the kiln has been ignited, the air inside the stone expands, as a result either of being constricted as the cold recedes, or of turning into vapour and increasing in size, as the stone eventually heats up; then, shattering the prison where it has been confined, it bursts out with a loud noise in its violent fury and totally demolishes the whole kiln. Many different*

animals have been seen flourishing in the centre of those stones, including worms with hairy backs and many legs; these can cause great damage to kilns' [4]. Although the information was highly unreliable it once again initiated observation and documentation of lime.

The 18th century saw a rise in interest in the subject of durable natural and artificial cements, occurring as a response to new, adventurous building and civil engineering works undertaken by early pioneering engineers. New materials were sought which were capable of asserting a hydraulic set (that is to say, the ability to set underwater), and which would thereby satisfy the rigour of the new engineering projects. Research was undertaken by a number of engineers and scientists of the day such as Semple (1758) and Smeaton (1797). Smeaton's work on the Eddystone lighthouse (1757) is considered as an essential leap forward in the science and technology of natural and artificial cements. He undertook experiments in which he calcined clays and chalks individually, and then subsequently blended them together to create an artificial cement. He observed that the combination of the silicates, aluminates and calcium oxide, led to the formation of a material which was extremely strong in hydraulic capacity.

Vicat, 1818, was one of the most significant post-Smeaton researchers whose pioneering work on artificial hydraulic cements and more specifically the development of the H.I. (Hydraulic Index), may be considered the true forerunner to Aspdin, the man associated with the discovery of ordinary Portland cement. Joseph Aspdin, a bricklayer from Leeds, published his patent for a new material named 'Portland cement' (1824). His use of the name 'Portland' for his cement was derived from the colour of the set cement, which resembles the colour of natural Portland limestone. In addition he wished to convey the impression of quality and durability that Portland limestone represented. Aspdin discovered that high temperature calcination of clays and limestones (which were traditionally fired at 700°C) could be blended (post sintering stage) in specific proportions, to attain desirable cements. These cements were capable of achieving relatively high strengths and had a greater ability to set underwater. This was due to the hydraulic properties of the material formed by the correct blending and a specifically high calcination temperature as aforementioned.

However, Aspdin's son, William set up his own cement works for the manufacture of improved cements in 1843. He discovered that clinkered or over-burnt material

substantially increased the strength of his cement' [5]. Within his calcination process he had serendipitously manufactured the compounds which create alite (α-C_3S), which is the primary cementing component in Portland cement.

By the beginning of the 20th century Portland cement's perceived advantages were leading to the demise of the use of traditional lime mortars. This saw an increase in the ideological stance associated with *'new is synonymous with good, old is synonymous with bad'* which ultimately led to the loss of almost 10000 years of developed empirical lime based knowledge within a relatively short period of time. The late 1960s saw the final demise of the use of lime in new building when lime plasters were superseded by gypsum based materials. The oligopoly of Portland cements, gypsums and plasterboard manufacture were to predominate the 60's and 70's. However, a resurgence in the interest of historic buildings and conservation was developing and questions were raised as to Portland cement's suitability for use upon irreplaceable historic building stock.

1.2 Specification of cementitious materials based upon strength

Within the last 60-100 years, the specification of mortars or concrete have been based upon relatively new ordinary Portland cement based materials. These incur properties such as the ability to resist high compressive strengths, faster curing times and greater hydraulic activity, the latter of these affording a greater ability to set under water. None of those properties could be truly matched by its predecessors, such as proprietary cements, natural hydraulic and non-hydraulic lime. The belief that durability of cementitious materials must be attained via strength and impermeability, [6] renders limes practically useless in these terms.

The shift in the choice of materials seemed well founded and at the time fully defensible as the modern construction industry was pioneering new innovative structural design forms, primarily enabled by the revolutionary cementitious binder, Portland cement. These structures could not have been built adopting even the best eminently hydraulic limes and pozzolanic mixes. However, the construction techniques adopted for traditional or vernacular buildings and that of modern buildings are quite different. The adoption of dense impermeable Portland cement materials applied to a traditionally built structure, which is relatively permeable, can lead to moisture entrapment and consequent deterioration.

Conversely, Bonen has revolutionised the thinking of the last 100 years as demonstrated by the following rather controversial statements *'The outstanding performance of ancient concrete structures implies that thermodynamic stability rather mechanical strength is a key point for a long-term durability'* [1] and *'to what extent is Portland cement concrete durable? Or in other words, is the main hydrated product of Portland cement, the C-S-H, capable of withstanding the test of time? This question becomes relevant in the light of the outstanding performance of a few ancient structures, some of which are continuously subjected to sequences of drying and wetting and salt attack'.* [1]

All historic buildings have unique requirements and operate upon construction principles that may be considered radically different to modern construction. However, high strength is not generally an essential design parameter for historic buildings. Hence, most historic mortars may have low strength requirements but will require greater permeability and flexibility to attain a forgiving structure enabling higher overall levels of durability. This makes us question the performance of modern cementitious materials, as did Bonen. Hence, the fixation upon strength within modern construction must be questioned, especially when this technology is insensitively used for conservation work.

As stated earlier, lime attains superior permeability to Portland cement via a relatively large interconnected pore structure. These pore systems also allow ice crystal growth, in frost periods, accommodating the crystals within the pore structure without causing deterioration of the matrix. This allows lime a greater propensity than Portland cement to be forgiving, which is essential in historic buildings. Unfortunately, Portland cement is still being specified and adopted all to frequently by ill-informed professionals and tradesmen. It has been empirically shown that these works will lead to long term and accelerated deterioration of finite historic built heritage.

1.3 Implications of lime research within a building conservation context

Using Portland cement for repair of historic buildings tends to disrupt the natural moisture equilibrium to which the buildings are accustomed. This results in exacerbated stone decay and increased moisture content within building components with resulting moisture entrapment and deterioration within the areas which have been repaired.

Plate 1: Deterioration of sandstone masonry due to dense impermeable Portland Cement mortar [7]

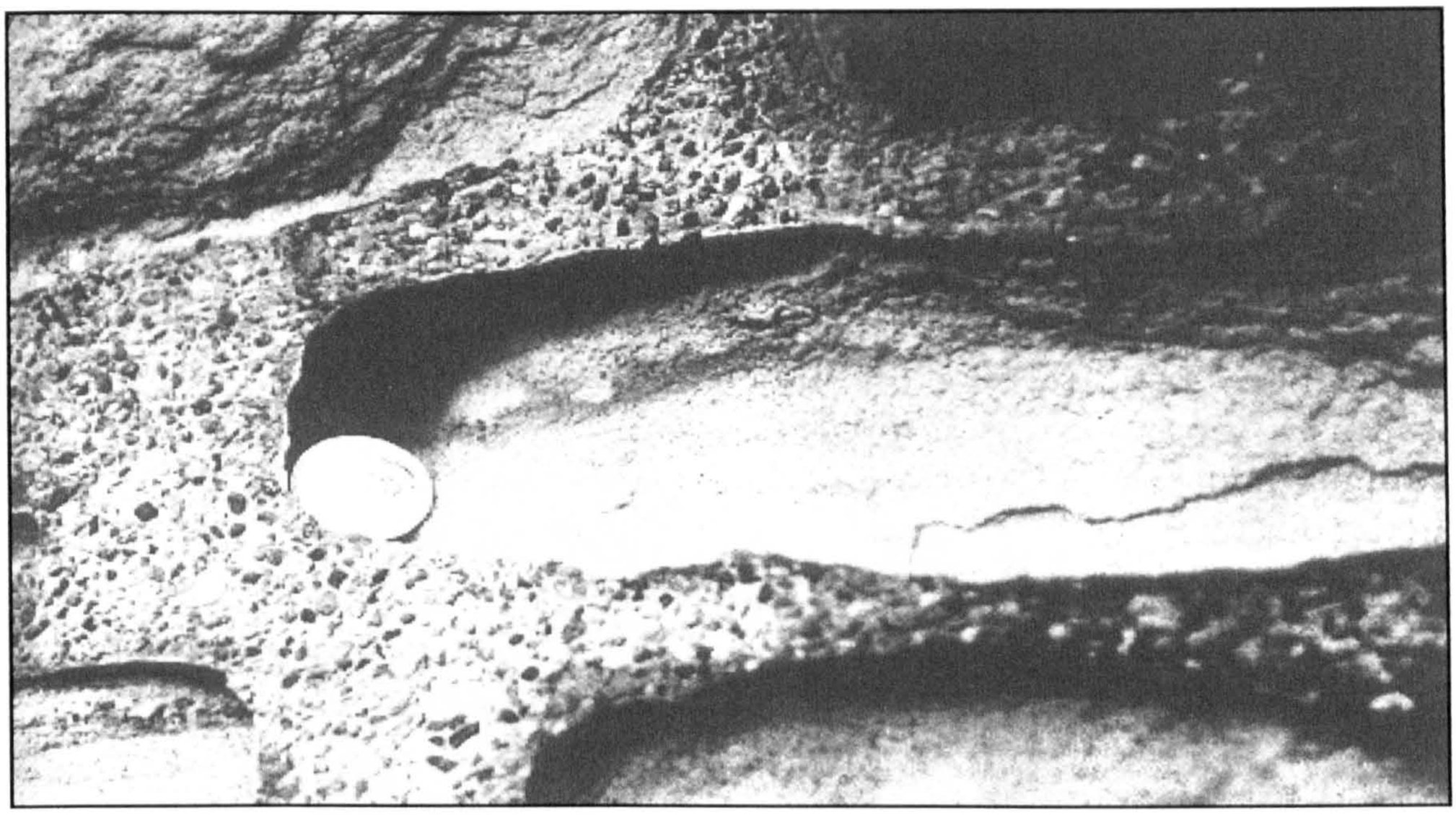

In addition to this the design concept of adopting a mortar which is softer than the substrate materials is difficult to achieve when using Portland cement, especially for traditional Scottish vernacular materials such as sandstone. Concerns about the deterioration of historic buildings which had adopted Portland cement instead of traditional lime based mortars and harl-coats was evident post 1970-80 (a phase in which many *'restoration'* projects were poorly undertaken). Today we are left with the legacy of insensitive repairs, which in most cases are irreversible and have been extremely detrimental to the historic building fabric, necessitating costly stone repair, and the replacement of internal elements and components.

A prime example of this is the refurbishment of Brodie Castle, Morayshire, in 1979 [7], where an insensitive Portland cement harl coat was adopted to replace the once lime harled masonry. Moisture entrapment ensued and led to irreversible damage to the internal joists and irreplaceable decorative plasterwork.

Plate 2: Stained (Portland cement) harling on the south west tower of Brodie Castle [7].

Such repairs contravene the principles of building conservation, [8] which state among others that all repairs should, replace materials like for like, avoid conjecture, be reversible and, where possible, adopt a least intervention approach to the historic building fabric. This is reinforced by Historic Scotland who state that *'The authenticity of an historic building depends most crucially on the integrity of its fabric and on its design, which may be original or may incorporate different periods of addition and alteration. The unnecessary replacement of historic fabric, no matter how carefully the work is carried out, will have an adverse effect on the appearance of a building or monument, will seriously diminish its authenticity, and will significantly reduce its value as a source of historical information'* [9].

Consequently, empirically tested lime based materials are today beginning to be appreciated once again and are recognised as the true binding material to be used upon our finite resource of historic buildings. Unfortunately, the science and technology of lime, whether hydraulic or non-hydraulic has been little researched when compared with Portland cement. Therefore, total adoption of hydraulic lime is difficult to justify scientifically and is still being debated today. It was therefore necessary to investigate the empirically tested functions which afford these materials the ability to allow a

relatively free moisture dissipation whilst allowing satisfactory durability characteristics. This was the starting point for the research undertaken.

1.4 Technological differences between traditional and modern construction

Traditional buildings relied upon several mechanisms to prevent moisture ingress and entrapment from occurring. These included thick walls and the ability to freely dissipate moisture from the external environment via permeable materials (see figure 1). Historic buildings constructed in this manner are empirically tested and work well with their age standing testimony to the performance and longevity of the structure. This makes the choice of traditional materials and techniques extremely important to ensure the continued satisfactory performance of historic buildings. If we consider the materials traditionally adopted within the remit of this construction then it becomes apparent that they are invariably permeable (to greater or lesser degrees). These materials and techniques are deemed to aid *'breathing'*.

Modern construction technology relies upon the adoption of relatively impervious materials and moisture resisting design to prevent moisture from gaining access to the internal environment. Modern buildings also rely upon ventilation systems to minimise the problems of condensation arising from internally generated moisture. The design of these structures adopts cavity walls which separate the internal and external leaves of masonry using wall ties. These have the twin function of aiding stability and also to prevent water crossing the cavity and gaining access to the internal environment. These walls are free draining, with weep holes at ground level. Generally, modern materials are relatively impermeable but those that are not are isolated from moisture paths by designed-in drainage or impermeable coatings. These materials and techniques are deemed not to *'breathe'*. Both traditional and modern forms of construction work well but when new impermeable materials are adopted upon traditionally built structures problems may occur. Figure 1 indicates the performance and material differences between traditional and modern construction technology and materials.

Figure 1: Differences between traditional and modern construction (after Hughes) [10]

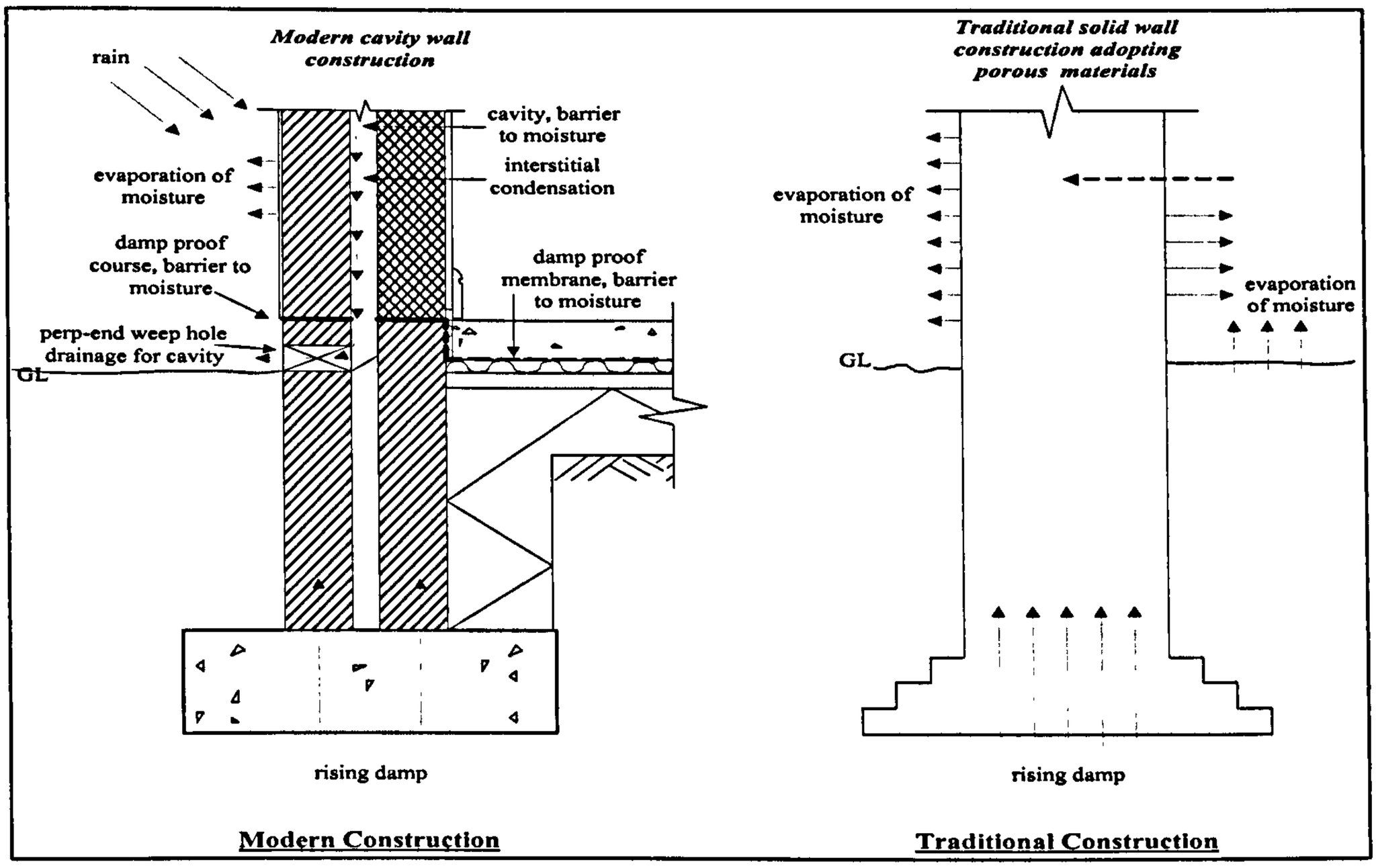

1.5 'Breathing' of traditional buildings

It is well understood that lime mortars and renders allow historic buildings to 'breathe', a particularly important requirement in northern climates, and that repairs done with cement-based materials have caused considerable damage due to their impermeability. However, what constitutes *"breathing"* has never been objectively defined with the result that it has become too nebulous a concept for rational use by professionals involved in the selection of materials for conservation. To say that a material *'breathes'* is difficult to substantiate as no real information has been written upon the subject. For example, if non-hydraulic limes are deemed to be permeable and therefore have the ability to *'breathe'*, and feebly through to eminently hydraulic limes have the ability to *'breathe'*, but Portland cement lacks this ability then at what point does a material cease to be breathable? This is particularly questionable considering that hydraulic limes and Portland Cements both derive their binding characteristics via the development of C-S-H.

This problem may be more clearly explained with the adoption of a conceptual materials permeability and hydraulicity scale (Figure 2).

Figure 2: Hypothetical hydraulicity / permeability scale (Author)

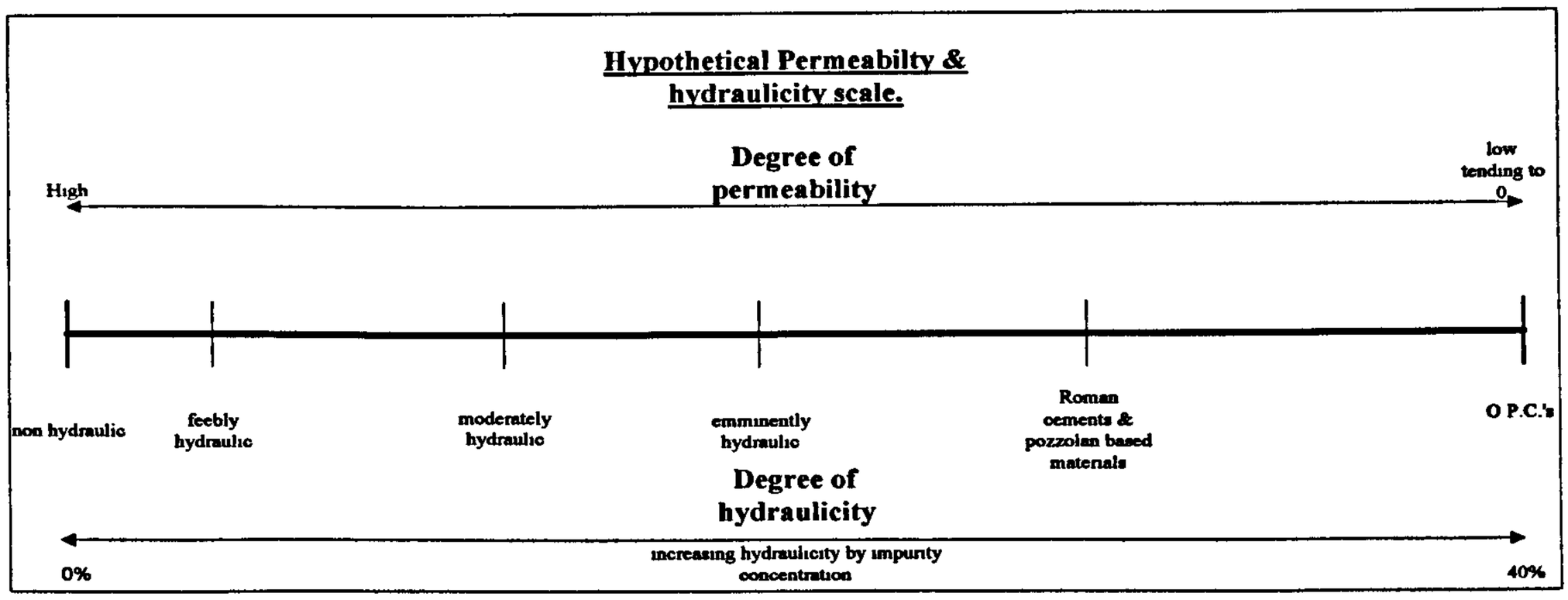

If this concept is valid the water vapour permeability and hydraulicity of these materials must be realistically assessed to truly evaluate the 'breathing' functions of lime.

1.6 Deterioration of historic building fabric as a consequence adopting insensitive materials

As has been previously stated; modern and traditional materials work well in the situations for which they were designed to be used. However, problems arise when modern relatively impervious materials are adopted for use upon traditional structures which rely upon traditional materials to allow moisture equilibrium to occur. This leads to problems associated with moisture entrapment, and consequent failure of components within the traditional buildings' fabric. To exacerbate the problem Portland cement contains a reserve of soluble salts not present in hydraulic limes. These salts are detrimental to soft impermeable materials because they easily form a saturated solution and re-crystallise within the substrate causing disruption.

1.6.1 Decay mechanisms caused by insensitive repair techniques

Within the last 20 years, an increase in the decay of sedimentary stones and soft-fired brick has been noted [7,9]. The primary cause of exacerbated decay is attributed to insensitive impermeable Portland cement being adopted for repairs which should have been undertaken in relatively permeable lime based materials. The most commonly occurring problems derive from re-pointing and harl coats, which in the short term may seem satisfactory, however, costly deterioration will be noted in the medium to long term. Plate 3: indicates such a problem. It would appear that the use of Portland cement has led to rapidly exacerbated stone decay.

Plate 3. Delaminating impermeable Portland cement from permeable substrate: Livingstone Place, Edinburgh. (Author)

As depicted in plates 2 and 3 the moisture flow from internal environments may be severely disrupted and in many cases will result in the delamination of an impervious cementitious coating from the relatively permeable substrate.

Plate 4: Paye House, Cromarty. Portland cement harl-coat sheet failure. [7]

1.6.2 Moisture entrapment and frost attack

Traditional lime based mortars offer little resistance to moisture flow and thereby allowed free moisture dissipation. These materials also act sacrificially and deteriorate in preference to the substrate, which increases the longevity of the structure and enhances the performance of the materials and structure holistically. They were designed to be renewed at intervals. However, when replaced by modern impervious Portland cement re-pointing and harl coats the capability of the building to allow free moisture dissipation is severely disrupted. The moisture generated from the internal environment, or that which has been absorbed into the fabric of the building from the external environment will naturally seek an alternative path for moisture dissipation. This diverted moisture has two common paths available; namely, egress through the relatively permeable stones and bricks which form the mass of the structure, or ingress into the structure where they become trapped within the walls and components bedded within.

Figure 3: A comparison of the technology of Portland cement and lime based harl coats [11].

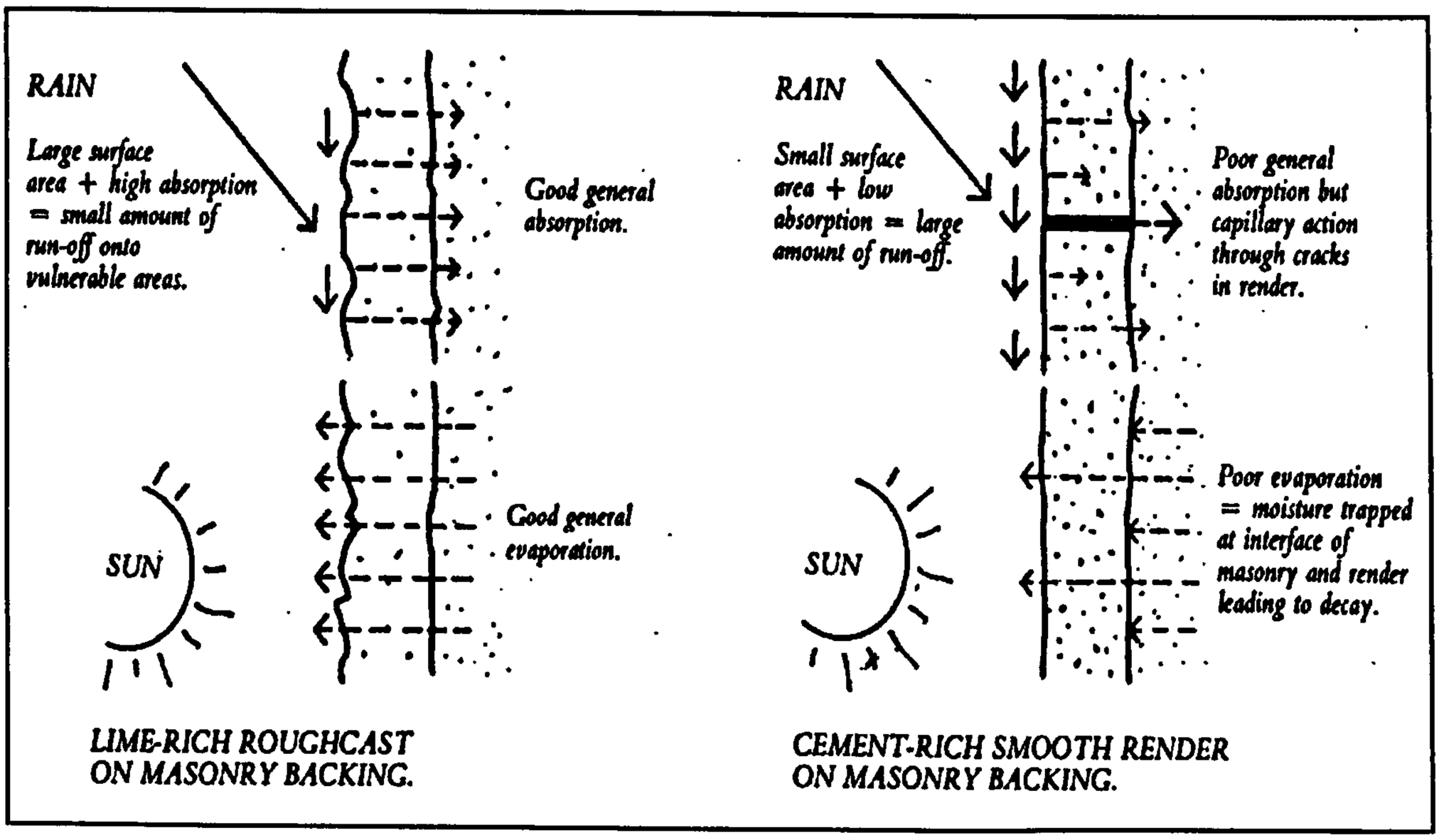

When the moisture content of the porous stone increases spalling occurs and leads to a Portland cement ridge which protrudes further than the deteriorating pervious stones. This ridge acts as a pool in which water can lie and increases the moisture content of the stone and leads to rapid deterioration of the stonework via frost action. This can clearly be seen in plate 5.

Plate 5: Much harder cementitious pointing has contributed to the excessive decay of the brickwork. [9]

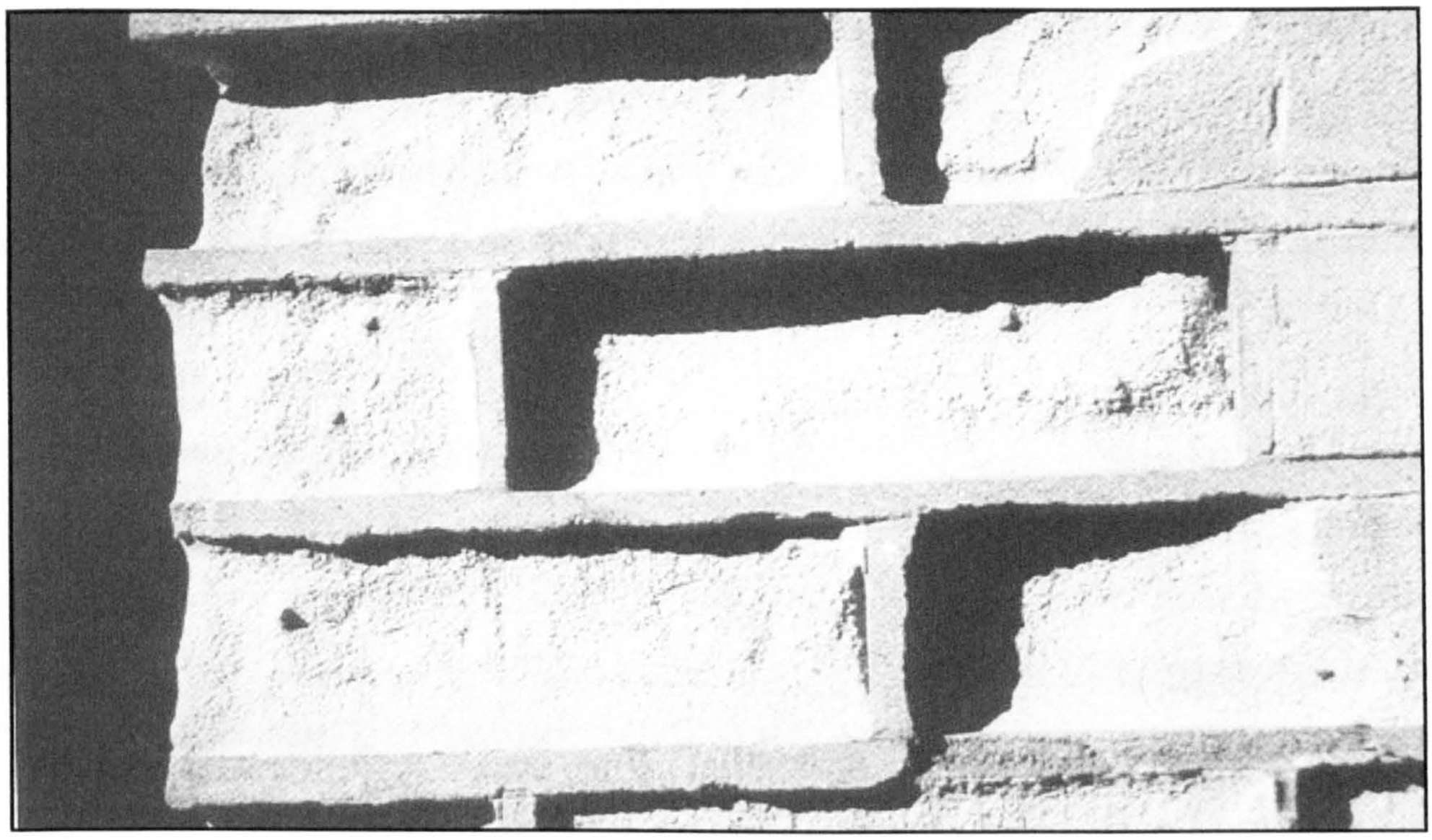

1.7 Development of a defensible hypothesis

As a consequence of deterioration seen in historic buildings repaired with dense, impermeable Portland cement instead of the relatively permeable lime mortars, a resurgence in interest in the latter has developed. A dense Portland cement mortar has a high resistance to the passage of water vapour whereas a feebly hydraulic lime mortar has low resistance. Portland cement brings about binding through the growth of a dense micro-crystalline network of calcium silicate hydrate (C-S-H) and calcium aluminate hydrates (C-A-H) which fill the voids left by free water in the mix, leaving a very fine pore size distribution. Hydraulic limes bind via C-S-H, formed from di-calcium silicate (β-C_2S, also known as *'belite'*), and calcium hydroxide ($Ca(OH)_2$) (also known as *'Portlandite'*), which also grow within the voids left by the free water. C_3S is not found in hydraulic limes due to the lower calcination temperatures associated with lime firing. Hardened limes have a much coarser pore size distribution which theoretically gives the material increased water vapour permeability. As with the hydration of cement, the hydraulic components of an eminently hydraulic lime are formed from the interaction of clay impurities during the firing process. It is therefore, reasonable to expect that greater hydraulicity results from a larger proportion of the cement-like components and in consequence low permeability might be expected from more hydraulic limes.

Holmes and Wingate reinforce this theory, stating *'Hydraulic lime mortars not only have this extra power of setting, but are stronger than non-hydraulic lime mortars. Thus they have often been used with the intention of giving durability to non-hydraulic construction works, but they can give rise to the same sorts of decay problems as mortars containing modern cements - undue stiffness and lower permeability which can allow soluble salts to cause damage to the masonry units, rather than to the more easily repaired joints'.* [12]

Thus a relationship between hydraulicity, (and consequent C-S-H formation) and water vapour permeability of cementitious materials is to be expected. The tangible aim of this research is to explore the concept of 'breathing' and if possible relate the findings on a hydraulicity index against permeability scale. Hence the working hypothesis is that *'There is a correlation between the hydraulicity and permeability of lime mortars for use within the historic building and conservation industry'.*

Chapter Two: Literature Review

2.1 General Introduction

The format for the literature review has been sub-divided into the primary constituent parts of the overall thesis namely, hydration, water vapour permeability and Environmental Scanning Electron Microscopy (E.S.E.M) analysis. It is hoped that this will aid the clarity of reading of the somewhat wide ranging subject matter, without becoming fragmented and tangential to the initial focus of the literature review. Whenever possible a historical perspective has been integrated into each area of study, enabling sound foundations to be established.

2.2 Historical development of hydraulic limes and artificial cements and the properties they impart.

The historical development and understanding of cementitious materials has an extremely long history. It has been shown that lime was used as a building material within the Epipaleolithic period [1], some 10,300 years ago (8300 BC). Numerous examples of ancient structures built in lime dating post this period are evident throughout Israel, Egypt, Turkey and Italy. However, it was the Romans (with their strong observational and philosophical influences derived from the Grecian Empire) who where the first of these civilisations to attempt to document observations regarding the physical and chemical properties of lime.

Vitruvius documented empirical functions of limes and pozzolans in his works *'The Ten Books On Architecture.'* [3] Vitruvius was an enlightened engineer who understood the importance of traditional knowledge to guide the then present developments. His documentation of pozzolans written in the first century B.C. gives us an insight into his beliefs and understanding upon the effects of pozzolans, stating, *'There is also a kind of powder which from natural causes produces astonishing results. It is found in the neighbourhood of Baiae and in the country belonging to the towns round about Mount Vesuvius. This substance, when mixed with lime and rubble, not only lends strength to building of other kinds, but even when piers of it are constructed in the sea, they set hard under water.'* [3].

His discovery of pozzolans is the first documented evidence of volcanic ash and pumice having very effective hydraulic properties which significantly affects the strength and

durability characteristics of these early concretes. This led Vitruvius to correlate the attainment of a hydraulic set in mortars with pozzolanic additives. Vitruvius realised that adhering to certain specifications and construction principles could lead to the attainment of superior structures. One such principle included; *'Walls which are to be under water should be constructed as follows. Take the powder which comes from the country extending from Cumae to the promontory of Minerva, and mix it in mortar trough in the proportion of two to one.'*[3].

These observations allowed the Romans to develop domestic, ceremonial and engineering structures that clearly surpassed those of any civilisation previously seen. The remains of these structures can still be seen and stand testimony to the ability of Roman structural engineering and early material science. One such building is the Pantheon in Rome with its innovative light weight lime concrete dome (see plate 6).

However, for all of Vitruvius's innovations and observations his works seemed to fade into obscurity with the fall of the Roman Empire and the beginning of the early medieval period (early medieval 500-1000AD). A period of approximately 1000 years passed with almost no scientific development or study of lime based materials. Consequently this period is associated with a regression in the understanding of mortar technology.

Plate 6: Pantheon (section), Rome

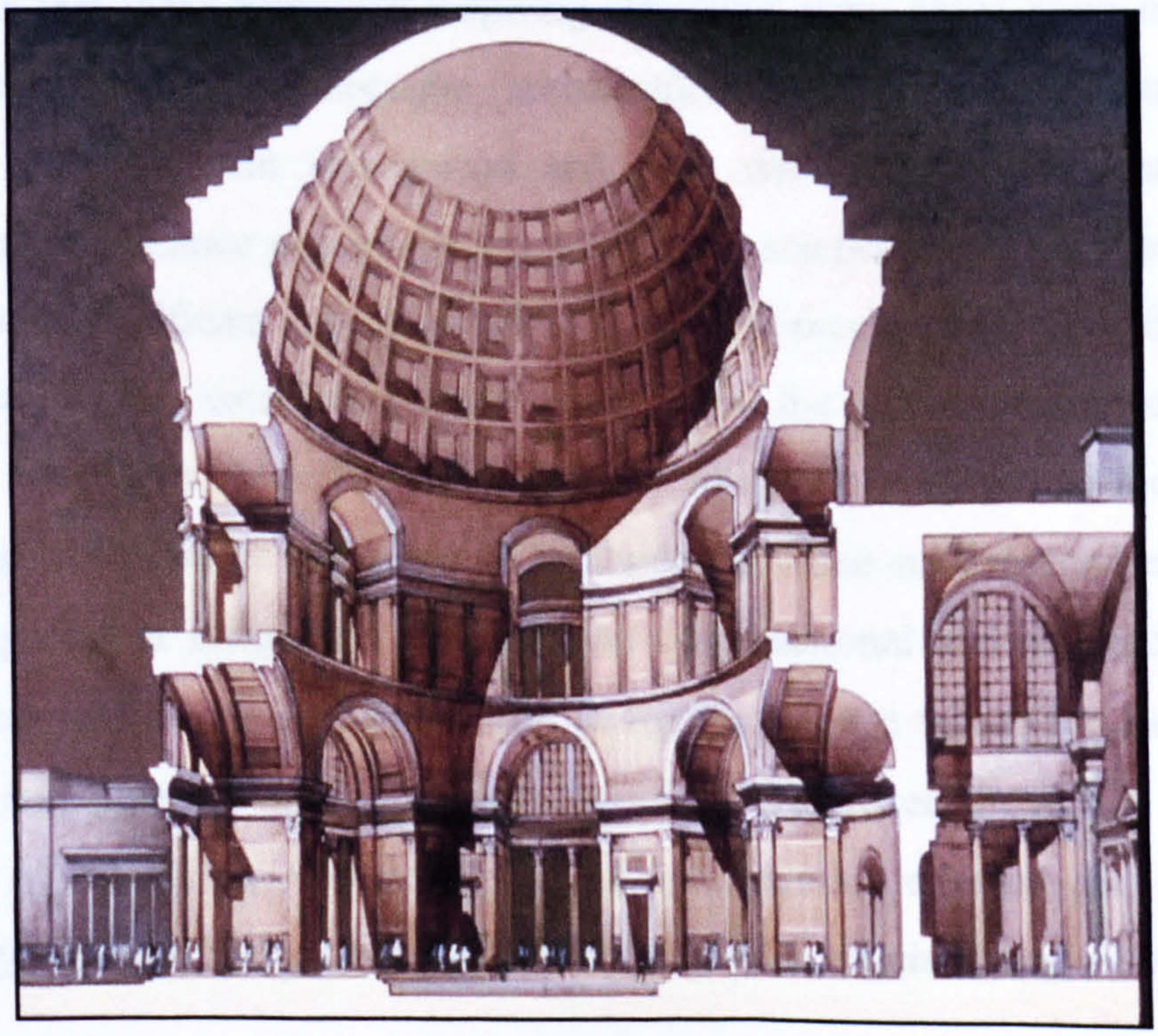

The early medieval period (the dark ages) saw the continuance of the use of traditional construction techniques and materials, and more specifically, the use of lime mortars. Unfortunately no real documented advances were made, or survived from this period. However, this does not mean to say that they did not understand how the material was to be used. This is reinforced by the Norman builders who obviously understood the application of lime mortars, to which their cathedrals stand testimony (Plate 7 shows Durham cathedral). It is interesting to note that structures such as this have lasted for approximately 1000 turbulent years, but now suffer from decay mechanisms associated with modern cements which have been adopted within the last 30 years.

Plate 7: Durham Cathedral dominating the Durham City skyline.

It is obvious that these truly awe inspiring structures were based upon Roman design concepts, hence, the Romanesque architectural style. However, little scientific knowledge emerged from this period and only with the development of the late medieval and renaissance period did any advance in science prevail. The renaissance or 'rebirth' saw a significant leap forward in the development of ideas of those building the structures, which were once again based upon the Roman design concepts. The developing interest in natural physical science and philosophy led to the initiation of what we know of today as the scientific methodology. One such researcher was Alberti, who although rather misguided did write on constructional and architectural matters. Alberti's texts indicate a significant loss in the knowledge which the Romans had so studiously and possibly serendipitously acquired. However, it would be wrong to dismiss all of Alberti's works, as certain observations are relevant and follow logical methodology. Unfortunately, certain beliefs prevailed which indicate the influence of

superstition upon observation. A good example of his beliefs on calcination was quoted in chapter 1 [4].

Prior to Semple and Smeaton it was believed that the most suitable lime mortars were those produced from hard limestone. This is noted by Pasley who emphasised traditionally held beliefs that *'lime prepared from the hardest limestones and preferably from moist, shady quarries should only produce hard mortars. In contrast soft stones, such as chalk, should only produce soft mortars'* [13]. This confusion about durable hydraulic mortars prevailed until Smeaton undertook his research for the construction of the Eddystone Lighthouse in 1757, with observations being published in 1791.

Smeaton paved the way for a myriad of research by engineers who were all working to attain a paragon in cementitious binders. Pasley described this with his analogy 'the race to the moon' [13]. The subsequent development of Portland cement was attained through the perfect blending and calcination temperature. One of the researchers was Vicat (1812), whose works upon the nature and use of hydraulic limes had initially been born out of his interest in engineering applications, as had Smeaton approximately 50 years previously. From these early works he compounded and reworked an array of papers and published a comparatively holistic text on ordinary lime mortars for construction in 1828 [14]. He was the first to develop a system of calculating the 'hydraulicity' of limes, in the form of the Hydraulic Index (H.I.). Although this was a significant advancement the calculation method was overly simplified and only considered *'the ratio between the percentage of silica to the percentage of lime CaO'* [15]. A strong influence upon Vicat's research was Descotils, who is reported by Bergoin as having stated that *'insoluble silica in calcareous materials became soluble when this material was burned at the necessary temperature'* [16], and also believed that *'silica combines with lime and it was this process that gave hydraulic properties to some limes'* [16].

However, for all the knowledge developed over the later decade, it was Aspdin (a brick layer from Leeds) who is commonly associated with the first Portland cement. Aspdin established a patent *'for making artificial stone'* in 1824. Within this patent he adopted the words Portland cement. Wingate states this aimed *'to give an impression of excellence and the suggestion of an attractive colour by association with Portland stone'* [13]. However, this material was simply comparable to a myriad of products also

considered to be artificial cements. Although Aspdin had recognised the need for higher temperature calcination and correct blending proportions, it was his son William Aspdin who (working at his own cement works near Gateshead) discovered that sintering temperatures must be achieved to attain cement with superior strengths.

In 1906 Candlot published *'Ciment et hydrauliques'*. According to Bergoin, he recognised the importance of Vicat's work undertaken almost a century before and stated: *'in 1818 Vicat demonstrated that all calcareous materials contained a percentage of clay finely dispersed in their mass, able to give, after burning hydraulic properties'* [16]. Candlot believed that *'the transformation of a calcareous rock when burned at a certain temperature causes the determination of the setting and hardening'* [16]. However, more importantly, he went a stage further than Vicat by understanding that *'during burning lime reacts with the clay and combines itself with silica to form calcium silicate'* [16]. It would be difficult to refute that this discovery paved the way for the birth of modern hydration theory in cementitious materials.

2.3 Traditional hydration theory and its historical development

Smeaton's experimental work on limes and artificial cements were initiated by a necessity to manufacture a cementitious material with high durability and strong hydraulicity (that is to say having the ability to set underwater). This was essential for the forthcoming re-construction of the Eddystone lighthouse (Commenced building in 1756, observations documented in 1791). Smeaton observed that *'strength for the toughest conditions could be achieved from impure limes'* [13] and therefore, recognised the importance of the combination of the clay and lime components within the quarried limestones. This marked a significant leap forward in the understanding of the principles of hydraulic activity. Among the basic experimental processes adopted by Smeaton was the 'kitchen sink' test, which showed that *'the limes which developed a firm set for "water building" where those made from limestones or chalks which contained a suitable proportion of clay'* [13].

In 1796 Parker patented *'a certain cement of Ferras to be used in Aquatic and other buildings, and stucco work'* [13]. These cements were manufactured by using naturally occurring Septaria (a concretion of limestone and clay). The proportion of clay / lime within Septaria are good when compared with modern cement proportions. Hence, certain hydraulic properties would be attained if thorough calcination was achieved. The

effects of this calcinated septaria cement was described by Wingate, who stated that, 'when fired at an appropriate temperature and then ground to a fine powder they produce a very quick setting cement quite unlike anything which had been seen before' [13]. This cementitious material became known as 'Roman Cement'. Once this patent ended in 1810 an influx of alternative artificial cements ensued.

Pasley undertook experiments upon lime and artificial cements for military purposes, and was specifically interested in the proportions of lime and clays within these materials. He summarised the existing knowledge in his seminal publication '*Observations on lime*' [13].

The twentieth century saw a radical advance in the understanding of complex hydration theory. Advances in individual crystalline formations were undertaken by a new breed of researcher, equipped with quick moving technological developments such as X-ray diffraction (XR.D), conduction calorimetry and Environmental Scanning Electron Microscopy (E.S.E.M) techniques. The complexity of modern hydration theory requires a specific look at those components that are essential to the hydration of hydraulic lime and Portland cement. Hence, the following section aims to highlight those hydration components whether, individual or collective, that are essential for early, medium and long term strength development in cementitious binders, including hydraulic limes.

2.4 Modern Hydration Theory

The aim of this section of the literature review is to describe, explain and discuss those primary texts that are deemed to be essential in modern hydration theory. To achieve this a logical sequence has been developed discussing primary hydration products, and where necessary indicating the development of polymorphism and polytypes of the respective compounds.

It is often considered that Portland cement and natural hydraulic lime (NHL) are opposing materials with no relation to each other. However, all cementitious binders whether natural or artificial have certain common hydraulic components. It is therefore necessary to look at the primary hydration products in both Portland cement and hydraulic lime, assessing the interrelationship as they occur. In addition the quantity of information pertaining to hydraulic lime hydration is somewhat dwarfed by that published for cements. Therefore, in situations where no information could be found for

hydraulic limes it was necessary to look to the cement industry to shed light upon the subject area.

2.4.1 Hydration of Portland cement

Taylor defines hydration as the 'totality of the changes that occur when an anhydrous cement, or one of its constituent phases, is mixed with water' [17].

Jawed, Skalny and Young describe hydration as an 'overlapping of chemical reactions between clinker components... leading to cement stiffening and hardening' [18]. He continues to define the stiffening process as the change from 'a system of flocs in concentrated suspension to a viscoelastic skeletal solid capable of supporting applied stress at least for the short time, without significant deformation' [18]. Thereby continuing to emphasise that this process has an effect upon the porosity of the material and ultimately leads to hardening. This may be deemed to be the basis of the formation of a complex elastic and brittle material. This is a 'chemico-physical process' [18] that leads to the strength development of the material. This will continue until 'inadequate reactants (i.e. cement components and water) and space to deposit the hydration products cause the reaction to cease' [18].

Odler defines hydration as 'reaction of anhydrous compound with water, yielding a new compound, a hydrate' [5], which is 'both a chemical and physico-mechanical change in a system, i.e. setting and hardening' [5] He continues to subdivide hydration into two subsets, namely partial and full hydration. Partial hydration may be formed in the presence of humid air, (the higher the humidity then the greater the hydration reaction) and or by an inadequacy of water in the batch. Full hydration is attained by the use of sufficient water, defined by the adoption of the correct water / cement or water / lime ratio. However it is important to realise that the respective water / lime or water / cement ratio affects the rheological properties and pore structure development of cementitious materials and may be responsible for differing forms of hydration products.

Odler discusses setting of Portland cement, indicating that it is synonymous with 'a rather sudden loss in the plasticity of the original paste, and consequent conversion to a solid material' [5] Setting is generally considered a period of low strength in Portland cement with the subsequent hardening phase leading to increased strengths. He believes

that Portland cement may be considered as a 'multi-compound system with a multi-component system consisting of individual chemical reactions, occurring in parallel and successively' [5]. Reaction is spontaneous as soon as water makes contact with the binder, with heat evolution occurring instantly. The heat of hydration may vary over time with acceleration, deceleration and dormant periods of hydraulic activity.

Many factors affect the hydration of both hydraulic lime and cement. Odler [5] indicates some of the primary considerations to take into account when assessing the hydration of cement, indicating that the phase composition of the cement and the presence of foreign ions, will ultimately affect the prevailing crystalline lattices. Also the phase composition of cement / lime will be affected by the calcination temperature, duration and the materials proportions, with foreign ions occasionally being incorporated either as impurities or purposely introduced to initiate synthesis and consequent formation of specific hydration products (especially in cement manufacture).

The particle size of the anhydrous material is very important in determining the rate of hydration and the particle distribution through out the matrix. This ultimately affects the pore structure development. However, it must be emphasised that the water / binder ratio must also be considered of primary importance.

The fineness of the cement / lime affects its particle size distribution and therefore its respective specific surface area. This has a significant affect upon the heat of hydration of the material.

The curing temperature, including prevention of conditions in which the loss of evaporable water may occur. Generally an elevated temperature twinned with a suitable relative humidity in the air will increase the rate of hydration and the consequent hydration products. However, the rate of set may be manipulated by the presence of chemical admixtures and additives such as pozzolans.

Jawed, Skalny and Young [18] believe that the concept of the hydration in cementitious materials may be seen as a dissolution and precipitation process of individual clinker products that may proceed in isolation or simultaneously. Indicating that 'the dissolution of anhydrous phases enable formation of compounds whose solubilities are lower than those of the anhydrous clinker materials, thus leading to the precipitation of colloidal

and crystalline hydrates that form the hardened paste. The speed of clinker solubility is different for the different phases and as a consequence generally those with high solubilities, such as the aluminate, sulphate and alkalis tend to hydrate in advance of the others.

Recent advances in hydration theory have been made with the use of modern scientific equipment, of which Odler [5] emphasises 3 specific tests, all of which are based upon the measurement of either non-reacted clinker (titration), viscosity (determination of the level of formed hydrates) and finally heat liberated from hydration reactions (rudimentary thermopile and heat sink). The latter has been adopted for my own research into hydraulicity. Odler believes that all of the aforementioned tests are classified as single parameter studies (singular selected parameters) or, alternatively multi-parameter studies [5] which as the name suggests measures several functions of the sample to derive the hydration properties. All tests of hydraulicity mentioned are time reliant and various sample forms will be tested under the same conditions after the same duration.

Both hydraulic limes and cements are composite materials. They are composed of individual crystalline hydrates that generate heat during their formation. This will continue at a reduced rate until the consumption of anhydrous particles has occurred. The heat evolution rates of the primary cement compounds may be seen in table 1. Some of these hydrated forms are common also to hydraulic limes.

Table 1: Results of statistical analysis of heat of hydration of cement (21°C) [19].

Period of hydration	Calculated heat evolution (in cement paste) expressed as calories per 0.01 gramme of compound			
	C_3S	C_2S	C_3A	C_4AF
3 Days	0.58	0.12	2.12	0.69
7 Days	0.53	0.10	3.72	1.18
28 Days	0.90	0.25	3.29	1.18
3 Months	1.04	0.42	3.11	0.98
1 Years	1.17	0.54	2.79	0.90
6 $^1/_2$ Years	1.17	0.53	3.28	1.11

Odler [5] believes that the rate of Portland cement and hydraulic lime hydration depends on several primary factors, including;

- The rate of dissolution of the involved phases
- The rate of nucleation and crystal growth of the hydrates to be formed

- The rate of diffusion of water and dissolved ions through the hydrated material that have already formed
- The phase composition of the clinker and the quality and quantity of the foreign ions incorporated in the crystalline lattices of the individual clinker materials will encourage or discourage interim and final hydration
- The processing history of the clinker, including the heating rate, maximum burning temperature and cooling rate, therefore, holistic calcination has an integral role to play in hydration kinetics
- The quantity and form of calcium sulphate present in the cement also affects the hydration properties. However, this will be less notable in lime as low sulphate concentrations are exhibited as opposed to Portland cement
- The fineness of the cement
- The technology employed for comminution of cement
- The water / cement ratio of the mix (discussed in water for hydration), curing conditions, and the hydration temperature

Several of the aforementioned factors may affect the structure of the hydrated forms. However, on a nano-structure level they are primarily dependent upon composition. Odler [5] believes that hydrated forms are significantly affected by the composition of the original binder, the starting water / cement ratio, the temperature of hydration, the absence or presence of chemical additives and finally, the time of hydration. These will have an affect upon the suitability of the hydration products within the set material.

The hydration of Portland cement is extremely complex and as Odler indicates the C-S-H phase may exist in various morphology, including, fibres, flakes, honey combs, and finally tightly packed grains and / or seemingly featureless dense material. However, when assessing them upon a nano-metre scale they are considered as having only one C-S-H type.

The aforementioned phases may be encountered at the different stages of hydration, to a greater or lesser degree, with C_3S hydration undergoing the following morphological changes; within the initial few seconds the formation of minute particles occur. At the early stages a foil like C-S-H or fibrous formation is seen and finally, at the longer hydration stage the material gradually loses its original character, and becomes tightly packed, eventually become featureless.

Odler [5] believes that C-S-H in mature pastes is not evenly distributed, and that formation of an inner product and an outer product will be encountered. The inner product is formed in-situ from anhydrous grains, these appear to be dense and fall out-with anything that may be considered as a structure. The outer product forms in the space originally filled with water, it is less dense than the inner product and is fibrous in texture. In addition to the outer product calcium hydroxide [$Ca(OH)_2$] precipitates and forms relatively large crystalline particles (portlandite) which are several micro-metres in diameter. These form in the same region as the outer product, namely within the space where the water once occurred.

Taylor [17] has discussed the hydration of anhydrous silicates and aluminates that are derived from the clinker phases in cement manufacture. He indicates that the ability of a substance to act hydraulically depends upon 2 primary factors. These being, the ability to react with water at a sufficient rate and extent and secondly, the capability to react and yield solid products of low solubility and lead to the attainment of a microstructure that gives rise to good mechanical strength and volumetric stability.

This may be practically illustrated when looking at the properties of C_3S and β-C_2S, both of which satisfy the aforementioned criteria. In contrast when looking at C_3A or certain polymorphs of belite, namely γ-C_2S it is clear that they are unsuitable for the physio-chemical performance required, with C_3A having poor cementing ability (in isolation) and the γ-C_2S having almost zero reactivity at normal temperatures.

Taylor has hypothesised that the reactivity of cementitious materials and more specifically individual components are affected by the relationship with oxygen molecules within the water, believing that 'any structural feature that draws electrons away from the oxygen atoms renders them less reactive' [17]. This led Taylor to develop the following predictions [17].

I) Oxygen atoms attached only to atoms of a single element will be less reactive as the electronegativity of that element increases. Thus, C_3S and lime both contain oxygen atoms linked only to calcium, and are more reactive than β-C_2S, in which all the oxygen atoms are also linked to silicon, while α-Al_2O_3, in which all are linked to aluminium, is inert. However, the reactivity of lime decreases if it is strong burned.

II) Oxygen atoms forming parts of silicate, aluminate or other anionic groups will be less reactive as the degree of condensation with other groups increases. β-C_2S, in which the tetrahedra do not share oxygen atoms, is more reactive than any of the C_3S_2 or CS polymorphs, in which they do.

III) Oxygen atoms forming parts of anionic groups similar as regards degree of condensation will be less reactive as the central atoms in the groups become more electronegative. In contrast to the C_3S_2 and CS polymorphs, CA, $C_{12}A_7$ and C_3A, in which the AlO_4 tetrahedra share corners, are all highly reactive.

Taylor continues to emphasise that irregular co-ordination of calcium will tend to lead to high reactivities.

Odler discusses the interaction of the clinker phases and more specifically the β-C_2S – C_3S systems, believing that β-C_2S in the presence of C_3S develops at a faster hydration rate, however, data at present is contradictory. In the proportions for cement the C_3S and C_2S do not really have a profound influence upon each other. For that reason he [5] believes that individual hydration products are similar to those hydration products which are combined.

C-S-H formation and structure is further complicated when assessing polymorphism of the material. Taylor has discussed the variations in polymorphs and affects of substitution of ions relating to developed crystal structures. He believes that variation in polymorphs and the consequent introduction of foreign ions into the crystal structure has a significant affect upon the development of the material. It is extremely complex and he believes that many factors can affect the aforementioned development including: chemical composition and polymorphic change: concentration and types of defects: particle size, mechanical stress, presence of micro-cracks and the mono or polycrystalline nature of the grains [17].

Taylor [17] elaborated upon work by Sakurai et al in which he reports that under Electron Microscopy studies the presence of screw dislocations where seen at grain boundaries (where the reaction was greatest). However, for all the defects Taylor believes that reactivity is dependent 'not so much on the amount of substituent or nature of the polymorph, as on the types and concentrations of defects' [17].

2.4.2 General hydration of hydraulic lime

As Portland cement chemistry and technology developed, great advances were made with chemical characterisation of the material. As Portland cement and natural hydraulic limes (NHL) may be considered as relatively close in a chemical context, it would not be unrealistic to group these materials within the same family of cementitious binders. The study of Portland cement may therefore shed a great deal of light upon the chemical and physical interactions within NHLs.

Radonjic et al undertook studies upon both NHL and high calcium limes, the first having a high level of Ca - silicate and aluminate components, with a consequently low CaO content >90%. They emphasise that the setting characteristics of the 2 materials are significantly different with partial carbonation and hydration in the NHL and purely carbonation within the calcium lime. The setting characteristics of both materials were 'reflected in the physical properties and microstructures of the lime mortars, and consequently their ultimate durability and strength' [20]. They found that the NHL mortars where denser than the relatively fragile non-hydraulic (CL) lime mortars.

Radonjic et al explains that the carbonation reaction is fundamentally important in the ageing and durability of mortars. Emphasising that in NH limes 'most of the portlandite is transformed to carbonate', whereas in the high calcium (fat limes) the carbonation rate is a great deal slower and in some cases ancient mortars have been found with 'particles of un-carbonated lime being present after thousands of years' [20]. Radonjic indicates that 'the concentration of carbon dioxide altered the rate of reaction but not the mechanism of carbonation' [20].

Carbonation and set propagation of the range of lime based materials is based upon the type of material, i.e. non-hydraulic limes relying purely upon carbonation, whilst hydraulic limes rely upon what Radonjic calls a 'side reaction'. This reaction is secondary to 'a more rapid, hydraulic setting' [20] process. They indicate that within a hydraulic set the 'lime (CaO) is mainly combined with aluminate and silicate components and water, resulting in a much smaller amount of portlandite being available for carbonate formation' [20].

Radonjic et al describe calcination as 'an endothermic reaction (requires heat) in which an oxy-salt (eg. carbonate or hydroxide) decomposes leaving an oxide as a solid product

with the emission of liberated gas.' [20]. Emphasising that when calcination occurs at higher temperatures (1200°C), the silicates found as impurities within the limestone form calcium silicates, which they call the 'strategic components' [20] of hydraulic limes.

Hughes and Swann reviewed research upon pozzolans and hydration and this led them to believe that different clay minerals burnt under certain conditions would have an effect upon the resulting pozzolan [21]. They therefore realised the importance of studying the minerals in their original form to establish phase constitution of the consequent hydrated product. They [21] emphasise the fundamental processes of setting in lime mortar with the development of the micro-structure mechanisms, occurring as a result of both pozzolanic and carbonation activity. This dual function of hydration and carbonation determines the rate of set in the lime-based material. Hughes and Swann [21] indicate that the calcination of hydraulic limes or, *'fat limes'* with aluminates and silicates from elsewhere will produce calcium silicates, calcium aluminates and / or alumino-silicates. In addition to the aforementioned products, calcium oxide and unconverted calcium carbonate are present and play an integral role in the hydration process. They [21] believe that the dominant calcium silicate is di-calcium silicate (C_2S). Upon mixing with water they lead to the formation of calcium silicate hydrates (C-S-H), with the addition of calcium hydroxide [$Ca(OH)_2$] acting as a primary lattice for the C-S-H.

This is reinforced by Holmes and Wingate [22] who indicate the primary active clay components within natural hydraulic limes, are soluble silica dioxide (SiO_2), alumina (Al_2O_3) and ferric oxide (Fe_2O_3), of which soluble silica dioxide (SiO_2) is the most active component. The proportion of these materials and the calcination temperature is very important for the respective phase composition of the clinker. They [22] indicate that when a natural hydraulic lime containing high levels of clay constituents is sintered then slaking may be problematic. These materials generally require an additional grinding phase to break down the clinkered material to attain the required particle size. These materials are known as natural cements and are quick setting and have high strengths [22]. They may be considered as the closest relative to Portland cement and include cementitious materials such as serpentine etc.

The calcination temperature of hydraulic lime is vitally important as alteration of the temperature will greatly effect the resulting hydration product. Hughes and Swann [21] indicate that spurrite ($2C_2S.CaCO_3$) is formed at calcination temperatures ranging from 800-1000°C. They state that this occurs due to a direct reaction between the calcium carbonate and silica. In addition at temperatures between 1000-1200°C, gehlenite (C_2AS), tetra-calcium aluminoferrite (C_4AF), and calcium aluminates (CA) are formed.

Hughes and Swann [21] indicate that the di and tri-calcium silicate phases (C_2S and C_3S respectively) are mainly responsible for giving the set in OPC. However, it is noted that 3 forms of di-calcium silicate have been discovered, namely alpha, beta and gamma. In addition they [21] indicate the primary complex calcium compounds, which include mono-calcium silicate (CS), di-calcium silicates (C_2S), calcium aluminates (CA) and di-calcium ferrite (C_2AF). From the information above it would not be unrealistic to assume that hydraulic limes fired at high temperatures would tend to act in a similar manner to Portland cement rather than limes.

Calcium silicate reactions may be conferred via natural and artificial pozzolans. The reactivity of these pozzolans varies greatly depending upon the quantity, fineness, and reactivity of the silica present. In addition the purity of the lime must also be considered. It is interesting that no reaction between lime and ordinary sand takes place. Generally, pozzolans adopted for use upon historic buildings and more specifically, ancient mortars are of the soft-fired brick or tile variety.

Hughes and Swann [21] discuss the effects of the presence of gypsum within a limestone deposit. When this material is calcined, anhydrite ($CaSO_4$) forms. However, they [21] still attribute the primary setting characteristics of hydraulic limes containing anhydrite, to those predominant reactive silicates. Comparing Portland cement and hydraulic lime, they emphasise that Portland cement forms tri-calcium silicates, achieved by higher calcination temperatures (1300°C) rather than those associated with hydraulic lime calcination (750°C). However, the set in C_3S is achieved via similar mechanisms to C_2S, albeit much faster.

Reinforcing this belief Eckels [15] has produced a table showing the relationship between strength and time for C_2S and C_3S. It is clear to see that C_3S attains over 50% of its total strength within the first 7 days after hydration. This correlates with work

undertaken by Taylor [17] in which he indicates that approximately 70% of C_3S has reacted at 28 days and almost 100% had reacted at the 1 year stage, with the consequent products being calcium hydroxide and amorphous C-S-H. Whereas the β-C_2S had a much slower reactivity and generated much smaller quantities of calcium hydroxide with 30% being reacted at 28 days and 90% in 1 year. Although C_3S and β-C_2S are activated at different rates Taylor emphasised that in terms of general hydration the two acted in a similar manner.

Table 2: The hardening of both belite (C_2S) and alite (C_3S), determined by strength development (Kg/cm^2) of pure compounds [15]

-	*7 days*	*28 days*	*180 days*	*365 days*
C_3S	322	466	512	584
β-C_2S	24	42	194	325

Hughes and Swann [21] indicate that $Ca(OH)_2$ is present in hydraulic limes, both at slaking and also from the hydration of the C_2S. However, water must be present in sufficient quantities to ensure full hydration of the C_2S. The $Ca(OH)_2$ reacts with the carbon dioxide from the atmosphere to initiate the set, however, this process is slow. Hughes and Swann [21] believe that the compressive strength of an eminently hydraulic lime increases by a factor of 3, within a period from 45 days and 365 days. This is very different from the hydration of Portland cement in which strength gain is predominantly seen within the first 28 days, with a subsequent small increase in the strength after that period.

Calcium hydroxide cannot be underestimated in the setting process of hydraulic limes; as it is this compound which initiates a hydraulic / pozzolanic effect upon the reactive silicates and aluminates. It has been proposed by Hughes and Swann [21] that the particle size of the silicates will affect the speed of the reaction. However, it must be emphasised that this is with respect to specific pozzolans manufactured from soft-fired clay bricks. In addition they [21] believe that the pozzolanic additive would also affect the rate of carbonation due to differing porosities and densities of the cementitious material. Therefore, carbon dioxide diffusion would be greatly enhanced in those materials with higher porosities.

The mechanisms of carbonation in lime-based materials have obvious effects upon the durability and binding properties of the aforementioned systems. The implications of

carbonation have been assessed by Radonjic et al [20]. The reactions are believed to occur within a time frame that may range from hours (or even less) through to many hundreds of years. However, Radonjic et al believes that generally the carbonation process must be viewed as a long-term process.

Radonjic et als' tests were applied to a range of samples including lime pastes (of varying pH) and hydraulic limes with a range of hydraulicities. Important primary factors to be considered were the 'CO_2 / relative humidity (RH) ratio' [20] and the duration which in this case was 28 days. They believe that the RH and temperature has an effect upon the conversion of portlandite to $CaCO_3$. However, it was emphasised that carbonation and general curing conditions had traditionally been based upon empiricism.

The set propagation of lime has been defined by Radonjic et al as its' 'carbonation reaction', continuing 'where portlandite [$Ca(OH)_2$] reacts in air due to contact with carbon dioxide in the atmosphere, causing transformation into calcite ($CaCO_3$), consequently producing hardening of the lime paste binder' [20]. It was also emphasised that although the NHLs have lower strengths than O.P.C.s they do impart higher porosities and lower flexural strength which are essential within the conservative repair of historic buildings.

Radonjic et al's work on carbonation used weight gain, in-situ observation via ESEM and chemical changes via X-ray photoelectron spectroscopy (XPS). The parameters for the assessment of carbonation kinetics are influenced by the following: solid / water ratio, CO_2 concentration, relative humidity and temperature.When they considered the C-S-H forming products, it was evident that the most important set characteristic in lime was not solely derived by the aforementioned but by carbonation, chemically '$Ca(OH)_2$ + CO_2 → $CaCO_3$, calcium hydroxide → mineral calcite' [20].

Radonjics' ESEM work used NHL pastes which were only partially hydrated. The samples were exposed to changing cycles of CO_2 and H_2O vapour. The samples exhibited 'rapid crystal growth of elongated crystal phases aggregated into radiating features.' [20] Radonjic indicates that these reactions where generally seen at the edge of the sample and attributes this to 'dissolution, evaporation, saturation and precipitation reactions.' [20]. It was interesting to note that the areas between the elongated crystal

phases were 'filled with sub-crystalline particles' which Radonjic associates with areas of 'higher water condensation.' When an increase in the concentration of water vapour within the ESEM chamber was exhibited, elongated crystal phases showed a noticeable densening in their network. Radonjic et al importantly indicates that water is linked to the 'stability of the highly hydrated gel-like phase, underlying and embedding most of the portlandite crystals' [20]. It was interesting to note that the calcium silicate and aluminate formations associated with the NHL paste appeared rich in potassium.

When Radonjic et al further studied the NHL samples after approximately 48 hours, it was evident that the crystalline phase had formed with a morphology resembling aragonite, with short leaves radiating in a rosette type texture' [20]. Radonjic also indicates that 'large stacks of portlandite were observed, with bimodal crystal orientation observed. That is to say 'plates parallel to the carbonate growth and others perpendicular to underlying carbonate phases' [20]. These crystalline formations are somewhat odd and can best be explained by the altered / variable dissolution rates and precipitation rates. In addition Radjonic et al believes that 'space availability for crystal growth was present whilst in the ESEM, hence different growth orientation occurred with the 2 mineral phases. Some of the phases formed initially were not stable under CO_2 / water exposure conditions, and as a result of their dissolution or alteration in the presence of new mobile species, a second generation of portlandite was produced [20].

The ESEM tests upon CL (non-hydraulic lime, in the form of a dry hydrate) were interesting. Radonjic et al exposed a small quantity of CL powder to water vapour and CO_2 cycles and observed the hydration in the ESEM. They explained that within minutes of being exposed, the 'formation of cubic crystals were observed' [20] and that 'portlandite crystals were forming a network of intersecting plates sometimes aggregated in radiating rosette' [20] formations. After 120 minutes and with an alteration in the quantity of CO_2 and water vapour, the presence of stacks of portlandite had appeared to form.

Radonjic et al had expected nucleation of the lime samples in such a rich CO_2 environment. The transformation of portlandite plates under the moist CO_2 environment was exhibited, with what they called 'preferential re-organisation of species in which Ca-rich zones acted as centres for CO_2 incorporation' [20]. Radonjic et al continued to

emphasise that although this occurred most of the sample was 'covered with radiating rosettes of carbonates inter-dispersed with portlandite stacks' [20].

2.4.3 Hydrates relating to hydraulic lime and OPC

2.4.3.1 Calcium Hydroxide (CH) - Portlandite [$Ca(OH)_2$]

The calcium hydroxide content of a cement or hydraulic lime is essential for hydraulic activity, leading to the propagation of a primary framework upon which C-S-H and other hydraulic components can form.

The atomic structure of CH is octahedrally based with oxygen atoms tetrahedrally co-ordinated and weak inter-layer forces being exhibited. Taylor [17] emphasises that CH has a unit cell that is hexagonal and also has good cleavage (0001 cleavage) following, $\alpha = 0.359nm$, $c = 0.49nm$. The stacking of the unit cell occurs leading to larger crystal development, however, faults in this stacking arrangement may occur with alteration of the structure being noted.

Figure 4: Structure of single layer of $Ca(OH)_2$ [17]

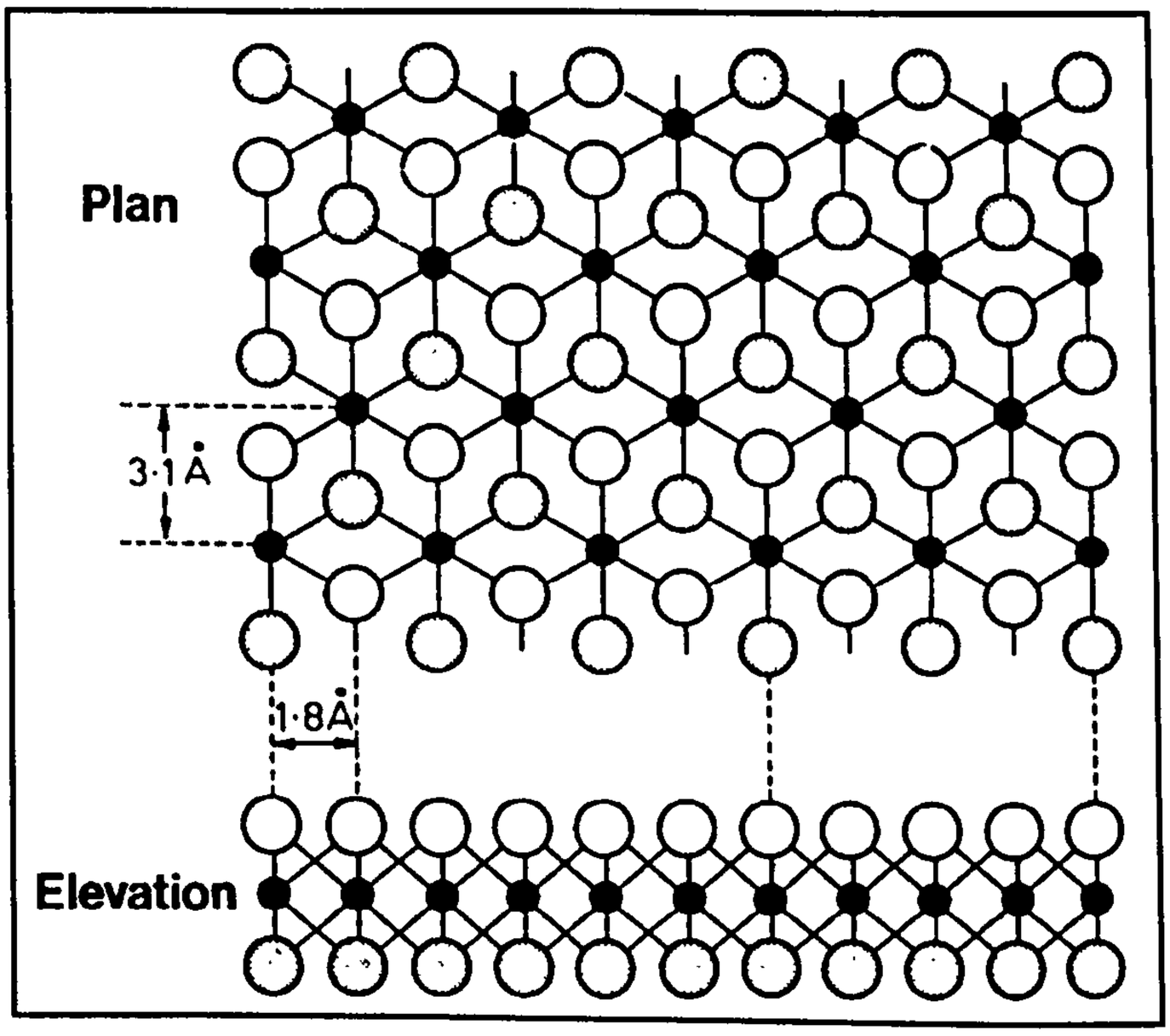

In its naturally occurring form CH is known as Portlandite [17]. The portlandite crystals form hexagonal plates, however, when they are subjected to further hydration they become somewhat 'massive and of indeterminate shape' [17].

The insolubility of calcium hydroxide decreases with rising temperatures and the size of the crystals can range from tens of a nano-metre thick [17] through to several millimetres in thickness (when raising the temperature in a saturated solution).

The concentration of $Ca(OH)_2$ within certain hydraulic limes may be seen in table 3.

Table 3: The $Ca(OH)_2$ concentration in common hydraulic limes (Author after Hughes) [21]

Natural Hydraulic lime type	$Ca(OH)_2$ %
NHL 2	43
NHL 3.5	28
NHL 5	23
Jura-Kalk	2

Odler emphasises that calcium hydroxide is essential for hydration. He believes that C_3S formation is always accompanied by the formation of $Ca(OH)_2$. The degree of formation will vary depending upon the level of saturation and or, dilution of CaO / SiO_2 molar ratio. For example Odler states that in *'highly diluted suspensions the CaO tending to $Ca(OH)_2$ formation will have a propensity to leave the calcium hydroxide dissolved in the liquid phase'* [5].

Odler [5] reinforces work by Taylor believing that when the calcium hydroxide does precipitate then crystals called *'Portlandite'* will form. Portlandite crystals are hexagonal in structure and consist of octahedrally co-ordinated calcium ion layers and tetrahedrally co-ordinated oxygen layers with hydrogen bound to oxygen. These may be up to several tenths of a micrometre in diameter, and will distribute evenly within the hardened paste. The degree of formation may be determined by titration and differential thermal analysis (DTA).

2.4.3.2 Calcium Silicate Hydrates (C-S-H)

Taylor [17] indicates that C-S-H is a generic name for any amorphous or poorly crystalline calcium silicate hydrate, emphasising that C_3S and β-C_2S are particular varieties of the aforementioned seen in Portland cement.

Odler [5] believes that C-S-H may be described as an amorphous calcium silicate hydrate product with the general formula, $CaO_x.SiO_2.H_2O_y$. Where x and y may vary widely. The complexity of C-S-H cannot be underestimated with many forms of

calcium silicate and respective polymorphs existing, under differing conditions of cement and lime manufacture.

The dashes adopted in C-S-H indicate that no particular composition is implied and are necessary because CSH in cement nomenclature specifically denotes $CaO{\cdot}SiO_2{\cdot}H_2O$. The term C-S-H gel is sometimes used to distinguish the material formed in cement, C_3S or β-C_2S pastes from other varieties of C-S-H

The complexity of the interaction of CaO-Si is best expressed visually in the form of a binary phase diagram. This may be seen below in figure 5 indicating the relevant phase transitions at varying temperatures.

Figure 5: Binary phase system CaO-SiO_2 (Author after Taylor) [17]

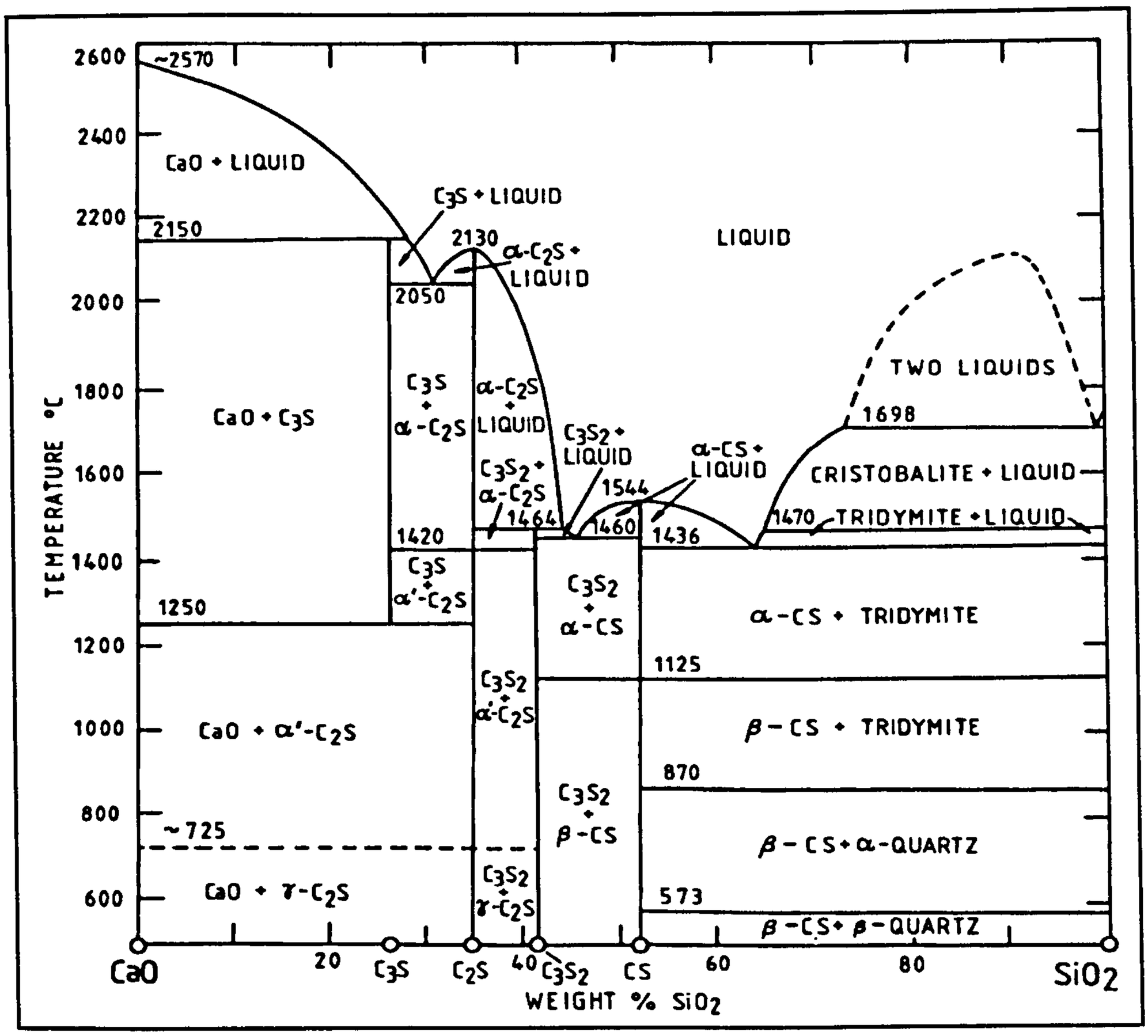

It can be seen that phase transformation of primary hydraulic components occur at different temperatures and or at altered compositions. Phase diagrams such as this can

give a good indication of the expected hydrated forms of the material and are commonly used in cement chemistry and technology.

Taylor emphasises that many crystalline calcium silicate hydrates are known, however, most of these do not occur under natural conditions, indicating that 'various types of semi-crystalline calcium silicate hydrate are intermediate in structure between these compounds' [17].

The fundamental difference between the C-S-H types are the layer thickness (nm), for example tobermorite has a thickness of 1.4nm and jennite 1.05nm. This may be seen in figure 6.

Figure 6: Single layers of tobermorite (*bc*- and *ac*- projections) and jenite *(ac*-projection)

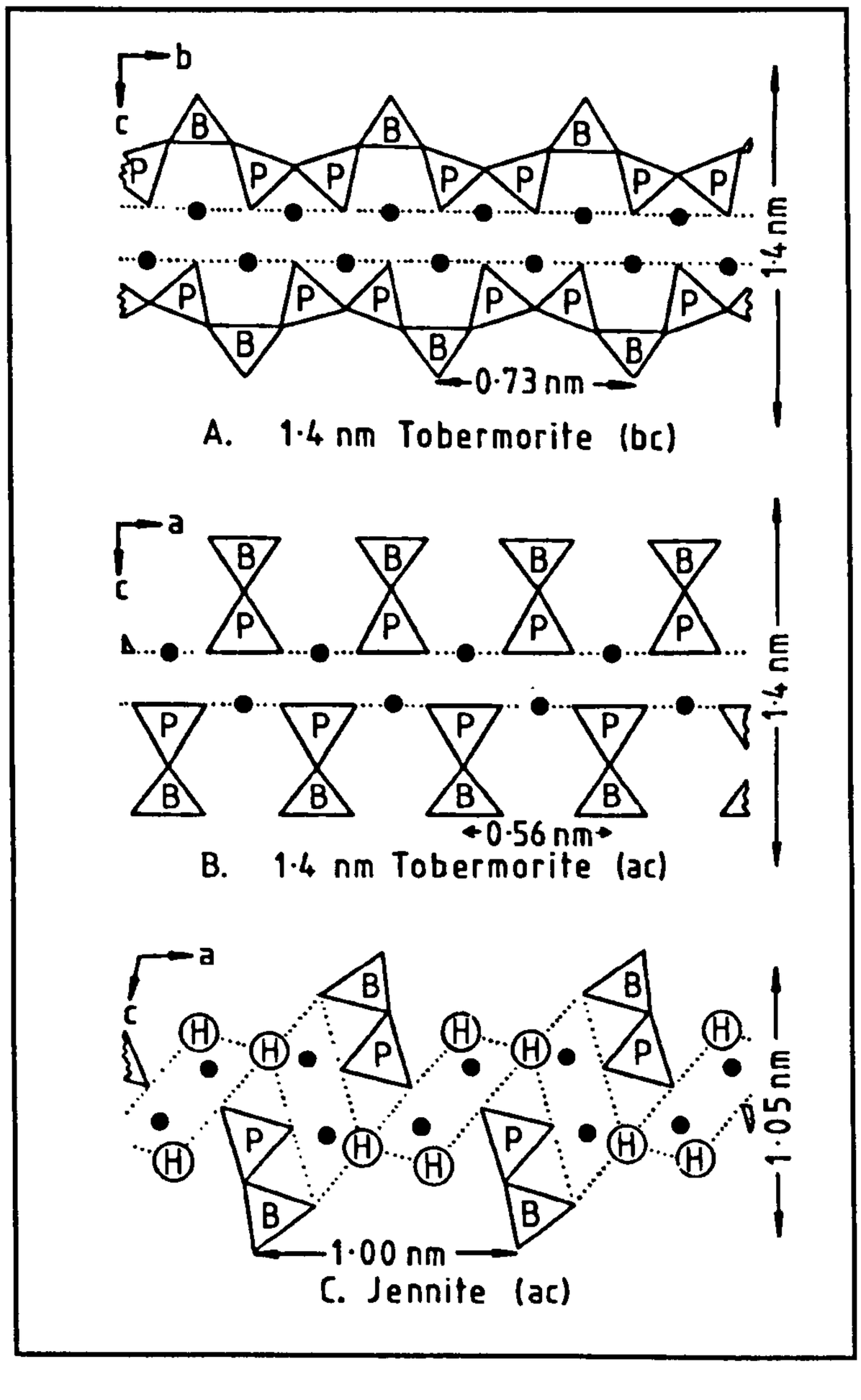

Odler [5] explains that jenite and tobermorite, primarily form by linear SiO_4 tetrahedra chains. These are known as *'Dreierkette'* with an empirical formula of Si_3O_9. Tobermorite formation develops in layers with a basic formula of CaO_2, which shares oxygen atoms with SiO_4 tetrahedra. These form at the sides of the CaO_2 to envelop it, and hence-with it becomes a paired tetrahedra.

C-S-H acts as an umbrella to encapsulate many varying forms of hydration product. OPC has different C-S-H forms when compared with hydraulic lime and this may be due to many factors including, composition, calcination and manufacture of the materials. The two most important forms of C-S-H in OPC and hydraulic limes are C_3S and β-C_2S respectively. Although C_3S is not exhibited in hydraulic lime it is discussed in an attempt to explain the differences in performance of the materials.

The initial hydration of C_3S and β-C_2S with its subsequent micro-structural development has been explained by Taylor [17], believing that differences occur between the hydration of the aforementioned. Both C_3S and β-C_2S have variation in calcium hydroxide formation and distribution into the water filled regions, when assessed at the same time frame post initial wetting. The C_3S exhibits much more growth than the C_2S. This $Ca(OH)_2$ growth occurs from relatively few centres with crystals grouping in isolated masses (1/10 of micrometer).

The anhydrous cement particles / grains then start to form a gel layer which obviously begins at the grain / water interface, however it spreads to and consumes the original water filled space. Taylor believes that this gel layer was separable into what he called a 'inner product' and 'outer product'. The inner product being that gel type formation which appeared to be in more or less direct contact with the anhydrous cement particle and the outer product' was those C-S-H forms which where a result of the gel that had developed in the water filled region. Taylor [17] described the inner product as 'massive and seemingly almost structureless', whereas the outer product appeared to 'form columns or fibres radiating from the anhydrous grains'.

Four morphological varieties of C-S-H gel and pastes have been noted by Taylor [17], namely; Type I through to type IV. Type I is related with early stage hydration and is associated with fibrous material, generally 2μm in length. Type II also relates to early stage hydration however, honeycomb or reticular networks are predominant rather that

the type I C-S-H morphological gel products aforementioned. Type III is associated with longer-term hydration products which Taylor describes as 'tightly packed equant grains up to 300nm'. Type IV is associated with featureless and massive forms that were the inner product. These may be seen in plate 8.

Plate 8: C-S-H formation (author after Mindess) [18]

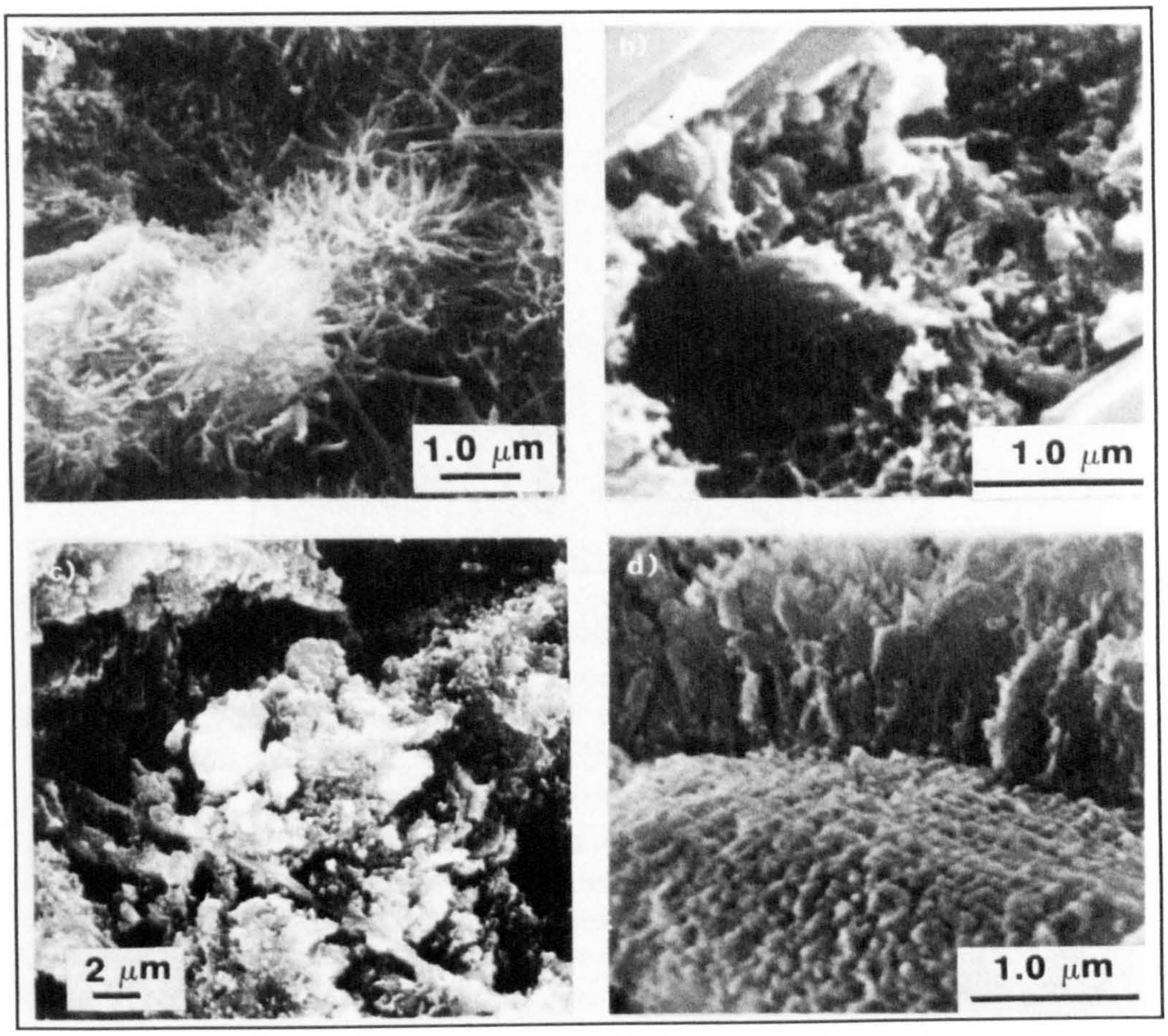

Taylor discusses work that was initially undertaken by Jennings et al [17] believing that in C_3S pastes, 3 stages of hydration occurred, namely, early, middle and late. The early stage products formed at approximately 4 hours, the middle stage formed at approximately 4-24 hours and finally the late stage forming post 24 hours. Taylor indicates that other research upon early hydration of C_3S was undertaken by Fujii et al [17] indicating that several surface forms exist consisting of 'foils, flakes and honeycombs' that tend to exfoliate from the C_3S particle surface.

The complexity of the hydration products are further increased when assessing the honeycomb type of C-S-H. Taylor indicates that at this stage the honeycomb may dehydrate and collapse leaving a crumpled or rolled up type of product that forms a fibre. This has also been alternatively called 'type E' C-S-H.

Taylor believes that the hydration of C_2S appears to be similar to that of C_3S, however the rate of reaction tends to be slower and generally forms at the grain boundaries and exsolution lamallae [17].

Taylor [17] discussed works by Menetrier et al in which he indicates that at early stage hydration the surface of the C_3S particle is attacked in an unevenly distributed form, with the first product seen being minute particles of calcium hydroxide.

The formation of C-S-H and $Ca(OH)_2$ is rather rapid in the middle stage of hydration with type I hydration products developing. In the latter hydration stage C-S-H formation following type III and IV with the addition of $Ca(OH)_2$ was noted. When these products where assessed via thin section, type III were shown to be of interlocked and interleaved thin foils and type IV was of a featureless mass even at 100nm, with a fine pore structure being exhibited.

2.4.3.3 Di-Calcium Silicate - Belite (C_2S)

The full chemical formula for di-calcium silicate is $2CaO.SiO_2$ [5] abbreviated to C_2S. β-C_2S is a very important modification of C_2S as it is a commonly occurring constituent within Portland cement and hydraulic lime. Odler [5] indicates that C_2S is a mixture of CaO and SiO_2 (calcium oxide and silica respectively), however, doping agents may also be present. It is interesting to note that the fineness and therefore, the level of grinding of C_2S and C_3S will accelerate the hydration reaction, having a great effect upon the temperature of the hydration reaction, and the water / solid ratio. The importance of C_2S cannot be over emphasised within the context of C-S-H formation, with β-C_2S never attaining the same high strength associated with C_3S C-S-H formation. β-C_2S has a slow induction time when compared with C_3S. Odler [5] discusses the synthetic form of β-C_2S, emphasising that it may be generated with $CaO{\cdot}SiO_2$ attaining increased reactivity, when compared with naturally occurring C_2S.

Odler [5] continues the discussion of polymorphism, believing that αC_2S is not well understood, when placed into context with other polymorph knowledge and that γ-C_2S only exhibits low hydraulic reactivity at ambient temperatures.

Jawed, Skalny and Young [18] indicate that the study of C_2S has not received the same attention as C_3S and that this omission requires rectification. However, for all the

deficiencies in research data, he believes that a great deal of information may be derived from assessing C_3S hydration.

Jawed, Skalny and Young [18] indicate that the fundamental difference between the hydration of C_2S and C_3S is the level of C-S-H formed and the rate of the hydration reaction. The hydration of C_2S occurs at a rate of approximately $1/20^{th}$ of that of C_3S. Upon initial hydration the grain boundaries of the C_2S particles show signs of non-uniform etching with the subsequent precipitation of C-S-H occurring very slowly. The heat of hydration is low in comparison with C_3S and the supersaturation of $Ca(OH)_2$ is not seen. The growth of large $Ca(OH)_2$ crystals do start to form even with a reduction in the Ca^{2+} concentration within the solution.

The continuance of hydration is believed to occur especially in C_2S, and will develop until space cannot allow further hydration, or exhaustion of the clinker grain.

Generally the C-S-H products derived from β-C_2S are similar to those associated with C_3S, however, certain differences are explained by Jawed, Skalny and Young. These include:

- The hydrated shell that forms from the anhydrous C_2S core may separate when the product shrinks [18].

- The late phases of C-S-H morphology in β-C_2S are variable when compared with the same age product in C_3S. This is attributed to different stabiliizers that eventually lead to alternative type III and IV morphology [18].

Jawed, Skalny and Young have emphasised that in all forms of C_2S whether, α, β or γ have different degrees of impurities that are present and lead to an alteration in the stability and or reactivity of the material. This has been attributed to the 'differences in ionicity' [18] of the stabilizers and crystal imperfections.

As aforementioned the hydration of C_2S is similar to C_3S although, the timing of events may differ significantly. It is believed by Jawed, Skalny and Young that nucleation and growth of $Ca(OH)_2$ in C_2S is not necessarily as important as in C_3S, but, he does

indicate that it is of utmost importance to have a 'calcium sink' [18] to allow continued hydration to occur.

Odler [5] reinforces both Taylor [17] and Jawed, Skalny and Young's [18] beliefs, indicating that the hydration of β-C_2S is similar to that of C_3S in that it is associated with the release of calcium and silicate ions into the liquid phase. Ca^{2+} increase in concentration until the saturation point has been reached (generally after a few hours). Hence, $Ca(OH)_2$ concentration / saturation is reached and silicate ion concentration decreases. Odler [5] indicates that 2 exothermic reactions are associated with C_2S, however, formation of the second of these is hardly noticeable. The mechanism of hydration of C_2S is similar to C_3S, however, it is much slower. For example it has similar hydration phases, similar oxygen and silica constituents, which combine to form C-S-H through precipitation. The post-hydration material is similar to C_3S, especially when looking at the free lime concentration [5]. C_2S also has longer average chain lengths than C_3S, enabling Odler [5] to hypothesise that the extended chain length is the reason for the continuation of hydration in the material. The stoichiometry of C_2S in C-S-H formation includes: Si-O-Ca, Si-O-Si, Ca-OH and possibly Si-OH. In addition it is important to note that the $Ca(OH)_2$ levels within C_2S are significantly smaller than those seen in C_3S. However, this is not to say that the same level of hydration is not occurring.

Taylor has shown that 5 polymorphs of belite (C_2S) exist at ordinary pressures, namely, α, α'_H, α'_L, β and finally, γ. These may be seen in figure 7.

Figure 7: Polymorphs of Belite C_2S (author after Taylor) [17]

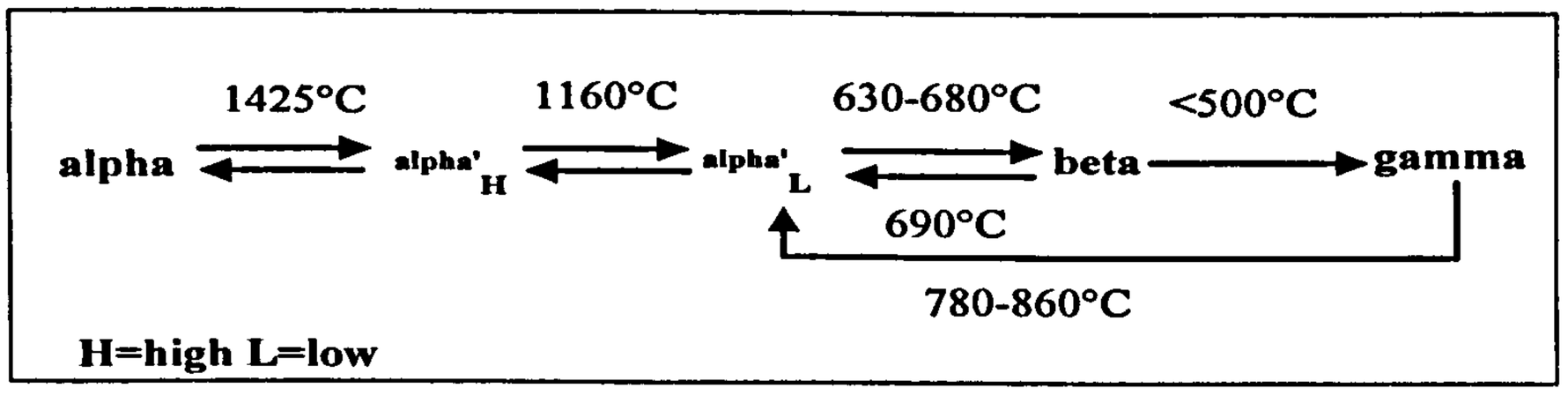

All of the above are formed from Ca^{2+} and SiO_4^{4-} ions with Taylor indicating that the α series and β have a similar arrangement with γ being different. Taylor has shown that the polymorphs that are formed at higher temperatures are difficult to preserve upon cooling. Generally their stability may only be achieved at room temperature by

stabilization via foreign ions. The γ form of C_2S is less dense than the other forms of C_2S and when the sintered γ form transfers to β it has a tendency to crack upon cooling. This tends to increase the volume of the crystal and cause fragmentation of the crystal, this is known as dusting. The presence of foreign ions within the C_2S generally prevents the transformation of the γ form occurring.

The unit cell of the α series and the β polymorphs are closely related in terms of unit cell. However, Taylor believes that βC_2S is derived from αC_2S with a decrease in symmetry that arises from 'orientation changes in the SiO_4^{4-} tetrahedra and small movements of Ca^{2+} ions'. It is interesting to see that the quantity of stabilizing agent required for C_2S reduces from α to β. This is also true for C_3S and its polymorphs. Taylor [17] believes that the transformation and stabilization of these crystallographic orientation changes is relative to the starting material rather than the traditional belief that total reorganisation of the structure occurs.

Figure 8: Crystal structures of C_2S polymorphs [17]

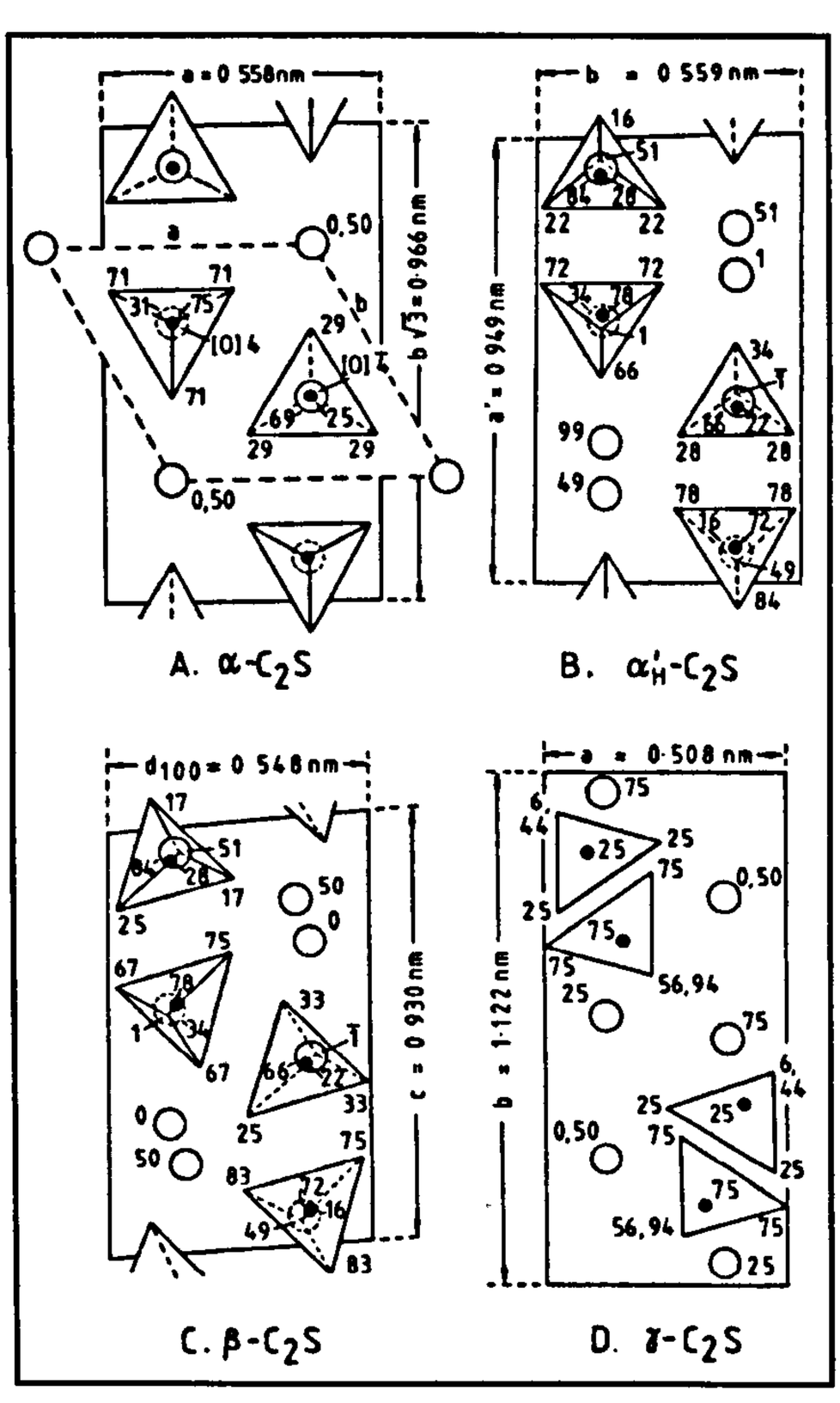

Taylor has indicated that belite grains in OPC clinkers have a complex striated structure. Two types of C_2S clinker grain striations exist namely, I and II. Both are formed via alternating the transition temperatures for crystallisation from the liquid or via slow cooling from αC_2S.

In cement manufacture the majority of belite is in the form of βC_2S with rounded particles with a mean size of approximately 20-40μm. However, the presence of αC_2S and $\alpha' C_2S$ cannot be disregarded from cement anhydrous compositional analysis.

Taylor [17] discusses work of synthetic belite formation undertaken by Yamaguchi et al believing that grain boundaries and material exsolved between the lamellae tended to generate amorphous or crystalline phases that are far removed from C_2S and were better defined as C_2AS, C_3A or C_3S_2.

The composition of belite clinker has been assessed by Taylor in which he found that pure forms of C_2S are 34.9% SiO_2 and 65.1% CaO. In impure belites it is more common to find between 4-6% oxide impurity that are generally composed of iron and aluminium. He continues to indicate that naturally occurring βC_2S is known as larnite.

2.4.3.3.1 High reactivity belite cements

Lawrence, C. D. [5] in his work on the production of low energy alternative cements has indicated that modern construction cements may be manufactured with low CO_2 emissions. He believes that this will be reflected in the content of CaO within the material. This in turn leads to the formation of a binder consisting primarily of belite ($2CaO{\cdot}SiO_2$) rather than the usual alite ($3CaO{\cdot}SiO_2$) form.

Lawrence [5] indicates that modern OPC is based upon the formation of calcium silicate. These may be produced in high or low emission forms, namely, Alite ($CaO_3{\cdot}SiO_2$) and Belite ($CaO_2{\cdot}SiO_2$) respectively.

The term high lime cement and low lime cements has been used by Lawrence [5] to describe β-C_2S, and C_3S respectively. Traditionally high lime cements yield belites with low reactivity.

Portland Cements with improved reactivities may be achieved by fast cooling of the clinker. This process leads to the formation of smaller alite and belite crystals that exhibit faster strength and growth during hydration. Hence the traditional method of high temperature calcination of alite and belites is believed to generate highly reactive hydraulicity of the material. However, reactivities may be altered by the adoption of various manufacture processes for example, the presence of fluoride will reduce the hydraulic activity, however, this is countered by adding SO_3. When fluorine is introduced into the material it results in high reactivities, although it must be emphasised that this has been associated with a compromise in the strength.

Lawrence [5] indicates that work on belite cements may be classified into 3 primary sections. These include:

- Hydraulic activity of the C_2S phase
- Hydraulic activity of belite rich cements without additional cementive components
- Hydraulic activity of belite rich cements with additional cementive components such as C_4A_3S

Lawrence [5] has indicated that the reactivity of C_2S may be improved via 3 primary processes. These are:

- Rapid quenching of the clinker in order to stabilise a high temperature polymorph
- The introduction of impurity ions during formation at high temperatures. These impurities are generally alkali in nature and are introduced into the crystal structure to attempt to stabilise the high temperature polymorphic form
- The addition of normal Portland cement clinker to the C_2S clinker in order to accelerate the rate of hydration

Lawrence [5] concurs with work undertaken by Taylor [17] in which he believes that 5 polymorphic forms of C_2S exist (see figure 7). These are all variable depending upon the formation temperature and pressure. Lawrence believes that all forms of C_2S are metastable with the exception of the γ-C_2S form.

Lawrence [5] emphasises that in OPC the β-C_2S form is slow to react with water forming cementitious hydrates. However it must be emphasised that the α and α' forms are also hydraulic.

It is believed that the reactivity of the β-C_2S may be increased by 'imparting a stressed condition through thermal shock, or through the formation of small crystallites manufactured using gel techniques or spray drying the material in the preparation of the raw feed' [5].

The lime saturation factor (LSF) is expressed as the ratio of CaO / 2.8 SiO_2 + 1.18 Al_2O_3 + 0.65 Fe_2O_3. This calculation can indicate the presence of free lime. The LSF will affect the compressive strength of the binder but may also affect the reactivity of the cement.

Lawrence continues to indicate that those materials with lime saturation factors of between 80-90% and altered alkali concentrations may lead to the formation of α-belite when being subjected to a quenching process. If this is undertaken upon materials of a low alkali nature then the formation of a new polymorph β^* may be produced. [5] This form of C_2S has higher hydraulic reactivity. He continues to emphasise that the stabilisation of these forms of C_2S has been attempted via the introduction of what Lawrence [5] calls 'impurities ions' into the crystal lattice. However, it must be emphasised that this has only been tentatively explored.

Table 4 indicates the alteration in compressive strength between the polymorphic forms of C_2S.

Table 4: Compressive strength (MPa) of cement paste cubes (water / cement = 0.6) formed from belite-rich clinkers (lime saturation factor II = 70-80%) [author after Lawrence] [5]

Main Belite Phase	Cooling rate (°C/min)	3 days	7 days	28 days	90 days
α	50000	3.1	8.9	20.9	29.6
α'	3000	1.4	2.0	6.7	10.0
β^*	50000	-	2.8	8.2	21.8
β	2.0	2.2	3.3	3.9	8.3
β^* annealed for 2 h at 850°C giving α'	50000	1.4	2.0	2.4	13.5

The activation of belite cements can therefore be achieved by thermal or chemical means. The lime saturation factor is important and is believed by Lawrence [5] to fall between 75-85%. When under these conditions the quenching at temperatures of between 1300-900°C with a cooling rate of at least 800°C / min will lead to thermal activation.

Lawrence [5] believes that the stabilising affect of high strength α belite is caused by quenching. This process allows the introduction of alkalis (or alternative foreign ions) which act as stabilisers. He continues to emphasise that the addition of foreign ions without the quenching process fails to stabilise the polymorphic form of C_2S. When P_2O_5 was adopted as the stabilising agent for α' C_2S its rate of hydration was faster than the β-C_2S form.

The hydraulic reactivity of belite cement has been attributed by Lawrence [5] as the 'calculated strength of the Ca-O ionic bond'. [5] He continues to emphasise that an assessment of the relationship of the crystal structure and hydraulic activity has been proposed. He believes that 'the electric field strength at the site of the Ca^{2+} ions in the crystal lattice determines the hydraulic activity'. [5] He continues to emphasise that early hydration of quenched (in CCl_4) pure C_2S is increased.

This is a marked difference between those forms of C_2S (generally considered as impure) that are extracted from Portland Cement as they have lower reactivities. The rapid cooling of belite may increase the amount of α modification which survives up to 40%. It is believed by Lawrence [5] that this may be attributed due to the α modification being 'sandwiched' within the fine lamellae of disordered β-C_2S.

It is interesting to note that no hydraulic sequence between the polymorph forms exist (i.e. α > α' > β > γ') [5]. However, the hydraulic strength has been associated with the following:

- Burning temperature
- Cooling rate
- Foreign oxide content

Lawrence indicates that both highly reactive and inactive forms of C_2S may be generated for all of the belite modified forms. The rate of cooling of the clinker is attributed to being pivotal in the determination of the activity and strength of belite in those materials with a lime saturation factor of 90% and below.

The cooling of the lime clinkers has been shown by Lawrence [5] to affect the hydraulic reactivity of the material with the low lime clinkers showing higher reactivities and the high lime clinkers exhibiting no real increase in performance.

This is reflected in table 5 which depicts the differences in the cooling rates of clinker with alternative phase compositions of low - lime clinker.

Table 5: An example of the phase composition of low-lime clinker cooled at high and normal rates (author after Lawrence) [5]

Cooling rate (°C / min)	1000	100
Alite	30	24
α'-C_2S	48	7
β-C_2S	0	44
C_3A	10	15
C_4AF	9	6
MgO	3	4
Amorphous glass	0	0

Belite cement used in concrete has been shown by Lawrence [5] to have favourable durability performance characteristics in terms of frost and carbonation resistance, when compared to regular O.P.C. The strength characteristics were also comparable after 4 years. Lawrence indicates that these cements had a lime saturation factor of between 80.5 and 81.7, a silica ratio range of 2.7 and 2.6 and finally, an aluminium ratio in the range of 2.3 and 2.6. He continues with an assessment of the mineralogical components of the aforementioned cement, indicating that the composition followed: alite 27-29%, α'-C_2S 21-30%, β-C_2S 14-36%, C_3A 6-7% and ferrite 16-18%.

Lawrence [5] has shown that high belite clinkers manufactured with lime saturation factors between 69-97 have resistance to freeze / thaw cycles greater than that of regular OPC.

It is extremely interesting to note that Lawrence believes that the primary deficiency in terms of microstructure of the cement is caused by the concentration of the $Ca(OH)_2$

crystals. The amount of $Ca(OH)_2$ generated upon hydration is lessened by the belite cements as opposed to the alite cements formation.

Lawrence [5] continues to indicate that the resistance to frost is decreased by the increase in the $Ca(OH)_2$ crystals. He attributes this to the fact that 'reduced temperatures increase the solubility of $Ca(OH)_2$ and thus cause an increase in the porosity of the microstructure at the surface of the portlandite crystals during freeze / thawing cycles' [5].

Alkali stabilisation and increased reactivity of high temperature forms of C_2S has been assessed by Lawrence [5]. He indicates that the introduction / inclusion of K_2O into the α' form of C_2S leads to stabilisation, and the addition of other chemicals such as barium, magnesium, manganese and boron oxides [5] has lead to the stabilisation of α'_L forms. The hydraulically active α' C_2S may also be successfully stabilised by rapid cooling of the clinker.

The high alkali cements that were quenched in water or air led to higher strengths. The higher the alkali levels in the C_2S oxides were shown by Lawrence to increase the compressive strength of the material. Lawrence [5] continues to indicate that the early strengths and higher late strength of active belites are less than alite rich cements.

The addition of chromium into β-C_2S prevents 'dusting' of the γ modification and in turn led to high early strength. However, Lawrence has emphasised that γ-C_2S is to be considered as non-hydraulic.

Lawrence has discussed the rate of hydration and heat of hydration in the presence of SO_3 and blast furnace slags believing that the 'hydration of belite was significantly retarded by the presence of blast furnace slag. The presence of alite, or normal Portland cement clinker, greatly accelerated the hydration of belite and it was suggested that the presence of $Ca(OH)_2$ is required to ensure a full hydration rate for both blast furnace slags and belite' [5].

Lawrence [5] also discusses the development and formation of aluminous belite in which he emphasises that the primary consideration is avoidance of those hydraulically non-reactive components, namely: C_2AS and CAS_2. Aluminous belite cements have

been produced with continuing strength development up to 3 years, and exhibit good sulphate and freeze / thaw cycle resistance.

This behaviour may have significant implications for understanding the behaviour of hydraulic limes, which are produced by firing at temperatures within the range at which these reactive belites are produced.

2.4.3.4 Tri-Calcium Silicate - Alite (C_3S)

Jawed, Skalny and Young [18] believe that C_3S is the most important component in OPC in terms of early strength and it has therefore been heavily researched. However, he believes that limitations of C_3S studies may occur due to the different preparation of the materials. This will lead to different reactivities of the material and hence different results.

Odler [5] shares Jawed, Skalny and Young's beliefs, that the manipulation of C_3S during preparation is common. This has the effect of either accelerating or retarding the hydration of the C_3S particles. In addition foreign ions may also be used to stabilize the crystalline lattice of the hydrated product. The use of $CaCO_3$ may also increase the rate of C_3S hydration, especially if present in a finely dispersed form. The composition of the liquid phase has been described by Odler, indicating that when the water interacts with the calcium and silicate ions, they rapidly pass into a solution, with Ca^{2+} / SiO_2 with a molar ratio of 3:1, hence, congruent dissolution of C_3S. He explains the hydration of C_3S upon a molecular level, indicating that an initial fast reaction between the water and C_3S starts almost instantaneously with rapid protonolysis [5] of the oxygen at the surface interface of the C_3S. Consequent dissolution of the material is seen. Therefore, O^{-2} ions in C_3S crystalline lattice form a liquid phase, with OH^- ion formation and SiO_4^{-4} ions dissociating, although by very little into H_4SiO_4.

Hence, chemically [5]

$$O^{2-} + H^+ \rightarrow OH^-$$
$$SiO_4^{-4} + nH^+ \rightarrow HnSiO_4^{(4-n)}$$

Odler continues to indicate that the positive Ca^+ ions within the liquid phase out balance the negative OH^- and silicate ions. C_3S dissolution rate is high, actually too high for the

ions to be diffused away from the C_3S and hence, an ion concentration build up occurs. An over saturation occurs in the liquid phase, with C-S-H (calcium silicate hydrate) precipitation at the surface of the C_3S. Dissolution is believed to be incongruent rather than congruent, leading to what Odler describes as a 'SiO_2 rich layer formation at the surface which subsequently adsorbs Ca^{2+} ions dissolved in the liquid phase' [5]. Consequently, an electric double layer is formed at the C_3S surface. Odler emphasises that no one really understands why hydration accelerates and consequently decelerates. However, several theories exist: These include impermeable hydrate layer theory, electrical double layer theory and finally the theories of nucleation of $Ca(OH)_2$ and C-S-H. Those will be discussed later in this chapter.

Jawed, Skalny and Young believe that C_3S hydration into its respective C-S-H is not perfect and therefore the generated product does not follow the classically accurate C-S-H composition, $C_3S_2H_4$. He describes C-S-H as an 'amorphous material of variable composition' [18]. In contrast he believes that calcium hydroxide is crystalline in nature with a fixed composition.

The hydration of C_3S is not yet fully understood, however it is known that the products of hydration form an amorphous calcium silicate hydrate phase. This has a CaO/SiO_2 molar ratio of less than 3.0 called the C-S-H (calcium silicate hydrate) phase, plus calcium hydroxide [$Ca(OH)_2$]. Odler emphasises that when calculating C_3S hydration as a function of time then it is essential to evaluate the specific surface area (Blaine) and the water / cement ratio. This is elaborated upon by Taylor, believing that 'moderate variations in specific surface area have little effect on the length of the induction period, but with finer grinding, may have a greater significance as the acceleratory period increases' [17].

The formation of C-S-H is complex with variable stoichiometry, understanding in this area has been aided by measuring the amount of non reacted C_3S as a function of hydration time. The consumption of C_3S has been graphically represented in figure 9 in which the following phases are expressed: A-B, pre-induction, B-C, induction, C-D, acceleration and finally, D-E, deceleration period. In order of hydration, these are pre-induction, induction, acceleration, and finally the deceleration phase.

Figure 9: Concept of C_3S consumption as a function of time. (Author after Odler) [5]

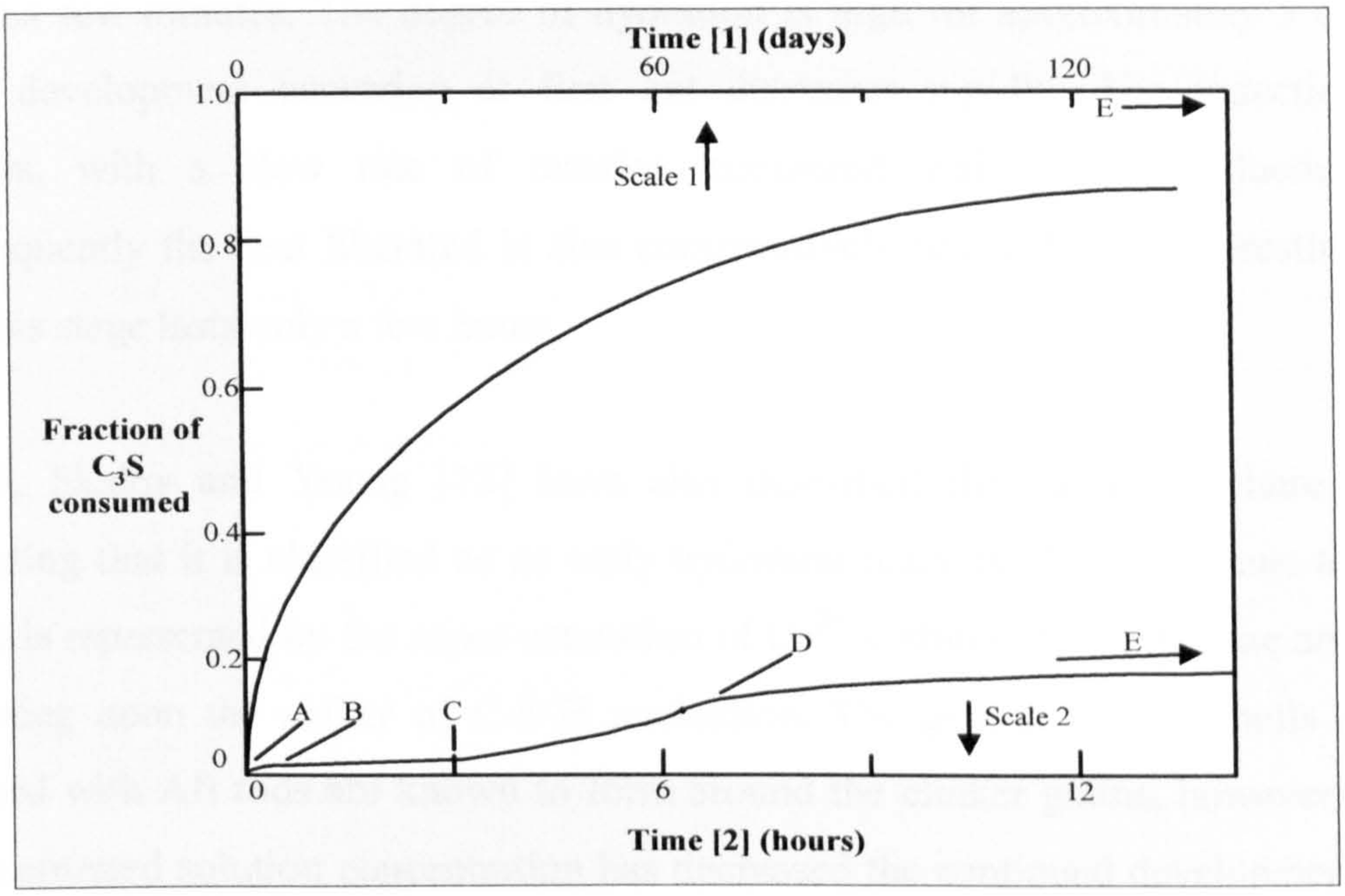

This is reinforced by work undertaken by Taylor [17] in which he also indicates that the consumption of C_3S follows the aforementioned stages. He elaborates this by emphasising that periods A-B correspond with early stage reaction, period C-D, with the middle stage and period E is associated with the later stage. Continuing to indicate the setting of the material occurs within the acceleration stage namely; C-D.

Further explanations of these specific phases require elaboration as they may share similarities to C_2S formation within hydraulic lime. This is a view shared by Taylor, believing that the mechanisms of β-C_2S hydration are closely related to those of C_3S, however, he does indicate that they are at a much slower rate. He also indicates that the products are similar in β-C_2S with the exception of having a lower calcium hydroxide concentration.

Taylor believes that the determination of the heat of hydration for β-C_2S (via conduction calorimetry) may be difficult to ascertain due to lower heat evolution. However, when he initiated tests he found the existence of an induction period that closely related to C_3S. This was reinforced in his assessment of the connectivity of silicate tetrahedra that increased in a similar manner to that seen in C_3S (end of induction period 24h at 50°C).

Upon initial contact with water the anhydrous C_3S particle starts the pre-induction phase. This is associated with the generation of heat of hydration, being observed within the first few minutes. The degree of hydration is high for approximately 5 days, with rapid development occurring at first but decreases rapidly. The induction period follows, with a slow rate of reaction compared with the pre-induction phase. Consequently the heat liberated is also comparatively reduced. It is interesting to note that this stage lasts only a few hours.

Jawed, Skalny and Young [18] have also described the induction phase in OPC, indicating that it is classified as an early hydration reaction. They continue to indicate that it is represented by the super-saturation of Ca^{2+} within the liquid phase and this has a bearing upon the ability of C-S-H nucleation. The growth of thin shells of C-S-H twinned with Aft rods are known to form around the clinker grains, however, until the supersaturated solution concentration has decreased the continued development of C-S-H is postponed. Jawed, Skalny and Young continue to emphasise that 'thin platelets of $Ca(OH)_2$ twinned with C-S-H growth begin to form contacts between the grains and a continuos skeleton of hydration products that develop' [18]. The formation of ettringite (C_3A + Sulphates) also known as Aft, occurs rapidly. If insufficient quantities of sulphates are present the ettringite will dissolve and consequently reacts with the $Al(OH)_4^-$ and in doing so forms monosulphoaluminate hydrates a.k.a. Afm phase.

The acceleration period (a.k.a. post induction phase) follows the induction period with a rapid increase in the hydraulic activity exhibited. A maximum point develops between 5-10 hours post initial wetting with decreasing activity after this point.

Odler indicates that the kinetics of the acceleration phase follow Avrami's equation [5]. This can be seen in equation 1:

Equation 1: Avrami's equation

$$\left[-\ln(1-\alpha)^{1/3}\right] = k_N t$$

Where:

Symbol	Associated with function
α	Degree of hydration
T	Time
${}^{K}N$	Reaction rate constant for a nucleation controlled process

Odler believes that the $Ca(OH)_2$ concentration in the liquid phase attains a maximum at this time, coinciding with the beginning of the second, main heat evolution peak. After this point it declines via precipitation into crystalline calcium hydroxide.

The deceleration phase of OPC is associated with what Jawed, Skalny and Young calls the 'diffusion of various reacting species and deposition of hydration products into the relatively dense pore system' [18].

Odler [5] explains the deceleration phase in which maximum hydration occurs, with the hydration exhibiting a reduction which is quite gradual. However, this does not mean that reaction ceases, as in reality hydration may continue for months after curing, with the non-reactive C_3S being consumed within the cementitious matrix.

Odler indicates that the kinetics of the deceleration phase follow 'Jander's equation' [5] for diffusion-controlled processes. This can be seen below:

Equation 2: Jander's equation

$$\left[1-(1-\alpha)^{1/3}\right]^2 = K_D t$$

Where:

Symbol	Associated with function
K_D	Reaction rate constant for a diffusion controlled process (other variables as before)

Jawed, Skalny and Young [18] reinforce work undertaken by Odler [5], concurring that the formation of the C-S-H products follow a sequence namely, pre-induction, induction, acceleration and deceleration. The pre-induction stage for C_3S is associated with calcium silicates passing into solution when in the presence of water. Jawed,

Skalny and Young [18] believe that silica concentrations are transitory, reaching a maximum of 1.7 mmol litre^{-1} with a decrease that occurs rapidly, however, Ca concentration increases. The rate of decrease of silica entering solution depends upon the water solid ratio.

The Ca concentration has a great effect upon the hydration of C_3S especially within early stage hydration with the Ca/Si ratio decreasing at a slow yet steady rate. This is combined with a thickening of the hydrated material and after approximately 1 minute and the precipitation of globular particles occur upon the surface. The surface of the C_3S particle then becomes progressively damaged by pitting as the dissolution takes place. Jawed, Skalny and Young emphasise that this process is non uniform across the grain surface. At this stage no hydration products are seen except the globular precipitates. Following this, products resembling flake and foil C-S-H morphology are exhibited growing from the surface. These grow quickly at the surface and lead to honey combed type II structures that may be seen in Plate 9.

Plate 9: SEM micrographs of C_3S hydration in early stages of reaction: (a) 30s; (b) 1 min; (c) 5 min; and (d) 30 min. [18]

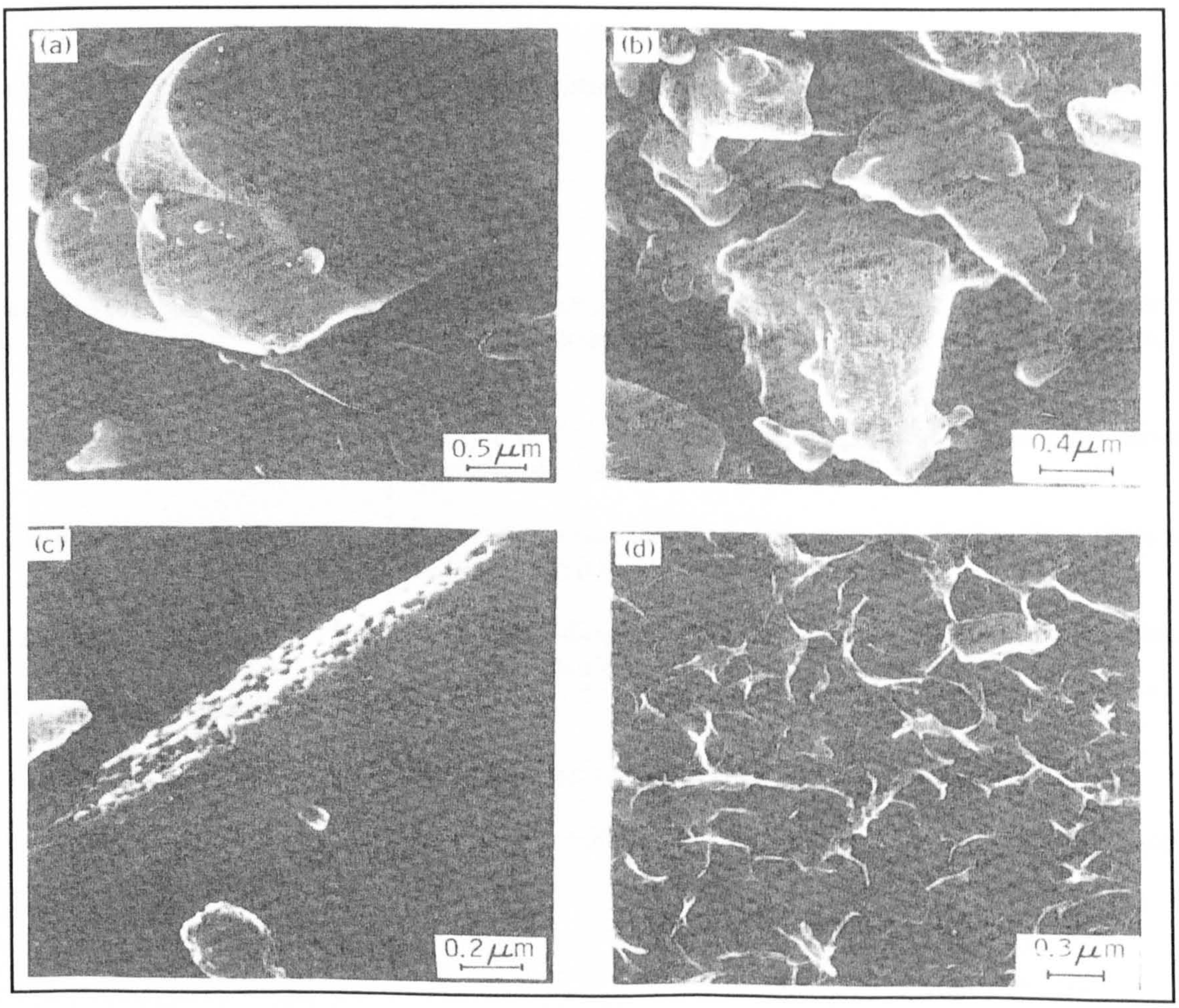

The induction period of C_3S is associated with low heat of hydration and corresponds with stage II in table 6. The concentration of Ca^{2+} and OH^- continue to increase, but Jawed, Skalny and Young [18] believe that this occurs in a non linear manner. He continues to emphasise that a large degree of super saturation of $Ca(OH)_2$ is seen prior to maximum level occurring, with the time taken for saturation depending upon the water / solid ratio, thermal history of the material and the concentration of crystal defects at the surface. A high water / solid ratio will restrict the attainment of super saturation and this will ultimately greatly affect the course of the hydration.

The quantity of hydrated products exhibited at the end of the induction period is only 1-2%, with the crystallisation of $Ca(OH)_2$ also starting. This is associated with new morphological forms of C-S-H being noted; namely types O-I.

Jawed, Skalny and Young [18] discuss the mechanisms of early hydration in C_3S believing that this is best categorised by the onset of initial wetting through to the termination of stage II. The subsets associated with these categories may be seen in table 6, however, it must be emphasised that these mechanisms are far from being fully understood and are only in hypothesis form.

Table 6: Theories for onset and termination of stage II : the induction period (author after Jawed, Skalny and Young)

Hypothesis	Description
A. Onset of Stage II	
Hydrate barrier	Initial dissolution of C_3S. Formation of a 'first' or 'primary' hydrate (C-S-H) which forms a physical diffusion barrier around the grains.
Lattice defects	The rate of C_3S hydration and the length of the induction period depend on the number of lattice defects.
Boundary layer reaction	C_3S dissolves congruently and the rate of hydration slows down as the $[Ca^{2+}]$ and $[OH^-]$ in solution increase.
Electrical double layer	Incongruent dissolution of C_3S forms a silica-rich layer which creates an electrical double layer at the surface.
B. Termination of stage II	
Nucleation of C-S-H	Nucleation and growth of C-S-H now become rate-controlling.
Nucleation of $Ca(OH)_2$	Nucleation and growth of $Ca(OH)_2$ crystals are necessary conditions.

It is believed that the initiation of the induction period may be tentatively explained by diffusion control, however, this theory is based upon indirect evidence only and critics have indicated that water attack seems to be non uniform over the surface and observable hydration products take some time to develop.

An alternative theory is that of the 'reaction at the boundary layer of the C_3S particle. However, this theory is believed to be directly linked with C_3S lattice defects that effects the rate of hydration. This is due to the lattice defect and the composition of the pH of the solution in contact with it. This theoretically effects the thermodynamic equilibria and ultimately effects the surface atomic layers but not the underlying atomic arrangements below. This effects the rate of dissolution and is dependent upon the Ca^{2+} and OH^- in the solution.

The hydration phase previously discussed reflect in the formation of varying C-S-H morphology (based upon both TEM and SEM) that may be seen in table 7.

Table 7: Classification of C-S-H morphologies (author after Jawed, Skalny and Young) [18]

-	Early products	Middle products		Late products	
TEM Designation Morphology	E	O Amorphous	I(I') Needles radiating from grains	3 Crumpled foils	4 Dense gel
SEM					
Designation Morphology	II Reticulated	I Needles radiating from grains		III Indefinite	IV Spherical agglomerates
Probable degree of silicate polymerisation	Monomeric? + Dimeric	Dimeric		Dimeric (+ Polymeric?)	Polymeric (+ Dimeric)

The hypothesised theories of C_3S hydration have also been discussed by Odler [5] who believes that an impermeable hydrate layer may develop. As the disolving C_3S particle begins to precipitate it causes a protective barrier which reduces the ability of the water to migrate to the non-reacted surface. This phenomenon prevents Ca^{2+}, OH^- and silicate ions entering the liquid phase and consequently reduces the reactivity of the hydration process. The initial reaction slows down after a certain period. However, as time passes the formed C-S-H becomes permeable and makes way for rapid hydration once again.

Odler indicates that the C-S-H layer is not yet fully understood. The ability of C-S-H to become permeable may be attributed to phase transformation, morphology and / or ageing.

Odler [5] indicates that the simplest explanation for this phenomenon may be derived from the idea that a membrane develops around the C_3S particle. This takes time to deteriorate and is associated with osmotic pressure generation between the liquid and the non-reacted C_3S. However, Odler also indicates that another theory known as 'imbibition of water' [5] and may be responsible for the breakdown in the C-S-H.

Table 8: Theories on the mechanisms of C_3S hydration (author after Odler) [5]

Mechanism	Impermeable hydrate layer theory	Electrical double-layer theory	Nucleation of CH theory	Nucleation of CSH theory
Pre-induction period		First stage C-S-H formed		
Beginning of induction period	First-stage production acts as diffusion barrier	Electrical double layer forms and impedes passage of ions	Super-saturation of liquid phase with respect to CH stops further rapid dissolution of C_3S	
Changes during induction period	Phase transformation or ageing of C-S-H layer	Osmotic pressure phenomena across the first-stage product layer	Gradual weakening of double layer	Slow nucleation of second stage C-S-H
End of induction period		Breakdown of C-S-H layer due to osmotic pressure and/or imbibition	Breakdown of double layer	Slow nucleation of CH	Nuclei of second stage C-S-H reach critical size
Acceleratory period		Accelerated dissolution of C_3S, growth of second stage C-S-H and CH		CH nuclei reach critical size

Odler [5] believes that in addition to the impermeable layer theory an alternative explanation has also been put forward known as the electrical double layer theory. It is assumed that a SiO_2 rich surface layer absorbs Ca^{2+} ions, and this leads Odler to believe that initial incongruent C_3S dissolution occurs. This tends to create asymmetrical dissolution, which in-turn, leads to concentrated hydration zones. This phenomenon causes the formation of an electric double layer which prevents the flow of ions to the solution and is consequently responsible for the dormant period associated with C_3S hydration. However, this eventually breaks down and allows ion flow to continue, with reactivation of the hydration process.

Figure 10: Electrical double layer theory in C_3S [18]

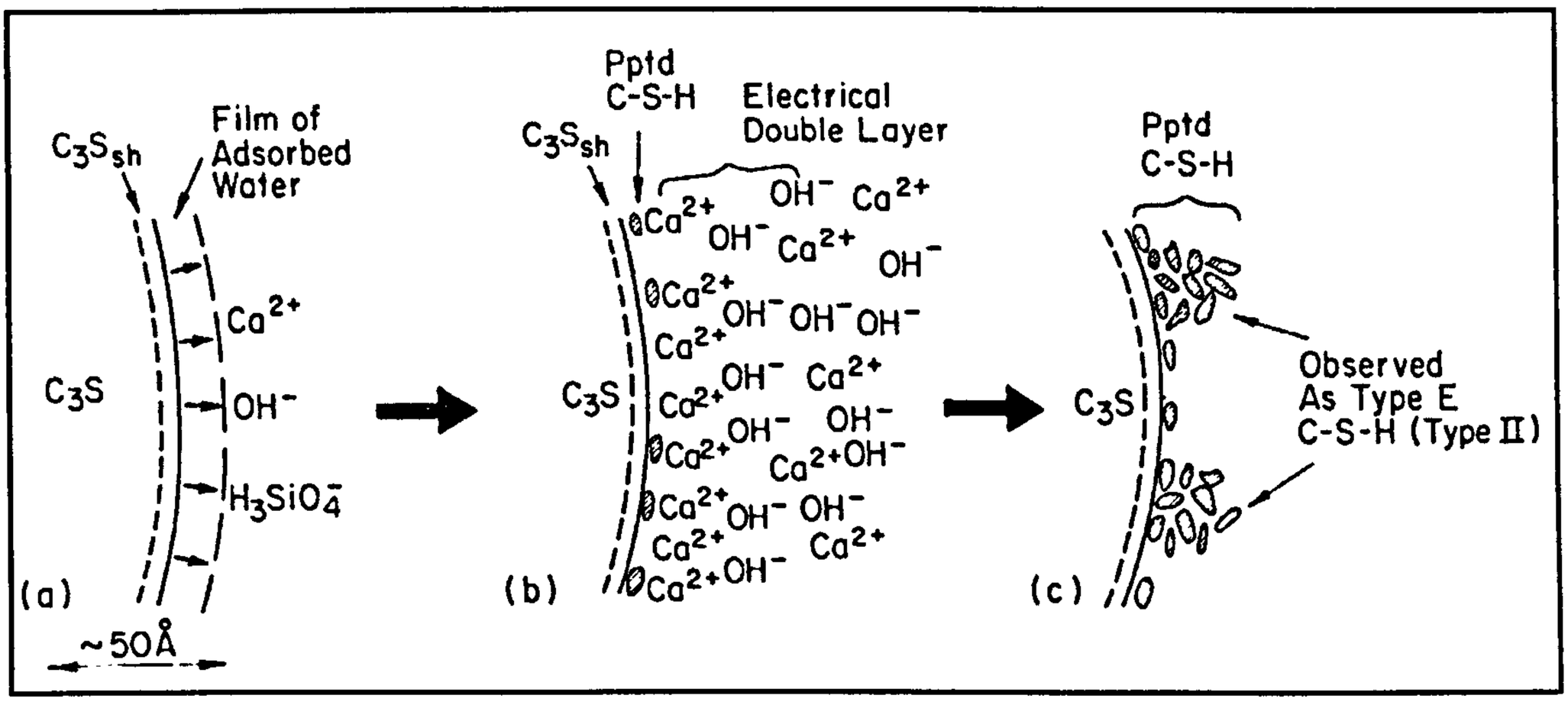

Odler discusses nucleation theory of $Ca(OH)_2$ and C-S-H believing that CaO/SiO_2 ratio within the C-S-H phase is always lower than C_3S (3:1). Therefore, C_3S hydration is correlated with the liberation of $Ca(OH)_2$ within the sample. Hence, during C_3S hydration, the $Ca(OH)_2$ dissolves into the liquid phase, however, any solid $Ca(OH)_2$ present will not dissolve into the liquid phase even below the liquid saturation point. This occurs due to the *'poisoning'* [5] of the $Ca(OH)_2$ nuclei surface by the silicate ions. Both C_3S and C-S-H require Ca^{2+} and OH^- to enable holistic dissolution. It is therefore important to realise that a finite quantity of $Ca(OH)_2$ is present within cementitious materials and may cause exhaustion of the aforementioned. However, over a long enough period poisoning will be overcome and will allow the precipitation of the silicate ions and the $Ca(OH)_2$ to act as a sink for the Ca^{2+} ions which in-turn will allow C-S-H formation to occur.

Odler [5] emphasises that the nucleation and consequent formation of C-S-H up to the induction phase follows a different form of morphology than that which develops from the C-S-H at the acceleration period and beyond. These are known as first and second stage C-S-H or alternatively as inner and outer product.

Odler [5] believes that first stage C-S-H formation is determined by the $Ca(OH)_2$ concentration within the liquid. Hence an increase in the $Ca(OH)_2$ concentration within the liquid phase will lead to the reduced formation of first stage C-S-H. However, Odler emphasises that $Ca(OH)_2$ is found in both soluble and insoluble forms and will therefore be effected by the solubility ratios. Once the thermodynamic barrier has broken down then second stage C-S-H formation may proceed.

The formation of first and second phase hydration products are visually represented for C_3S particles in figure 11.

Figure 11: C-S-H primary and secondary formation, indicating effect of electrical double layer theory

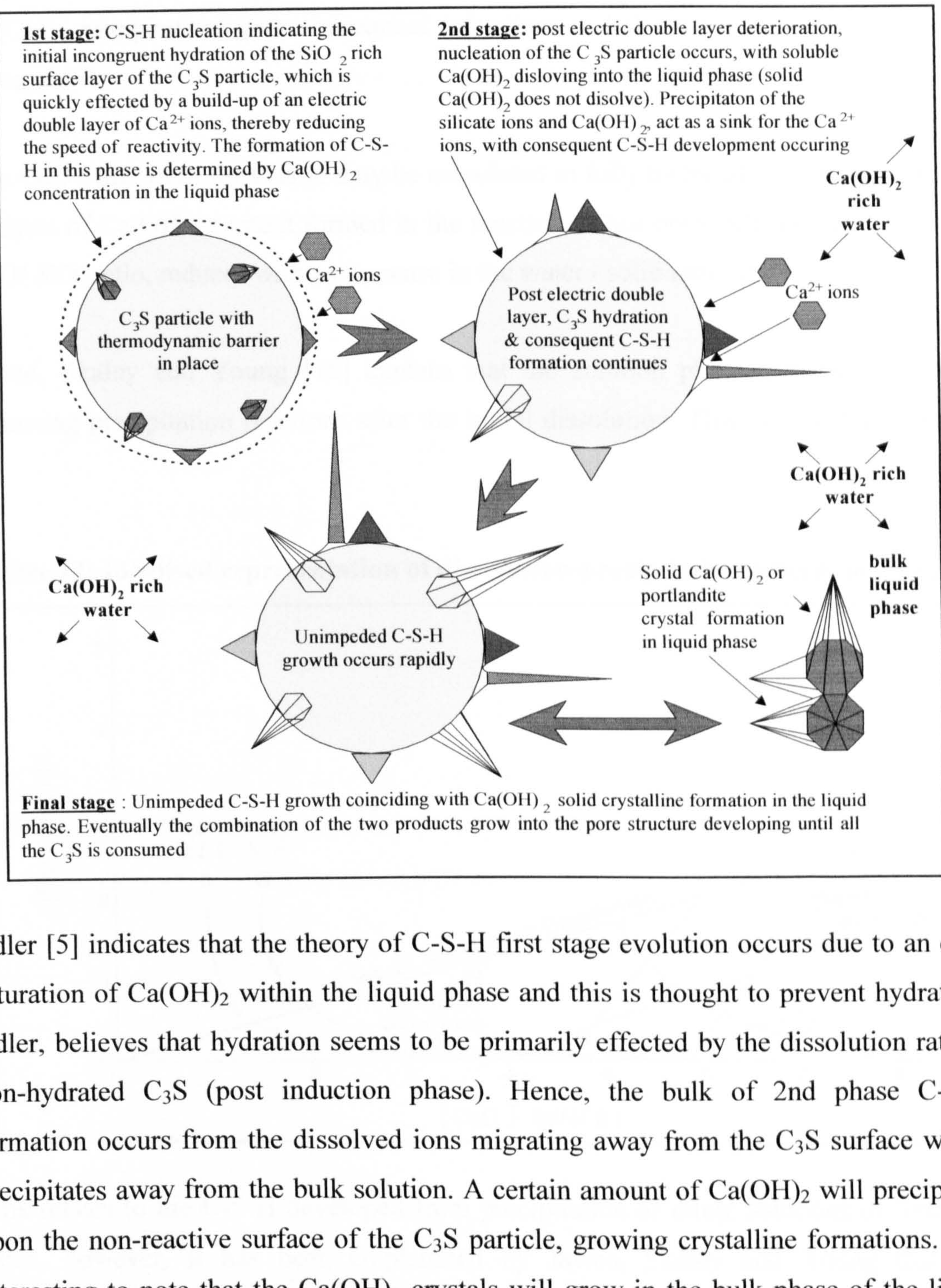

Odler [5] indicates that the theory of C-S-H first stage evolution occurs due to an over saturation of $Ca(OH)_2$ within the liquid phase and this is thought to prevent hydration. Odler, believes that hydration seems to be primarily effected by the dissolution rate of non-hydrated C_3S (post induction phase). Hence, the bulk of 2nd phase C-S-H formation occurs from the dissolved ions migrating away from the C_3S surface which precipitates away from the bulk solution. A certain amount of $Ca(OH)_2$ will precipitate upon the non-reactive surface of the C_3S particle, growing crystalline formations. It is interesting to note that the $Ca(OH)_2$ crystals will grow in the bulk phase of the liquid and form larger portlandite crystals.

The growth of C-S-H and $Ca(OH)_2$ crystals will eventually develop into the space where the water once resided forming a dense crystalline matrix. As the crystal growth

increases, a reduction in the water volume will obviously be seen. Odler indicates that the rate of hydration is related to diffusion and is affected by the dissolved ions ability to migrate as the level of non-reacted C_3S reduces. Consequently, hydration will stop when the C_3S is consumed or a low W/C ratio prevails. Mixes with low W/C ratios will tend to generate an environment which lacks sufficient space for C-S-H growth and $Ca(OH)_2$ precipitation, with consequent reductions in holistic cementitious formations being noted.

The CaO / SiO ratio for C-S-H may be calculated in fully hydrated C_3S paste, from the analysis of $Ca(OH)_2$ content formed in the reaction. It has been indicated by Odler that CaO/ SiO_2 ratio, reduces with an increase in the water / solid ratio of a starting mix.

Jawed, Skalny and Young [18] explain that the solution phase directly effects the following precipitation reactions after the initial dissolution. This is reflected in figure 12.

Figure 12: Idealised representation of dissolution-precipitation process in C_3S [18]

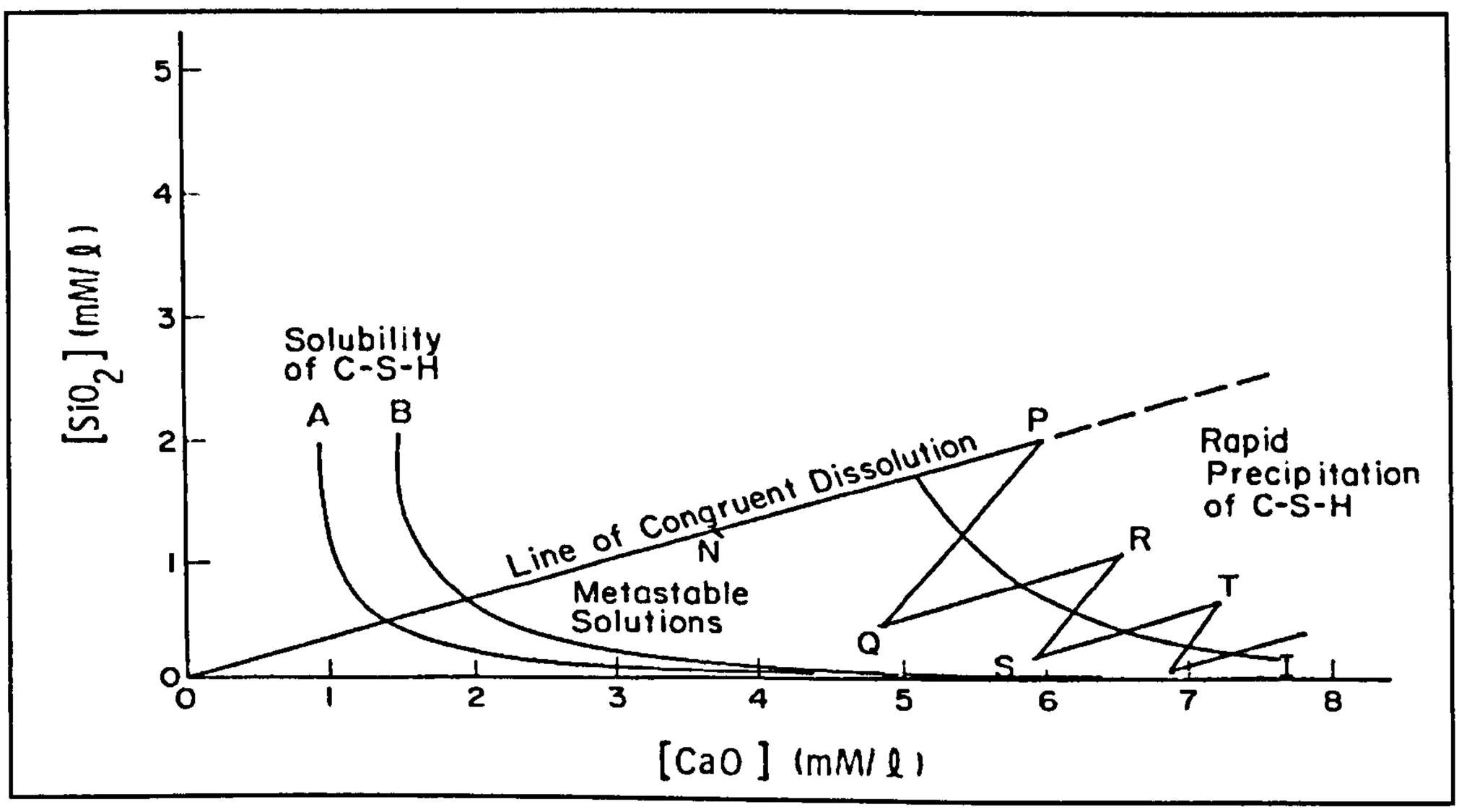

This relates to the C-S-H developed from precipitation of dilute solutions of lime and silica, however, it has been emphasised by Jawed, Skalny and Young that this precipitation does not occur until the super solubility curve for C-S-H reaches point 'P'. After this point precipitation occurs following line P-Q. Line Q-R denotes more congruent dissolution, R-S, re-precipitation and finally S-T representing dissolution.

The nature of the concentration of the Ca/Si ratio is determined by the composition of the solution.

Jawed, Skalny and Young [18] explain that early stage hydration of C_3S is effected by the initial dissolution of the particle, with incongruent Ca^{2+} and OH- moving rapidly into solution leaving a silica rich surface layer. Following this the adsorption of Ca^{2+} on the negatively charged surface creates an electrical double layer.

Figure 13: Dissolution of C_3S to form a silica-rich layer [18]

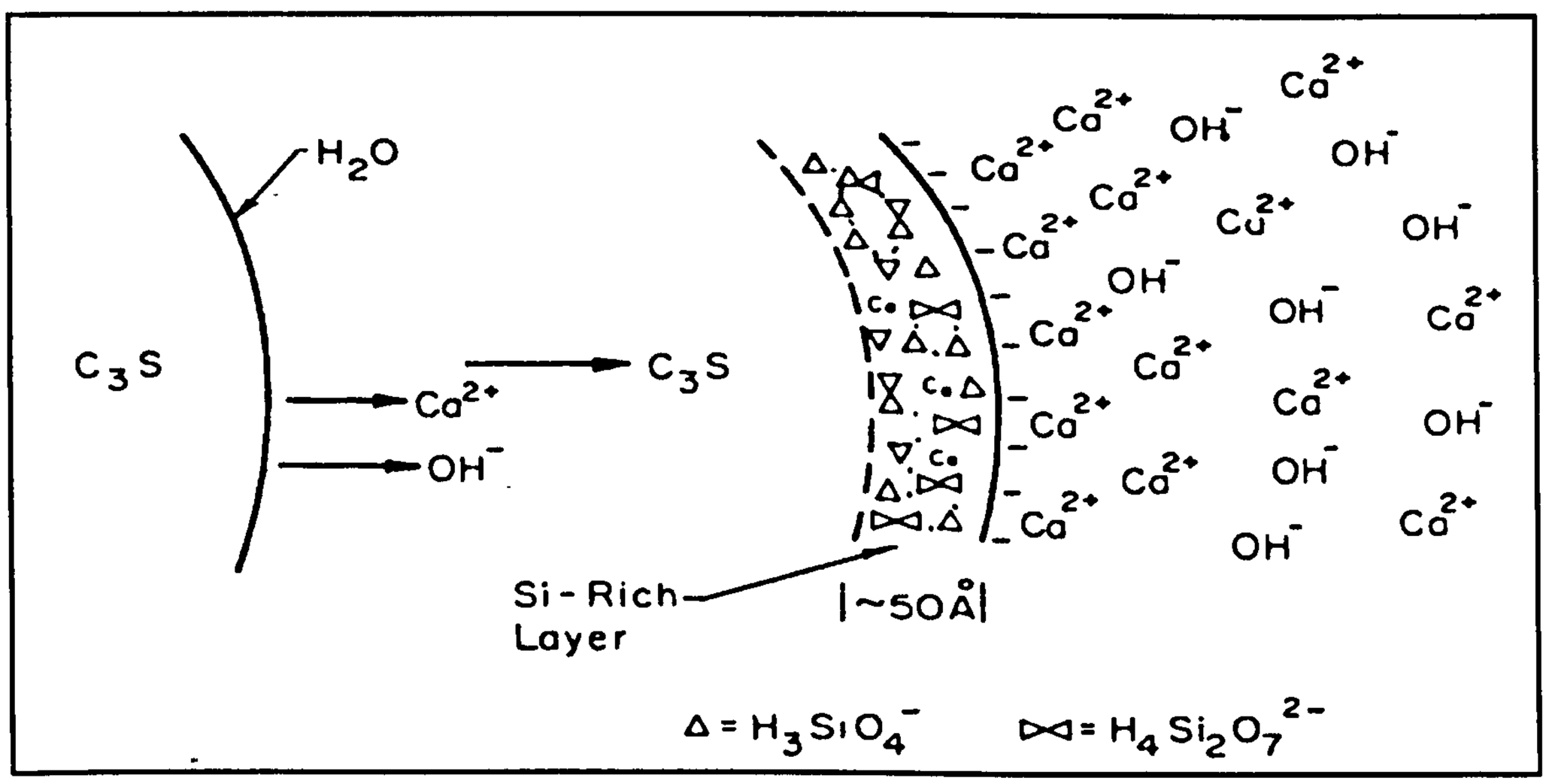

This layer will continue via incongruent dissolution until C-S-H (type E) forms. It has been suggested by Jawed, Skalny and Young [18] that the silica rich layer is maintained until the quasi-solid that is rich in water, dissolves slowly to form C-S-H.

The end of the induction phase is seen with the nucleation of the new phase. Barnes et al believes that nucleation is the transformation of the unstable E-type C-S-H into a stable stage I C-S-H. However, it has also been hypothesised by Young et al [22] that the induction period ends when the maximum Ca^{2+} has occurred in the solution with the nucleation of $Ca(OH)_2$ developing. The growth of $Ca(OH)_2$ crystals is related to heat evolution in stage III. Jawed, Skalny and Young believe that 'delayed growth of $Ca(OH)_2$ nuclei has been attributed to the adsorption of silicates on the faces' [18], thereby delaying the precipitation of $Ca(OH)_2$ in the presence of soluble silicate. The rapid hydration of cements during the induction period can be partially explained by 'thermal shocking' which is the increasing of the hydration temperature. This promotes $Ca(OH)_2$ crystallisation from the super saturation.

The acceleration of C_3S hydration does not occur with super saturated $Ca(OH)_2$ solution. It is also believed that the $Ca(OH)_2$ crystal growth may become 'poisoned' [22] by silica adsorption. However, in stage III hydration the increased $Ca(OH)_2$ concentration will lead to increased hydration.

Jawed, Skalny and Young [18] indicate that the study of early hydration is somewhat hindered by the speed of the initial reactions and variability of the C_3S preparation that will ultimately affect the rate of dissolution and ionic fluxes that prevail. He believes that for all the uncertainty with the aforementioned theories, certain factors are reliable. These factors being that when the dissolution - precipitation takes place it is generally congruent in nature and is linked with a silica rich layer development.

The consequent precipitation of C-S-H occurs within the absorbed water layer, however only precipitates that are a few atomic layers thick may grow. This process will ensue in a continuous solution - precipitation process that allows the development of what Jawed, Skalny and Young [18] calls 'discontinuous layers'. These occur at the surface and are associated with large amounts of water and electrical double layer. This layer would slow down hydration, and it would not prevent ions passing. The C-S-H that subsequently precipitates will be highly disordered with a variable composition. This layer although variable in thickness will control the rate of Ca^{2+} and OH^- release into the solution, due to its ability or lack of it to diffuse through the surface hydrate electrical double layer and thereby enter into the solution. Jawed, Skalny and Young [18] emphasises that this rate of diffusion is obviously affected by the ionic concentration of the bulk solution. This escape of Ca^{2+} and OH^- is known as the nucleation of $Ca(OH)_2$. For continued hydration of C-S-H to ensue it is necessary to allow the nucleation of $Ca(OH)_2$ to occur. After this has taken place the C-S-H is believed to be amorphous however, upon an increased silicate concentration it agglomerates into solid particles. The high level of silica with relatively low solubility leads to the development of small surface particulate C-S-H. The $Ca(OH)_2$ crystals form from this layer and develop into relatively few crystals.

The following middle phases are associated with a significant increase in the formation of hydration products. Jawed, Skalny and Young believes that a 'gradual change from reaction kinetics controlled by the rate of dissolution of C_3S or the rate of crystal growth of $Ca(OH)_2$ to diffusion control' [18] is seen.

Stage III heat of hydration is generally associated with rate of $Ca(OH)_2$ crystal growth. This is twinned with the continued C_3S dissolution. At this stage the precipitation of C-S-H is rapid with coinciding formation of $Ca(OH)_2$ crystals. The ensuing C-S-H that engulfs the C_3S particle is believed to 'show no definite form in wet state' and continuing he states that 'this is common in amorphous material forming in a random arrangement of particles with a high water content' [18].

The impending phase is an important one in which the C-S-H dehydrates and then shrinks, splitting and consolidating into what Jawed, Skalny and Young calls 'spines or needles' [18]. He attributes the formation of these rods to a 'crumpling and rolling up of sheet like material' [18].

These crystals form into the areas in between the hydrating particles. This stage is the transition between the anhydrous and hydrated silicate particulate.

Jawed, Skalny and Young [18] believe that Stage IV C-S-H is effected by the materials particle size and particle distribution. This has an affect upon the diffusion control of the material and is a gradual process as the C-S-H coating thickens. The C-S-H layers thickness is effected by the particle size with the larger grain having the thickest layer of C-S-H and vice versa.

The seeding of crystalline hydrates is of critical importance in the ensuing major hydrated product.

Late hydration or Stage V hydration is associated with the densification of the C-S-H and is believed by Jawed, Skalny and Young to occur due to the relative absence of space for the growth to be accommodated.

The morphology of C-S-H between stage III and IV are believed to show no significant difference however, the $Ca(OH)_2$ crystals do grow and it is believed by Jawed, Skalny and Young that they may 'engulf some of the hydrating C_3S grains, thereby limiting their potential for complete hydration. The large $Ca(OH)_2$ crystals always contain low levels of silica that will be dispersed throughout the structure due to the nature of dissolution and precipitation of the material.

2.4.3.5 Tri-Calcium Aluminate (C_3A)

Odler [5] states that the chemical formula for tri-calcium aluminate (C_3A) is $3CaO{\cdot}Al_2O_3$, continuing to indicate that it is a cubic orthorombic structure and or, monoclinic modification of the previously explained C_2S. However, the latter only develop through the presence of foreign ions (ie: Na^+). However, all of the above have similar hydration properties. The sequence of hydration in C_3A is initiated firstly by an initially unreacted particle of C_3A, secondly, a gel formation at the surface of C_3A particle. The third phase is a hexagonal crystal growth precipitated from the liquid phase, following the general chemical formula: C_2AH_8 and C_4AH_{19} and finally, hexagonal phases form cubic C_3AH_6.

Figure 14: Hydration of C_3A in the absence of $Ca(OH)_2$

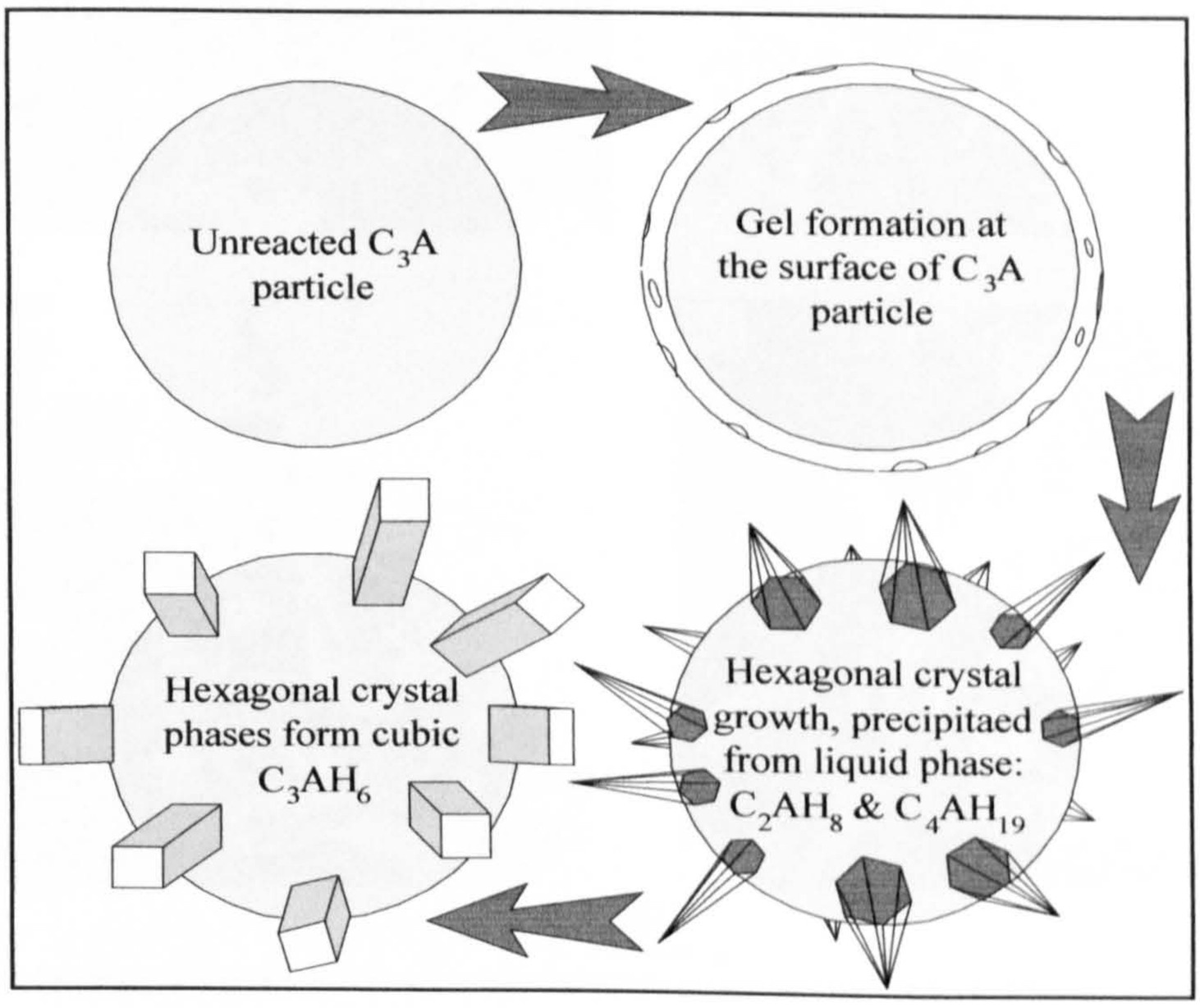

Odler [5] believes that C_3A hydration accelerates depending upon a change in temperature, the grain size of the C_3A, the water / Solid ratio and presence / absence of CO_2. It is interesting to note that $Ca(OH)_2$ will slow down the C-A-H formation and only forms C_4AH_{19} as a primary product. However, this will convert to C_3AH_6 with the continued hydration process. Generally, C_3A hydration slows down soon after initial hydration due to the formation of the hexagonal hydrates (C_2AH_8 and C_4AH_{19}) which acts a protective barrier upon the surface of the C_3A particle. Once these hexagonal formations develop into a cubic formation (C_3AH_6) the barrier can be easily disrupted. Hence, hydration may commence.

Odler [5] indicates that C_3A's reactivity reduces with the presence of calcium sulphate due to limited solubility of C_3A in the presence of sulphates. Odler [5] briefly discusses calcium alumino-ferrite [$C_4(AF)$], believing that it reacts in a similar manner to C_3A, although at different reaction rates. However, the reaction in the presence of lime allows the formation of $C_4(AF)$ only.

Plate 10: Hydration products in C_3A [18]

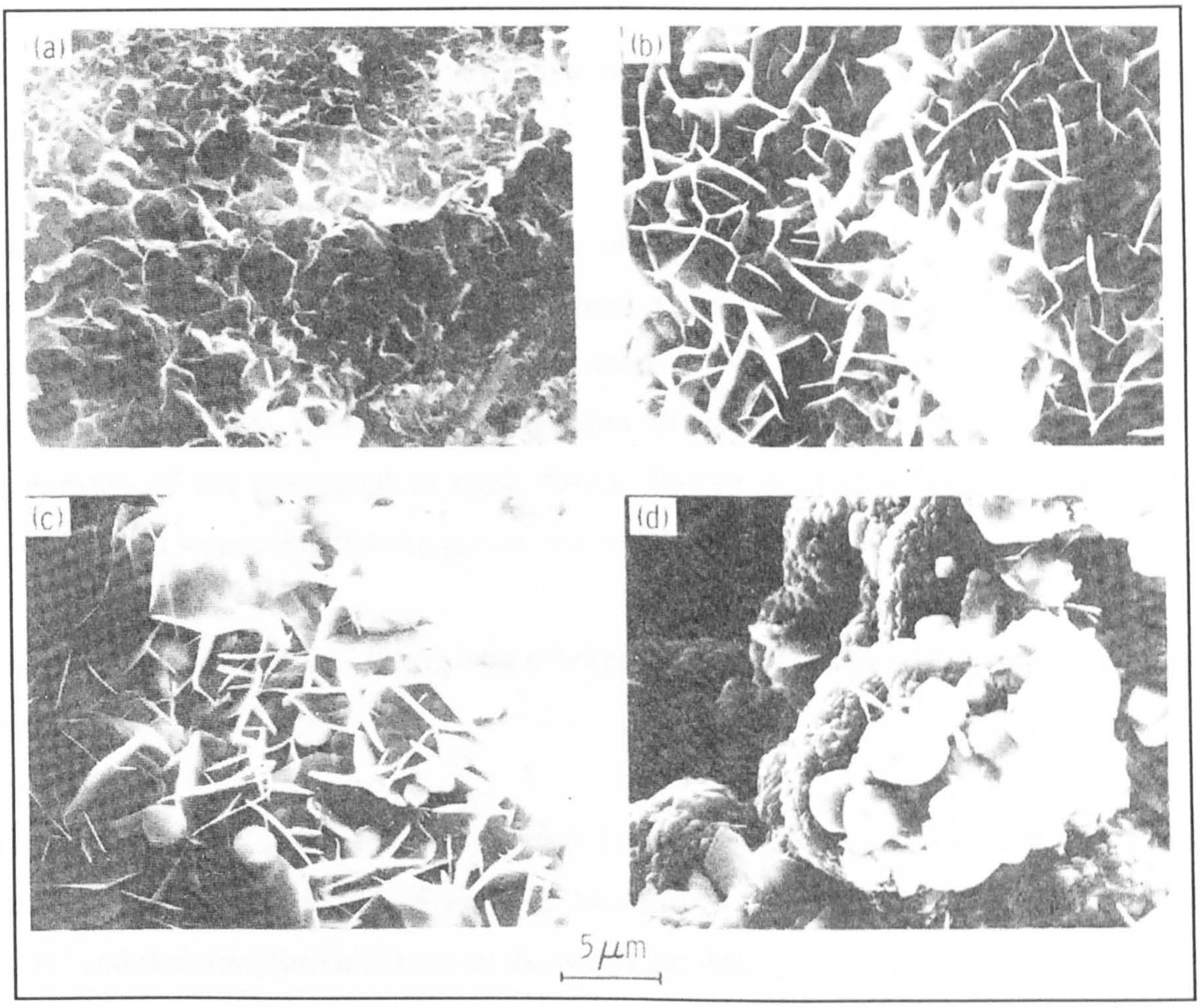

Plate 10 indicates: a)gel consisting of irregular foils; b) hexagonal flakes of C_nAH_{lg} c) hexagonal CAH_9 and cubic C_3AH_6 and d) mostly cubic C_3AH_6.

2.4.3.6 Hydration of the Ferrite phases

Jawed, Skalny and Young define ferrite solid solution (Fss) as 'the iron containing phase which varies in most cements between C_6A_2F and C_6AF_2 with a mean close to C_4AF'. He continues to define both AFm and AFt phase as follows:

AFm 'the phase formed in the hydration of Portland cement which is considered to be derived from pure monosulphoaluminate with the partial substitution of A by F, and SO_4^{2-} by other anions' [18].

AFt as 'the phase formed in the hydration of Portland cement which is considered to be derived from pure ettringite with the partial substitution of A by F, and SO_4^{2-} by other anions' [18].

The ferrite phases are similar to C_3A hydration phases, although they are somewhat slower in terms of reactivity.

Hexagonal hydrates are associated with C_4AF and it has been hypothesised by Jawed, Skalny and Young [18] that the hexagonal crystallography may alter into cubic morphological form. This includes $C_2(AF)$ and $C_4(AF)$ that both have hexagonal habits that alter into cubic forms. The substitution of Fe and Al are responsible for the conversion of the hexagonal to cubic forms. Barnes et al also believes that the Al component is responsible for the general stability of the material.

The hydration of calcium ferrite and calcium alumino-ferrites will increases with an increase in the A / F ratio.

The formation of C_4Fm has been associated with the hydration of C_2F and amorphous $Fe(OH)_3$. The formation of C_3F and C_4F are derived from the intimate mixture of C_2F and C and therefore the behaviour of the two is similar.

2.5 Calculation of Hydraulic Index and Cementing Index

The definition of hydraulic set in limes has been stated by Holmes and Wingate as 'the chemical combination of lime, burnt clay or other pozzolanic material and water to form a stable compound, even under water' [12]. Holmes and Wingate continue to indicate that 'the hydraulic limes contain lime and clays which have already formed intermediate compounds in the firing' [12]. This has a direct relationship upon the calcination and subsequent hydration products noted. Odler has devised a more scientifically rigorous definition of hydraulicity and hydration, believing that hydraulicity is the ability to harden underwater, through hydration rather than carbonation, and that hydration is believed to be a 'reaction of an anhydrous compound, a hydrate..., it is associated with

both chemical and physico-mechanical changes in a system, in particular with setting and hardening' [5]. It is clear to see that Portland cement hydration and lime hydration are close relatives and their consequent hydraulicity has been traditionally calculated in a similar manner to each other.

Traditionally, the calculation of a material's hydraulicity has been undertaken with the adoption of a series of cementitious and hydraulic indices, C.I. and H.I., respectively, twinned with chemical evaluations. The hydraulic index was defined by Eckels in 1928 as *'the ratio between the percentage of silica and alumina to the percentage of lime CaO'* [15]. Unfortunately, Eckels' hydraulic index is indiscriminate and does not subdivide the percentages of alumina and silica into reactive and non-reactive components within the lime sample. Eckels believed that the aluminium and silica attain equal reactivities and this was later shown by Bergoin [16] to be incorrect.

In addition to the aforementioned problems, Chandlot (1906) recognised that discrepancies within these indices were apparent. He states that 'this classification cannot be absolute because... if a certain proportion of clay is necessary to achieve hydraulicity, its degree will also be subject to the manufacturing process and to the uniformity of the raw materials' [16]. This early understanding of calcination effect was invaluable and would have almost certainly had an influence upon other researchers work upon hydration.

Equation 3: Hydraulicity Index (Eckels)

$$\text{Hydraulic Index} = \sum {}^{(Si + Al)}/_{CaO}$$

Cementitious indices were an advance upon the older H.I. as they not only considered the percentage of lime, silica, alumina, but also the additional components within the material, namely iron and magnesia. However, problems with both of the H.I. and C.I. calculation methods occur because not all the silicates and aluminates are necessarily reactive and must be considered simply as aggregates.

Equation 4: Boynton's cementitious index (C.I.) [23]

$$C.I. = \frac{2.8(\%S) + 1.1(\%A) + 0.7(\%F)}{(\%)C + 1.4(\%M)}$$

Livesey assessed Vicats' calculation for hydraulicity of cementitious materials,

$$I = \frac{SiO_2 + Al_2O_3 + Fe_2O_3}{CaO}$$

and found the calculation showed a poor relationship with performance [24]. Kuhl's [24] formula for hydraulicity,

$$CI = \frac{2.8(SiO_2) + 1.1(Al_2O_3) + 0.7(Fe_2O_3)}{CaO + 1.4(MgO)}$$

is more advanced in terms of oxide components but it was still deficient due to its assumption that the silicates etc are all of a reactive nature. However, as he emphasises 'it is clear that calcium, present as $CaCO_3$ and any silica, alumina and iron remaining inert as insoluble material, has not converted into hydraulic components.' [24].

Eckels' cementitious index (C.I.) assumes that silica and lime combine to form C_3S, but this only forms at higher firing temperatures than normally associated with lime calcination. In addition it was assumed that other components were also hydraulically reactive when in actual fact they were not. These non-hydraulic components cannot therefore add to the strength development of the material.

The classification of hydraulic limes and their consequent cementitious index values can be somewhat confusing and inaccurate. There have been three primary investigators in this area, namely; Vicat, Eckel, and finally Boynton; whose conflicting views are summarised in table 9.

Table 9: Conflicting classification and hydraulic indices for limes.

Research Undertaken by	Classification Of lime	Cementitious Index (C.I.)
VICAT; 1837 [16]	Feebly Hydraulic	0.10-0.16
	Hydraulic	0.16-0.31
	Eminently Hydraulic	0.32-0.42
ECKEL; 1928 [15]	Feebly Hydraulic	0.3-0.7
	Eminently Hydraulic	0.7-1.1
BOYNTON; 1980 [23]	Feebly Hydraulic	0.3-0.5
	Hydraulic	0.5-0.7
	Eminently Hydraulic	0.7-1.1

Issues are further confused when the addition of Holmes and Wingate's results upon C.I. for various types of lime are integrated. They adopted a range of limes to be assessed using the C.I. calculation method, and as aforementioned more conflict prevails.

Table 10: Cementitious Index for various types of limes (author after Holmes and Wingate) [12]

Lime description	Cementitious Index (C.I.)	Active clay content in the limestone.
Fat limes	Close to zero	Very little clay
Slightly hydraulic limes	0.3 to 0.5	Around 8%
Moderately hydraulic limes	0.5 to 0.7	Around 15%
Eminently hydraulic limes	0.7 to 1.1	Around 25%
Natural cement	1.7	Up to 45%

It is easy to see how confusion could prevail as the leading authorities all have different values for the same cementitious materials. Hughes and Swann reinforce this belief by stating that: 'Setra Marketing Ltd, the UK importers of St Astier hydraulic lime, describe NHL2 as feebly hydraulic whilst from the setting time measurements it would be classified as better than eminently hydraulic' [21]. The consequence would undoubtedly be confusion for those attempting to specify the materials, believing that they have applied a feebly hydraulic lime which in reality performs, under the above classification system, as an eminently hydraulic lime.

Livesey [24] drew attention to the urgent need for the development of a new code of practice for the design and use of lime. He believes that problems are encountered because the traditional methods of assessment for the hydraulicity of limes are slow and often inaccurate. New performance assessments must be closely linked with results and vice versa and Livesey aims to develop a new 'system for calculating constituent compound mineralogy' [24]. Elemental oxides present in hydraulic limes are the same as those in cement, although their relative proportions are different [24] and basic

differences in mineralogy, particularly the high proportion of crystalline $Ca(OH)_2$ had influenced the traditional calculated results.

Livesey considered several methods of elemental component analysis: X-ray fluorescence - pellet type and boron bead type and thermo-gravimetric methods which analyse weight change when the materials is heated. In this case the thermo-gravimetric analysis assessed the loss of water from the binder, whether it be loosely bound, adsorbed or combined with respect to silicate phases, other hydrated lime hydration products and CO_2 combination.

It is interesting to note that the development of the CI for cement was derived from the use of phase diagrams for hydraulic components. Livesey emphasises that a newly developed hydraulicity index must 'take into account that silica exists in some low-activity soluble forms, even in natural chert sands.' [24] 'Some forms of C_2S are less reactive than in normal Portland cement belite, and, as in Portland cement, slower burning can result in coarser, less reactive forms of silicates' [24].

X-ray diffraction is often adopted for OPC quality control and Livesey used this process for the assessment of hydraulic lime, leading to the identification of known crystal forms such as βC_2S (belite). As expected, Livesey found no C_3S (alite) in any of the commercially available limes, but did find C_4AF (Brownmillerite) [24] in relatively significant quantities. The general quantities of C_2S were found by Livesey to be major in class 5 lime, significant in class 3.5 lime and minor in class 2 lime [24]. Importantly the role and detection of alumina phases were believed by Livesey to increase 'the plastic and hydraulic properties of hydraulic lime' [24].

C_3A and other aluminate compounds, such as C_2AS (di-calcium alumino silicate) (gehlenite) and C_4AF, were found in all of the hydraulic limes. Livesey considered this to be particularly important for the higher alumina content limes since it confirms that only a small proportion of alumina is converted to the reactive C_3A compound and therefore contribute to the hydraulic activity and also react detrimentally when exposed to sulphate' [24].

Livesey proposed a new method for estimating the hydraulic properties of lime, based on belite, aluminate, sulphate, hydrate and carbonate concentration, all of the which

would be calculated via the process of 'deduction of insolubles.' [24] In this process, successive stages determine C_4AF from remaining iron oxide, C_3A and C_2AS from remaining alumina, C_2S from remaining silica, $CaSO_4$ from remaining sulphate excess over alkali content, $CaCO_3$ from carbonate content; and $Ca(OH)_2$ from remaining calcium [24] and the calculation was cross checked against the surplus post hydration lime.

An assessment of limes from crushing strength alone has too many anomalies to accurately represent performance, so consequently, Livesey summarised the results as shown in table 11. Livesey stated that the NHL 2 lime 'is clearly of different composition to the others having lower silica, alumina and iron and higher calcium content as well as lower strength than most others' [24]. Interestingly when Livesey assessed the NHL 3.5 limes, he found that an anomaly exists due to the 'higher silica, alumina and iron and lower calcium content, compared with other class 3.5 limes, indicative of greater hydraulicity than the strength shows' [24].

Table 11 : Analytical calculated compound composition and physical properties of natural hydraulic limes, Author after Livesey [24]

Type	NHL	NHL	NHL	NHL	NHL	NHL	NHL
Class	2.0	3.5	3.5	3.5	3.5	5.0	5.0
Sample Ref	2A	3A	3B	3C	3D	5A	5B
Chemistry							
SiO_2	6.0	18.7	10.3	11.7	19.5	20.8	21.4
Al_2O_3	0.3	6.1	3.7	1.2	1.8	1.8	10.4
Fe_2O_3	0.7	2.3	1.5	0.6	0.8	0.8	3.2
CaO	63.3	46.2	60.0	59.1	58.8	58.0	39.4
MgO	1.4	1.2	1.5	2.0	1.3	1.3	2.8
K_2O	0.20	0.49	0.93	0.26	0.29	0/27	1.44
Na_2O	0.06	0.23	0.11	0.06	0.06	0.06	0.14
SO_3	0.80	1.09	1.43	1.37	0.48	0.37	2.49
Cl	0.01	0.01	0.01	0.01	0.01	0.01	0.01
LOI	27.0	22.9	20.2	23.0	16.3	16.1	18.5
Total	**99.75**	**99.22**	**99.71**	**99.29**	**99.34**	**99.51**	**99.74**
Insolubles	0.7	14.8	0.9	4.0	4.8	3.9	10.6
CO_2	14.0	19.9	9.2	11.1	9.4	8.9	6.0
Soluble SO_3	0.28	0.28	0.52	0.25	0.20	0.15	0.52
Compounds							
C_2S	15.4	7.3	24.7	21.4	41.1	47.4	23.9
$Ca(OH)_2$	47.5	10.0	36.2	40.8	24.3	18.7	3.5
$CaCO_3$	31.8	45.2	20.9	25.2	21.4	20.2	13.6
$CaSO_4$	0.9	0.6	0.8	1.8	0.3	0.1	1.8
C_4AF	2.1	7.0	4.5	1.7	2.4	2.4	9.7
C_3A	0.0	6.1	3.7	1.1	1.7	1.7	11.1
C_2AS	0.0	6.2	3.8	1.1	1.7	1.7	11.2
Total (inc insols)	**98.4**	**97.3**	**95.5**	**97.3**	**97.6**	**96.1**	**85.5**
Indices							
I	0.14	0.59	0.30	0.21	0.37	0.42	0.77
CI	0.33	0.85	0.63	0.49	0.90	1.03	1.23
Physical EN-196-1 mortar compressive strength (MPa)							
@ 7 days	-	0.8	1.5	2.9	1.9	2.8	6.4
@ 28 days	3.5	2.3	4.1	6.6	4.0	7.7	10.3
Whiteness							
Reflectivity	80	51	65	77	74	68	49

It is also the authors' view that a new classification system for hydraulicity is urgently needed to prevent ambiguity.

2.5.1 Conduction calorimetry

Bergoin previously indicated that only reactive silicates and aluminates can confer hydraulicity, therefore, a new test for hydraulic reactivity must be adopted. One such test may be based upon measuring the heat of hydration of those active components only. Such a test is widely used in Portland cement research, and takes the form of the J.A.F conduction calorimeter.

The development of the isothermal conduction calorimeter and associated techniques were initiated by Tian [25]. This work spurred a great deal of interest in the area with J.A. Forrester subsequently publishing a paper in 1970 entitled *'a conduction calorimeter for the study of cement hydration'* [26] and subsequently went into production manufacturing the first purpose built calorimeter for the study of cementitious materials. This specialised calorimeter was known conveniently as the J.A.F. calorimeter. This enabled conduction calorimetry work within cements to develop rapidly.

Forrester [24] studied the characteristics of heat evolution rates in OPC which lead to the development of the basic graphical representation shown in figure 15.

Figure 15: Characterisation of heat evolution in O.P.C. Author after Forrester [24]

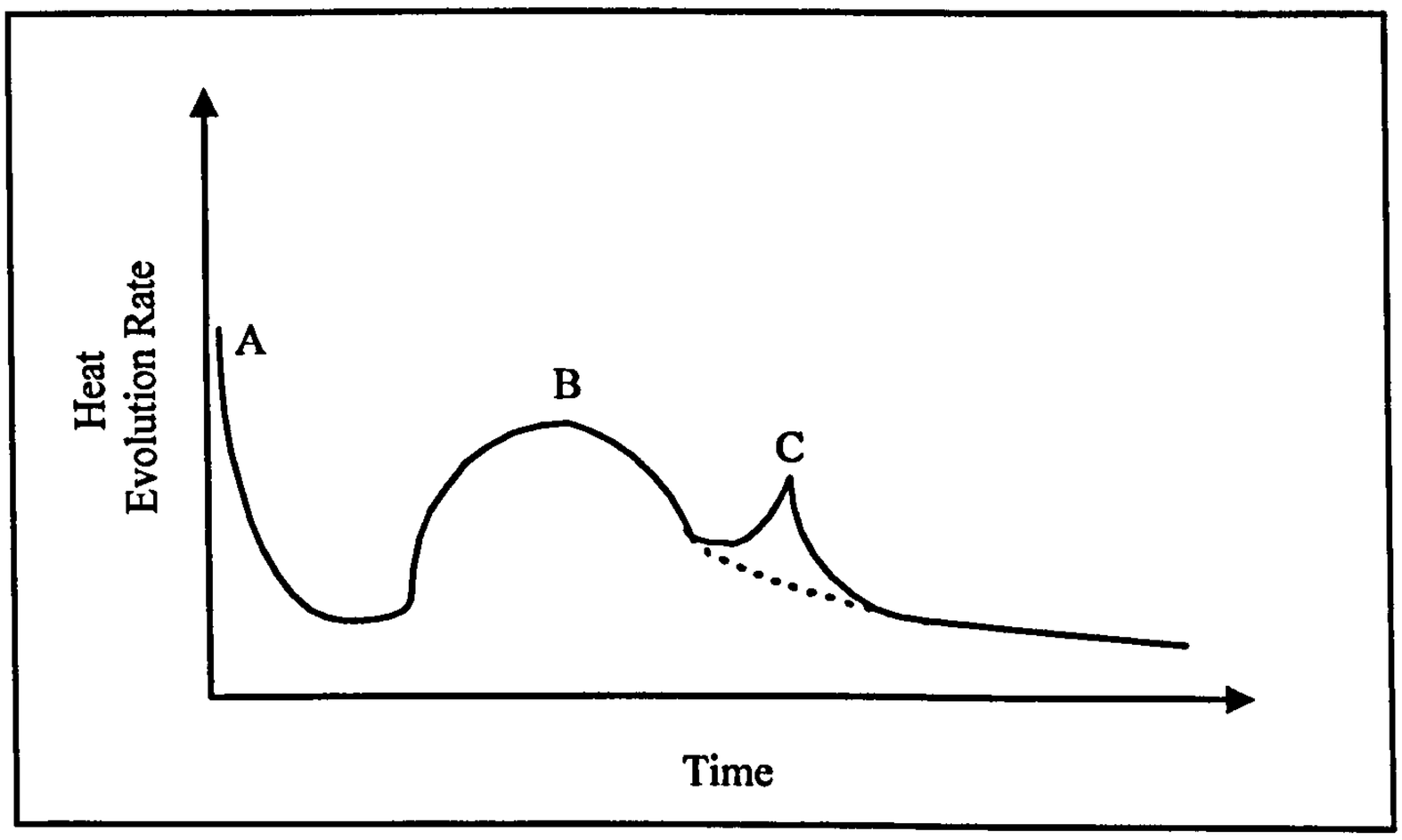

Forrester indicates that the 3 significant heat peaks namely; A, B and C that are all associated with different hydraulic activity within the material. The first of these; (A) is

associated with the heat of wetting and the hydration of free lime. This reaction is generally exhibited for approximately 2 hours at which point the minimum rate of heat is ascertained. Forrester indicates the measurement of this process can only be partially assessed due to the nature of the 'large calorimeter can'. The wetting phase therefore appears to decelerate only however, it is obvious that the acceleration phase is simply not recorded due to the nature of the aforementioned calorimeter experimentation process.

Once peak (A) is dormant then the activation of what will become heat peak (B) commences (in Portland cement only). This activation is associated with the early hydration of alite (C_3S) and ettringite (C_3A + gypsum). This phase generally lasts between 10 and 14 hours, however it must be emphasised that the alite (C_3S) is not generally exhausted. Forrester [26] believes that this area requires greater study as the true behaviour is not understood.

Forrester indicates that heat peaks (A) and (B) always occur in OPC hydration with (C) being variable. Heat peak (C) is associated with excess C_3A hydration, that is to say hydration over that required to combine with the sulphate to form ettringite. Lerch [26] believes that the commencement of peak C coincides with the disappearance of the sulphate ions from the solution phase of the paste. A marked reduction in C_3A hydration after peak (C) is seen and is associated with the formation of mono sulphate. This is derived from the high sulphate form of calcium sulpho-aluminate hydrate. The rate of heat evolution post heat peak (C) falls to a very low level. This main deceleration occurs for 2-3 days however, it must be emphasised that this reaction may still be detected post 28 days.

It is interesting to note that no evidence for heat evolution in belite or ferrite phases existed. It is believed that the ferrite phase forms immediately after the ettringite to mono-sulphate transformation.

Jawed, Skalny and Young [18] have shown early, medium and late hydration phases in graphical form. The first 2 relate to Forresters heat peaks A and B. See Figure 16.

Figure 16:Heat of hydration in early, middle and late phases [18]

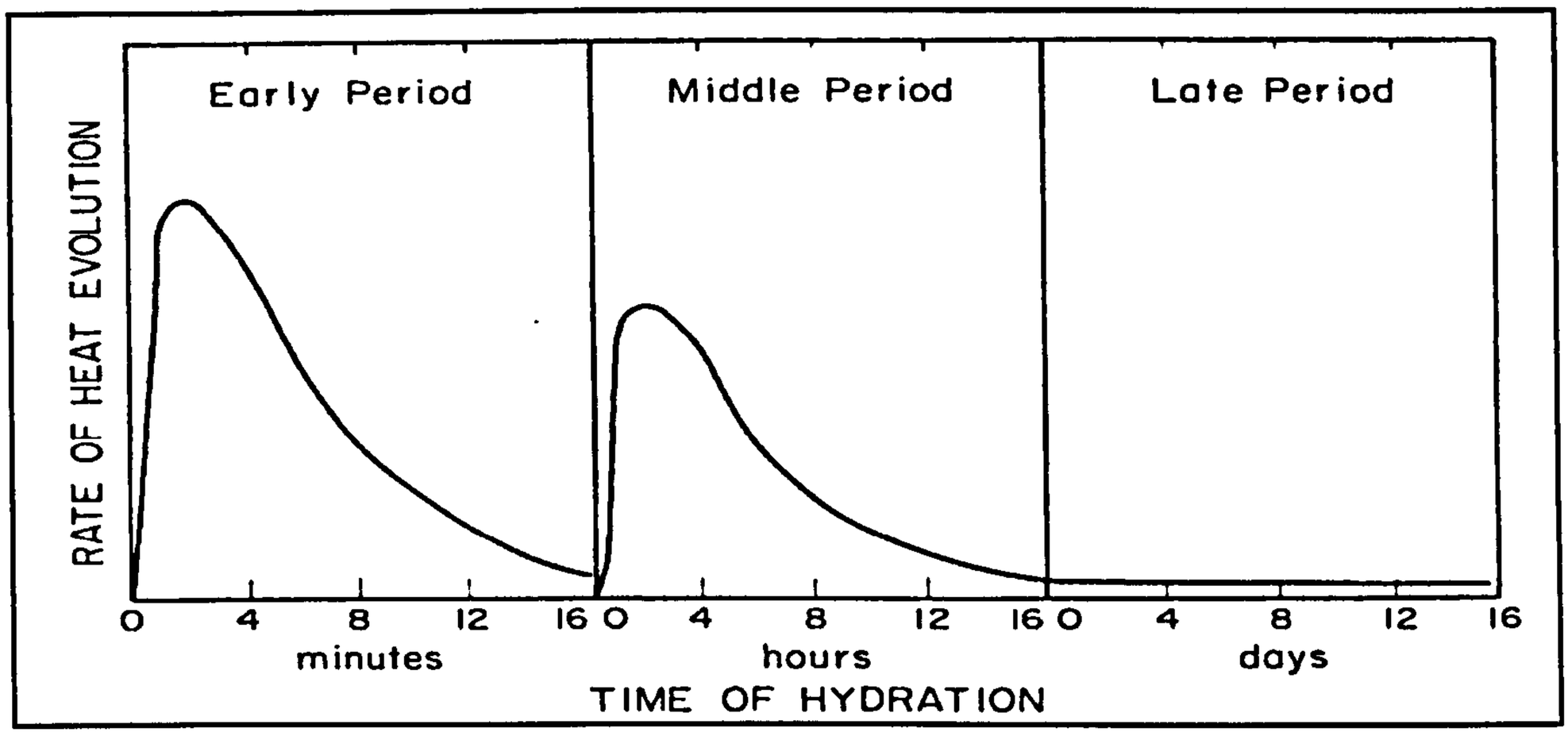

Traditional studies of C_3S via conduction calorimetry have led to the development of idealised conduction calorimetry data such as that seen in figure 16. The release of calcium hydroxide into solution obviously affects the formation of portlandite and this in turn has a bearing upon the conduction calorimetry results. This may also be seen in figure 17.

Figure 17: Schematic representation of changes taking place in C_3S-water systems (w/s ratio < 1.0) [18]

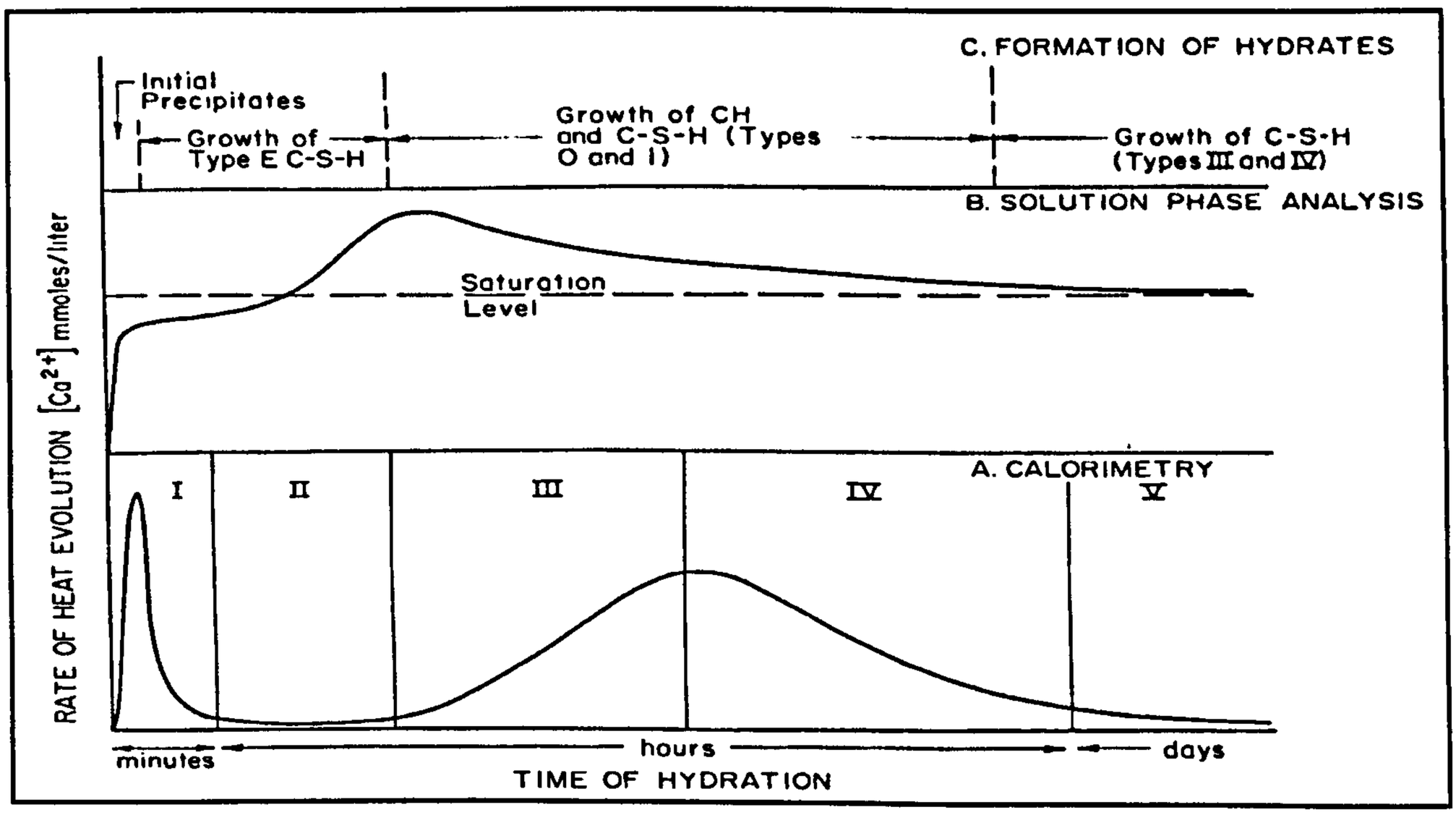

The mechanisms of hydration seen in Figure 17 are summarised in table 12.

Table 12: Sequence of hydration of C_3S (author after Jawed, Skalny and Young) [18]

Period	Reaction stage	Chemical processes	Overall kinetic behaviour
Early	I. Pre-induction	Initial hydrolysis; release of ions	Very rapid. Chemical control
	II. Induction period	Continued dissolution; formation of early C-S-H	Slow. Nucleation or diffusion control
Middle	III. Acceleration period (post induction period)	Initial growth of permanent hydration products	Rapid. Chemical control
	IV. Deceleration period	Continued growth of hydration products; development of microstructure	Moderate. Chemical and diffusion control
Late	V. Diffusion period (steady state period)	Gradual densification of microstructure	Very slow. Diffusion control

It is important to realise that the above conduction calorimetry plots represent the 'dynamic balance between the heat evolved by hydrating sample of C_3S and the heat lost by the calorimeter to its surroundings' [18], the exact shape and position of the peaks depend on the particular instrument used.

When assessing the hydration phases associated with figure 17 it was emphasised by Jawed, Skalny and Young that although 5 stages were indicated only 3 are of primary importance. This was due to the arbitrary nature of the divisions between them. He believes that it may be simpler to only consider the 3 phases namely; first peak, second peak and finally, the steady state situation. These categories may be better described as the early, middle and late hydration phases and correspond to stage I+II, III + IV and finally V respectively

Jawed, Skalny and Young [18] state that stage I corresponds to the first few minutes of hydration in cementitious materials, with the transition between stages I and II being affected by parameters such as the water solid ratio and temperature. Early stage hydration is the most difficult to study due to rapidity of the hydration reaction and the limitations of time taken with respect to sample preparation. This may be overcome by the adoption of injection methods of sample preparation.

The level of accuracy attained by the adoption of conduction calorimetry has been discussed by Lawrence [5] in which he believes that it is extremely good when compared with the traditional method of heat of solution (assessed via standard

deviation). Lawrence continues to indicate that the total heat evolved has an accuracy measured with less than 1% error. His studies were undertaken adopted the JAF conduction calorimeter similar to the one used in this research. He believes that with this method of assessing heat of hydration 'a separation of the hydration reactions for the different cement minerals present' [5] may be ascertained.

In addition to the determination of the individual hydration products, Jawed, Skalny and Young's research has shown that the shape of C_3S hydration plots may lead to the assessment of admixtures such as accelerators or retarders. Figure 18 indicates 4 alternative mixes including, accelerated set, A, Fast hardening, B, normal, C, and finally retarded set, D.

Figure 18: Effect of admixtures upon conduction calorimetry plots [18]

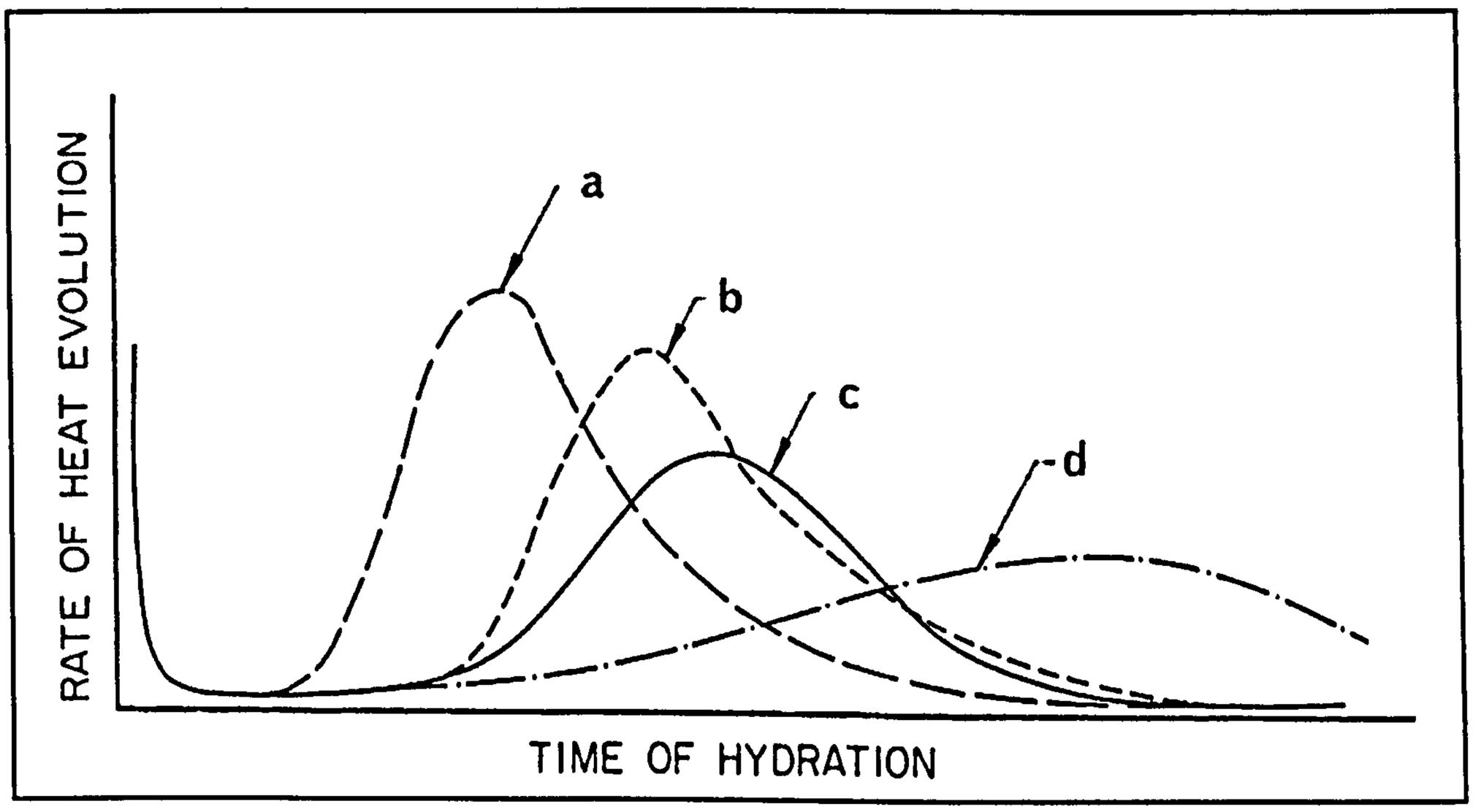

Lawrence's [5] study provided graphical representation of OPC samples in the form of heat evolution curves adopting varying water / cement ratios, These may be seen in figures 19 and 20.

Figure 19: Heat of hydration curves adopting 0.375 w/c ratio [5]

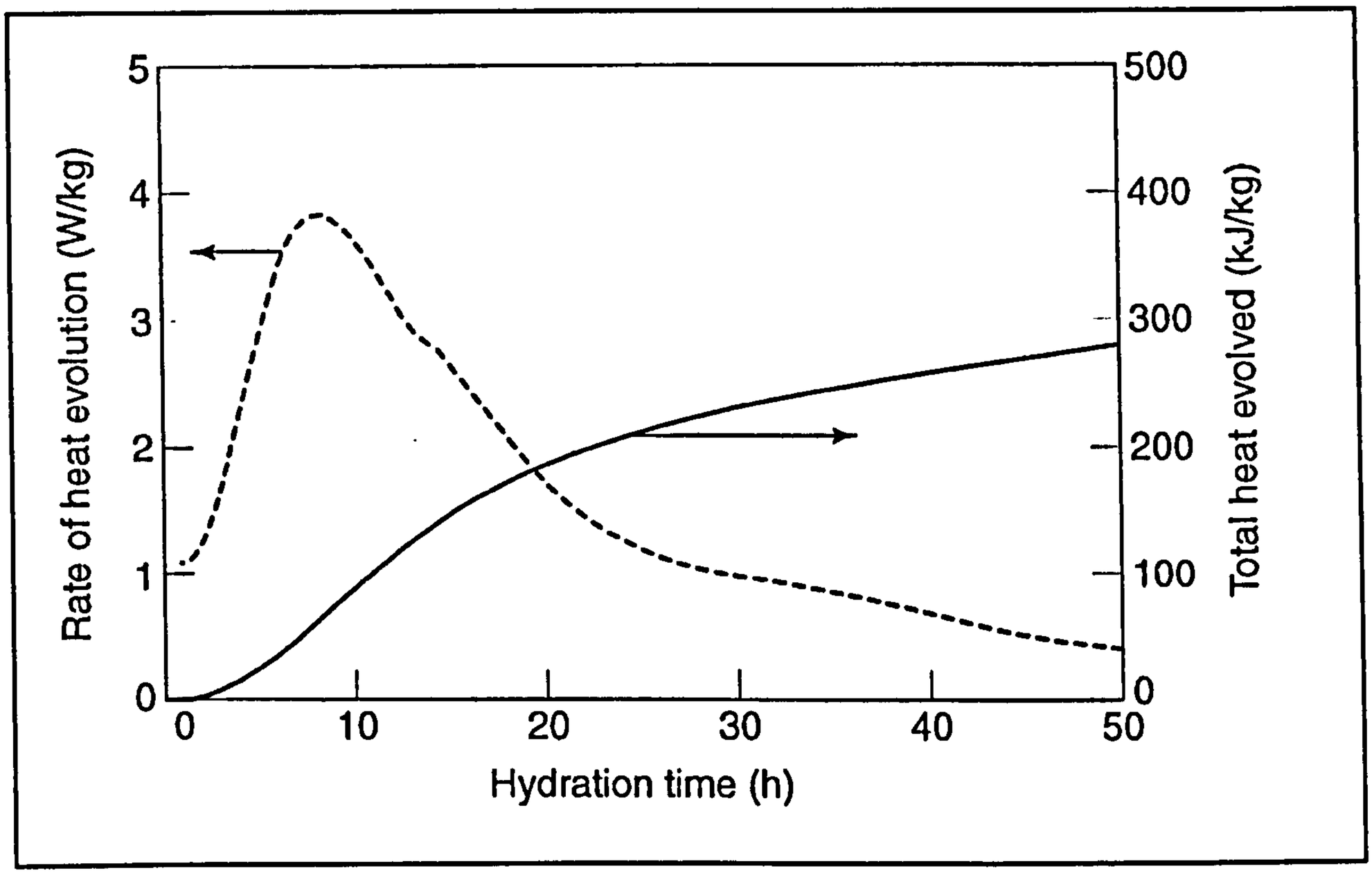

Figure 20: Heat of hydration curves adopting 0.440 w/c ratio [5]

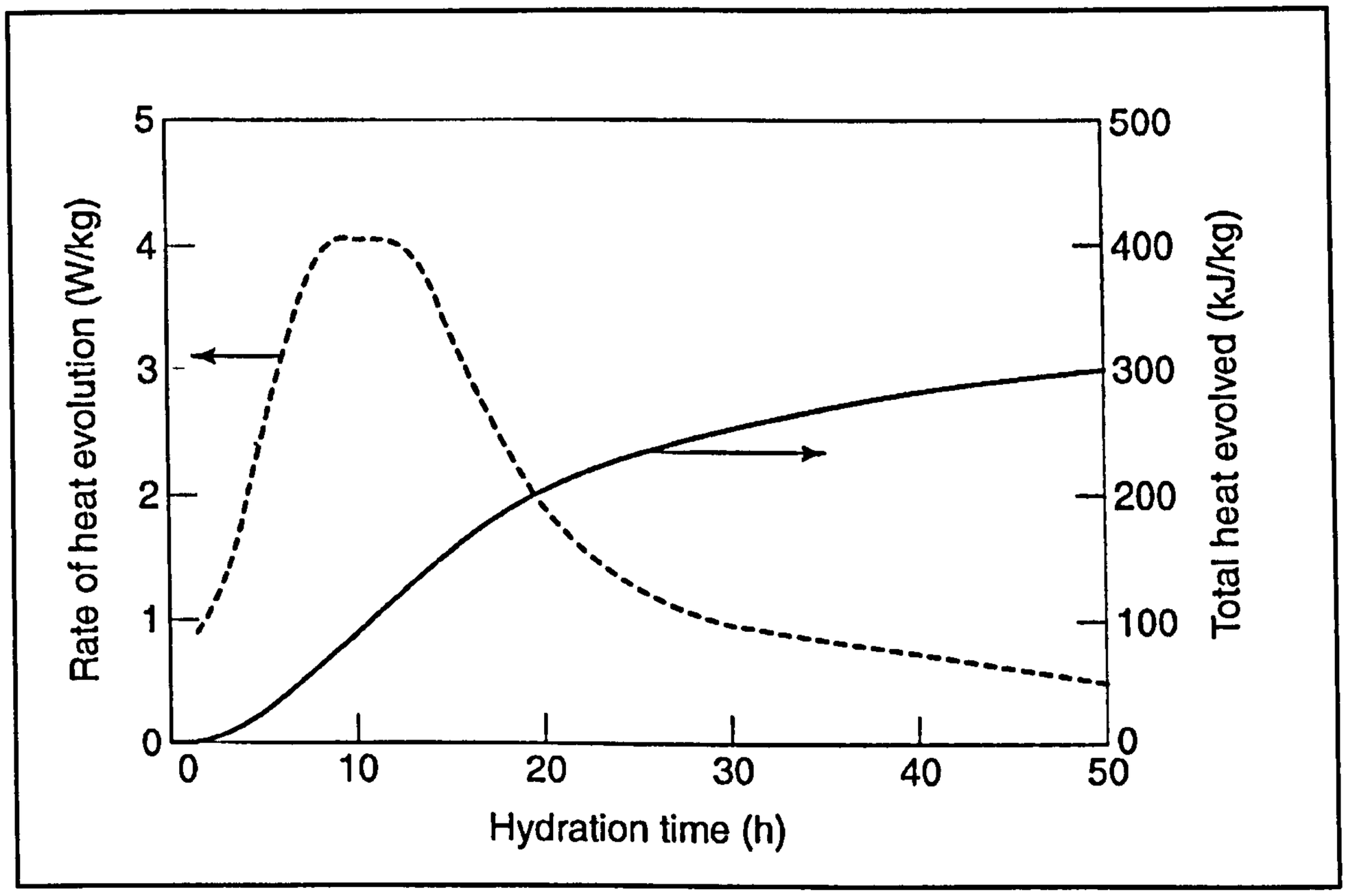

Jawed, Skalny and Young [18] elaborate upon the former authors work upon cement hydration via conduction calorimetry. They note that hydration is a complex dissolution - precipitation process in which various hydration reactions proceed simultaneously and at different rates and may be influenced by each other. The result of the dissolution of anhydrous phases enables the formation of compounds whose solubilities are lower than

the anhydrous clinker materials leading to the precipitation of colloidal and crystalline hydrates that form hardened pastes [18].

The fundamental process of ionic exchange between clinker species of cement when in contact with water has been explained by Jawed, Skalny and Young [18] as an exchange between solid and liquid. They indicate that different clinker types have varying solubility rates that will ultimately affect the concentration of the liquid phase and will have specific relevance to the calcium aluminate, sulphates and alkalis phases that react extremely quickly when compared with other products. This may be graphically seen in figure 21 [18].

Figure 21: Schematic representation of cement hydration [18]

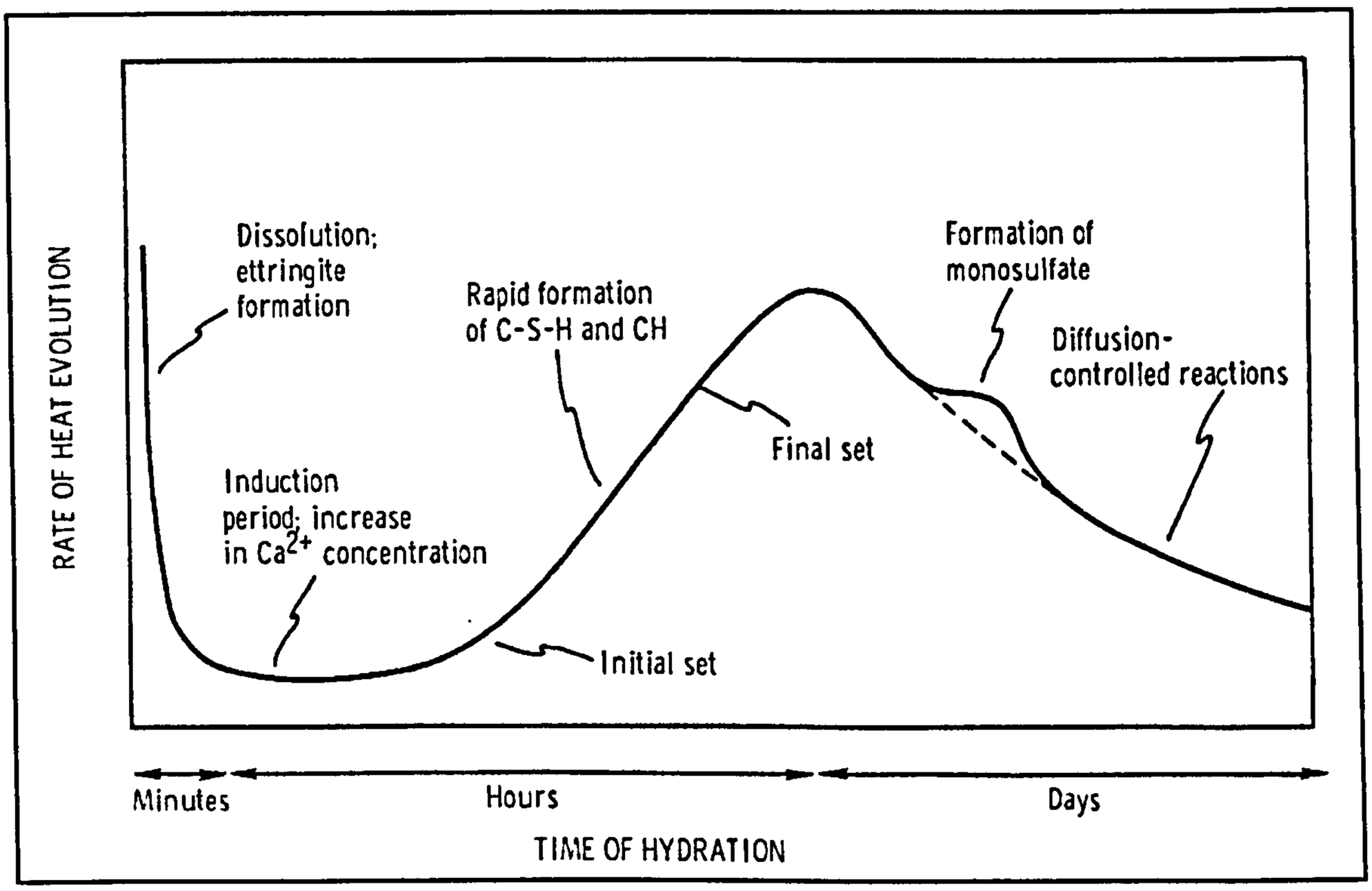

Jawed, Skalny and Young's research has led to the description of the reactions in cement in both tabular and graphical representations. Emphasising that heat evolution curves may be produced for individual pure components or for the holistic material. This is reflected in table 13.

Table 13: Meaning of basic hydration reactions in OPC (author after Jawed, Skalny and Young) [18]

Reaction stage	***Chemical Processes***	***Physical Processes***	***Relevance to mechanical properties***
First minutes	Rapid initial dissolution of alkali sulphates and aluminates; initial hydration of C_3S; formation of Aft	High rate of heat evolution	Changes in liquid phase composition may influence the subsequent setting
First hours (induction period)	Decrease in silicate but increase in Ca^{2+} ion concentration; formation of CH and C-S-H nuclei begins; Ca^{2+} concentration reaches a supersaturation level	Formation of early hydration products; low rate of heat evolution; continuous increase of viscosity	Formation of Aft and Afm phases may influence setting and workability. Hydration of calcium silicates determines initial set at end of induction period
Approximately 3-12h (acceleration stage)	Rapid chemical reaction of C_3S to form C-S-H and CH; decrease of Ca^{2+} supersaturation	Rapid formation of hydrates leads to solidification and decrease in porosity; high rate of heat evolution	Change from plastic to rigid consistency (initial and final set); early strength development
Post acceleration stage	Diffusion-controlled formation of C-S-H and CH; recrystallisation of ettringite to monsulphate and some polymerisation of silicates possible. Hydration of C_2S becomes significant.	Decrease in heat evolution. Continuous decrease in porosity. Particle-to-particle and paste-to-aggregate bond formation	Continuous strength development diminishing rate. Decrease in creep. Porosity and morphology of hydrated system determine ultimate strength, volume stability, and durability

Jawed, Skalny and Young [18] have highlighted 3 cautionary factors to be considered when undertaking conduction calorimetry studies. These are:

I) The rate of heat evolution is not linearly proportional to the degree of hydration or development of physical properties.

II) Isothermal hydration studies do not properly represent hydration processes in engineering applications where concrete develops mechanical properties in semi-adiabatic rather than semi-isothermal conditions.

Cement hydration heat evolution curves represent the overall response of the calorimeter to a set of chemical reactions.

2.6 Non-hydraulic lime hydration.

The hydration of non-hydraulic limes differs greatly from that of hydraulic limes in so much as no hydraulic compounds exist in pure fat limes. The hydration or slaking of a non-hydraulic lime is essentially a reaction between CaO and water, yielding $Ca(OH)_2$. These materials do not set underwater.

Boynton defines hydration as *'the reaction of the lime and water'* [23] and continues, emphasising that hydration and slaking are essentially one and the same. The reason for the simplicity of the definition put forward by Boynton may be explained by his area of study which only relates to non-hydraulic limes, these have no or trace element of reactive silicates and aluminates and for that reason do not form C-S-H. He [23] explains that the hydration of non-hydraulic limes generates hydrates in both dry powder form, or a putty which is achieved by adopting an excess of water for the hydration / slaking process. Hydration yields a strong exothermic reaction but this is not due to hydraulicity but to a rather volatile reaction between the calcium oxide and the water, yielding calcium hydroxide. Substantiating this, Boynton [23] gives values emphasising the volatility of lime slaking, stating that the 'heat of hydration of 1lb (0.45kg) of pure quicklime is sufficient to heat 2.3lb or 1.04kg of water from 0°C to boiling point (100°C)' [23]. He also indicates that the hydration of non-hydraulic limes may be considered as a reversible reaction, hence dehydration recreates quicklime by volatising water into vapour. Boynton explains this chemically reversible nature within the following limes [23].

Table 14: Reversible reaction of non-hydraulic limes, $CaO \leftrightarrow Ca(OH)_2$ (author after Boynton) [23]

High Calcium Hydrate
CaO (h.c. quicklime) + $H_2O \leftrightarrow Ca(OH)_2$ (h.c. hydrate) + heat ↑
$Ca(OH)_2$ (h.c. hydrate) + heat ↔ CaO (h.c. quicklime) + H_2O (vapour) ↑
Normal dolomitic hydrate
$CaO \cdot MgO$ (dol.quicklime) + $H_2O \leftrightarrow Ca(OH)_2 \cdot MgO$ (dol. Hydrate) + heat ↑

Boynton indicates that the predicted hydrate values depend upon the oxide and lime solid content, namely, CaO and MgO. Boynton believes that high calcium limes will slake more effectively than dolomitic limes due to hard burning.

Boynton [23] indicates that the non-hydraulic limes may be produced post slaking in several forms, including dry hydrates, putties, slurries and milk and saturated solutions (hydrates).

2.7 Calcination considerations of non-hydraulic and hydraulic limes

The principles of calcination theory are explained by Boynton [23] in which he indicates that thermal decomposition is a principal chemical property of lime, following the basic formation of $CaCO_3$ to CaO, via the expulsion of CO_2. The calcination temperature and duration is important when assessing the production of hydraulic lime, as different temperatures will give rise to differing phase compositions which will have a direct relationship upon the C-S-H formation within the lime. This will influence the hydraulicity of the material. However, Boynton [23] indicates that calcination and therefore, thermal decomposition is affected by the dissociation temperature and rate of dissociation of CO_2, purity of the lime and crystallinity of the limestone. He noted that the highly crystalline limes tend to dissociate at lower firing temperatures and vice versa. However, in reality the process of calcination may be more complicated due to varying levels of impurities present with the limestones.

The possibility of attaining no impurities in limestone is explained in the St Astier manufactures data believing 'the composition of the earths crust shows the predominance of silica and its presence is almost inevitable in all limestone deposits' [27]. Both Boynton [23] and Glasser [5] indicate that silicates, aluminates and other impurities combine with CaO at high temperatures and form complex phase systems. Hence, during calcination, silica and alumina reactions increase within the elevated atmospheres enabling formation of basic hydraulic compounds within lime.

The calcination of hydraulic limes has been described by St Astier [27] (lime manufactures) in which they reinforce the aforementioned information, believing that the combination or partial combination of silica, aluminium and iron oxides with quicklime results in the formation of; silicates, aluminates and ferrites.

Generally, integral impurities do not combine at low temperatures, that is to say below approximately 900°C. However, Boynton [23] explains that with temperatures approximately above 900°C complex calcium compounds will form.

As aforementioned the calcination temperature is an imperative factor to be considered when assessing hydration. It must however, be emphasised that particle size also has a significant affect upon the rate of hydration.

2.7.1 Particle size of hydraulic materials

The particle size in hydraulic materials will influence the rate of hydration and also the distribution of the particles within a matrix. Hughes and Swann [21] have indicated that a hydraulic limes demand for water (w/l ratio) is reflected in the particle size and the $Ca(OH)_2$ content. The water demand is reflected in table 15, indicating that D_{50} and D_{70}, which refers to 'the particle sizes below 50 and 70% of the value of the lime particles' [21].

Table 15: particle size in hydraulic limes (author after Hughes) [21]

Limes	W/l ratio	D_{50}	D_{70}	$Ca(OH)_2$ (%)
St Astier NHL2	0.526	5.34	16.28	43
St Astier NHL3.5	0.436	11.64	27.51	28
St Astier NHL5	0.388	18.49	39.16	23
Jura-Kalk	0.300	23.84	53.30	2

A reduction in the particle size is generally associated with an increase in the rate of hydration. This occurs due to the increase in the rate of hydration. This occurs due to the increase in surface area in contact with the water. This will also reflect in the rate of dissolution and saturation of Ca^{2+} in the liquid phase.

Table 16 indicates the results of Blaine fineness of cement powders and more specifically individual hydrates, determined via SEM/X-ray imaging with the addition of optical microscopy. It is interesting to note that in Portland cement preferential grinding of the clinker may occur with the resulting material having altered properties, for example the increased grinding of C_3A over C_3S [28].

Table 16: Blaine, Volume fraction and surface area of primary hydration products

		Cement Powder				
		Blaine Fineness (m^2 / Kg)				
Phase	**Clinker**	654.0	540.7	370.0	279.0	197.0
	Volume Fraction					
C_3S	0.740	0.770	0.752	0.746	0.643	0.763
C_2S	0.163	0.142	0.134	0.130	0.212	0.089
C_3A	0.076	0.045	0.077	0.084	0.077	0.083
C_4AF	0.022	0.043	0.037	0.041	0.068	0.065
	Surface Area Fractions					
C_3S	-	0.713	0.712	0.692	0.599	0.713
C_2S	-	0.176	0.131	0.122	0.233	0.098
C_3A	-	0.061	0.110	0.123	0.098	0.116
C_4AF	-	0.050	0.048	0.064	0.070	0.073

The particle size of cements and hydraulic limes play an integral role in the pore structure development of hardened pastes and mortars. This will be briefly discussed in the following section, however, it must be emphasised that this is generally out with the remit of the research.

2.8 Pore structure development and characteristics

Jawed, Skalny and Young believe that the properties of hardened cement may be assessed by adopting what they call 'composite theories', [18] that is to say the development of the properties of individual components, aggregated to give a realistic impression of the hardened material. Therefore, cement and hydraulic limes may be viewed as complex composite materials, whose properties ultimately depend upon its components and their relationship to each other.

Cementitious materials are therefore porous with an 'intimate mixture of hydration products, both crystalline and amorphous' [18]. This is reflected in table 17, in which some of the primary hydration products in cement are emphasised.

Table 17: Properties of hydration products (author after Jawed, Skalny and Young) [18]

Compound	Typical morphology	Typical dimensions	Resolved by
C-S-H	Variable	~0.1μm	SEM, TEM
CH	Equant crystals	0.001-0.1μm	OM, SEM
Aft	Prismatic needles	10x1μm	OM, SEM
Afm	Thin hexagonal platelets or irregular 'rosettes'	1x0.1μm	SEM

The formation of the hydration products (as seen in table 17) in hydraulic lime and cement are greatly affected by the water used. Odler [5] discusses water and hydration in which he indicates that several categories exist, all playing a prominent role in the inter-relationship between the phases. These include:

- H_2O bound to the structure and within the structure of the C-S-H phase
- H_2O which is in the OH^- ions within the crystalline lattice of $Ca(OH)_2$
- H_2O which is bound to the surface of the hydrated phases (present via adsorption forces)
- H_2O which fills the gel and capillary pores of hardened paste

The latter of these directly affects the pore structure and performance of pastes and mortars. In addition Odler [5] indicates that two types of water exist within cement hydration however, this is also true for hydraulic limes. These are *'bound'* water and *'free'* water, bound water may also be known as combined or non-evaporable water, and free water is that which will ultimately lead to the development of pore structure of variable size. An increase in the water / solid ratio will see an increase in the pore system, however, this will decrease as hydration continues.

The affect of water ratios upon a cementitious materials ability to permeate water and water vapour is an integral factor to consider. This has been discussed in work by Neville and Brooks [6] who believe that a low w/c or w/l ratio will ultimately lead to low permeability. This is reflected in figure 22. In addition a reduction in the materials rheological properties will be encountered with a low water ratio and must always be considered in mortar manufacture.

Figure 22: Relationship between cement water ratios and permeability

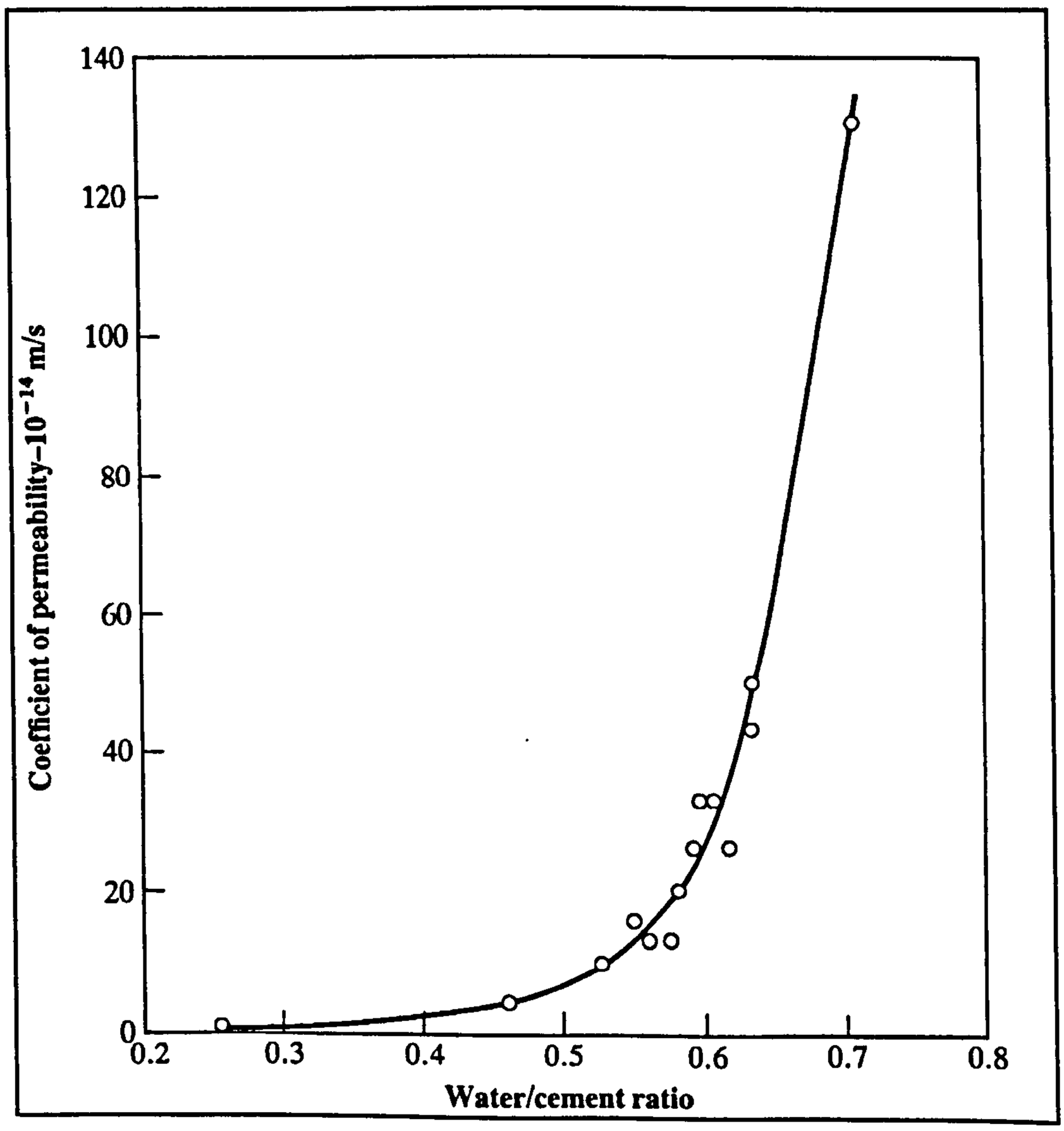

The pore structure of cementitious pastes may vary significantly in terms of size and distribution and this reflects upon the performance of the material. The size and importance of the pores may be seen in table 18.

Table 18: Pores in cement paste (author after Jawed, Skalny and Young) [18]

Classification	Size	Method of analysis	Origins	Importance
Large pores	>5x10^4 Å	Optical microscopy	Air entrainment; entrapped air; inadequate consolidation or curing; excessive mix water	Limit strength
Capillary pores				
Macropores	>500 Å	Mercury porosimetry	Remnants of water filled space in fresh pastes	Control permeability and durability
Mesopores	26-500 Å	Mercury porosimetry; gas adsorption desorption	Remnants of water filled space; smaller pores associated with C-S-H	Capillary effects create stresses during drying
Micropores	<26 Å	Gas adsorption-desorption	Associated with C-S-H	Disjoining effects may occur during wetting and drying

The determination of porosity in cement and limes alike is somewhat misleading when assessing performance, as it is the distribution and size of the pores that is of critical importance. Jawed, Skalny and Young [18] explain that cement may lack the interconnectivity of pores which greatly effect the permeability of the material. He continues to believe that micro pores should be considered a part of the C-S-H.

The porosity of the material decreases as the development of C-S-H continues and is further reduced by the development of $Ca(OH)_2$. These are relatively large hexagonal crystal types that 'engulf parts of previously formed C-S-H and the overall morphology becomes more and more featureless' [18] over time. Neville and Brooks [6] believe a decrease in permeability is caused by the densification of C-S-H types within the pore structure. This is reflected in figure 23.

Figure 23: Decreasing permeability with age [6]

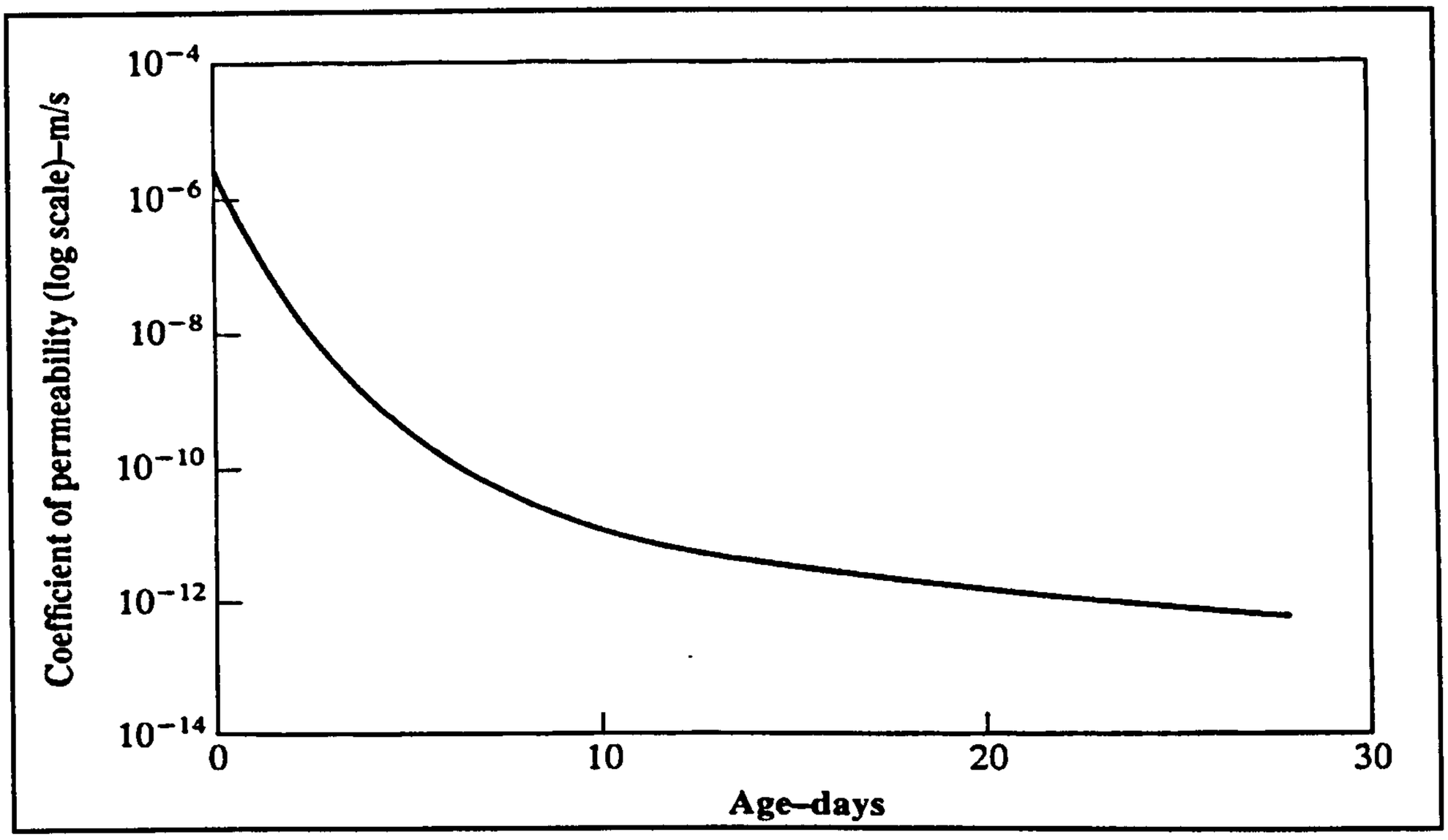

The concept of pore interconnectivity has been discussed by Neville and Brooks [6] in which they reinforce work by Jawed, Skalny and Young, believing that it is the nature of the pore structure rather than the total porosity that is the primary factor to consider when assessing permeability. Figure 24 indicates this theory with figure A, showing an interconnected pore structure and figure B, showing a relatively segmented structure, both of which have the same total porosity.

Figure 24: Idealised segmented and interconnected pore system in cement pastes [6]

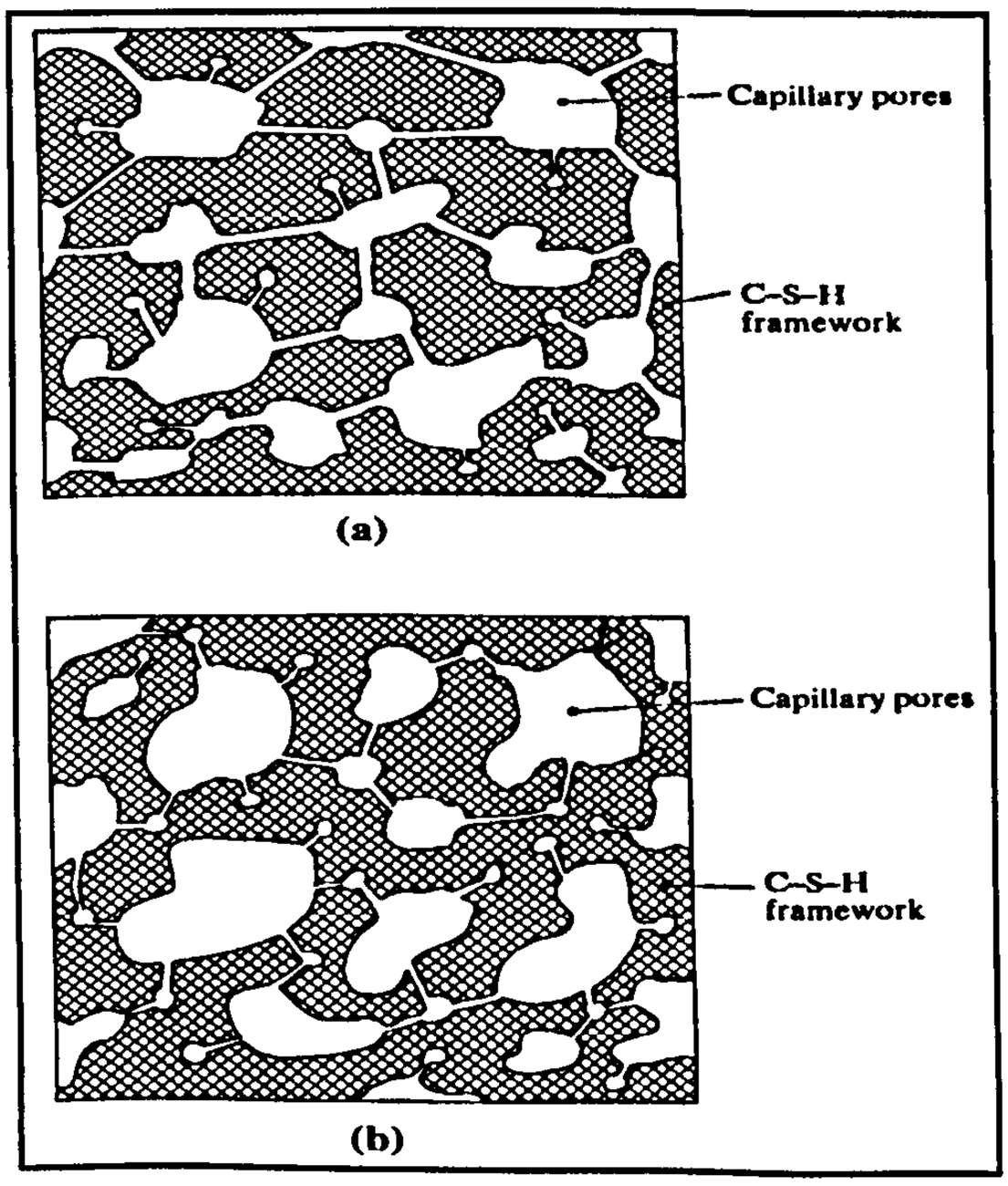

The relationship between the volume of free water and the level of pores formed, equates to the porosity. Odler [5] indicates that the porosity will reduce as hydration continues, being partially due to the water becoming bound within the formed C-S-H phase. He believes that cementitious pore systems include hydraulic radii, gel pores and capillary pores, defining the hydraulic radii pores as 'the ratio of the volume to the surface area of a pore fraction' [5], that are generally within the range of between <1 and 1000nm. He continues to emphasised that the greater the W/C ratio the higher the hydraulic radii pores tend to be, and as aforementioned these pores will decrease in size with the progression of hydration.

Very small pores which exist within the hardened pastes and must be considered as an integral part of the hydrated material, and are commonly known as 'gel pores' [5]. Pores whose diameter increase with increasing levels of W/C ratios are known as 'capillary pores' [5]. However, it must be emphasised that the distinction between the pore structure types may not necessarily be clear and they may be considered one and the same in certain instances.

The relationship between capillary porosity and fraction of connected pores in various cements and pozzolans is indicated in figure 25. It is clear to see that an increase in capillary porosity relates to an increase in fraction connected.

Figure 25 : The relationship between porosity and water/cement ratios [29].

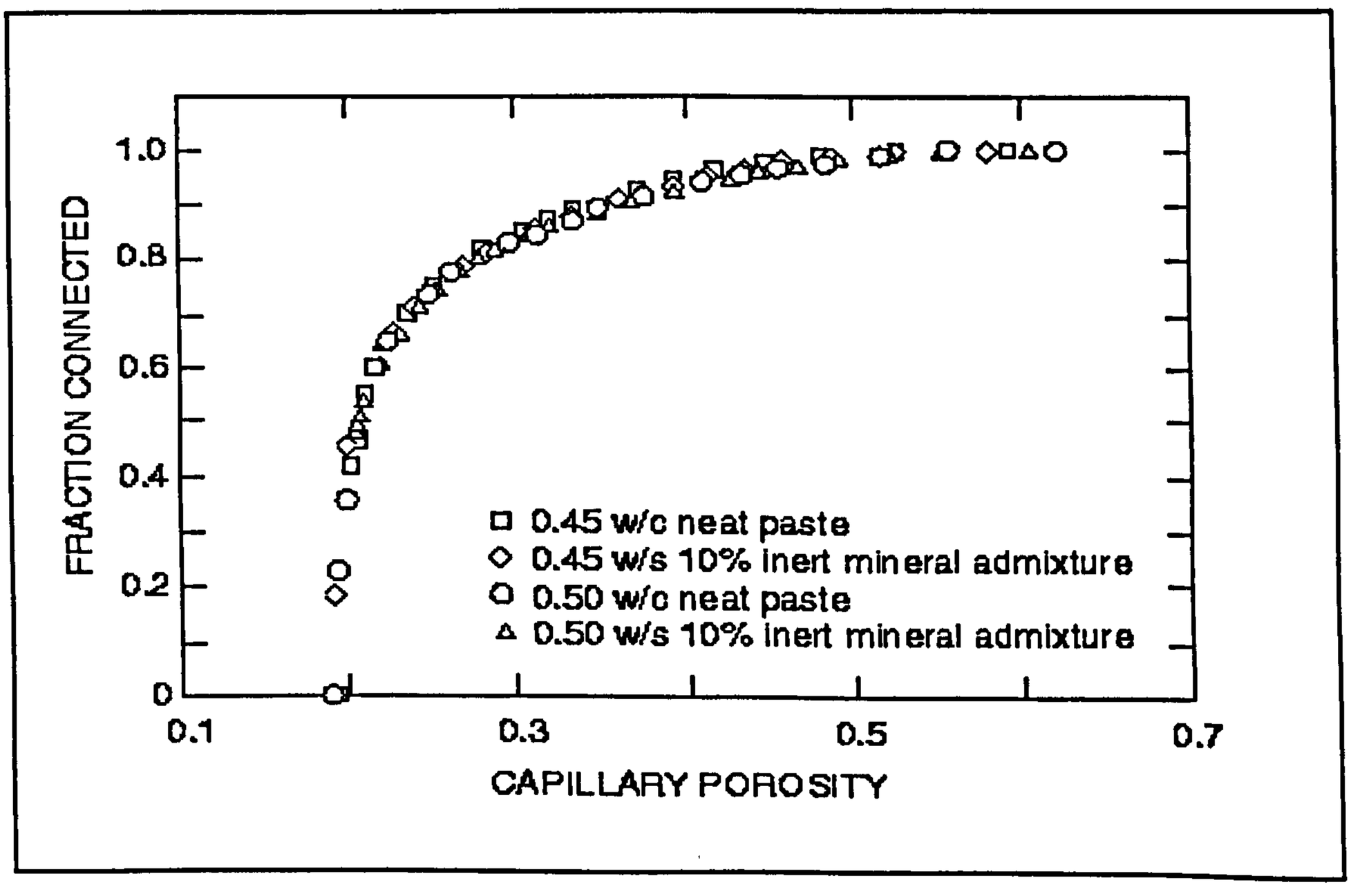

The degree of hydration effects the formation of interconnected pores, this is indicated in figure 26 below. This relationship suggests that with an increase in hydraulicity of the cementitious material, a decrease in the fraction of interconnected pores will be exhibited.

Figure 26: The relationship between hydration and the fraction of interconnected pores [29]

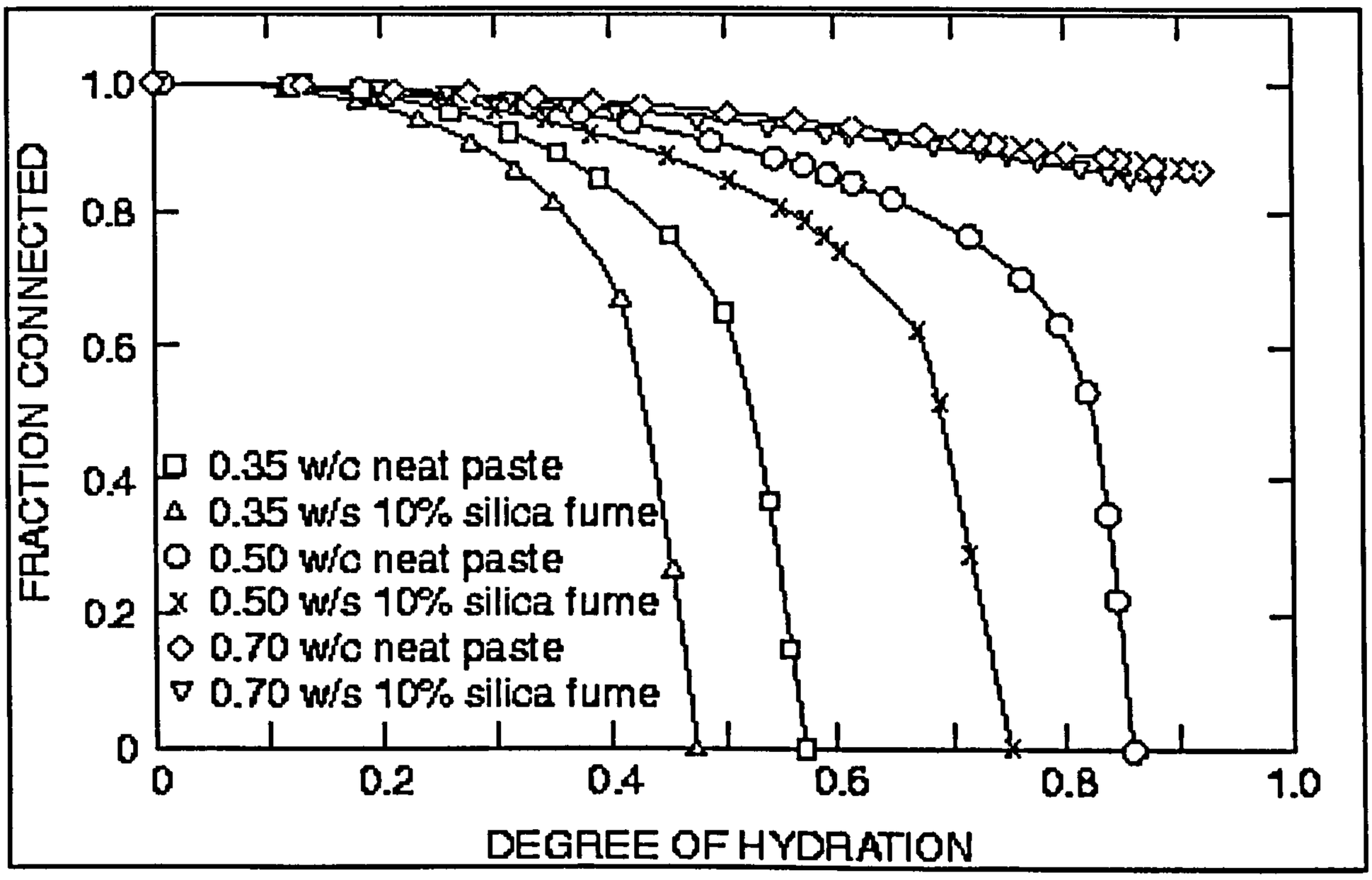

Lawrence discusses physicochemical and mechanical properties of Portland cement believing that Portland cement microstructure is 'complex and gives rise to time dependant physical and mechanical properties, with significant changes occurring over months or years' [5]. He continues to emphasise that it is not simply a case of hydration, as ageing processes do come into play within the colloidal hydration products. It is interesting to note that pore sizes in excess of 1 micron are capable of allowing water vapour to pass through their respective structure. However, below 1 micron, water vapour transmission will encounter great difficulty.

Lawrence indicates that the chemical binding of water to the hydrates allows a series of energies to be embodied, resulting in a ready loss of moisture over a wide range of humidities. The water molecules subsequently readjust between different micro-structural sites with a responding change in environmental temperature and humidity [5]. Lawrence discusses the inadequacy of existing knowledge pertaining to physico-mechanical and mechanical properties of Portland cement stating that 'The fundamental

relationships between practical performance and chemical or physical microstructure are not at present reliable' [5].

The pore structure is important, but it must be emphasised that it is not the only consideration in the permeability of the material. It is therefore also important to consider the relationship between the binder, aggregate and the physical characteristics of the aggregate.

Odler discusses the importance of the cement paste aggregate interface, believing that the physical and chemical properties of the hydration phase will alter depending upon the constitutional differences of the material. The interaction between the two is known as the 'transitional zone' [5]. In non-hydraulic limes the affinity between the lime particles and the aggregate are often poor and this affects the bond characteristics and the pore structure development. However, in cements and hydraulic limes this is somewhat different and is generally characterised by a thin layer of $Ca(OH)_2$ which forms after adhering to the aggregate, followed by a rod like formation of C-S-H gel particles which adhere to the $Ca(OH)_2$.This assemblage is known as the 'duplex film' [5], and is generally, only 1-2μm [5]. However, conflicting theories exist, offered by Scrivener and co-workers [5], in which they refute the idea of a total $Ca(OH)_2$ film and the consequent formation of the duplex film. However, they have formulated the theory that growth from the aggregate develops from whatever phase is in direct contact with the aforementioned. They also believe that it is the C-S-H phase which, generally interacts with the aggregate surface.

Figure 27 : Theoretical 'Duplex film' formation

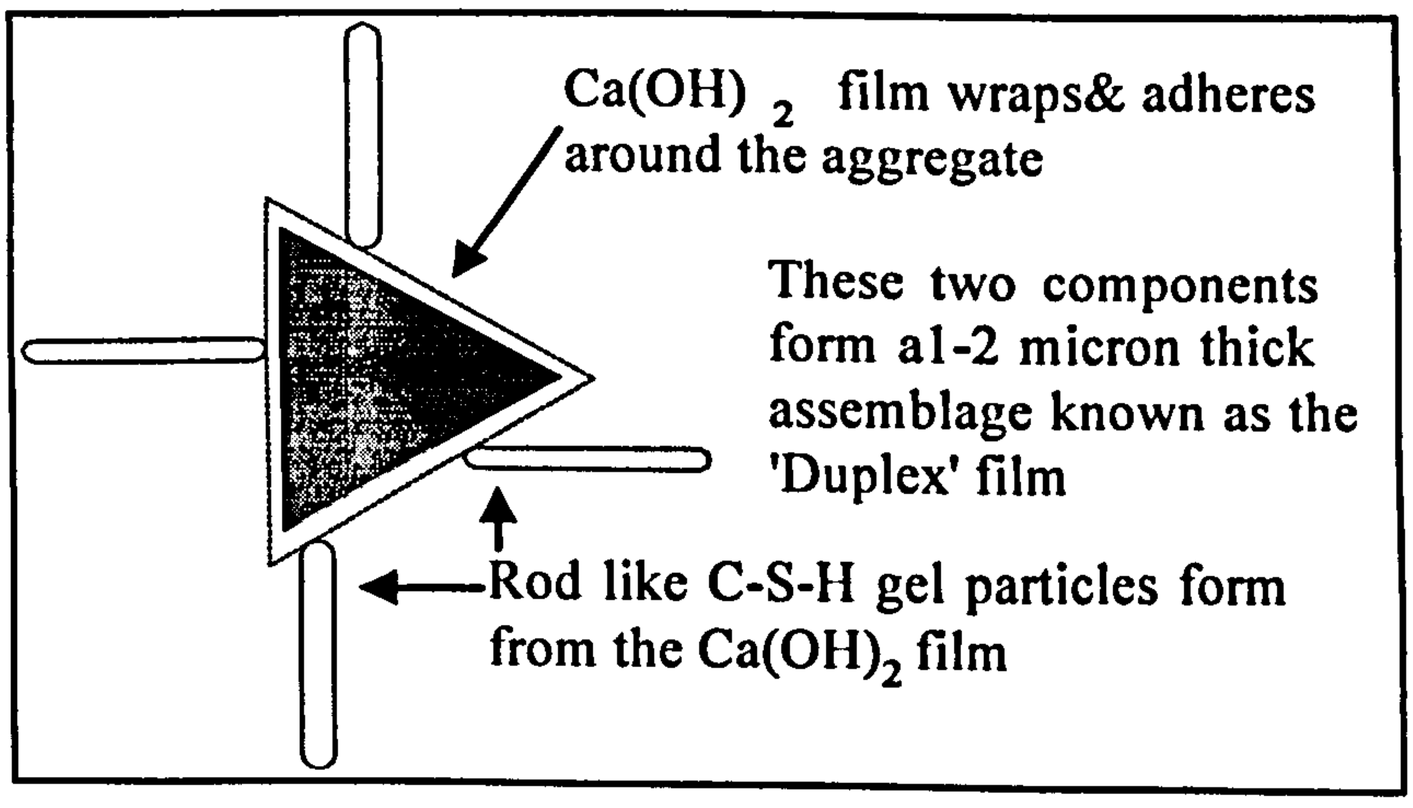

Odler [5] believes that differentials in the density of the cement paste are seen between the interface of the aggregate and that of the bulk cement paste. This is due to the formation of a water film, which is located at the aggregate surface. This region is rich in $Ca(OH)_2$ and hence, the ion flow and formation takes place from the cement paste to this zone. Hence, precipitation of these ions occur after migration within the transitional zone. It is believed that the transition zone is enriched by secondary $Ca(OH)_2$ and ettringite. It is interesting to note that the interface region is generally within the range of 30-60μm. Certain aggregates will induce a chemical reaction within the cement paste as well as being reactive themselves, e.g. calcium carbonate aggregates in the presence of C_3A will produce a calcium carboaluminate reaction. Unfortunately information pertaining lime based materials performance in this area is somewhat lacking and requires further attention.

2.9 Current testing and terms for water vapour permeability

The traditional tests of water vapour permeability in cementitious materials have a rather chequered history, with questionable testing methods, a lack of continuity of data and a lack of internationally recognised data. This has attributed to the confusion associated with water vapour analysis and information free flow transfer. An example of this lack of uniformity can be seen in table 19.

Table 19 : Differences in data collection and test procedures [30]

ASHRAE	*CIBSE*
Differentiates between homogeneous and non-homogeneous materials (conductance for stated thickness).	No differentiation, conductance determined from component part conductivities and air space resistances.
Quotes dry state values which are not representative of materials in use.	Compensates for moisture so that values are representative of materials in use.
Source of data well documented.	Source not well documented.
Known test procedures: ASTM C-518 (guarded hot plate) or ASTM C-177 (heat flow meter method).	Test procedures largely unknown (guess: pre-standard guarded hot plate). BS 874 for new entries.
For non-homogeneous material ASTM C-236 (guarded hot box) or (calibrated hot box) recommended.	Calculation recommended.
Data intended for computation of steady state U-values.	Data more useful for dynamic modelling.

It is hoped that this study will reduce the level of ambiguity in the area and lead to better understanding.

The study of the internal pore structure in lime based materials have been seldom broached. Those that have touched upon the subject have only developed empirical or very basic scientific data, which although useful is not independently rigorous enough. Once again this leads us to turn to limes closest relative, namely Portland cement, combined with general porous media studies to attain comparable information of their respective behaviour. The pore structure of Portland cement has been well studied and a great deal of information exists, this will be discussed later on in within this section.

The study of the flow of moisture in porous materials is generally believed to hinge upon two primary considerations, firstly the internal structure of the material and secondly, the laws that determine the moisture transfer within the aforementioned internal network of pores. Saidani-Scott [31] indicates that it is not satisfactory to define porous media as *'solid bodies that contain "pores" due to the fact that it does not allow us to attain information relating to the geometrical formation of the pore structure, continuing to believe that 'intuitively, "pores" are void spaces which must be distributed more or less frequently through the material if the latter is to be called "porous". Extremely small voids in a solid might be called "molecular interstices" very large ones might be called "caverns". "Pores" are therefore void spaces of volume intermediate between caverns and molecular interstices; the limitation of their size is therefore rather intuitive as well as their classification.'*

Alternatively, Walker and Morgan define pores as 'the spaces between the tangible particles of building materials ' [32], also stating 'the behaviour of the material is determined by the extent and the arrangement of the pores' [32]. They explain that adsorption of water into the building fabric is generally due to capillary action, although permeability also follows the same mechanisms. Water permeability must have an inter-connected route to allow water and water vapour transfer to occur.

Saidani-Scott [31] further believes that porous materials, whatever their constitution can be broadly classified into two areas, firstly, unconsolidated or consolidated which depends upon the rigidity of the matrix and secondly, ordered or random, depending upon the regularity of the pore geometry. Obviously all materials have varying water vapour diffusion characteristics, ranging from theoretically total impermeable to fully permeable. Figure 28 indicates the array of materials commonly adopted for

construction. It is clear to see that lime mortars (non specific) are placed between cellular concrete and gypsum plaster.

Figure 28: Water vapour diffusion coefficients for common building materials

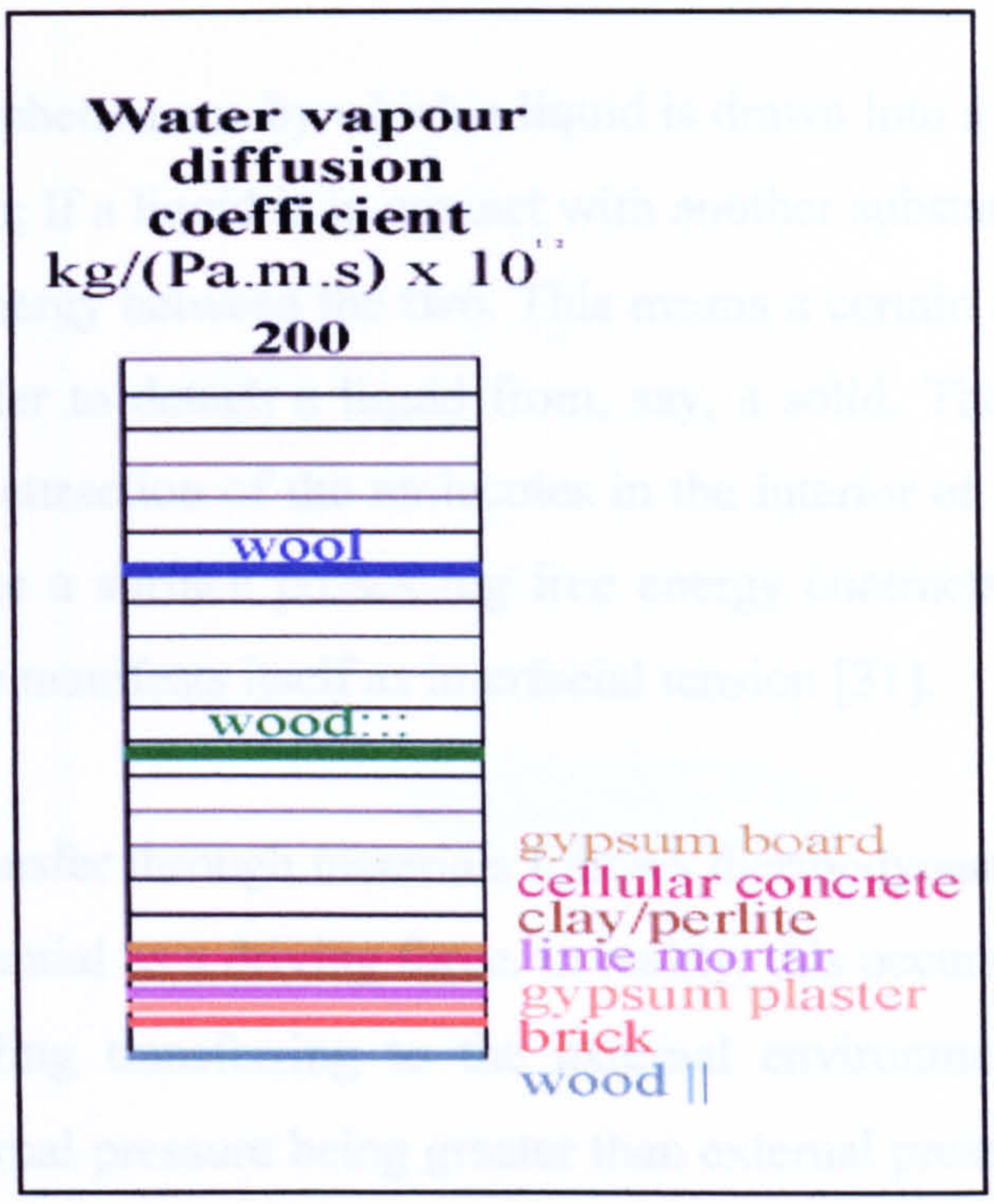

It is interesting to note that all of the materials mentioned fall within a similar numerical spectrum, namely x 10^{-12}.

The complexity of the study of moisture movement in porous media is hindered due to the number of terms used without clear definition. For this reason it is necessary to discuss certain essential terms which will be generally used throughout the document.

Permeability: has been described in the Dictionary of Science as 'the diffusion of gas or liquid under a pressure gradient through a porous material' [33]. This is the adopted definition for this work. Teutonico [34] defines permeability as in a more simplistic manner believing that it is 'The ability to transmit liquid or gas from one place to another'.

Porosity [35]: has been defined as the proportion (by volume) of the total volume of a material that is void.

Wettability has been defined as the extent to which a solid is wetted by a liquid, measured by the force of adhesion between the solid and the liquid phases [33]. The wetting of materials obviously depends upon the surface in contact with the water and is also dependent upon impurities within the water.

Capillarity is the phenomena by which a liquid is drawn into a narrow pipe by the forces of surface tension; If a liquid is in contact with another substance (gas or solid), there is free interfacial energy between the two. This means a certain amount of work has to be performed in order to detach a liquid from, say, a solid. The interfacial energy arises from the inward attraction of the molecules in the interior of a substance upon those at the surface. Since a surface possessing free energy contracts if it can do so, the free interfacial energy manifests itself as interfacial tension [31].

Water vapour transfer through materials follows thermodynamic activity that must have a pressure differential as a driving force. In reality, this occurs as a build up of moisture within the building transferring to the external environment (generally in northern climates the internal pressure being greater than external pressure). However, the rate of diffusion through a mortar must be a function of not only pressure and temperature but also the material's composition. The diffusion rate, or permeability through a sample requires a certain length of time to allow for a moisture equilibrium to occur within the sample. After a certain duration a steady flow of water vapour is traditionally believed to occur and this can then be recorded as the permeability function of the mortar sample. This diffusion follows Boyles' law once equilibrium is achieved within the sample and a steady rate of water vapour flow should be exhibited. Figure 29 shows the situation.

Figure 29 : Moisture flow in a diffusion experiment

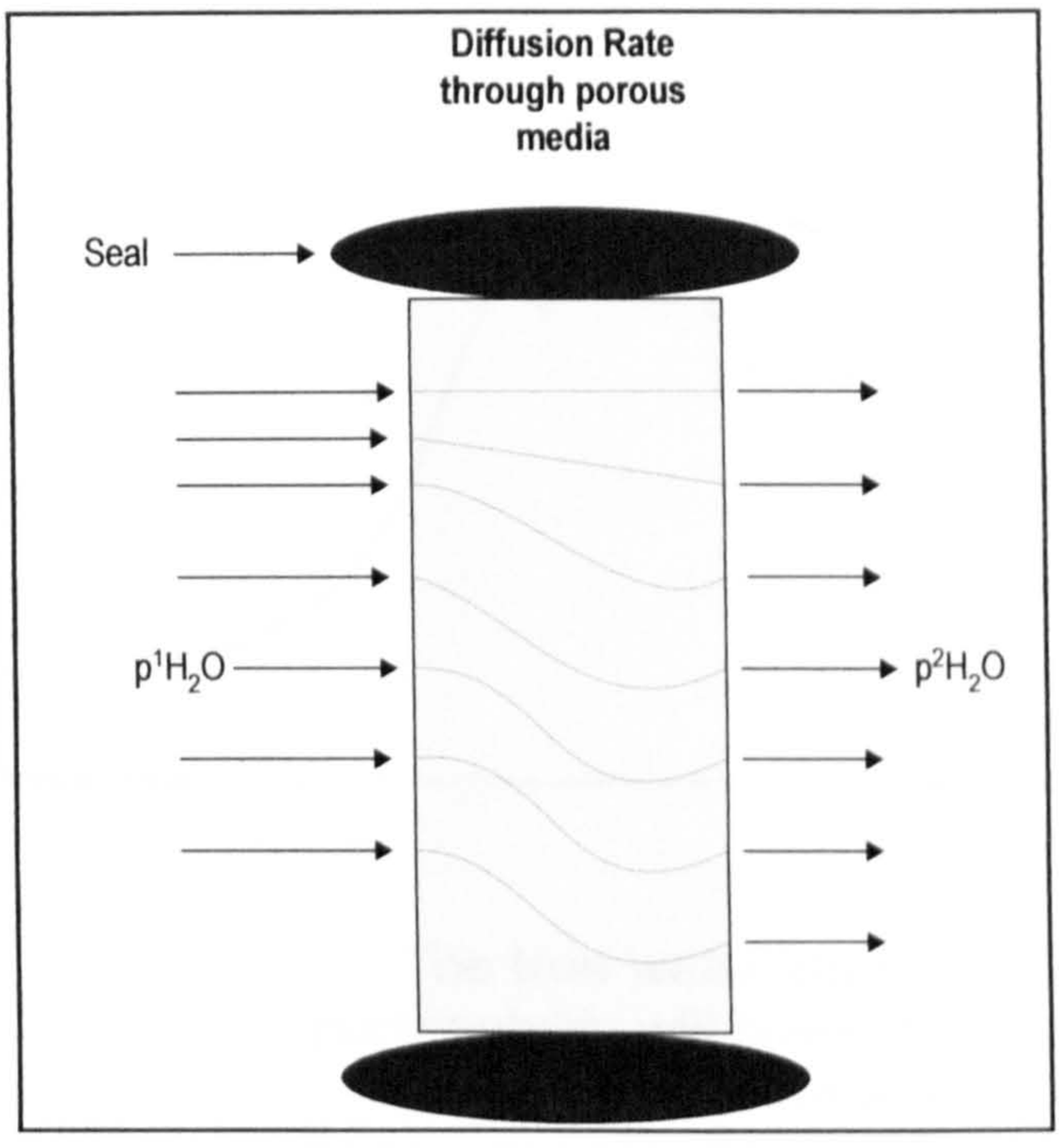

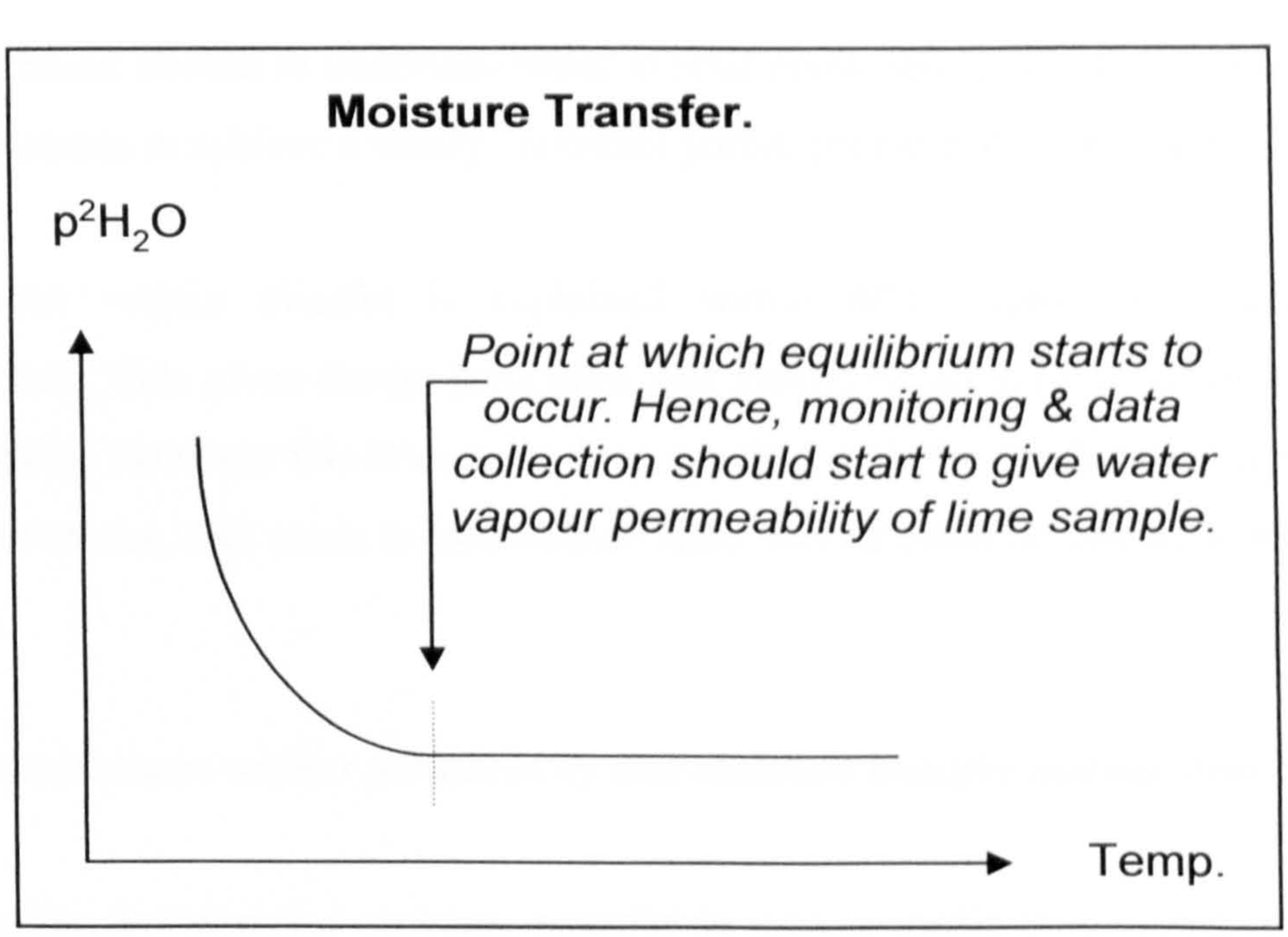

It is necessary to attain a constant water vapour pressure to allow for continuity of diffusion. In reality moisture transfer is not present at a constant rate and hence, a graph similar to the one shown in Figure 30 will occur.

Figure 30 : Non-steady state vapour diffusion

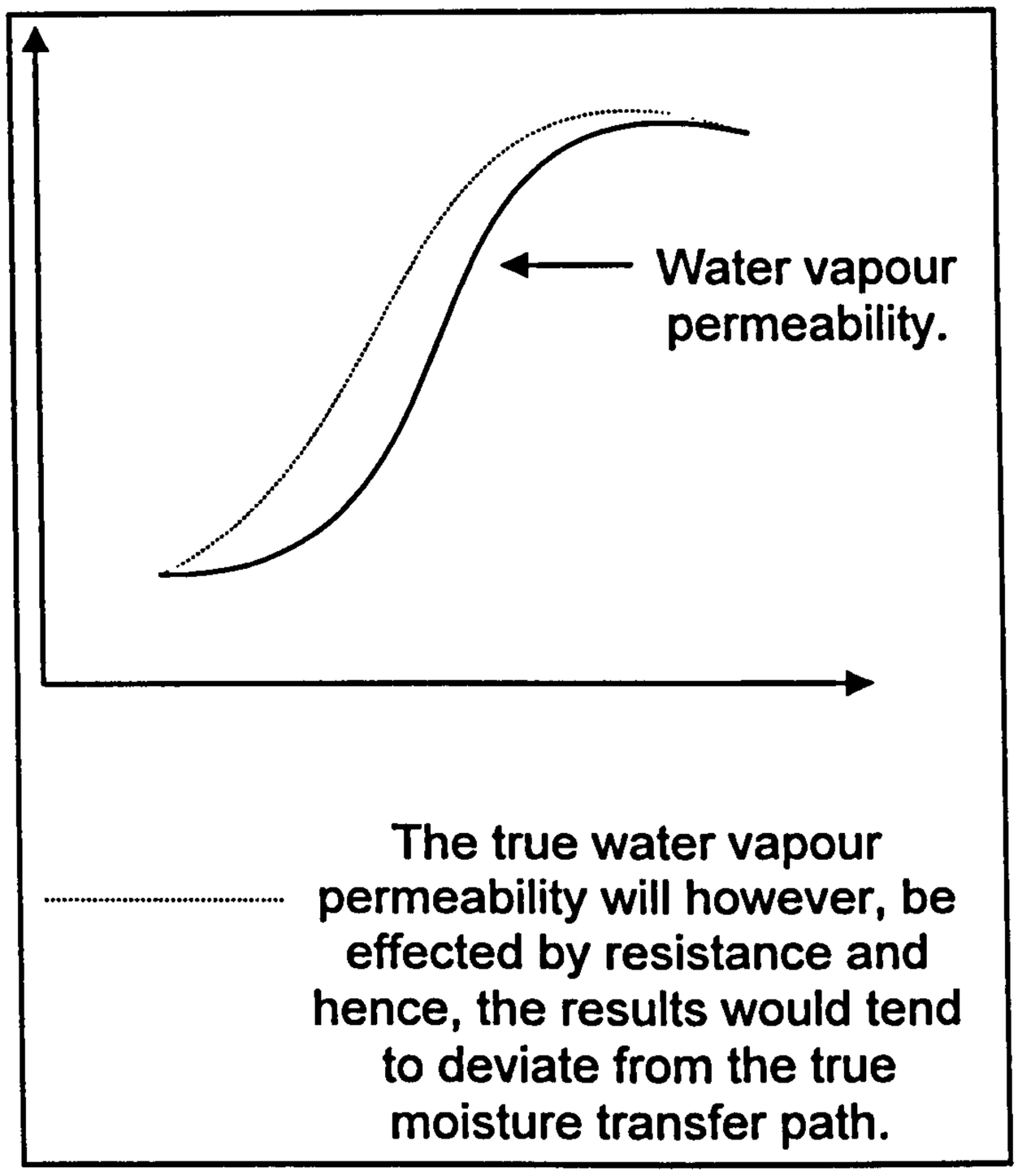

The experiment chosen to undertake water vapour permeability adopts a simple process using desiccants to achieve a steady / constant partial pressure of water vapour.

Basic water vapour transfer is explained within BRE digest 110 dealing with condensation. This gives design principles that should be adopted to avoid interstitial condensation. However this document does not deal with the mechanisms that lead to moisture transfer, and tends to concentrate upon the calculation side of water vapour transfer.

2.9.1 General water vapour permeability and moisture transfer mechanisms in porous media

Traditionally, the study of moisture transfer in porous media was rooted in research undertaken by Phillip and De Vries, in their works 'combined heat and moisture transfer in soils' [31]. In the 1960's and 70's Cary and Taylor (1964) and Valchar (1966) were developing the theories of irreversible thermodynamics [31]. This is important as these theories apply to porous building materials performance. Unfortunately, building materials are very complex and this makes the theory of irreversible thermodynamics difficult to apply to practical building situations.

Moisture movement through inorganic solids is complex to model and is hindered by the conditions generally being less than saturated and therefore, contents are non-uniform [31]. The concepts of wetting and drying follow the principles of energy transfer defined by irreversible thermodynamics. Cary and Taylor's work, developed models that allowed the study of the moisture movement within porous materials, based upon these principles. The primary force (or energy transfer mechanism) associated with moisture transfer is evaporation, which in-turn is driven by forced convection or by heating. Therefore, heat and water flow are related and generally involve steep temperature gradients.

Saidani-Scott in her works 'Analysis of moisture transfer in porous media' [31] emphasise that difficulties in predicting and measuring moisture transfer occur. These include:

- A steady state situation hardly ever occurs
- The moisture transport properties of a material vary significantly with moisture content and somewhat with temperature, so the problem is non-linear
- There is an appreciable spread in the material properties, even within different specimens of what appears to be the same material
- The boundary conditions for a calculation are not very well defined

Theoretically, a liquid surface will always tend to minimise surface area, with water molecules attracting the surrounding molecules with the result that the average force on an individual molecule, over a set duration is zero. Therefore, no surface tension exists between the water molecules, due to the nature of water bonding. However, at the boundary of the water and the material, tensions develop, with the resultant forces being equal and opposite.

Water vapour transfer in cementitious materials has been explained in simplistic terms by Cabrera and Claisse [40]. Their results showed that the flow of oxygen within dry cementitious materials followed Darcy's equation. Hence, oxygen transportation as a gas has a relatively easy flow across the material. Unfortunately water vapour flow does not due to the possibility of continuously changing moisture contents across the thickness of the material. Water will permeate cementitious materials in one of three mechanisms, namely: liquid, vapour and condensation.

Cabrera and Claisse [40] undertook wet cup experimentation believing that moisture transfer depends greatly upon local humidity and it was found that the rate of water loss was proportional to the amount of water remaining within the vessel with migration generally occurring exponentially. They continue to indicate that when they conducted their experiments they found that the rate of transport of water vapour was not found to vary greatly for the different samples and was proportional to the porosities of the samples. It is interesting to note that Cabrera and Claisse [40] believe that the adoption of silica fume can lead to the attainment of cementitious materials that are almost impermeable to oxygen and therefore to water vapour.

Bazant and Najjar [40] observed that the mean free path of a molecule of water at room temperature is many times greater than the size of continuous pores in concrete with Mills' observing that at 96% relative humidity, pores with diameters below 3.5mm will sustain meniscus. Hence, in cement based concrete at 100% RH. It is believed that the pores are all full of water or water vapour with the exception of the outer surface.

The principles of moisture movement and more specifically water vapour transfer in inorganic compounds have also been explained by Torraca [35]. His works are especially interesting as they are tailored to a building conservation. He [35] continues to explain that moisture transfer is predictable in inorganic compounds with certain material exhibiting properties that will aid or hinder moisture flow. He uses limestone as a prime example believing that they are rich in oxygen and hence, they are highly negatively charged, and as a consequence the oxygen molecules in the material repel the negative electrons within the water. This generates a weak bond between the water and the lime and encourages water flow within the solid.

It must be emphasised that although this may be true, lime mortars are by nature autogenous, with silica, quartz and other components comprising the matrix. These materials all have different electrical charges that either lead to attraction or repulsion of the water. Those materials that attract water are known as hydrophilic, and conversely those that repel water are known as hydrophobic. The capability of the materials to repel or attract water and the pore wall are affected by many factors, including, aggregate dispersal, C-S-H formation, pore size, pore distribution and internal geometric structure.

Torraca also discusses the concept of polar liquids that show weak bonding to material surfaces. This is due to the nature of their contact angles between the solid and liquid, indicating that water is to be considered a polar material. A large contact angle between the water and the material will create a weak attraction and vice versa. These contact angles are attributed to a liquids internal molecular formation. Hence, the internal structure of a liquid effects the attraction between liquid and solid.

Figure 31: Effect of contact angle [36]

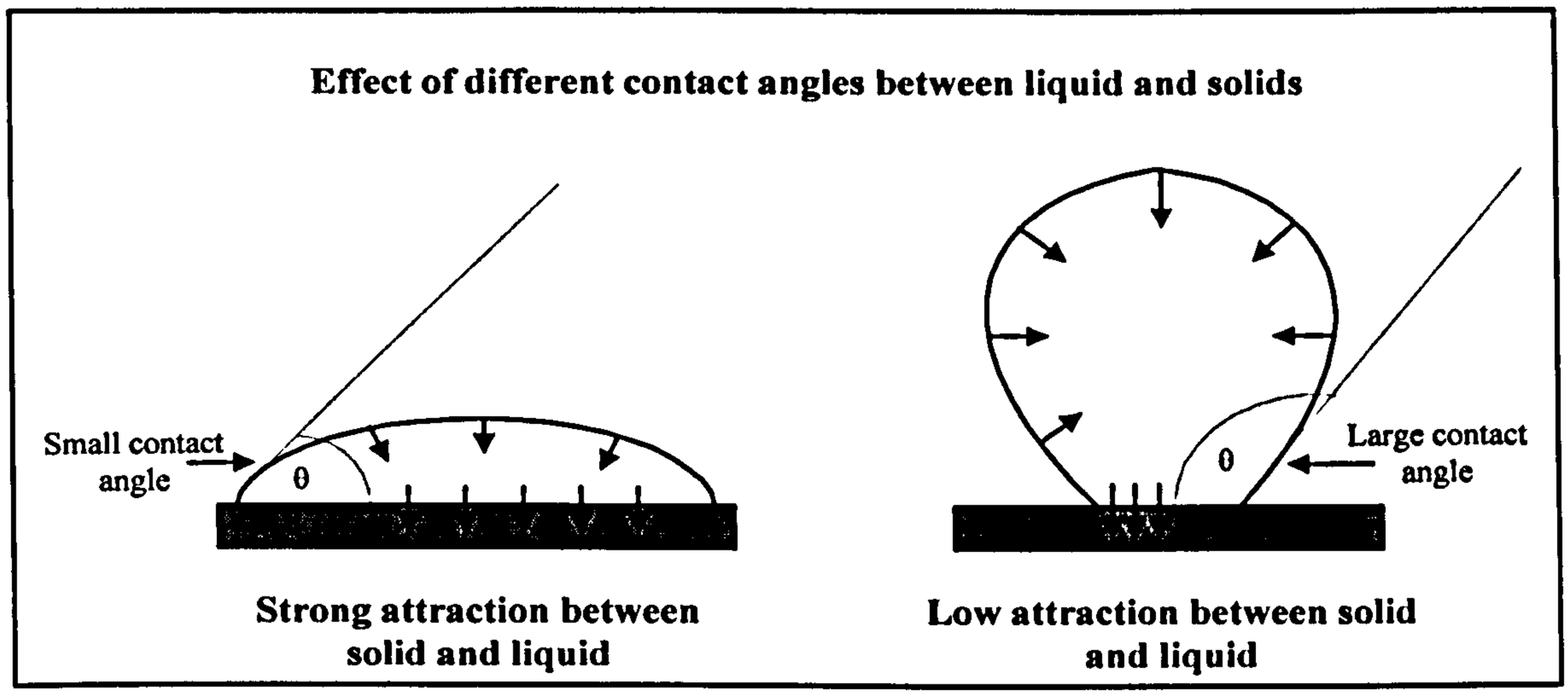

This is reinforced in work undertaken by Buckman [36] upon wettability of surfaces, believing that 3 basic forms of contact angle exist when assessing wettability conditions. The aforementioned may be seen in table 20.

Table 20 : Wetness classifications.

Wetness classification	Contact angle 0°
A) wet water condition	< 90°
B) Intermediate wetness	90°
C) Oil wet	> 90°

As the names suggest, they relate to the effect of the porous solid upon the moisture within the material. Hence, wet water conditions will only occur in those materials that have water attraction capabilities. Obviously, the term water wet relates to the material's moisture transfer capability and is not indicating that, rather ridiculously, some water is wetter than others.

The complexity of moisture flow in porous media is further increased if the material is non-uniform in characteristics. Hence, the flow of moisture will be affected by:

- Pore diameter and pore distribution and internal geometric structure
- Aggregate grading dispersal and shape
- Aggregate porosity
- Water / lime ratio
- Impurities within mortar or within the water which is transferring through the material
- Degree of hydraulic component formation

In addition flow characteristics due to micro regional variation in the materials constituents will also affect performance. This may be illustrated with lime mortars that are primarily comprised of Ca and SiO_2. Ca based products repel water due to large contact angles between the material and the water, whereas the SiO_2 will attract water due to small contact angles. It is evident that conflict may exist between the different components found within mortar and may increase the complexity of moisture transfer accordingly.

This may be seen visually within the following plates, indicating the properties of hydrophobic and hydrophilic materials. The more spherical the water droplets are then the greater the materials are in terms of hydrophobic nature, and vice versa.

Plate 11: Hydrophilic and hydrophobic material surfaces in quartz and illite [36]

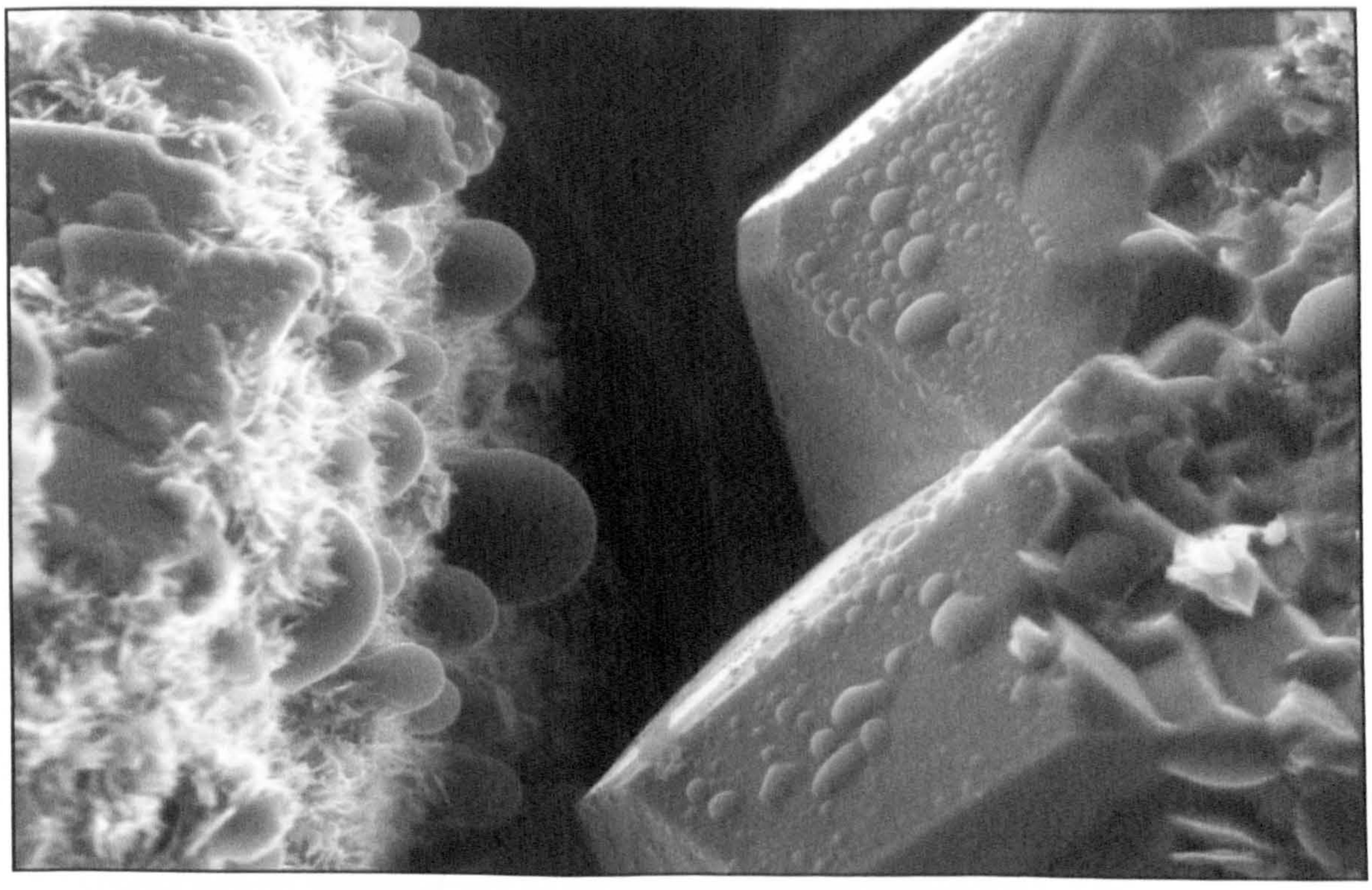

The water droplets can therefore aid in analyses of the physical characteristics that the materials may exhibit. For example, if the materials placed in contact with water tend to form dome shaped water droplets then these materials will tend to be of a low negative electrical charge and will bond with the water molecules readily.

Plate 12: Hydrophilic and hydrophobic material surfaces in illite [36]

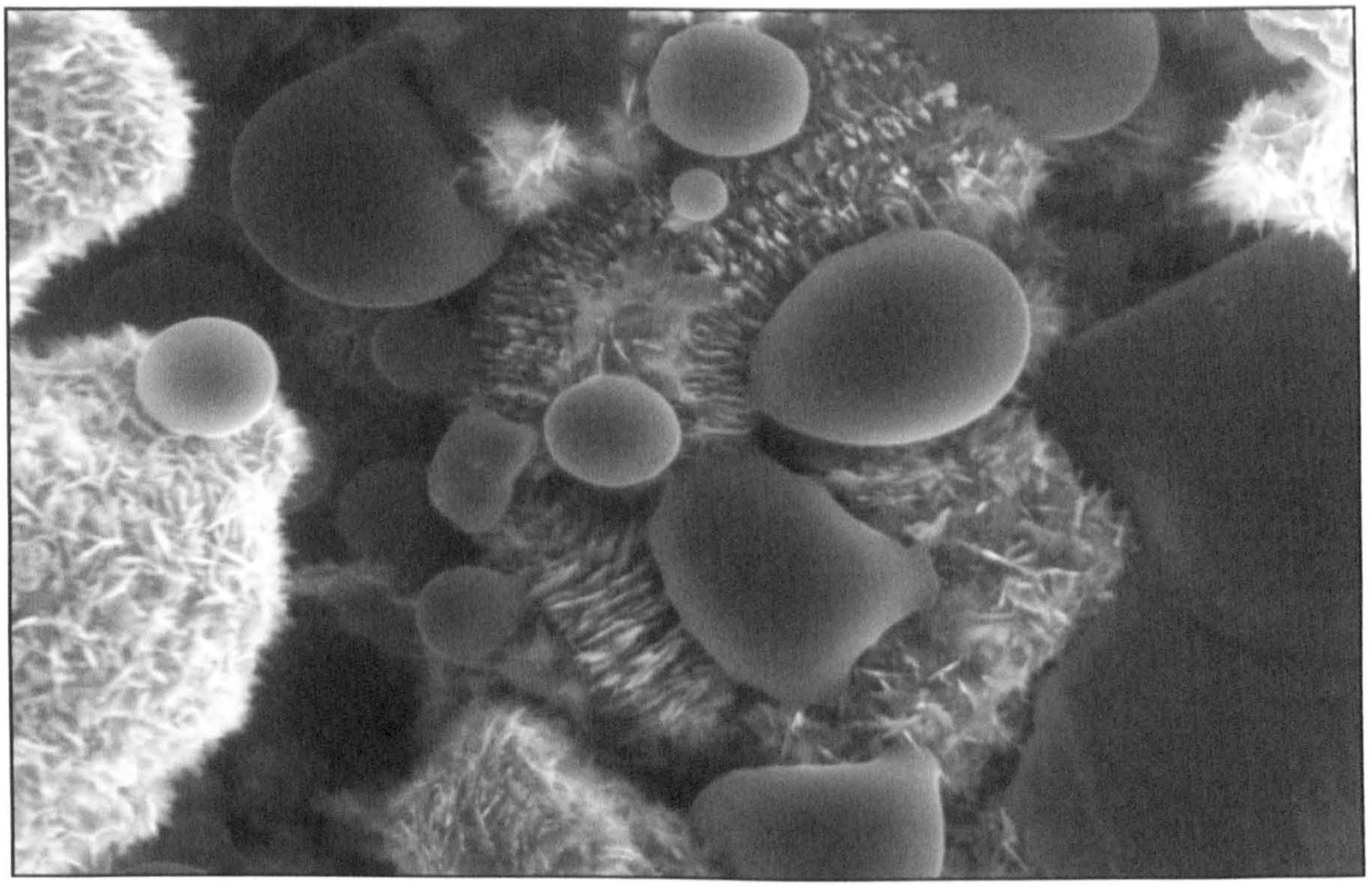

Plate 13: Spherical and dome shaped water drops [36]

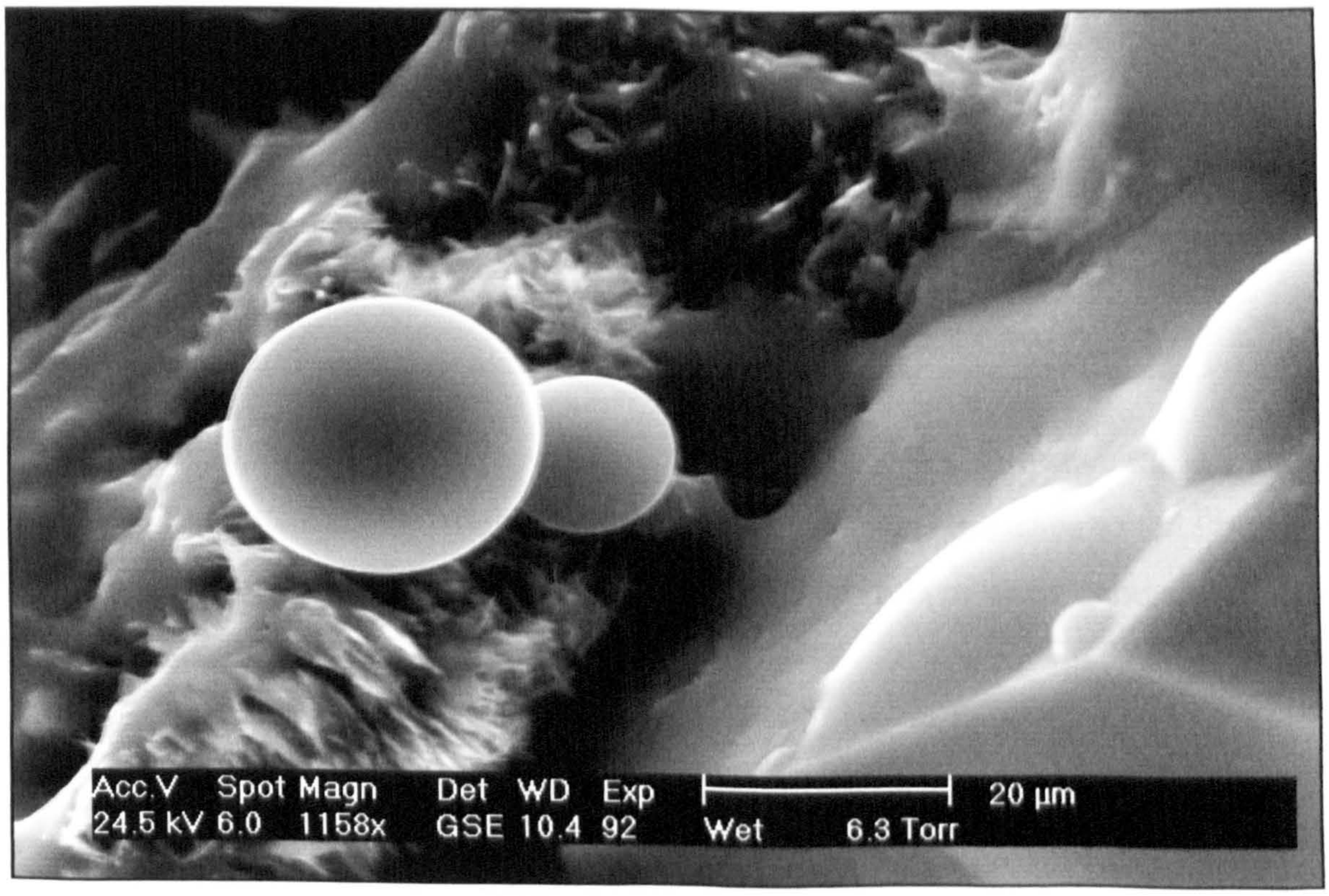

As expressed earlier the moisture flow characteristics are rather complicated due to the attraction or repulsion within the materials. This is clearly seen in plate 12 in which water droplets are following the contact angle relationship expected within the differing materials within the mortar.

This phenomenon has led to Torraca [35] to believe that the water within the limestone is induced into electrical movement via the atomic bonding structure. Electro-kinesis ensues and a physical movement phenomenon is generated by a potential difference between the water. This water flow will occur as long as sufficient water molecules are present to keep a continuous flow or, chain of molecules. He [35] continues; indicating that due to surface tensions within water molecules, (which are caused by the nature of hydrogen bonds) an attracting inward force will always be exhibited.

Torraca [35] also states that a meniscus is formed within the liquid and between the pore walls due to the liquid's inward attracting force generated by water's molecular structure. This is known as capillarity, which he defines as *"the spontaneous phenomenon of a liquid / water movement due to the attraction of the water towards certain surfaces"* [35]. Hence, capillary suction occurs when the attraction of the water to the surface of the solid is greater than to the water molecules bonding to themselves.

Figure 32: Surface tension forces within water [35]

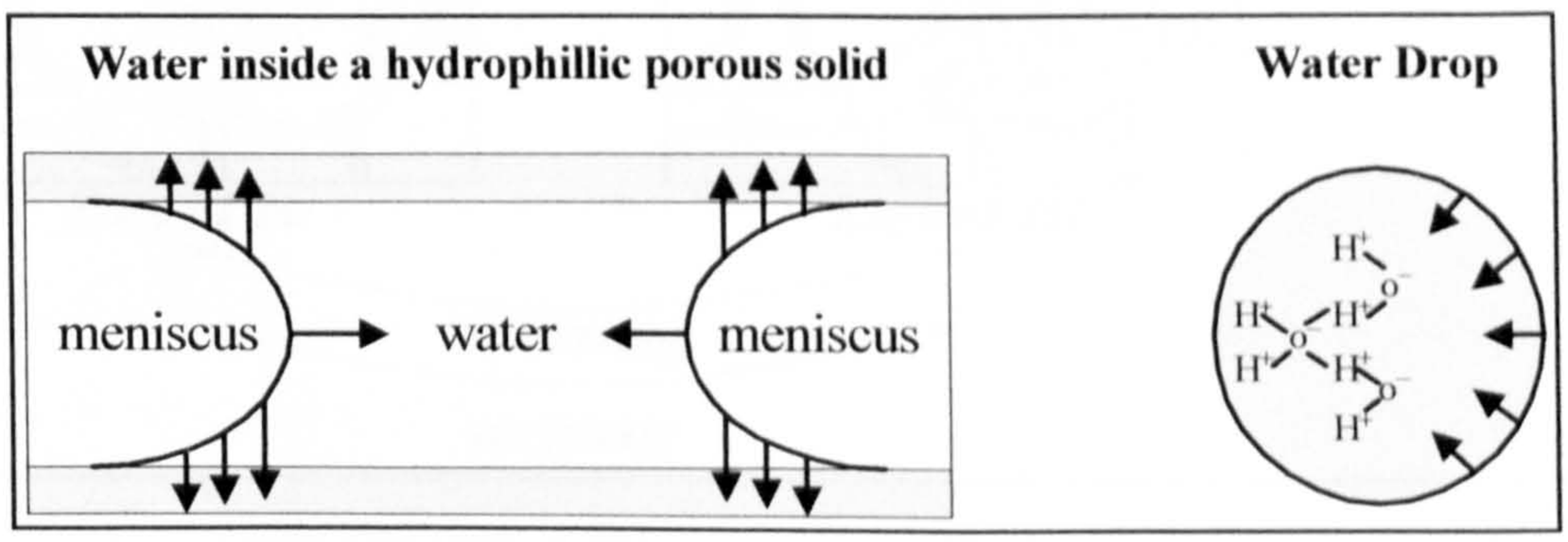

Generally, complications will ensue when the water attempts to evaporate, as porous materials tend to attract moisture readily, but have a greater resistance to the liberation of water as water vapour. Torraca [35] indicates that 4 levels of water content exist (see figure 33) within a material including:

Level 1: Pores empty, therefore, dry.

Level 2: Only small capillaries are full of water. Therefore, large diameter pores are dry.

Level 3: Small capillaries are full. Large diameter pores are covered with water but are not full (known as the critical water content which may be affected by the geometry and nature of the material and also the soluble salt concentration).

Level 4: All pores are full.

Figure 33: Water distribution in a porous hydrophilic body (after Torraca)

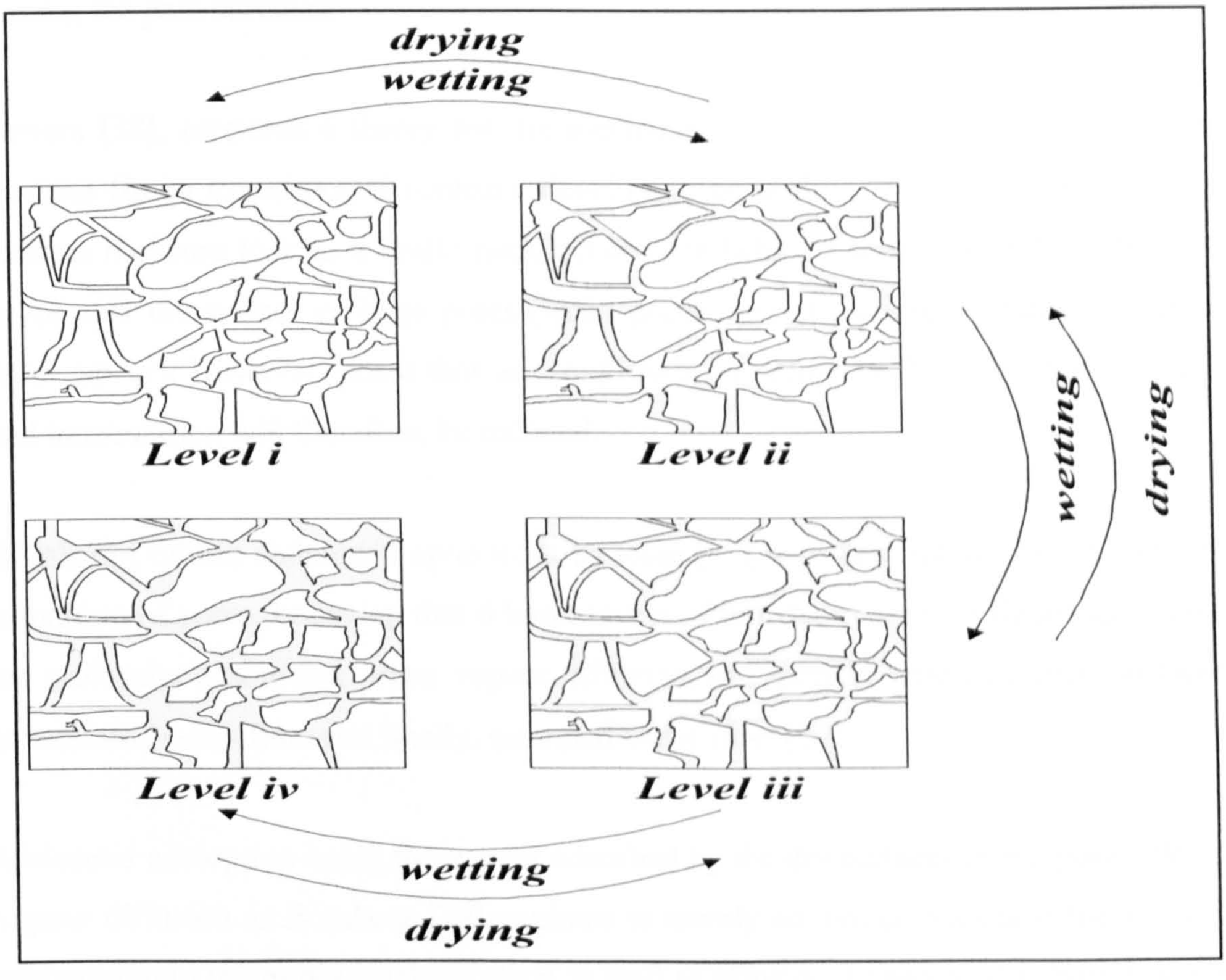

Scott-Hindi Sandani [31] believes that moisture contents within porous building materials rarely develop beyond level 2. Hence, full saturation very rarely occurs within porous materials and consequently water vapour transfer must be the predominant moisture flow mechanism. It must be emphasised that moisture movement must have a force or driving mechanism which will initiate transfer, and these take the form of one or a combination of the following:

- Suction
- Diffusion
- Osmosis
- Electrokinetics
- Heat and differential vapour pressures

Rose [37] elaborates upon the transmission of water in non-saturated environments stating two specific mechanisms of transmission occur. The first of these is that the necks of the pores are filled with water and vapour condenses on one side of the neck and evaporates from the other, and secondly, surface creep of a fine film of water coating the pore surfaces.

Powers [38], proposes a theory for the mechanism of loss of water from wet to dry surfaces (in an experimental context), developing an analogy of an 'ink bottle' which reduces moisture loss as a bottle neck occurs. He believes that water vapour bubbles occur near the surface of large pores (small pores are not sufficiently large enough to hold vapour). However, pores that are small will not allow bubble formation to occur and transmission will therefore, be reduced.

Bomberg [39] has elaborated upon work by Rose [37] with descriptions of the stages of saturation of pores, believing that 6 basic levels of transfer occur (see figure 35). These are molecular adsorption, water vapour diffusion, transport in series, parallel transport, unsaturated water flow and finally, saturated water flow [39].

Molecular adsorption being the vapour adsorbed by the dry surfaces of the pores. Water vapour diffusion as Bomberg [39] explains is mainly equimolar vapour diffusion with evaporation in micro pores taking place as well as effusion, however, Bomberg believes that these may be disregarded.

Transport in series is capillary condensation producing some unmoveable water drops. Bomberg indicates that 'evaporation from these drops, into vapour transport mechanisms with subsequent condensation at an alternative region usually increases the rate of transport'.

The parallel transport being an adsorbed layer of water in certain separate capillaries that are thick enough to allow localised flow of water. Bomberg believes that the transport series and parallel transport are difficult to distinguish from the whole region of water vapour transmission, continuing to indicate that when the boundary between the 2 is clear then this is known as the upper hygroscopic condensation boundary [39].

Unsaturated water flow occurs when the layer of water adsorbed by the capillary walls becomes thick enough to start a transport of liquid water. Bomberg believes that this phase is difficult to distinguish from the combined vapour / liquid transport as in the water vapour transmission process previously mentioned. He continues to emphasise that the limit called the critical moisture content represents the moment when the liquid phase flow has the same density rate as the vapour flow [39].

Saturated water flow begins when the adsorbed layer has become so thick that the small capillaries have become full of water and therefore no air transmission can occur. However, any air bubbles that may be contained within the relatively large macro-pores are engulfed by the water. Bomberg believes that this kind of flow occurs during the wetting run at the capillary saturation. He discusses 'absolute saturation' emphasising that both saturated and unsaturated flow may occur at higher moisture contents known as the saturated or unsaturated flow regions.

Bomberg believes that in general for materials with relatively constant pore sizes a sharp up and down diffusivity curve is characteristic, and for a pore size that is distributed in a linear manner it will produce a relatively continuous increase in diffusivity [39].

This reinforces the basic work undertaken by Torraca, with a greater level of elaboration upon the moisture transport mechanisms, indicating that moisture transport in porous media takes the following 5 steps (see figure 34):

i. Adsorption of water to surface. (The water molecules build up until a complete mono-layer is formed, vapour flux cannot be transmitted until this layer has occurred).
ii. Layer built and vapour flux ensues (Behaves like an ideal gas and pressure increases due to unimpeded flux of vapour)

iii. Condensation at the neck occurs (Impervious to inert gases, but pervious to vapour via distillation)

iv. Substantial water absorbed and thin liquid films may occur and flow (Also known as liquid assisted vapour movement)

v. Vapour pressure increases and condensation occurs hence, saturated flow begins in the porous system

Figure 34: Progress of moisture sorption in an idealised pore (author after Torroca)

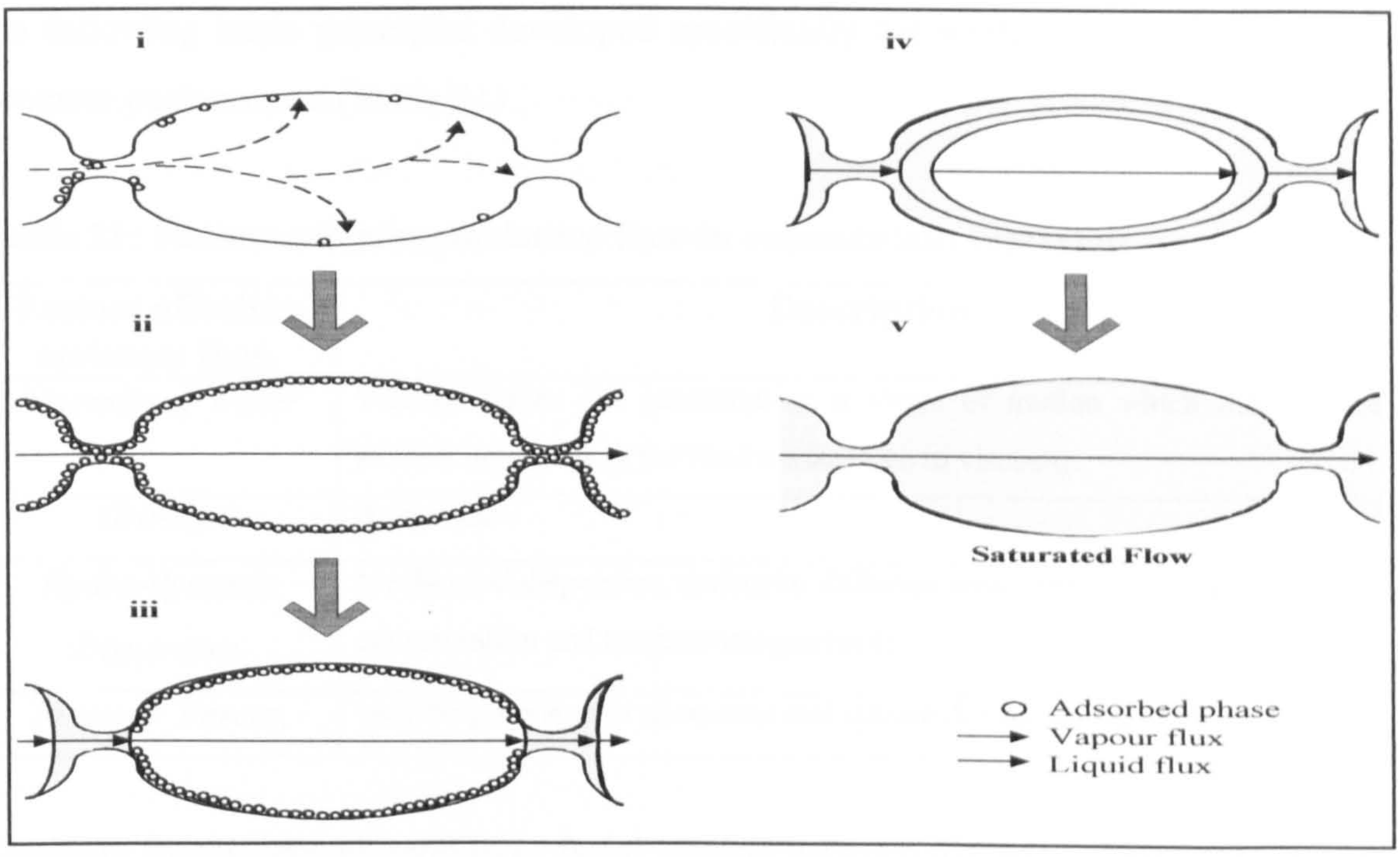

Figure 35: Different kinds of moisture flow through porous materials (author after Bomberg)

Pore Size	Moisture Flow Type		Comments on flow	Schematic of pore	Possibility of transport of:		
					Vapour	Liquid	Air
submicropores $r=10^{-9}m$	molecular adsorption	Wet	mainly monolayer adsorption		free wvt	unmoveable water	free air transport
micropores	water vapour diffusion & effusion	Wet					
	transport in series	Wet					
$r=10^{-7}m$	parallel transport	Wet					
submacropores $r=10^{-5}m$	unsaturated water flow	liquid flow			wvt only inside the air bubbles	water capillary flow	zero air transport
$r=10^{-4}m$	capillary saturated water flow	liquid flow	capillary transition zone			hydraulic flow	

Unfortunately mortars do not generally attain this condition with cementitious materials having a random geometric pore structures that are spread over a large order of magnitude. Bombergs therories indicate that even greater complexity is exhibited in porous materials with generally, transfer of moisture being slow, and consideration must be made for wetting and drying cycles [40]. He believes that the square root law generally gives moisture transfer values, but discrepancies evolve due to viscosity of the pore water.

The factors affecting moisture flow in cementitious materials may be summarised by the following basic principles developed specifically for work upon the modelling of concrete performance (Table 21).

Table 21: Factors affecting moisture flow in cementitious materials

Factors affecting moisture flow.	Description.
Viscosity of Water	Viscous forces are generated as a virtue of motion which induce shear stresses acting along the fluid surface due to viscosity.
Gravity.	As normal
Hydro-dynamic Dispersion.	Mechanical dispersion, molecular diffusion which may occur due to concentration and temperature gradients.
Pressure Forces.	May be generated in an unsaturated system due to capillary forces.

Capillary forces depend upon inter facial tension between different phases. The angle of contact between different phases and the angle of contact between interface water and the solid must be considered. It is believed that it is the difference of energy or potential difference that causes mass transport (higher to lower energy states always occur). Capillary force is therefore to be considered as the main driving force for water flow, however, it must be emphasised that, viscous drag acts as a retarding force upon the aforementioned.

With realistic materials the water vapour flux is affected by so many variables that permeability is capable of being predicted only with the use of complex mathematical models, which do not lend themselves to the rapid through put of comparative data that is required by the work in this thesis.

2.10 A general introduction to breathability

It is well understood that traditional buildings require the ability to transmit water and water vapour with a minimum of resistance. Oxley and Gobert, state that *'any wall which is porous must allow water vapour to diffuse through it, indeed this is one of the routes by which excessive water vapour within a building normally escapes to the exterior'* [41]. In addition Schofield reinforces this belief indicating that in traditional buildings 'damp was allowed to evaporate away harmlessly, and the 'soft but tough' materials worked in harmony with seasonal changes in humidity and temperature' [42].

When assessing the performance of historic buildings that traditionally adopted lime mortars and harl-coats then the choice of mortar is of the utmost importance. Historic Scotland emphasised that *'traditionally constructed buildings relied on mass walling with a sacrificial lime and coarse aggregate coating to protect the masonry and inhibit water penetration'* [7]. In addition *'cementitious renders are harder and impervious, properties which may be seen by some people as attractive for the repair of old buildings. However, the truth is that old buildings move, and renders crack and allow water in and behind their surface. That same impermeability then traps moisture and transmits it through the softer substrate leading to rising damp, fugal attack, salt and frost damage and accelerated stone decay'* [7].

This is reinforced by Carrington and Swallow who believe that *'it is vital to achieve a mortar that matches the original in texture, porosity, hardness and colour. In addition the mortar should also be softer and more porous, and thus sacrificial to a masonry substrate (because water should be encouraged to evaporate through the mortar, ensuring that any associated decay from soluble salt crystallisation, for instance, occurs there). He emphasises that in practice, the use of Portland cement in a repair mortar makes the aforementioned aims almost impossible to achieve. Lime mortar, almost invariably non-hydraulic lime putty, is found to provide the most satisfactory mortars for conservation work'* [43].

It is therefore evident that the non-hydraulic lime mortars are considered inherently more permeable than Portland cement mortars. Townsend believes that moisture must be both readily adsorbed and freely dissipated from historic mortars to ensure satisfactory performance. When discussing harl coats he states 'this can only be achieved by forming the covering from materials which are not denser or more

permeable than the walling they cover. Any substantial decrease in permeability will inhibit the free passage of moisture and decay is likely to occur at the interface of the wall and covering' [11].

Holmes and Wingate believe that 'Lime based renders allow walls to 'breathe' so that moisture can disappear without damaging the structure. Lime mortars are much more suitable than cement mortars…because they are less rigid and more permeable.'[12]

As seen previously a myriad of terms have been used in an attempt to define 'breathing'. The permeability of traditional mortars are essential, if not one and the same as breathing. However, the true definition of breathing has not been objectively defined. Holmes and Wingate believe that the definition of breathability is best described by the following: *'The extent to which a building material is able to allow moisture to move to the surface and evaporate harmlessly'* [12].

Hughes uses the term porosity to define the concept of breathing and states with respect to lime mortars and harl coats: 'the porosity of these mortars permits evaporation of moisture from within the wall' [10]. As aforementioned in this chapter porosity may be defined as 'the fraction of void to the total volume' [31], however, this does not take into account the interconnectivity or segmental nature of the pore structure and therefore fails to define breathing.

Hence, *'breathing'*, must be the material's ability to transmit water and water vapour with a minimum of resistance. Therefore, it could be said that the permeability and *'breathing'* (the ability to allow *'moisture which has been absorbed by the fabric to evaporate from the surface'* [10]) of a material are close relatives. This definition is similar to that used by Teutonico, where permeability is defined as *'the ability to transmit liquid or gas from one place to another'* [34].

All of these documents show the basic technical principles behind what 'breathing' should be, however, this has only been assessed via empirical testing. It is hoped that a definition of breathing can be attained when assessing the material under test.

2.11 Historic development of the Environmental Scanning Electron microscope (E.S.E.M.) and X-Ray diffraction imaging

Prior to discussing the historical development of microscopy it may be useful, as J.E. Gordon believed to briefly explain the very small units used in microscopy. Gordon [44] indicates that '1 micron (1μm) is $^{1}/_{10,000}$ of a centimetre, that is $^{1}/_{1,000}$ of a millimetre. The smallest thing that one can see in the ordinary way with the naked eye is roughly $^{1}/_{10}$ of a millimetre, that is about 100 microns across. The smallest thing one can see with an ordinary optical microscope is usually a little less than half a micron across'. The Angstrom unit (1Å) is $^{1}/_{10,000}$ of a micron, that is $^{1}/_{100,000,000}$ of a centimetre, hence 10 Å = 1 nanometre (nm) = 10^{-9} metre.

The development of the scanning electron microscope was primarily enabled by the invention of the scintillator and photomultiplier [45] in the early 1960s. From these early devices it was found that by using different inputs, various forms of information could be extracted. For example, inputs could vary with the number of primary electrons adopted (these act as information carriers) and the volume at which the primary electrons are produced. It is important to consider the characteristics of the carrier, including the penetration depth of the electrons into the sample.

The use of S.E.M. (Scanning Electron Microscopy) allowed the attainment of high resolution imaging. However, it has been emphasised by Philibert that 'sometimes a result is produced without an understanding of its origin or development; in this regard, there may be nothing more deceiving than an image' [45]. Viewing images must not be considered as a simple process and it is the translation of the specimen that is difficult. The scanning procedure is a 'point by point examination, line by line' which 'furnishes an image in the form of a signal S(t)' [45]. He continues to explain that 'on the basis of mathematical morphology, the texture analyser uses a <<structural element>> such as a bi-point, a polyhedron, etc....to determine the morphological functions - whence a characterisation and a quantitive recognition of the shape' [45]. Fortunately, the aforementioned are calculated automatically.

2.11.1 Operation and application of SEM / ESEM

In essence electron microscopes adopt X-rays which are bombarded at the specimen. Most of these electrons are 'scatter-back' which means that they are bounced away from the surface with little or no energy loss, however, some will interact with the surface

atoms to produce what Chandler calls 'secondary low level electrons' [46]. See figure 36.

Problems traditionally arose with micro-structural analysis as regional chemical differentials within the sample led to inaccurate data. Although this was true, modern ESEM technology allows simultaneous chemical and visual analysis, eradicating the aforementioned.

Figure 36: The various effects of electron-specimen interaction (author after Chandler) [46]

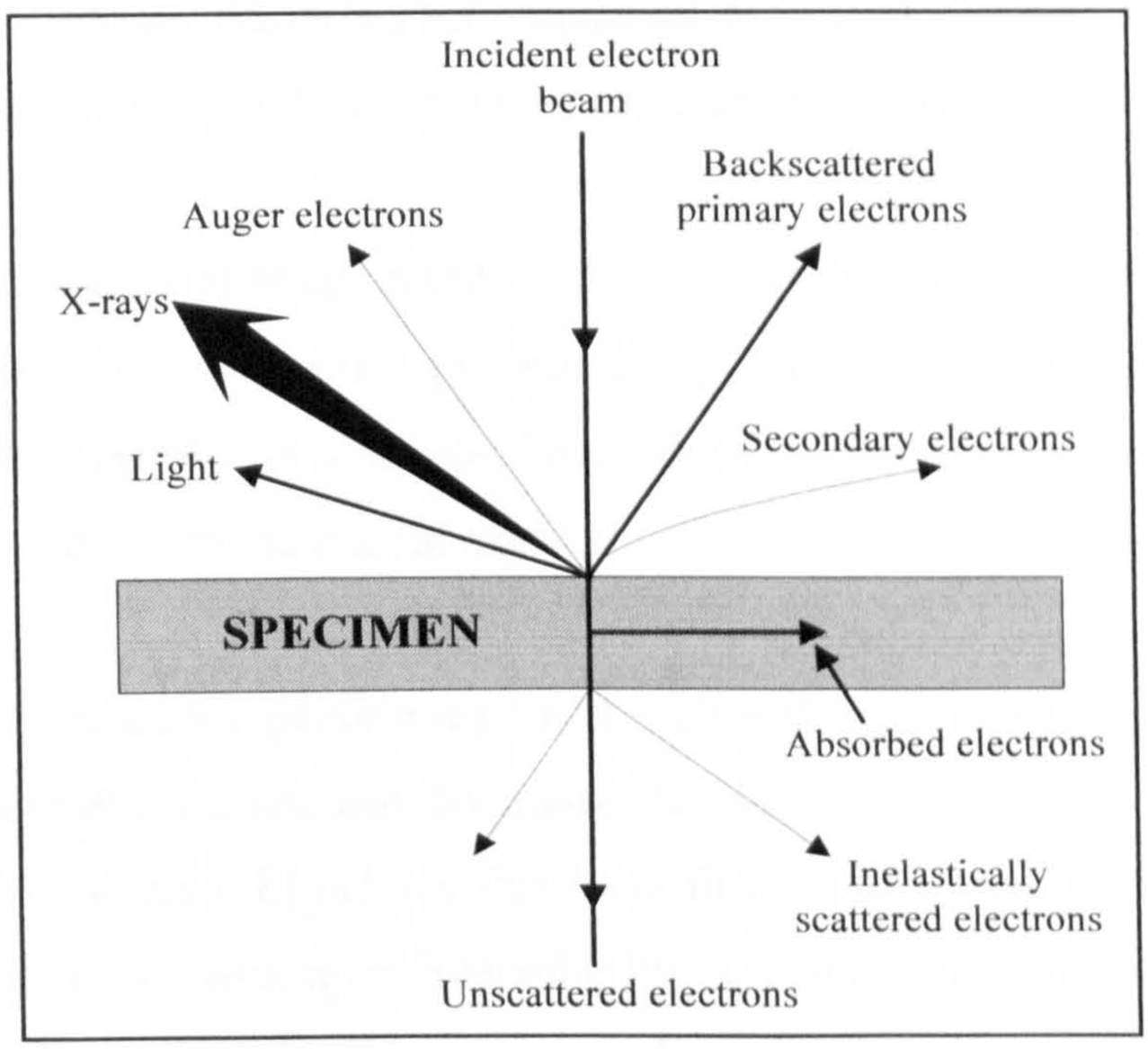

Chandler explains that all atoms have individual characteristics determined and composed by protons and neutrons, which in turn form the nucleus. The electrons spin in the orbits around the nucleus and follow strict quantum mechanics, that is to say that they follow specific energy levels. The greater the number of these orbits and respective energy levels, depends upon the state and size of the atom. The orbits are grouped together into major units known as shells. Therefore, the characteristics of elements may be determined by nuclear charge and energy distribution of respective orbital electrons. Today the same basic theory is used, however it is a specialised form of microscopy known as ESEM. This enables samples to be studied under controlled environmental conditions with the additional advantage of eradicating the need to apply specific coatings to the sample. The ability to environmentally study the sample allows an in-

depth understanding of the material in its natural state to occur, and is therefore a valuable tool.

The ESEM can create environments adopting, water vapour, air, Nitrogen, Argon, oxygen, etc. with the ability to access dynamic characteristics of wetting, drying, freeze / thaw, adsorption, melting, corrosion and crystallisation. In addition the ESEM can generate pressures without surface charging occurring due to the secondary electron detector which is designed on the principle of gas ionisation [47]. Hence, the primary electrons on the surface of the material are accelerated towards the detector, this is biased by a moderate electric field. The impact of the electrons and gas molecules liberates free electrons which in turn generate increased signals. The positive ions created in the gas neutralise the excess electron charge built up on the sample.

The ESEM can operate at temperatures within a range between -190°C and 400°C with a full capability for temperature programming. This may be twinned with a fluid injector and the ESEM can simulate freeze thaw cycles and the effect of chemical solution application upon the chosen sample.

2.11.2 Existing research pertaining SEM / ESEM high resolution imaging, EDX analysis upon hydraulic and non-hydraulic binders

Charola and Henriques [48] believe that identification of hydraulic components is not easy to achieve. Their work upon hydraulic limes manufactured from marly limestones indicated that the hydration products are similar to those seen in OPC. Continuing to emphasise that the general hydraulic reactions in hydraulic limes are known however, determination of the mineral phases is difficult.

Both Lewin and Radonjic have undertaken invaluable research into historic mortars using SEM and ESEM. Lewin S.Z. [49] undertook Scanning Electron Microscopy (S.E.M.), combined with X-Ray Diffraction (X.R.D.) analysis upon mortars used in the conservation of historic buildings. A range of mortars where tested by Lewin, including lime-sand, lime-pozzolana and lime-cement-sand mortars (Lewin subdivided his mortar batches into binary and ternary mixes; binary being those with 2 components and ternary being those with 3 components), all of which where cured for several months prior to testing. His study concentrated upon those transformations associated with the respective materials hydration.

ESEM analysis was undertaken by Radonjic et al [20] in which her study hoped to aid in the understanding of ancient lime mortar macrostructure via analysis of the microstructure. The samples tested included various ancient mortars including: A hydraulic lime mortar from Masada, Israel (Circa 10BC), a Greek mortar from Castello d' Empuries, Spain (Circa 500BC), a Roman mortar from England (Circa 50BC), a mortar from Jericho, Israel (Circa 7000BC), a mortar from Hurst castle, England (Circa 1540AD) and finally, a 19th Century hydraulic lime mortar from Barry docks, Wales. [20]

The results from Lewin's [49] analysis upon lime putty (non-hydraulic) indicated the presence of thin hexagonal plates (max dimension 2μm, minimum 0.07μm) of $Ca(OH)_2$, (a.k.a. Portlandite), trace element of C-S-H and a 1-2% calcite component. Within the binary lime putty-sand analysis no Portlandite was seen when assessed via XRD. Lewin believes that the portlandite with its hexagonal plate morphology had disappeared to be replaced by irregular particles of partially fused larger agglomerates of calcite. The calcite had adhered to the sand to varying degrees, with tiny calcite crystal growth seen upon the siliceous substrate. In addition to calcite the quartz and feldspar of the sand could also be seen clearly.

The crystallography of the samples altered from initial manufacture to the consequently aged sample. In the young samples $Ca(OH)_2$ was seen, however, the $Ca(OH)_2$ converted into calcite due to the chemical reaction of the atmospheric carbon dioxide and water vapour (carbonation). This mechanism is affected by the materials ability to carbonate, with Lewins believing that a relative humidity of between 50-75% is best for this transformation. Lewin [49] believes that this is substantiated in works by Roberts who indicated that at lower humidities very little carbonation takes place due to the lack of free water. The presence of large amounts of moisture also hinders the reaction by filling pores and reducing or preventing access of the CO_2 to the interior.

Lewin [49] believes that the poor mechanical strength of lime putty sand mixes occur due to the limited inter particle fusion developing at calcite-calcite contacts and secondly, the small affinity of calcite crystallites for quartz surfaces.

This was similar to Radonjics analysis of Greek mortars samples (circa 500BC) that exhibited a relatively 'fragile, easily powdered, fairly porous texture that were white in

colour' [20]. The mortar was composed of 'loosely packed angular crystals' [20] which had a low conductivity. Aggregate / lime interfaces were also seen, with proportions of the aggregate being barren. The presence of sub-micron cubic crystals were also seen, however, Radonjic et al was not specific about the crystal type.

When Lewins analysed the ternary lime putty-pozzolana-sand batch it was clear that the powdered silicate reacts with the calcium hydroxide. A chemical analysis of the pozzolan (from Salone, Italy) derived a composition of 46.7% SiO_2 (Soluble silica), 11.1% Fe_2O_3, 16.7% Al_2O_3, 9.8% CaO, 3.7 MgO, 6.5% K_2O and 1.9% Na_2O, with a particle size in a range of 1.5μm.

Lewin indicates that under XRD analysis the majority of the components showed as glass, however, 10-20% consisted of crystallite components, which upon subdivision were identified as $KA_1Si_2O_6$ (a.k.a Leucite), $Ca_2Al_2Si_8O_{10}$ (a.k.a Prehnite) and the presence of 3-5% of Yoderite, a magnesium aluminium silicate. $Ca(OH)_2$ was also present within the matrix at the 7 day period. C-S-H and C-A-H where present in small quantities due to the interaction between the $Ca(OH)_2$ and the pozzolana. This interaction takes the form of $Ca(OH)_2$ adhering and coating the glassy pozzolana shards. Lewin continues to explain that 'the calcium aluminate and silica reaction products occur as chunky polygonal crystallites' [49] which grow out of the pozzolana surface. It is interesting to note that with an increase in age a structural change occurs, with etching of the pozzolan and consequent increasing in the pozzolans surface area. The $Ca(OH)_2$ had been converted from its original morphological form by recrystallising and being incorporated into the network of masses bridging the pozzolan shards. Lewin explains that this is the reason for pozzolans improvement of the strength of mortars. At an age of 2 months increasing quantities of prehnite, and small amounts of mono-hydro calcite ($CaCO_3 \cdot H_2O$) were seen (approximately 5%).

The pozzolana results above show similarities to Radjonic et al's work and when she tested the Masada mortar she found a composition of ash-gauged plaster with a greyish coloured hydraulic mortar. At low magnification Radonjic found a uniform grain size with 'good connectivity of grains' [20]. Radonjic believes that the relationship between the angular aggregate and the lime (grain boundary) was derived due to pozzolanic reactivity of the components. The discovery of laminar / sandwiched crystalline phases

were seen with distortion of the stratified components due to heat / drying tending to generate a curing effect of the sheet minerals.

Lewin also indicates that within the binary lime putty - sand batches all the $Ca(OH)_2$ had converted into calcite within the first 2 months, as opposed to the ternary lime pozzolana - sand batches which had not. He continues to emphasise that this phenomena is associated with the fact that 'portlandite in lime putty is inherently readily reactive towards atmospheric CO_2' and that the 'rate of reaction is primarily limited by the porosity, i.e., gas permeability, of the mortar' [49]. Lewin believes that the small particle size associated with the pozzolana tends to create a lesser permeability within the mortar, with sand as the primary filler resulting in an increased permeability.

A similar non-hydraulic lime mortar was analysised by Radjonic et al, and although it must be emphasised that the morphological changes may have been significant over time it may still be useful to compare the results. Hence, Radonjic et al's [20] study of the Roman mortars (circa 100AD) revealed a fine grained lime matrix which enveloped the aggregates. Interestingly the presence of organic fibres (plant) were seen within the mortar. The lime was deemed as amorphous at 850x magnification, with a clearly large surface area. The lime was finely divided upon the aggregate, however, it was well bonded to the aggregate face (interface). The aggregate appears to have been effected with the dissolution of its face occurring, and therefore the interface had tended to deteriorate.

The analysis of the Roman mortar sample (circa 50AD) was markedly different from the aforementioned due to what would appear to be the presence of pozzolanic additives, with aggregate being generally enveloped by the lime paste which had formed into conglomerates. It was interesting to note that these conglomerates had large voids between them. The presence of closely packed angular calcite crystals were exhibited with the addition of what Radonjic et al calls 'inter-layers of fine hydrated material' [20], unfortunately she was non-specific with respect to the individual and / or combined crystallography. The bonding relationship between the lime / aggregate within this mortar was much higher than that of the aforementioned Roman mortar, with the presence of laminar crystal types which where much coarser.

The analysis of the Jericho mortar (Circa 7000BC) was found by Radonjic et al to have a dissolved appearance at the aggregate / lime interface (at relatively low magnification: 650x). It must be emphasised that this sample had been prepared not via fracturing, but by the traditional SEM method which adopts the process of thin section polishing. When the sample had been fractured and prepared in a manner similar to the others no evidence of aggregate / lime interface dissolution was noted. Radonjic et al indicated that the lime paste was evenly distributed and well adhered to the aggregate surface.

Interestingly Radonjic et al found the presence of large well formed calcite crystals and attributed their formation to high levels or, the ability of the mortar to readily carbonate. Radonjic et al believes that for this level of calcite to have formed it must have been initially derived from a 'vein rich in portlandite or some other Ca-rich medium' [20], this would also correlate with the suggestion that carbonation must have occurred readily with very little impedance to the CO_2.

Lewins' analysis of the lime putty - pozzolana - sand mortar (4:1:10) yielded interesting data, with calcite, quartz and feldspar being found to be present under XRD testing. However, when assessed under Scanning Electron Microscopy (S.E.M.) it was evident that an agglomeration of tiny calcite particles (0.06-0.03μm) had coated the sand grain and pozzolana shard surfaces. He indicates that certain regions of the sand grain were relatively bare. Lewin continues to indicate that due to the 'small reactivity of portlandite or calcite with quartz surfaces, the calcite-coated pozzolana shards were weakly bonded to the sand grains' [49]. As a large proportion of sand was present within this mortar, favourable conditions were exhibited for the entry of atmospheric CO_2, with the consequent conversion of the hydroxide into the carbonate. Lewin therefore concluded 'the addition of a small proportion of pozzolana to a lime sand mortar does not have a significant effect in improving its strength or ageing characteristics' [49].

Radonjic et al mortar sample from Hurst Castle, England (Circa 1540) was believed to have hydraulic components. However, the initial images by Radonjic et al indicate that well formed 'advanced crystal growth and well developed clean surfaces' [20] were commonly found at moderate magnification. At high magnification 4750x silicate forms were seen with what Radonjic et al called 'spongy phases' [20]. These phases were similar to those associated with the 1850 hydraulic mortar samples from Barry dock. Radonjic et al believes that it is the formation of silicate and aluminate phases which

occur along the grain boundaries of the fine aggregates (quartz) which are 'the most fragile interfaces in mortars' [20] and also, 'provides a sealing effect preventing water leakage'. [20] Radonjic et al continues, stating the silicate and aluminate phases are 'responsible for the dense and compact texture of hydraulic lime mortars' [20].

The analysis of Lewins' Portland cement pastes and mortars were manufactured adopting type 1 Portland cement and low alkali Portland cement types. Under X.R.D. the expected primary constituents were seen including C_3S (50%), βC_2S (25%), C_3A (10%), calcium ferrite solid solution phases, namely, C_2F and C_6A_2F (10%). Other secondary components were present and these include small quantities of CC, CS, MgO, Na_2O and finally K_2O. Lewin indicates that the only difference between the two types of Portland cement were their respective elemental alkali and aluminium content. When manufactured as a paste and left to cure for 6 weeks the primary reaction products seen under X.R.D. where calcite, C-S-H (a.k.a. tobermorite), afwillite and very small amounts of portlandite which occasionally formed within other constituents.

Portland cement ground clinker paste exhibited a dense crystalline network which Lewin believes may develop from a colloidal state prior to its formation into crystalline C-S-H compounds. This C-S-H may develop slowly in the initial curing period (2-7 days), however, it will rapidly develop after this period for approximately 6 weeks. The increasing ability to identify X-ray diffraction patterns of the individual components of C-S-H increases with the ageing of the colloidal gel into fully matured C-S-H, only when the cement has matured to a significant level can individual components such as the needle like afwillite crystals be clearly distinguished. Lewins X-ray diffraction of the C-S-H material revealed the expected orthorombic unit cell of tobermorite ($5CaO{\cdot}6SiO_2{\cdot}2^1/_2H_2O$). Lewin indicates that although tobermorite follows a known crystalline X-ray diffraction pattern, variations do occur with respect to the C-S-H orthorombic form.

Lewin [49] indicates that when looking at cement-water reactions under S.E.M. four distinct types of crystal morphology occur, namely, needle, fibre or rod like formations, sponge like texture formations, large well formed hexagonal plates and finally, rhombohedral crystals of calcite. The first of the crystal types, namely, needle like or fibrous are associated with growth upon the clinker grains. These are solid and have a straight appearance. The second sponge like formations occur due to tightly packed

platelets, which grow perpendicular out from the clinker grains forming a rather amorphous appearance. Lewin indicates that as these platelets grow, etching of the clinker grains occurs. In the regions between the clinker grains the third form of crystals grow, namely the well formed hexagonal plates. Finally, rhombohedral calcite crystals where exhibited upon the clinker grain surface. Lewin emphasises that although the aforementioned crystalline forms appear relatively amorphous they all clearly follow the holistic growth patterns associated with tobermorite.

Lewin states that 'a large proportion of the fibres are truly crystalline in character, and that there is little or no portlandite, despite the substantial proportion of the hexagonal platy crystals' [49]. In addition the calcium aluminate phases tend to form hexagonal plates which were found to be tubular arrays. The portlandite crystals within the Portland cement can often alter in character, namely from $Ca(OH)_2$ into $CaCO_3$. This alteration occurs via polymorphism with no external change to their shape.

Lewins elaborates upon the rod-like crystals believing that they have a cross section which is hexagonal. The platelet crystal forms have a six-sided outline which does not follow a general orhorombic crystal type, normally associated with tobermorite. However, he believes that in favourable growth formations a rectangular shape should be seen. Lewin believes that this anomaly may be explained, stating that 'the apparently hexagonal crystal habits observed in these preparations were produced in the course of the sequence of solid state transformation that result in the eventual formation of tobermorite from the initially formed C-S-H gel-portlandite 'eutectic' [49]. Furthermore, when Lewin assessed the work undertaken by 'Grudemo' he found that a 'topochemical transformation of $Ca(OH)_2$ into calcite' occurs '(i.e., there is no change in crystal habit accompanying the carbonation)' [49]. The low proportion of $Ca(OH)_2$ has been correlated with true crystalline tobermorites (as opposed to C-S-H forms of hydrated calcium silicate) which tend to form with a decrease in pH of the clinker grain. Hence, the formation of either crystalline or non-crystalline tobermorite is dependant upon the chemical characteristics of the cement and / or the preparation of the sample. Lewin believes that more specifically these characteristics may occur from the 'concentration and accessibility of atmospheric CO_2, or pH of the water... and not necessarily the age or weathering history' [49].

Lewins X.R.D. and S.E.M. analysis of the ternary lime - Portland cement - sand batches, consisted of various batch ratios namely; 3:1:10, 3:1:12, 4:1:10 and finally 4:1:12. His analysis indicated that although a high proportion of lime was adopted within the batches no evidence of portlandite occurred. However, in all the batches calcite was present with feldspar and quartz also being identified, obviously from the sand grains.

The rationale behind the conversion of the $Ca(OH)_2$ into calcite equates with the aforementioned theory that the sand grains allow a greater level of permeabilty within the mortar, thereby allowing entry of atmospheric CO_2 into the batch. This allows the conversion of $Ca(OH)_2$ (calcium hydroxide) into $CaCO_3$ (calcite) over a period of several months.

The proportion of cement within Lewins' mortar samples was low (some 6%) and the detection of this component could not be achieved via X.R.D. However, the S.E.M analysis did detect their respective components with the sand grain surface enabling C-S-H rods and fibre to grow outwards (quartz grains act as the host for the bonding rod growth). The C-S-H's molecular bonding to the quartz is attributed with the primary mechanical strength characteristic of the cement and therefore, the holistic strength of the mortar. Lewins indicates that due to C-S-H's very small nature it is almost impossible to detect them via optical microscopy.

Lewin explains that the lime within the mortar does no longer exist as $Ca(OH)_2$ and has therefore, converted into $CaCO_3$, however, the crystal structure generally follows 'pseudomorphs of portlandite'. The conversion of the $Ca(OH)_2$ into $CaCO_3$ (calcite) causes the re-arrangement of the internal crystal lattice whilst retaining the external shape. As aforementioned the general external shape of $Ca(OH)_2$ and / or $CaCO_3$ is that of a large, thin hexagonal plate.

Lewin describes the lime putty within the mix, believing that 'most of the portlandite of the lime putty was present originally as small, irregular crystallites, and these have been converted into the non-descript aggregates of calcite crystallites' [49].

The final mortar to be analysed by Lewin was a binary hydraulic lime and sand batch. Lewin emphasised that the X.R.D. analysis revealed that the mineral constituents of

hydraulic lime were the same as that of Portland cement with the addition of portlandite. He reinforced this belief by stating 'it is equivalent to a mixture of lime and cement clinker when mixed with sand and water to produce a mortar in the proportion of 1 part of hydraulic lime to 3 parts of sand, the result was similar to, but not identical with, that obtained from the lime, cement and sand mixtures' [49]. Lewin indicates that the only substantial difference between the 2 mortar types was that the hydraulic lime and sand mix had a substantial proportion of portlandite when aged. The lime-cement-sand mix showed no evidence of these portlandite components at a similar age. The reason for this phenomena is described by lewins believing that 'in the manufacture of hydraulic lime, the homogenization of the cement and lime phases is much more intimate than when the two ingredients are mixed by hand during mortar preparation, hence, in hydraulic limes the cement phase appears to coat and protect the portlandite from contact with atmospheric CO_2' [49].

In addition the sand (quartz) grains within the mix showed a profusion of what Lewin calls a 'felt-like mat of the hydration products of the cement' [49]. From these grow C-S-H rods and fibres. The cement clinker phase surface exhibited the spongy etched appearance, with platelets and fibres growing from them. Lewin believes this is a typical manifestation with C-S-H development, with the presence of 'large, thin hexagonal plates of portlandite also clearly seen.

This is a view shared by Charola [48] indicating that when hydraulic lime mortar samples were analysed via SEM the sand grains were 'covered with a felt like mat of fibres and needles typical of the crystallisation of C-S-H gels. Continuing to indicate that these fibrous crystals were more likely to be attributed to Al:Si:Ca with a molecular ratio of Al:Si:Ca (1:4:10), therefore C-A-S-(H) in nature.

2.12 Conclusion

This literature review has shown that much work has been done on cements leading to an extensive understanding of their nature and behaviour but that a comparable amount of literature on the nature and behaviour of limes is not available. The significance of the performance of lime based materials in historic buildings has been demonstrated and the possibility of a linkage between hydraulicity and permeability established. The work to be described in the rest of this thesis aimed to confirm the hypothesis that *'There is a*

correlation between the hydraulicity and permeability of lime mortars for use within the historic building and conservation industry'.

Chapter Three: Experimental Procedure

3.1 General Introduction

The data collection for the development of the thesis was undertaken adopting a multi-phase experimental approach;

- Phase 1: Hydraulicity / hydration.
- Phase 2: Water vapour permeability.
- Phase 3: Environmental scanning electron microscope and energy dispersive X-ray (EDX).

Phases 1 and 2 are data collection tools for the extraction of raw data, whereas the phase 3 work was adopted to allow a visual assessment aiding in the correlation between the first 2 phases.

3.2 Materials

3.2.1 Lime binders

A full range of lime binders in the form of calcium hydroxide [$Ca(OH)_2$] have been adopted, from non-hydraulic to eminently hydraulic. These limes were primarily in the form of a dry hydrate, however, several non-hydraulic lime putties have been adopted. These putties were used in gauged batches and also for binary pure fat lime mortars. It was important to attain a comparison between regional, national and international variations of lime as this is aimed at increasing the understanding of these commonly adopted lime types. The limes chosen were expected to lead to the attainment of a greater understanding of the set characteristics of the materials. In addition OPC was also used to act as a comparative analysis tool.

The choice of binders for the experimentation can be seen in table 22.

Table 22 : Binders

Batch #	Binder Type	Region / Area	Maturity
2,10-14(*g*).	Non-Hydraulic lime Putty	Shap, N. England.	6+ months
3	Non-Hydraulic lime Putty	Blair Athol, Scotland	6 months
4	Non-Hydraulic lime Putty	Isle Of Man	6 months
5, 10(*g*).	Natural Hydraulic lime NHL2	St. Astier, France.	(dry hydrate)
6, 11(*g*).	Natural Hydraulic lime NHL3.5	St. Astier, France.	(dry hydrate)
7, 12(*g*).	Natural Hydraulic lime NHL5	St. Astier, France.	(dry hydrate)
8, 13(*g*).	Natural Hydraulic lime NHL5	Jura Kalk, Jura-cement fabriken, Switzerland	(dry hydrate)
9, 14(*g*).	Ordinary Portland cement.	Blue Circle, UK.	(dry hydrate)

(*g*). Indicates where a gauged mix has been manufactured.

3.2.2 Water ratios

The water ratios adopted for the manufacture of the natural hydraulic lime samples can be seen in table 23.

Table 23 : Water lime / ratios (Author after Hughes and Swann) [21]

Limes	*W/l ratio*	*$Ca(OH)_2$ (%)*
St Astier NHL 2	0.526	43
St Astier NHL 3.5	0.436	28
St Astier NHL 5	0.388	23
Jura-Kalk	0.300	2

The water / cement ratio adopted for the OPC samples was 0.4 and approximately concurs with Odlers' [5] w/c ratios for conduction calorimetry experimentation and other tests.

As non-hydraulic lime is generally produced in a putty (for building conservation) form, no additional water was required for the manufacture of the mortar samples. However, the sand adopted for the mortar was pre-dried in an oven at 105°C for a 24 hour period to eradicate problems with probable moisture variations. Therefore it was necessary to include a moisture correction factor for the aggregate determined via the calcium carbide speedy moisture meter. The average moisture content for the aggregate was 7% which was accordingly adjusted for the batch.

3.2.3 Aggregates and moisture contents.

The batch ratios for the select mortars have been chosen for testing because of the following factors:

- Frequency of use in industrial practice.
- To allow continuity (in terms of mortar manufacture and data collection) of testing by fixing as many variables as possible.

The mortar mixes fell into 1 of 2 primary categories; namely, binary or ternary. That is to say the binary mortars were manufactured with only 1 binder type (therefore 2 components) and the ternary batches adopted 2 (therefore 3 components). It was deemed necessary to assess the performance of both of these mortar types as Scottish industrial working practice commonly adopts both types. It is believed by certain practitioners that the adoption of ternary mortars will lead to higher levels of durability when compared with binary mortars.

Table 24 indicates the mortar batch ratios that were adopted for the experimentation: (NB: # 1-9 non-gauged mixes, # 10-14 gauged mixes.)

Table 24 : Summary of mortar mixes

Batch #	Batch Ratios	Lime	Aggregate	Additions to batch
1 a,b,c	As manufactures specification	13mm Plaster Board, test samples to verify WVP test equipment.	NA	NA
2 a,b,c	1:3	Shap, non-hydraulic lime putty	Gowrie sharp sand. Agg, conforming to BS:812	100g (ml) H_2O. Comp. For sand mc
3 a,b,c	1:3	Blair Athol, feebly hydraulic lime putty	Gowrie sharp sand. Agg, conforming to BS:812	100g (ml) H_2O Comp. For sand mc
4 a,b,c	1:3	Isle of Man, non-hydraulic lime putty	Gowrie sharp sand. Agg, conforming to BS 812	100g (ml) H_2O Comp. For sand mc
5 a,b,c	1:3	Natural Hydraulic lime (dry hydrate) NHL2	Gowrie sharp sand. Agg, conforming to BS:812	0.526 w/l ratio + 100ml H_2O comp for sand
6 a,b,c	1:3	Natural Hydraulic lime (dry hydrate) NHL3.5	Gowrie sharp sand. Agg, conforming to BS:812	0.436 w/l ratio + 100ml H_2O comp for sand
7 a,b,c	1:3	Natural Hydraulic lime (dry hydrate) NHL5	Gowrie sharp sand. Agg, conforming to BS:812	0.388 w/l ratio + 100ml H_2O comp for sand
8 a,b,c	1:3	Natural Hydraulic lime (dry hydrate) NHL5	Gowrie sharp sand. Agg, conforming to BS:812	0.300 w/l ratio + 100ml H_2O comp for sand
9 a,b,c	1:3	Ordinary Portland cement	Gowrie sharp sand. Agg, conforming to BS:812	0.4 w/c ratio + 100ml H_2O comp for sand
10 a,b,c	0.5:0.5:3 (1:1:6)	Shap, non-hydraulic lime putty : Natural Hydraulic lime (dry hydrate) NHL2	Gowrie sharp sand. Agg, conforming to BS:812	0.526 w/l ratio + 100ml H_2O comp for sand
11 a,b,c	0.5:0.5:3 (1:1:6)	Shap, non-hydraulic lime putty : Natural Hydraulic lime (dry hydrate) NHL3.5	Gowrie sharp sand. Agg, conforming to BS:812	0.436 w/l ratio + 100ml H_2O comp for sand
12 a,b,c	0.5:0.5:3 (1:1:6)	Shap, non-hydraulic lime putty : Natural Hydraulic lime (dry hydrate) NHL5	Gowrie sharp sand. Agg, conforming to BS:812	0.388 w/l ratio + 100ml H_2O comp for sand
13 a,b,c	0.5:0.5:3 (1:1:6)	Shap, non-hydraulic lime putty : Natural Hydraulic lime (dry hydrate) NHL5	Gowrie sharp sand. Agg, conforming to BS:812	0.300 w/l ratio + 100ml H_2O comp for sand
14 a,b,c	0.5:0.5:3 (1:1:6)	Shap, non-hydraulic lime putty : Ordinary Portland cement	Gowrie sharp sand. Agg, conforming to BS:812	0.400 w/c ratio + 100ml H_2O comp for sand

The aggregate chosen for the mortar manufacture was kept constant through out all of the experiments. This allowed the isolation of variables relating to a graded sand ratios. The Gowrie sand was tested following *BS:812, part 1:1975. Sampling and testing of mineral aggregates, sands and fillers: part 1 sampling, size, shape and classification.* The classification test adopts the standard BS: sieve-testing apparatus which gives an accurate indication of the percentage of fines and coarse aggregates present.

The Gowrie sand is an angular sharp sand with a range conforming to BS:812 with a fineness modulus of 2.74(A) and 2.68(B). This sand is often adopted for mortar manufacture and harl coats. Although the sand is angular the rheological properties of the mortars are not compromised, as the workability gained by the use of lime as a binder far out weighs the resistance imposed by the aggregates. The relationship between limes and their aggregates has been hypothesised as increasing the compressive strength of masonry walling, as the relatively large irregular aggregates may lay 'point to point'. This will enable the lime mortars to carry higher compressive loadings as the aggregates are theoretically transmitting the load directly from sand particle to sand particle, and therefore not necessarily fully dissipated throughout the lime mortar matrix.

3.3 Hydraulicity / hydration experimentation

In an attempt to measure the hydraulicity of the cementitious binder it is necessary to use the conduction calorimeter. This apparatus operates upon the principle of cementitious materials (those with reactive components) hydration which releases energy from a high energy state to a lower energy state with heat being liberated in the process. This heat can be measured and gives precise data relating to the heat of hydration of the binder. The apparatus has the advantage of allowing the heat of hydration to be plotted through its primary heat evolution phases. This gives a great deal of information relating to the rate of heat and total heat evolution and thereby, evaluating the hydraulicity of the material. In addition, the mechanisms of hydration within lime may be better understood as the heat evolution peaks and troughs indicate reactive and dormant periods within the hydration process.

The calorimetery equipment measures the heat of hydration, whether assessing initial or long-term hydration functions. The heat of hydration is converted from directly

proportional electrical impulses (in milliVolts, converted into Kj/Kg and W/Kg) which are monitored and logged for further analysis.

The advantages of adopting the conduction calorimeter include:

- Only those hydraulically reactive components are measured (as they are the components that generate heat) as opposed to traditional methods of hydraulicity measurement, which measures all silicates and aluminates present whether they are reactive or not.
- Initial and early hydration phases up to 72 hours can be analysed.
- Data representation indicating all sub-phases of hydration can be graphically represented allowing an in-depth understanding of hydration to be developed.

3.3.1 Test procedure and manufacture of samples.

3.3.1.1 Calorimeter operation

The test for hydration of cementitious binders requires a 30g standard sample which is placed into a standard polythene bag. The calculated water / binder ratio allows the attainment of theoretically enough water for full hydration to occur. The specified quantity of distilled water is syringed into the 30g sample bag and mixed by kneading for a minimum of 2 minutes. This ensures that all the binder comes in contact with the water; enabling the analysis of the 30g sample to be a true and realistic datum. Once the sample is fully kneaded then all the air should be expelled from the sample bag and a knot should be tied tightly in the bag. The excess polythene protruding past the knot should be cut off to allow the sample to be accommodated within the 30g standard sample container, diagrammatically depicted in figure 37.

30ml of transformer oil must be placed within the standard sample can. This ensures good thermal contact between the sample bag and the strain gauge. The sample must be wrapped tightly around the strain gauge. The spun aluminium lid must then be pushed down into place to form a seal between the container and the lid, ensuring the 'o' ring seal is suitably closed.

Figure 37: Conduction calorimeter (schematic) [author]

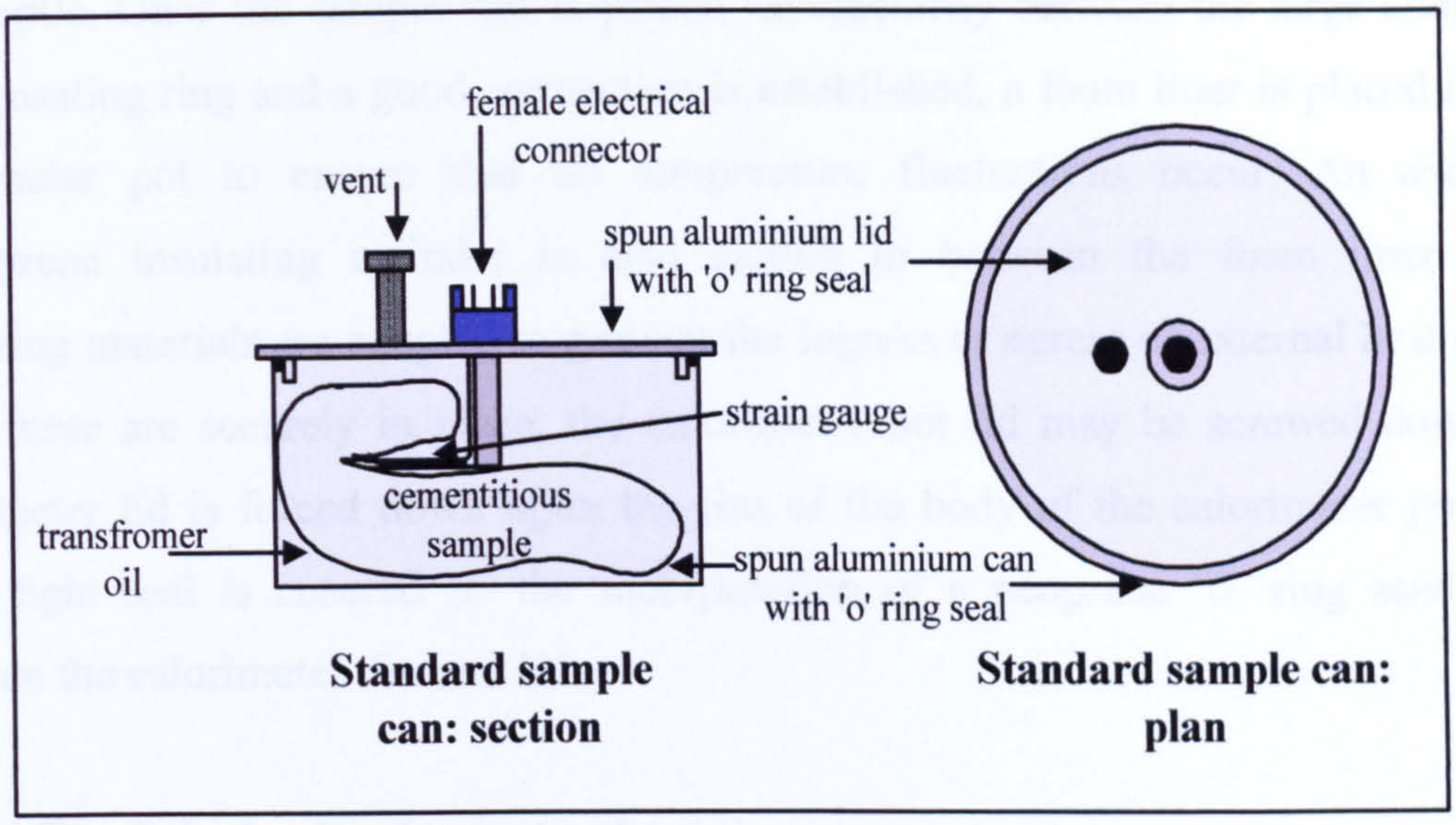

Plate 14: The Wexham isothermal conduction calorimeter (Wexham)

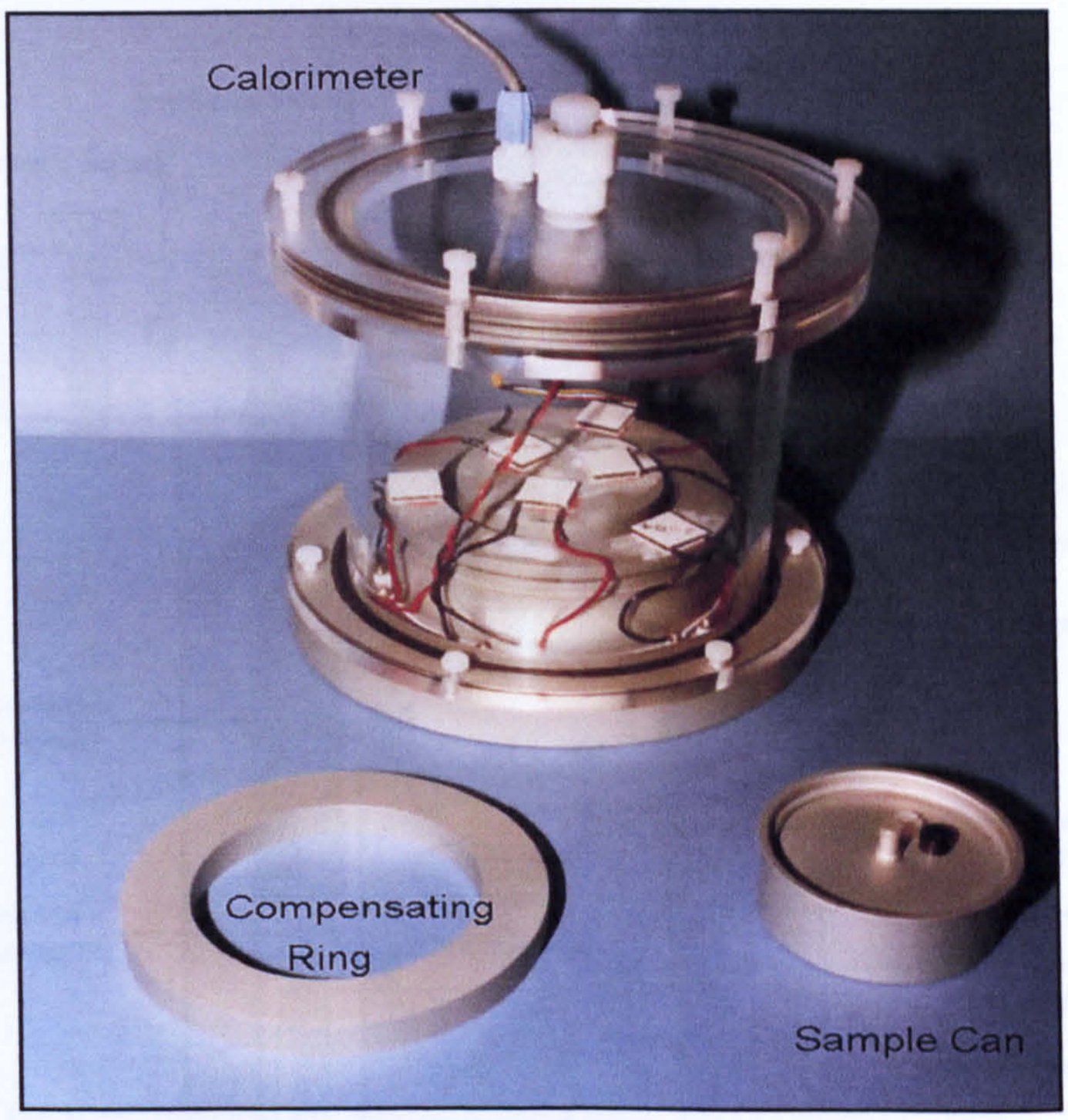

The large compensating ring (shown in plate 14) must be gently placed into the calorimeter pot. The 'male' electrical connection from the calorimeter must be attached into the 'female' socket located on top of the spun aluminium sample can. A secondary connector leading from the calorimeter pot to the electrical interface must also be connected adopting 'male' and 'female' connectors. The fully connected sample can must be slowly lowered in between the aluminium compensating ring and must come to rest upon the four ceramic thermopiles. The thermopiles must be clean, as any debris

could potentially affect the conductivity from the sample can connecting to the thermopile. Once the sample can is placed satisfactorily between the large aluminium compensating ring and a good connection is established, a foam liner is placed into the calorimeter pot to ensure that no temperature fluctuations occur. An additional polystyrene insulating cylinder is also slotted in between the foam liner. These insulating materials are adopted to prevent the ingress or egress of external heat energy. Once these are securely in place, the calorimeter pot lid may be screwed down. The calorimeter lid is forced down upon the rim of the body of the calorimeter pot and a water tight seal is ensured by the incorporation of a neoprene 'o' ring sandwiched between the calorimeter rim and lid.

Figure 38 : Calorimeter details (author)

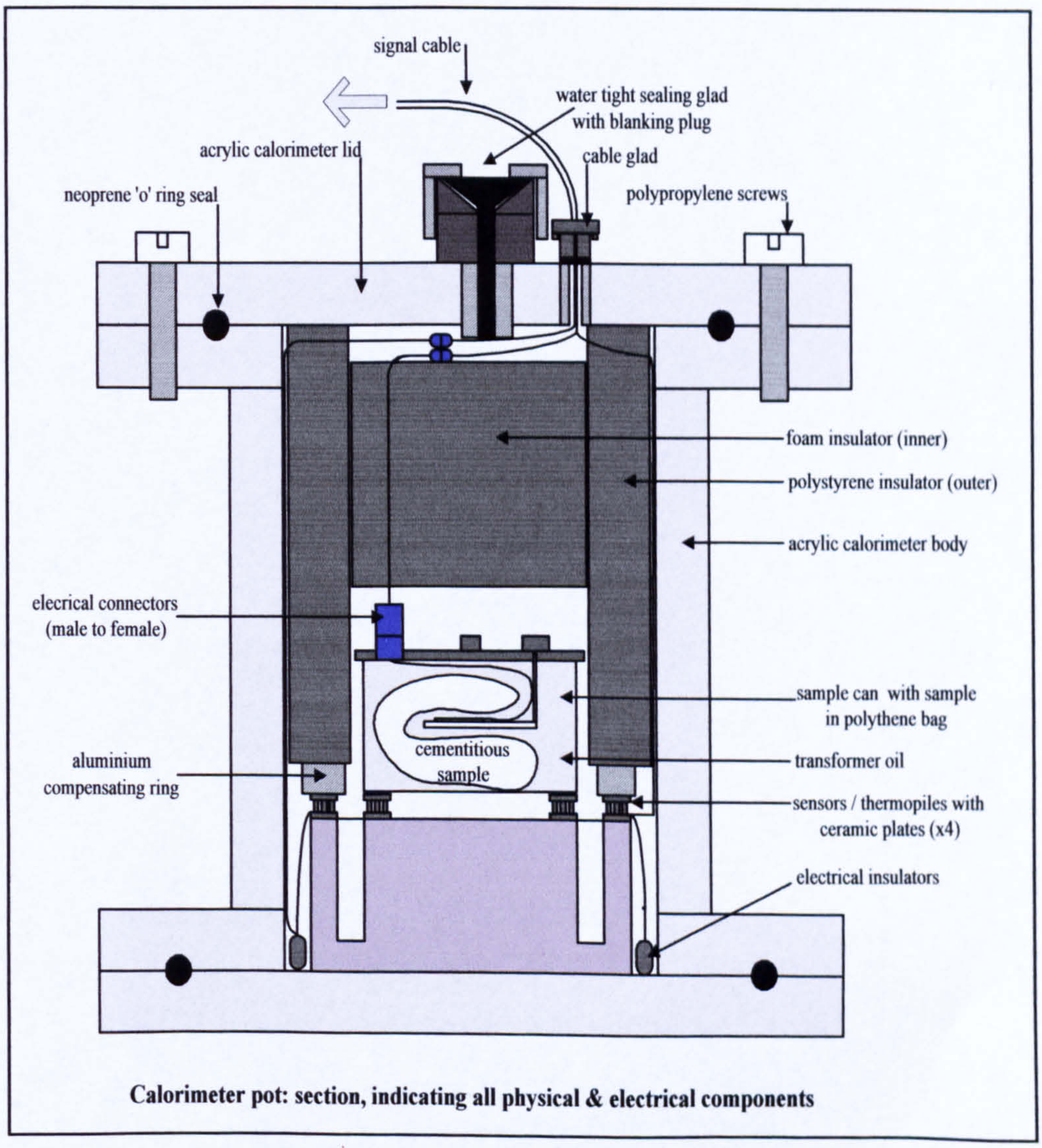

Calorimeter pot: section, indicating all physical & electrical components

The calorimeter pot is then lowered into the water bath and checked for leaks. If everything is satisfactory then a rubber isolating mat is submerged in the water and placed directly over the top of the sealed calorimeter pot. Finally, a metal lid is

positioned over the water bath aperture to ensure that no debris falls into the main water bath.

It must be emphasised that this procedure makes it impossible to observe heat evolution rates during the first approximate one hour of the reaction because the paste takes that long to reach thermal equilibrium in the water bath.

3.3.1.2 Data Input and calorimeter interface commands

The last stage is to establish the computational and electrical operations between the calorimeter pot, the interface and the logging computer. The test undertaken follows the graphical data collection format, which requires a mV scale (generally 50mV) to be entered and also a duration for the test run. Normally, the test duration is 72 hours (3 days). The computer programme that was initiated will require a channel input and also a calorimeter number, as it is possible to run up to 6 calorimeter pots simultaneously. However, in this case only two pots are operational and therefore, the numbers are limited to 1 or 2.

The test is allowed to run and a graph is plotted throughout the duration of the test, allowing a visual interpretation to be made prior to a data analysis once the test has been terminated. The graphical data can be regenerated via the use of a spread sheet computer package such as 'Microsoft Excel'©.

Figure 39 : JAF Conduction Calorimeter full system

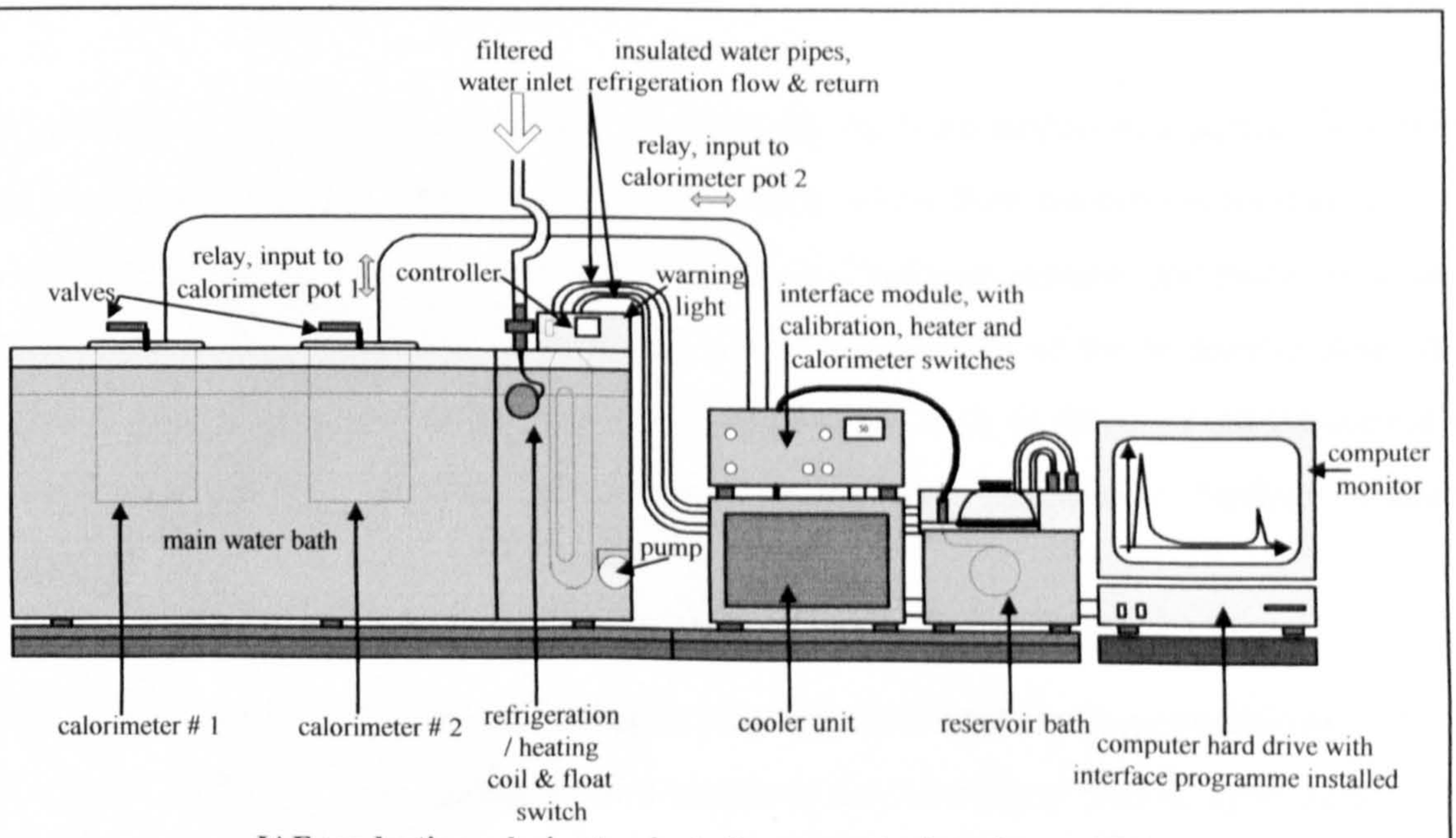

JAF conduction calorimeter, including computer interface and PC

The calorimeter must be calibrated for each run using an internal heater. It generally takes approximately 1 hour, with a minimum cycle time for the relay device of 0.5 minutes with a minimum of 50 cycles and is done after the end of the experimental run and before data analysis can begin. A typical trace obtained for cement is shown in figure 40.

Figure 40 : A typical experimental calorimeter trace including the calibration data.

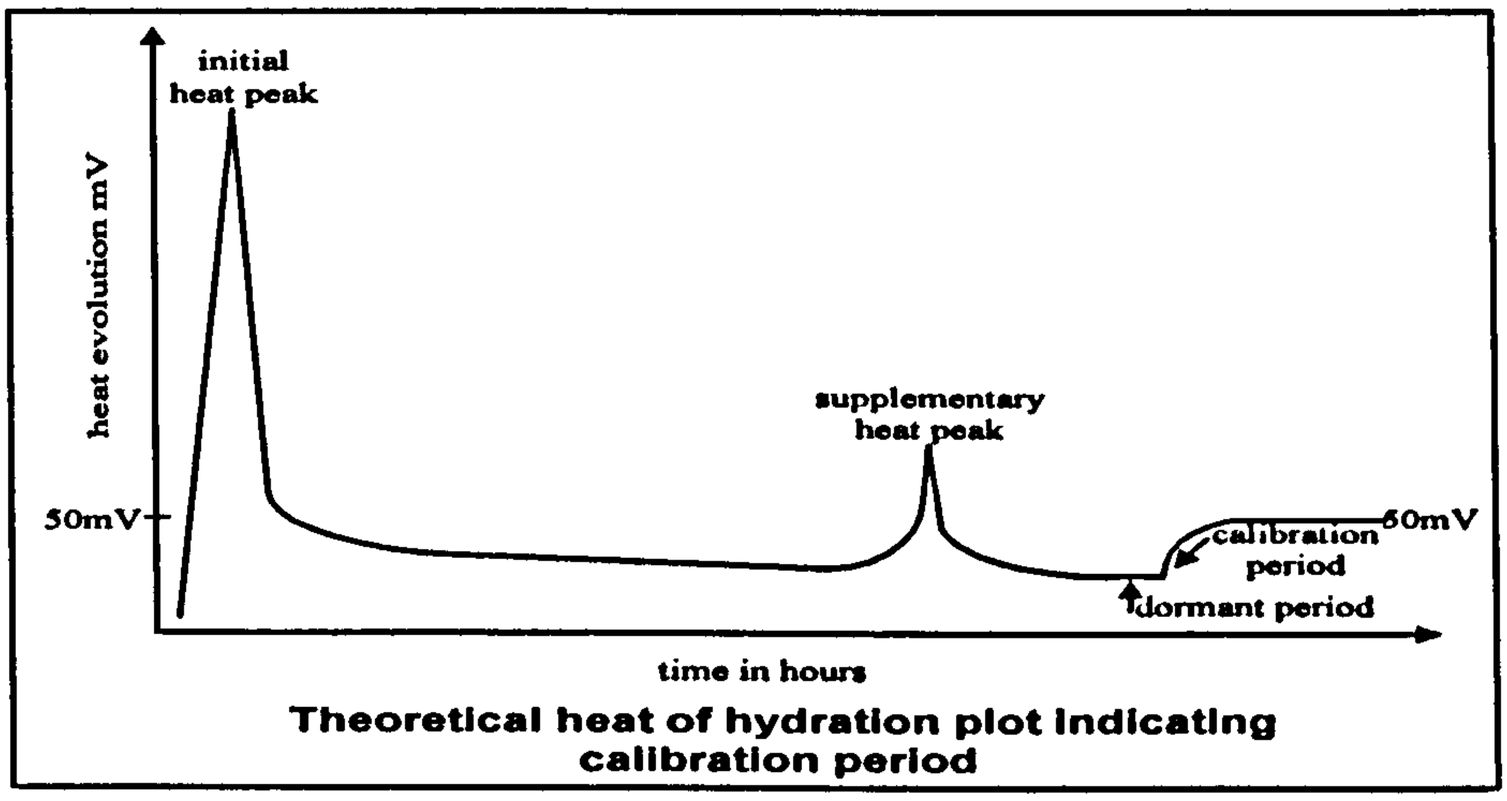

3.3.1.3 Test duration and associated factors

The study of hydraulic activity within cementitious binders is related to many factors, however, time has a major influence upon the formation and thermo-dynamic stability of C-S-H, A-S-H and $Ca(OH)_2$. The study of hydration within the first 3 days attempts to understand the hydration products which form within this period, and this differs from material to material. This depends upon the degree of hydraulicity, or reactive silicate and aluminate content within the material.

The growth of many of the hydraulic components do form within this period, however, several components lie dormant until such a time when they become activated. It is to be expected that $Ca(OH)_2$ growth will be seen in Portland cement, hydraulic lime and non-hydraulic lime. However, C_3S should not be seen in any of the hydraulic limes due to their lower calcination temperature. It is differences such as these which theoretically set Portland cement and hydraulic limes apart, and necessitate further in-depth investigation.

3.4 Water Vapour Permeability sample manufacture and curing conditions

The mortar samples were manufactured adopting the laboratory paddle type mixer. The mortars whether binary or ternary in nature were all 'knocked-up' for a minimum of 10

minutes (on setting number 2) and were considered to be thoroughly mixed and followed the 3 stages encountered by Hughes, [21] namely, bread crumb, balled and smooth well mixed. Colour consistency throughout the mortar reinforced the belief that the samples were suitable for use.

The water ratios seen in table 23 were adopted for the manufacture of the mortar samples. The workability of the samples was different depending upon the water demand of the material. However, it must be emphasised that in retrospect rheological measurements would be a more effective method of achieving consistency and reproducibility of sample manufacture. This method of assessing water demand for the mortars would also have greater relevance to materials used in practice.

The samples were manufactured via tamping the mortar into the sample container and troweling off the excess mortar to make a uniform surface and thickness of the sample. The curing of all of the mortar samples was undertaken in the curing room at Heriot-Watt University. The ideal curing temperature and relative humidity was 20°C +/- 3°C and 50% RH, +/-5%, with a duration of not less than 30 days. Every sample was sprayed intermittently with an atomising water bottle to ensure full hydration and to act as a catalyst for carbonation, however, this need occur only for the first few days. To prevent rapid drying of the samples from occurring it was necessary to cover all the samples in damp hessian sheet. This prevented excessive and rapid evaporation from occurring.

3.4.1 Water Vapour Permeability experimentation

The water vapour permeability experiments were based upon a variation of BS: 3177: 1959: *'Permeability to water vapour of flexible sheet materials'*. This was due to the fact that no specific British Standard existed at this time. This procedure was adopted for tests upon water vapour permeability of lime wash coatings by Boxhall and Trotman (1997) [50]. In addition to the aforementioned, English Heritage also adopted this test method upon the research exercise, 'the Smeaton Project" [51]. Subsequently, a new British Standard, BS EN 1015-19:1999: Methods of test for mortar for masonry- Part 19: *'Determination of water vapour permeability of hardened rendering and plastering mortars'*. came into effect in January 1999, halfway through the testing programme. Upon analysis of this new British Standard, it was not deemed necessary to alter the current experimental procedure as the existing system followed the new British

Standard closely, and both worked upon the principle of dry cup experimentation, similar relative humidity and test duration.

Although the authors test procedure was very similar to the new BS EN1015-19 test method certain differences did occur in terms of sample preparation and test methodology.

- The curing conditions for BS EN1015-19 samples were 20°C +/- 2°C and 95% +/- 5% relative humidity. These conditions were generated for the first 2 to 5 days depending upon the sample constituents. A reduction in the relative humidity to 50% +/- 5% was undertaken after this point for the remainder of the 28 days curing time. This differed from the authors' samples that were cured in an atmosphere of 50% +/- 5% at a temperature of 20°C +/- 3°C.

- All the samples were tested for water vapour permeability within a maximum 10 week period post manufacture. All of the samples should have been tested simultaneously but the large number of samples, twinned with desiccant variation, led to a slightly extended test period.

- The cured samples were then tested in the (Weyco) thermal cabinet at 100% relative humidity at a temperature of 25°C.

- The desiccants adopted for the authors' research also differed from BS EN1015-19. The BS adopted KNO_3, (Potassium Nitrate) and LiCl (Lithium Chloride) as desiccants as opposed to KCl (Potassium Chloride), NaCl (Sodium Chloride) and $NaNO_2$ (Sodium Nitrite).

The final difference between the experiments was due to the variation in the size of air gap between the sample and the desiccant. BS-EN 1015-19 adopted a 10mm air gap whereas the authors' samples had an air gap of 90mm. This should not affect the test as the calculation for water vapour permeability takes into consideration the distance between sample and desiccant and allows for adjustment in air gaps.

The mortar samples under test consisted of a range of binders. These include non-hydraulic, feebly hydraulic, eminently hydraulic, gauged limes and finally Portland

cement. Three samples for each type of binder were manufactured totalling 36 samples in all. These samples were then tested adopting three different desiccants, namely, KCl, NaCl and $NaNO_2$ the purpose of the desiccant adopted was to act as a driving mechanism generating a partial water vapour pressure differential across a closed sample container. Hence 108 sample disks were tested in all.

When the samples were exposed to a high relative humidity (100% RH) the weight of the sample increased, with a relationship between the exposure period and weight gain being noted. This was dependent upon the duration to which the samples were exposed within the environmental thermal chamber.

Figure 41: General arrangement of permeability apparatus

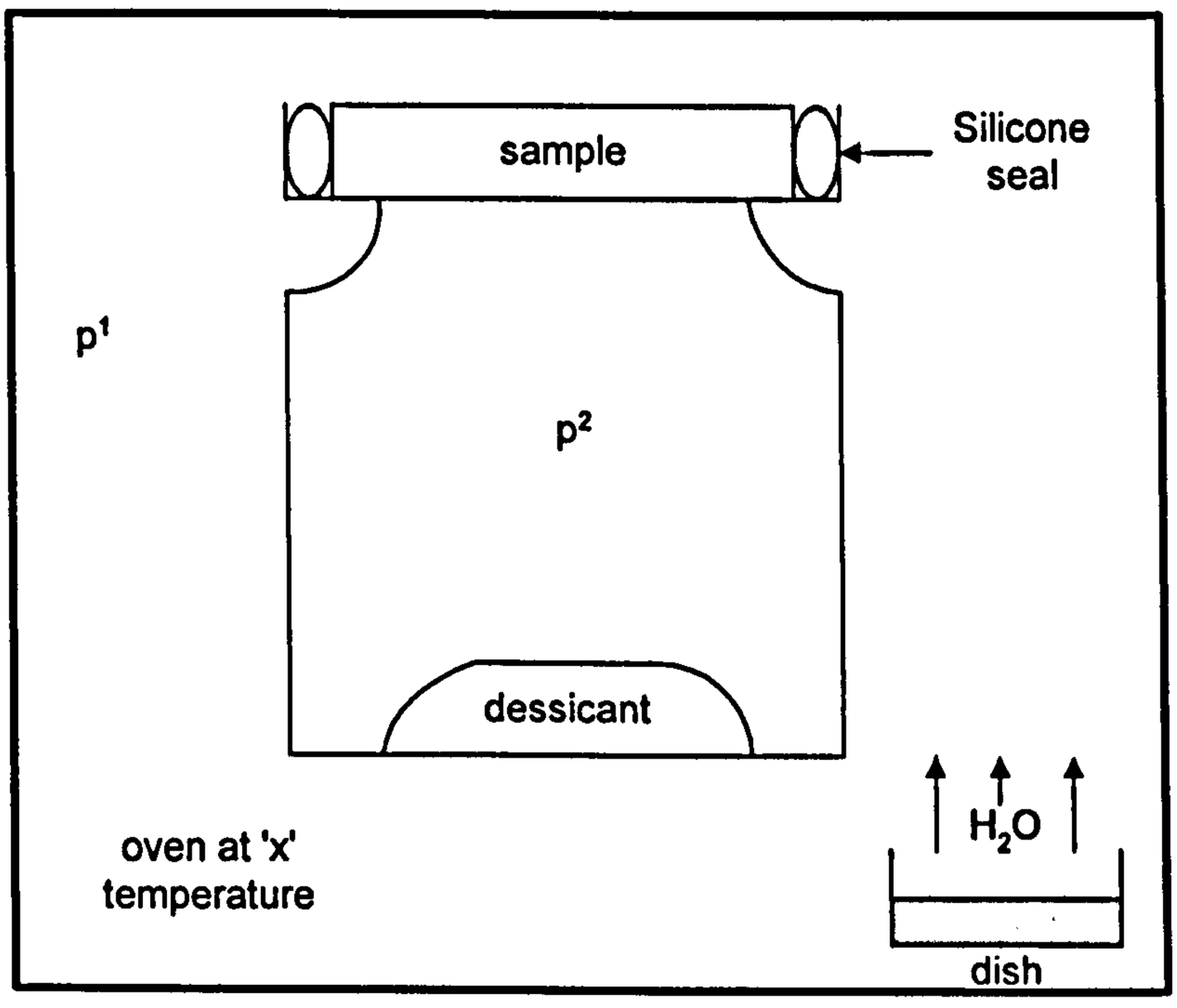

The set up had to be relatively inexpensive due to the large number of samples needed. The container for holding the samples needed to be adequately secured and seal the mortar samples. The mortar disk sample is then sealed in position adopting a silicone sealant. To activate a driving force a desiccant is placed within the container. The container is then weighed in its entirety and this weight is recorded. The container must be placed in a controlled humidity oven (Weyco controlled environment chamber) which will be set to a known temperature. Inside the oven, along with the sample vessels was a water source. This allowed a constant relative humidity to be achieved at

any given temperature. As the temperature within the oven is known it is quite easy to ascertain the relative humidity of the chamber by reading off a psychometric chart.

As water vapour penetrates through the sample from the high humidity outside the container through to the desiccant placed within the container and undergoes a weight change. At regular intervals the sample was removed and re-weighed, with the difference between the two weights being logged. From this data calculations were undertaken to evaluate the rate of permeability of the mortar sample.

The level of absorption exhibited by the desiccant must be known as all desiccants have different rates of absorption. Therefore, desiccants have different thermodynamic properties at different temperatures.

Hence, the graph of weight against time could be drawn (figure 42).

Figure 42 : Weight change with time.

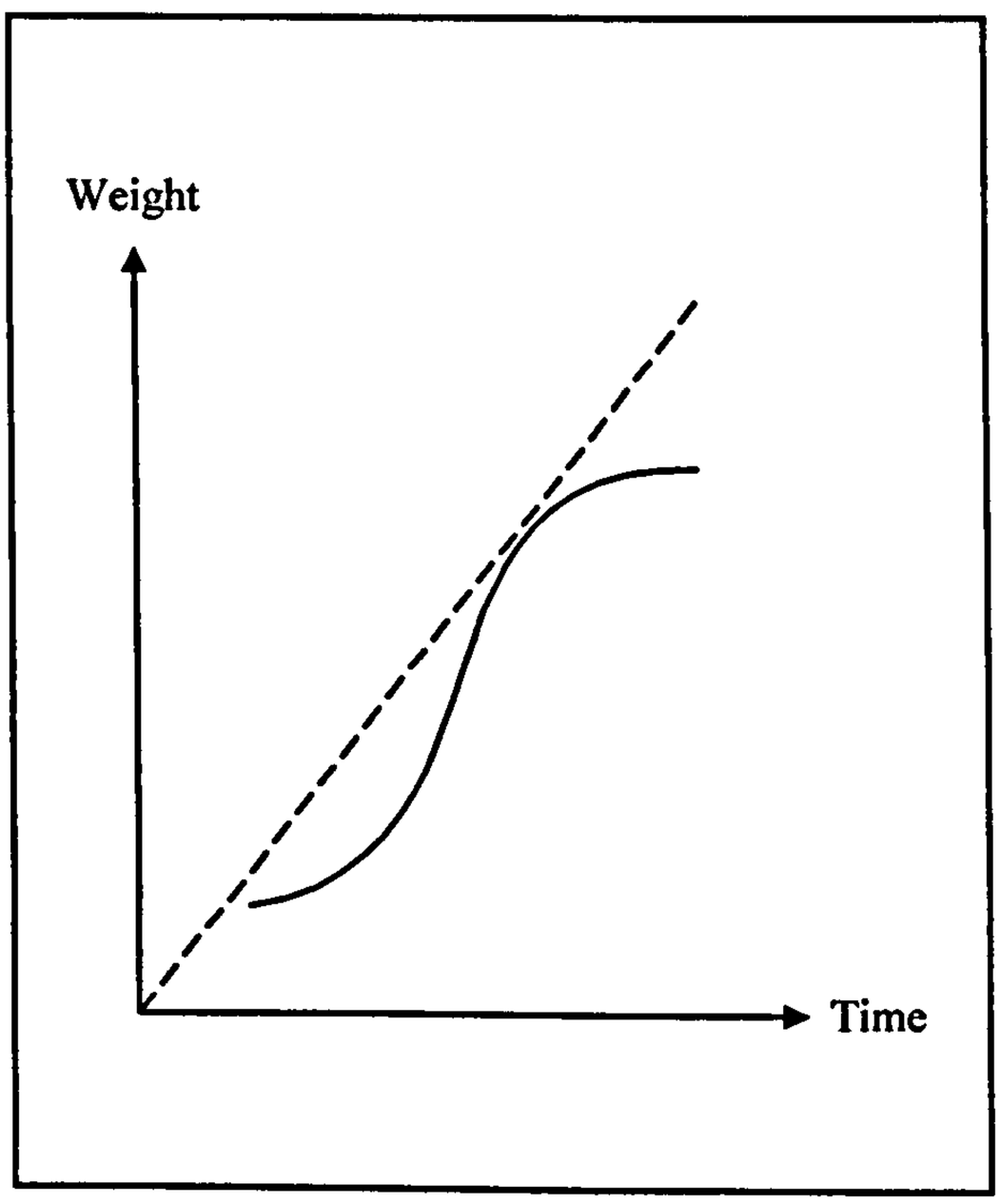

Therefore, following the calculation for permeability we can evaluate the level of diffusion.

The desiccating agents to be adopted were: Sodium Nitrite ($NaNO_2$), Potassium Chloride (KCl) and Sodium Chloride (NaCl). While referred to as desiccants, strictly speaking these are saturated solutions which provide a constant and reproducible relative humidity inside the sample container of 66, 76 and 86 % respectively.

The advantage of this form of experiment was its relative inexpensive nature and its simplicity in use. In addition a constant vapour pressure can be maintained easily. However, problems may be encountered when weighing the sample due to the fact that the time taken between removing the sample container and weighing it will allow for heat dissipation from the container. This may alter the weight of the container and give inaccurate data. The risk was minimised by keeping the time interval as short as possible and rotating (calculated from random charts) the order of the samples taken from the thermal cabinet.

Different samples were required for every change in relative humidity. This increased the time and number of samples required for the experiment. In addition to the lime mortars a small number of control specimens of plasterboard were also tested.

3.4.2 Water vapour permeability results

The permeability of the sample was calculated from the slope of the graph generated from plotting the cumulative weight increase of each container (weight in milligrams) against the total time of exposure in the cabinet. The required slope is that of the best straight line (following y=mx+c), drawn through those points which represent the constant rate of gain. Hence, it is measuring'χ' mg, weight increase over a period of 24 hours, for an exposed area of 50 cm^2. When 4 points lie in a straight line, upon the graph, steady state conditions are deemed to be attained. The graph below indicates the process of plotting the experimental data until at least 4 points along the straight line have been achieved. The curved section on figure 43 relates to the development of steady state conditions.

Figure 43 : Typical results (schematic)

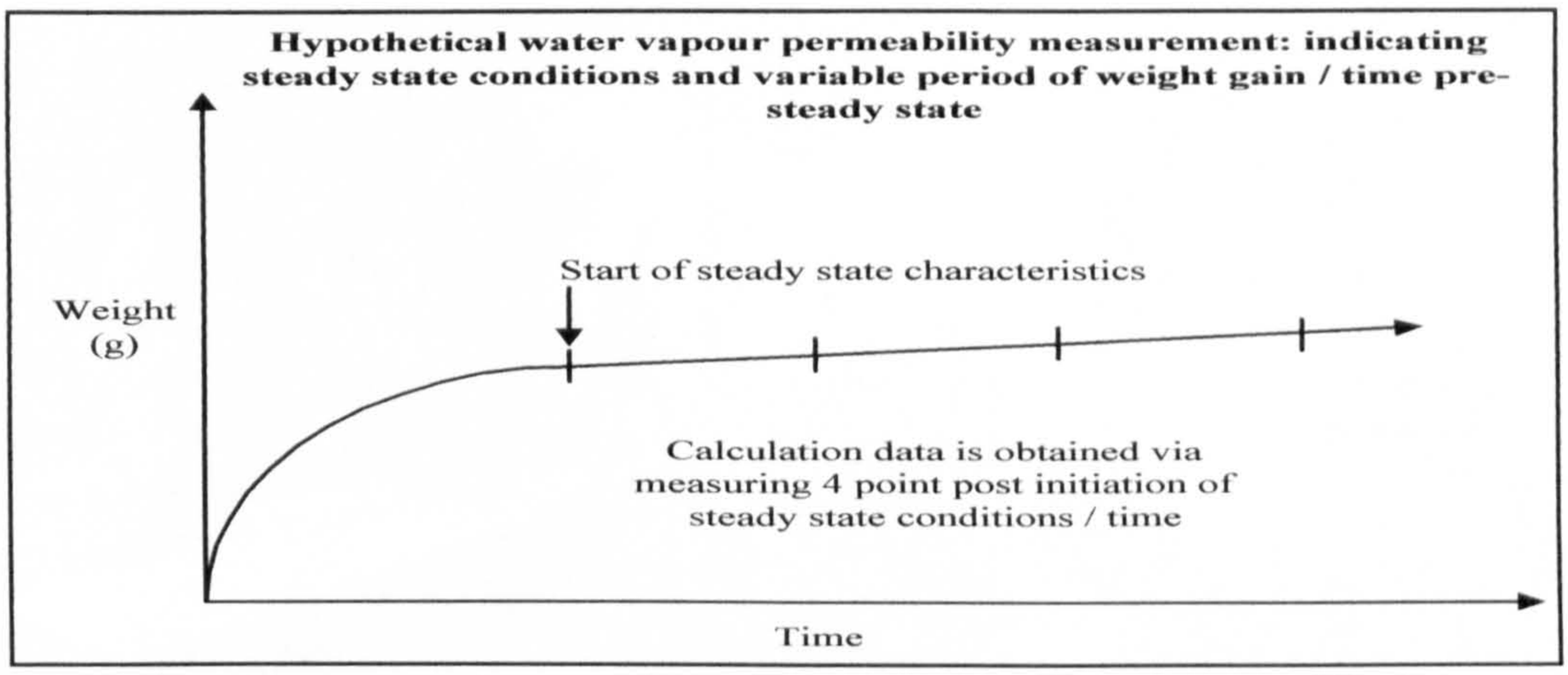

The sample was cast into the screw cap of the container which had been cut out to an internal diameter of approximately 80mm, this is therefore the dimension for calculation of the mortar sample. Therefore, πr^2 , $\pi 40^2$mm = 5027.7mm^2 or 0.005027m^2. The thickness of the mortar sample is approximately 10mm. A set of data is shown in figure 44.

Figure 44: A typical set of data for a lime mortar

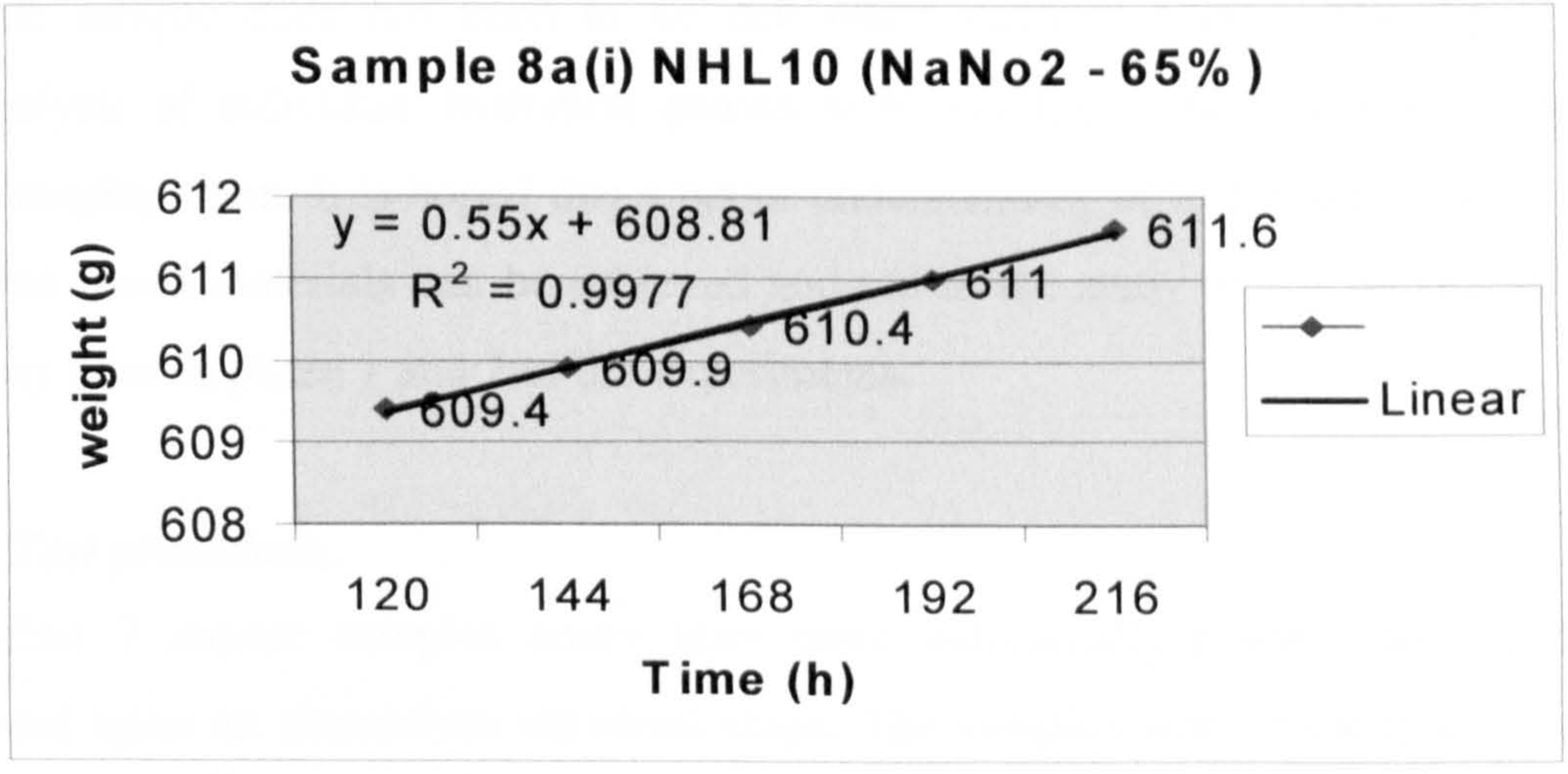

3.5 Environmental Scanning Electron Microscope (ESEM)

ESEM analysis of mortar samples was of interest to evaluate crystallography, mineralogy, pore size distribution, and also the bond at the aggregate interface. This was essential for the verification of hydraulically active components and subsequent crystalline growth. This will hopefully aid in understanding of the hypothesised relationship between hydraulicity and permeability of lime based materials.

Plate 15 : The ESEM set up at Heriot-Watt University

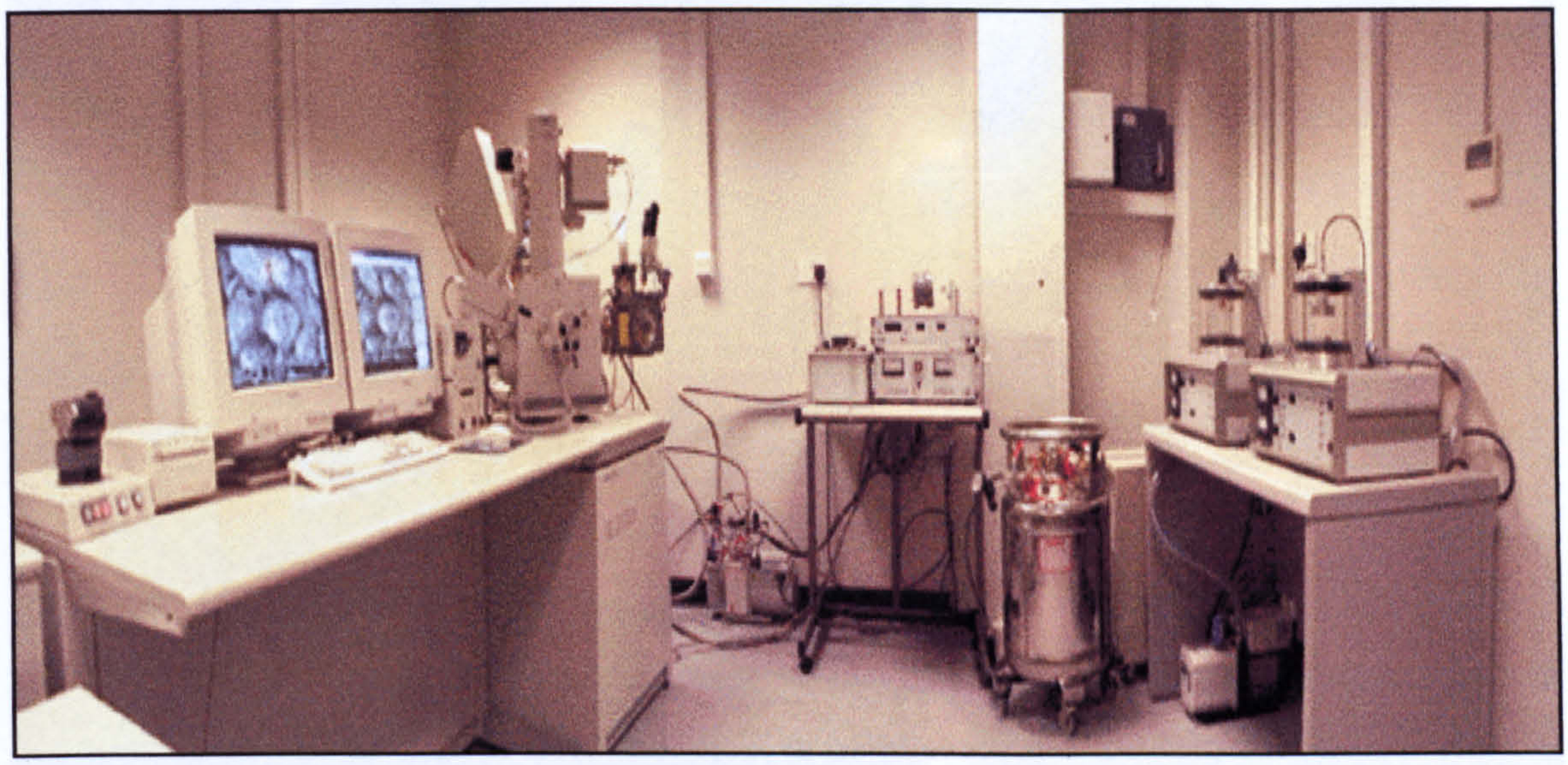

The advantages of adopting ESEM technology as opposed to conventional SEM microscopy, include:

- No need to coat the sample with gold prior to analysis.
- The sample does not need to be dry when analysis occurs. Thereby allowing analysis of individual hydration phases to be studied within the material without damaging them. It is hoped that a better understanding of hydration products within lime based materials can be achieved and aid in the study of any anomalies which may arise in phase 1 and 2 of the experiments.

3.5.1 Test procedure.

The first 7 mortar samples under tests were individually placed into the ESEM, mounted upon an aluminium universal stage. The samples were stuck to the universal stage adopting (C-Plast) plastic conductive carbon cement. Once all of the samples were secure they were placed into the ESEM chamber and a partial vacuum was generated. The partial vacuum was increased and stabilised at 0.6 torr.

Plate 16 : samples placed upon universal stage in ESEM chamber

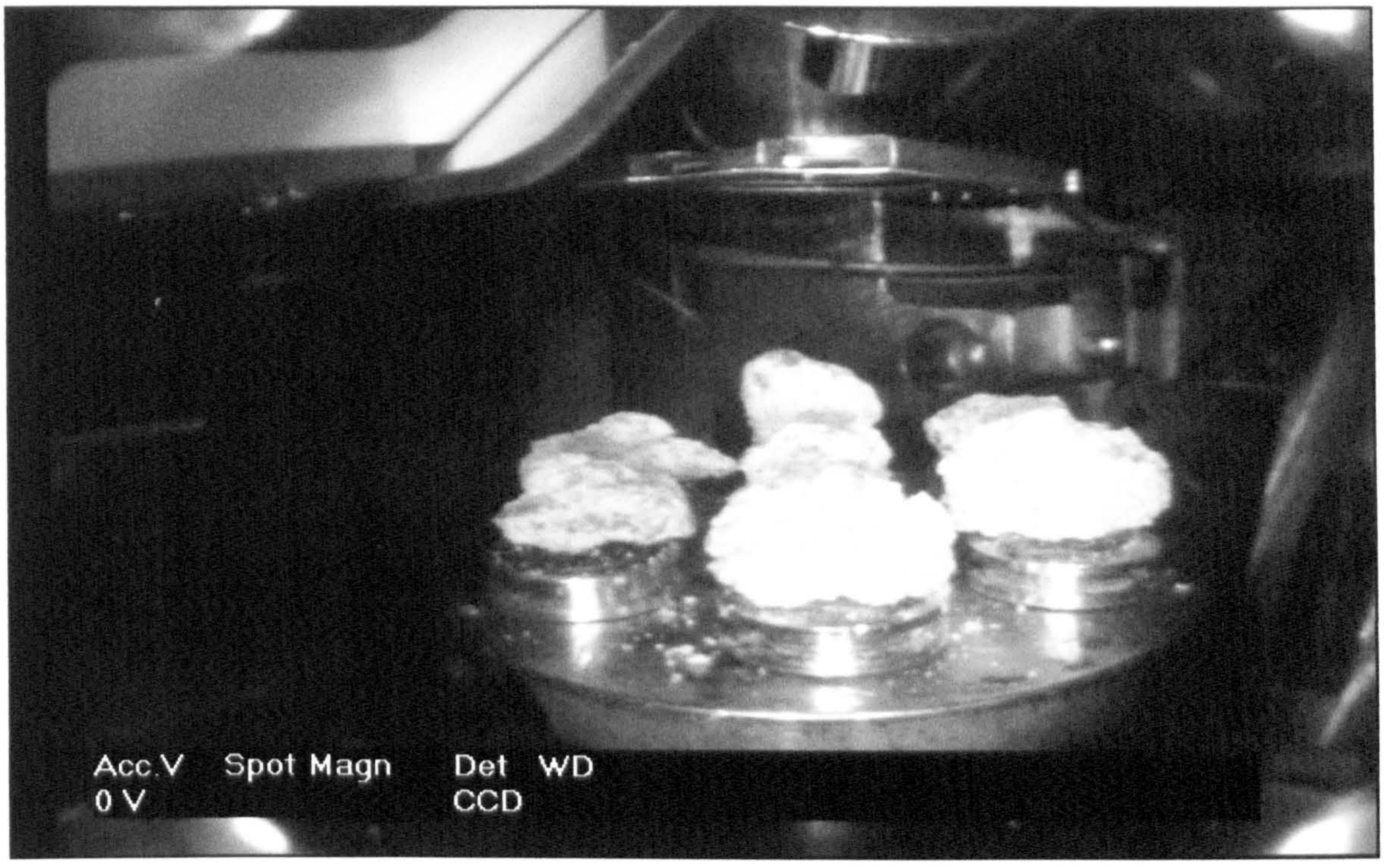

The image quality of the digital pictures received from the ESEM was enhanced by introducing an inert gas into the working chamber. In this case the gas adopted was water vapour, as it is believed to give the best conditions for experiments of this nature. The ESEM was set for 20Kv electrons, this being the standard for this operation. The ESEM tracked across the samples at low resolution. Once an area of interest had been established the microscope was slowly set for increased magnification. The maximum intensity achieved with clarity for these tests was in the region of 12000x, however to attain maximum information from the samples it was necessary to take images, twinned with EDX tests at various magnification.

The samples were examined for features that would explain any relationship between the water vapour permeability and the hydraulicity of the material and the results are presented in chapter 4.

3.5.2 Energy Dispersive X-ray (EDX) analysis

The EDX analysis is undertaken by the ESEM whilst simultaneously allowing a visual appreciation of the material under test. The area designated for analysis is mapped by the ESEM. Mapping is the process of scanning the surface of the material in a repetitive manner, acquiring layer upon layer of data. The chemical analysis is represented in both a graphical plot with respective chemical concentrations represented by peaks the

largest and most significant of these is the K-α peak. A secondary peak may also be noted within EDX plots and is known as the K-β peak. This is generally disregarded from the analysis.

Chapter Four: Results

4.1 General Introduction

As the experimentation was undertaken in 3 phases it would be logical to assess the data within these 3 areas individually. Hence, the hydraulicity, water vapour permeability and ESEM analysis will be collated and a brief assessment of the materials performance will be undertaken.

4.2 Hydraulicity Results

The three day conduction calorimetry tests were designed to show the level of hydraulic reactivity within the sample under test, and also simultaneously attempting to attain accurate information regarding significant changes in the hydration of the cementitious material. The full range of cementitious samples are discussed in this section.

4.2.1 Natural Hydraulic lime 2 (NHL2) samples

The initial hydration phase displayed in figure 45 sees a rapid rise in heat evolution at 1.68 hours, with a maximum rate of heat of 27.86 W/Kg. Following this point a slow but steady decline in activity occurs to zero at approximately 65 hours. The initial heat peak may be attributed with the formation of portlandite [calcium hydroxide ($Ca(OH)_2$)] crystals, and simultaneous low level C-S-H compound development.

The negative values at the very start of the experiment must be ignored because they are due to the sample reaching thermal equilibrium in this time.

The total heat generated by the NHL2 was 2054.16 kJ/kg over a 72 hour period. This relates to the average NHL2 total heat of 2067.02 kJ/kg. The total heat generated in the NHL2 sample is represented in figure 46, which follows an approximate parabolic function. The rate of heat generated increases until a maximum value at approximately 2 hours. After this point the rate of heat decreases and tends to zero post 70 hours, marking an end to the hydraulic activity.

Figure 45 : Rate of heat for NHL 2 sample (72 hours)

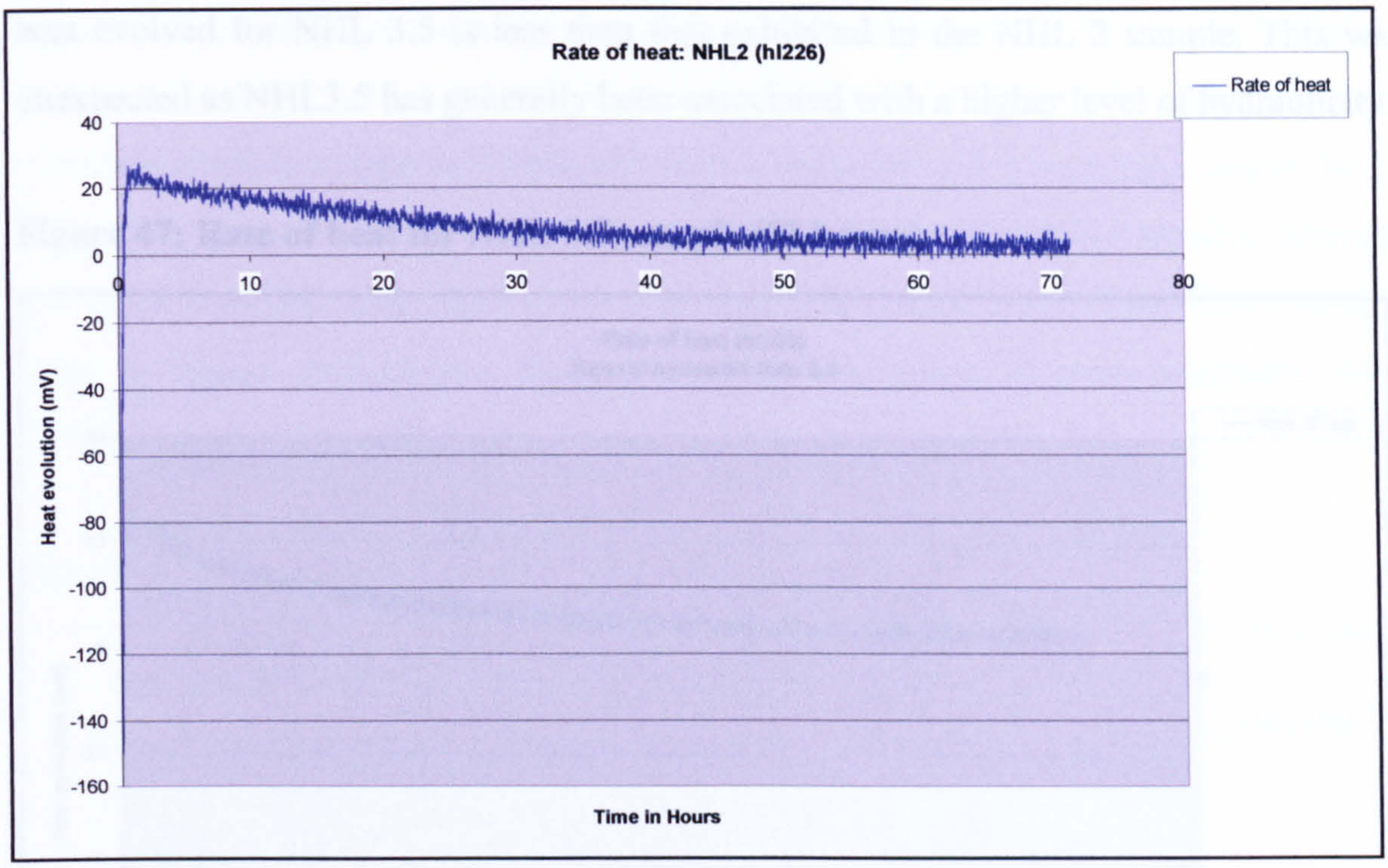

Figure 46 : Total and rate of heat for NHL 2 sample (72 hours)

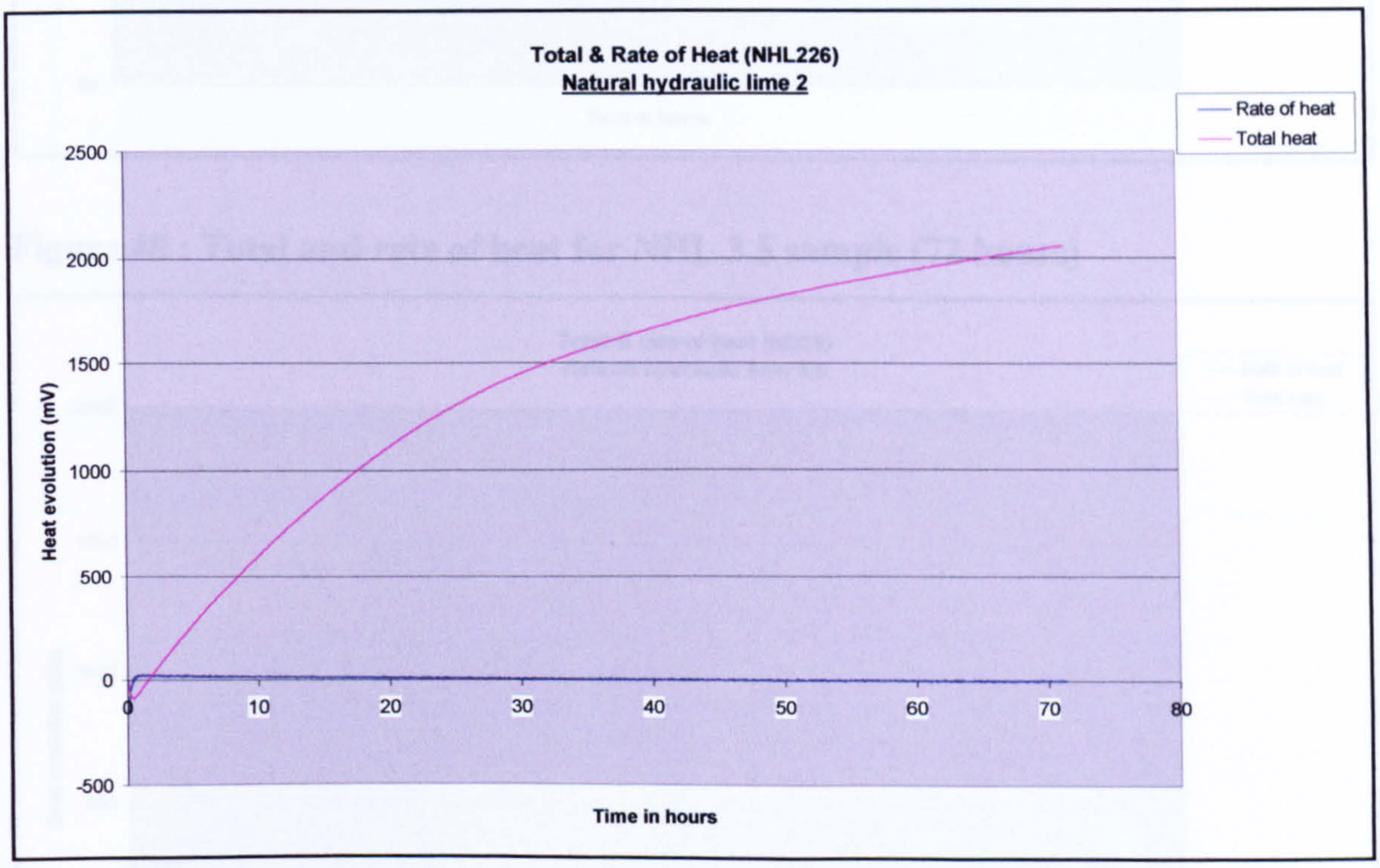

4.2.2 Natural hydraulic lime 3.5 (NHL3.5) samples

The initial hydration phase displayed in figure 47 shows the same rapid rise in heat evolution as that seen in the NHL 2 sample. This continues until a maximum point occurs at approximately 0.86 hours, with a maximum rate of heat of 27.73W/Kg. After this point a slow but steady decline in activity occurs with relative dormancy prevailing at approximately 70 hours. The total heat generated was 1828.53 kJ/kg (shown in figure

48), which was similar to the average NHL 3.5 total heat of 1517.33 kJ/kg. The total heat evolved for NHL 3.5 is less than that exhibited in the NHL 2 sample. This was unexpected as NHL3.5 has generally been associated with a higher level of hydraulicity

Figure 47: Rate of heat for NHL 3.5 sample (72 hours)

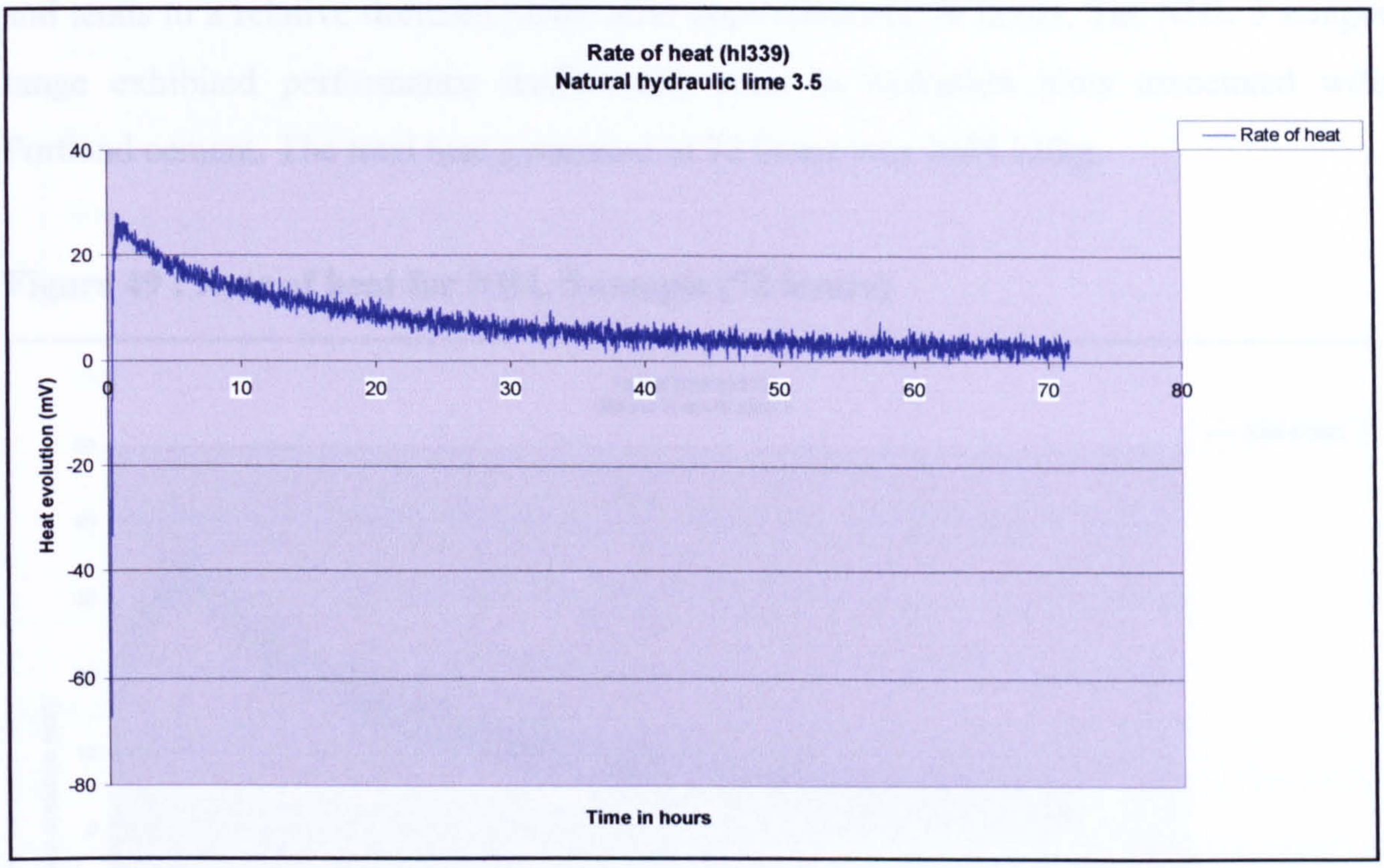

Figure 48 : Total and rate of heat for NHL 3.5 sample (72 hours)

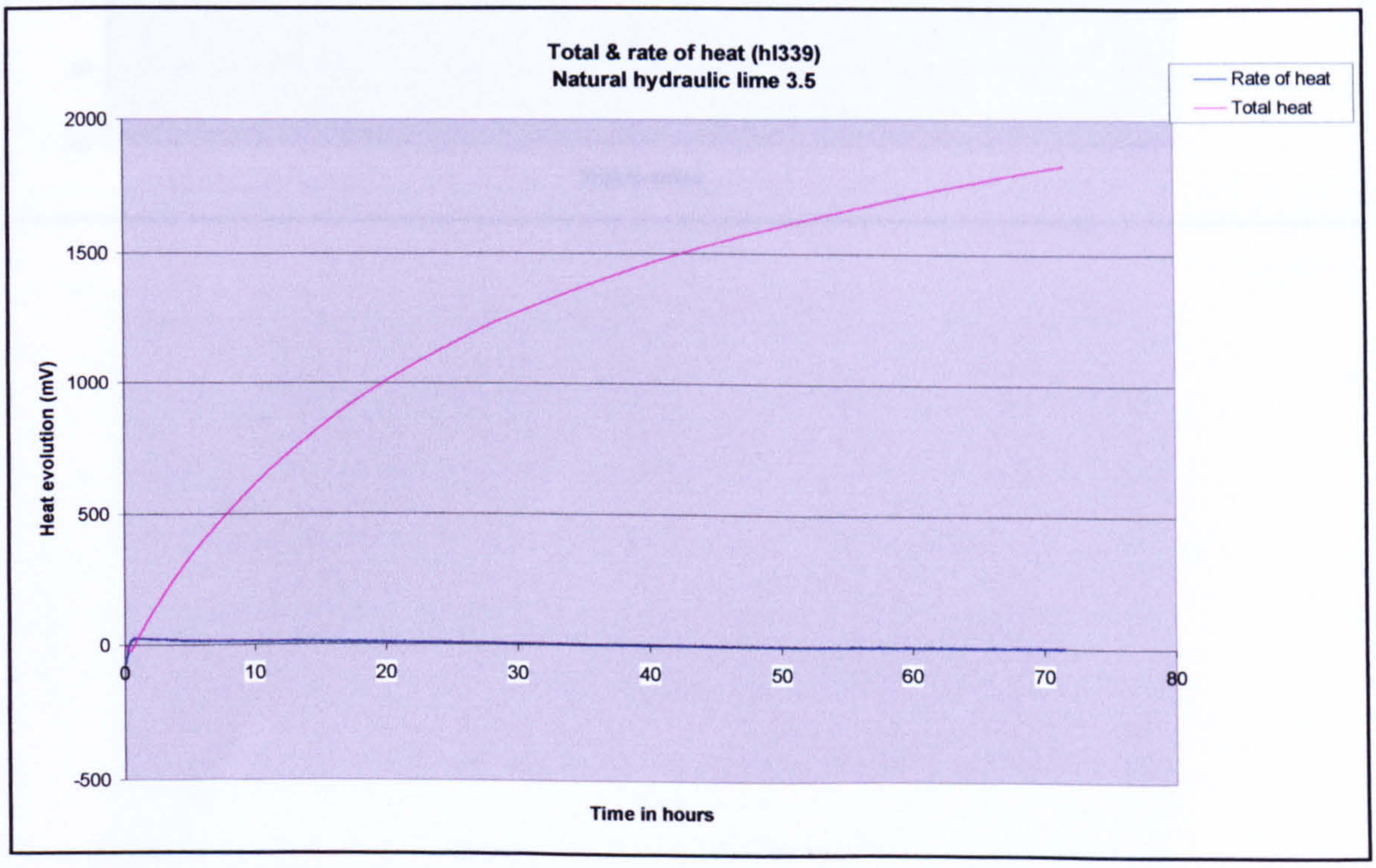

4.2.3 Natural Hydraulic lime 5 (NHL5) samples

The initial hydraulic activity displayed in figure 49 shows a rapid rise in heat evolution at approximately 1 hour, with a heat generated close to 27 W/kg. The rapidity of heat evolution starts to reduce and begins to form a shoulder with a maximum rate of 38.17 W/kg at 6.45 hours. The hydration of the NHL5 starts to slowly but steadily decrease and tends to a relative dormant phase after approximately 70 hours. The NHL 5 sample range exhibited performance traditionally seen in hydration plots associated with Portland cement. The total heat generated in 72 hours was 3044 kJ/kg.

Figure 49 : Rate of heat for NHL 5 sample (72 hours)

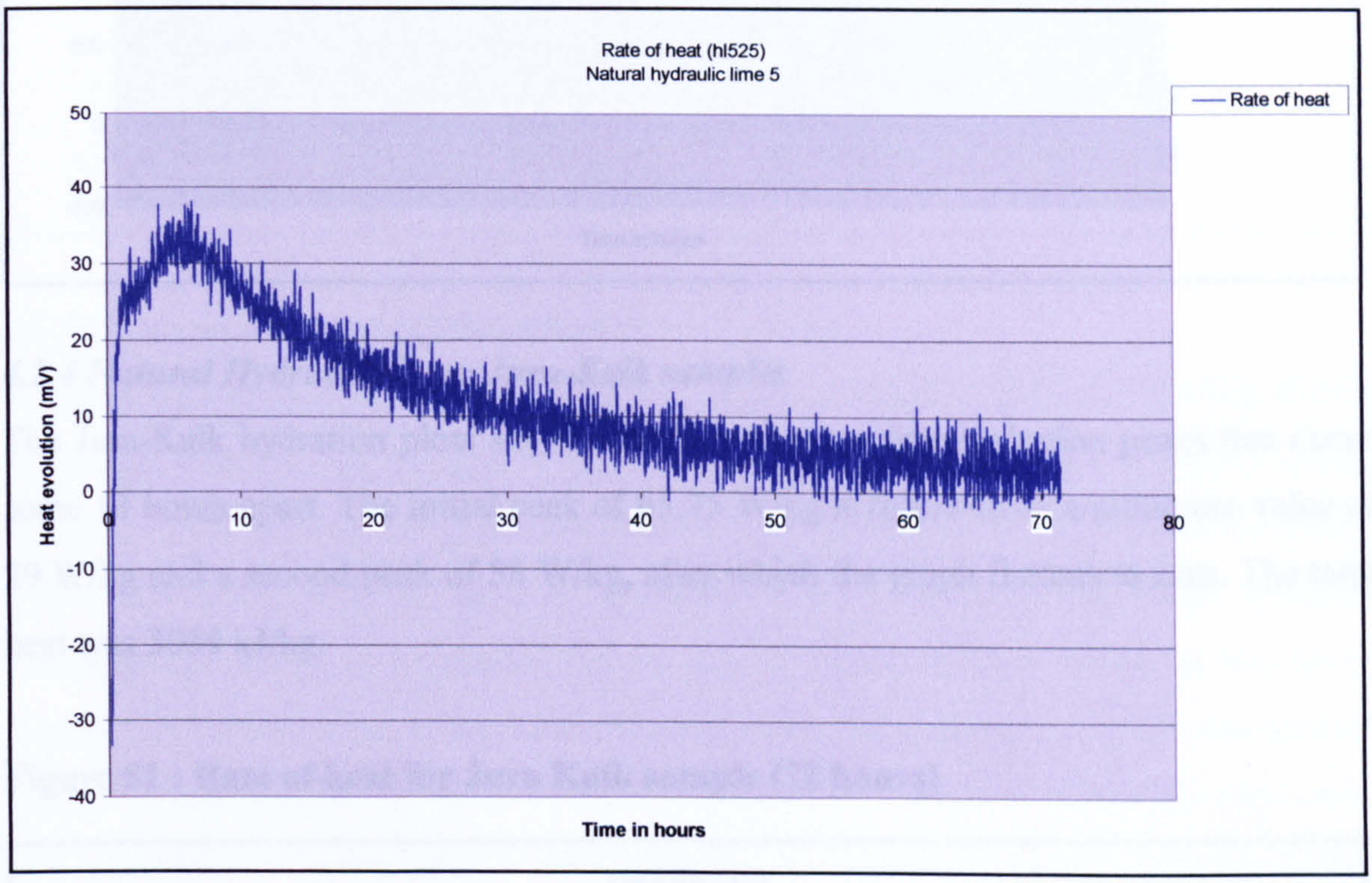

Figure 50 : Total and rate of heat for NHL 5 sample (72 hours)

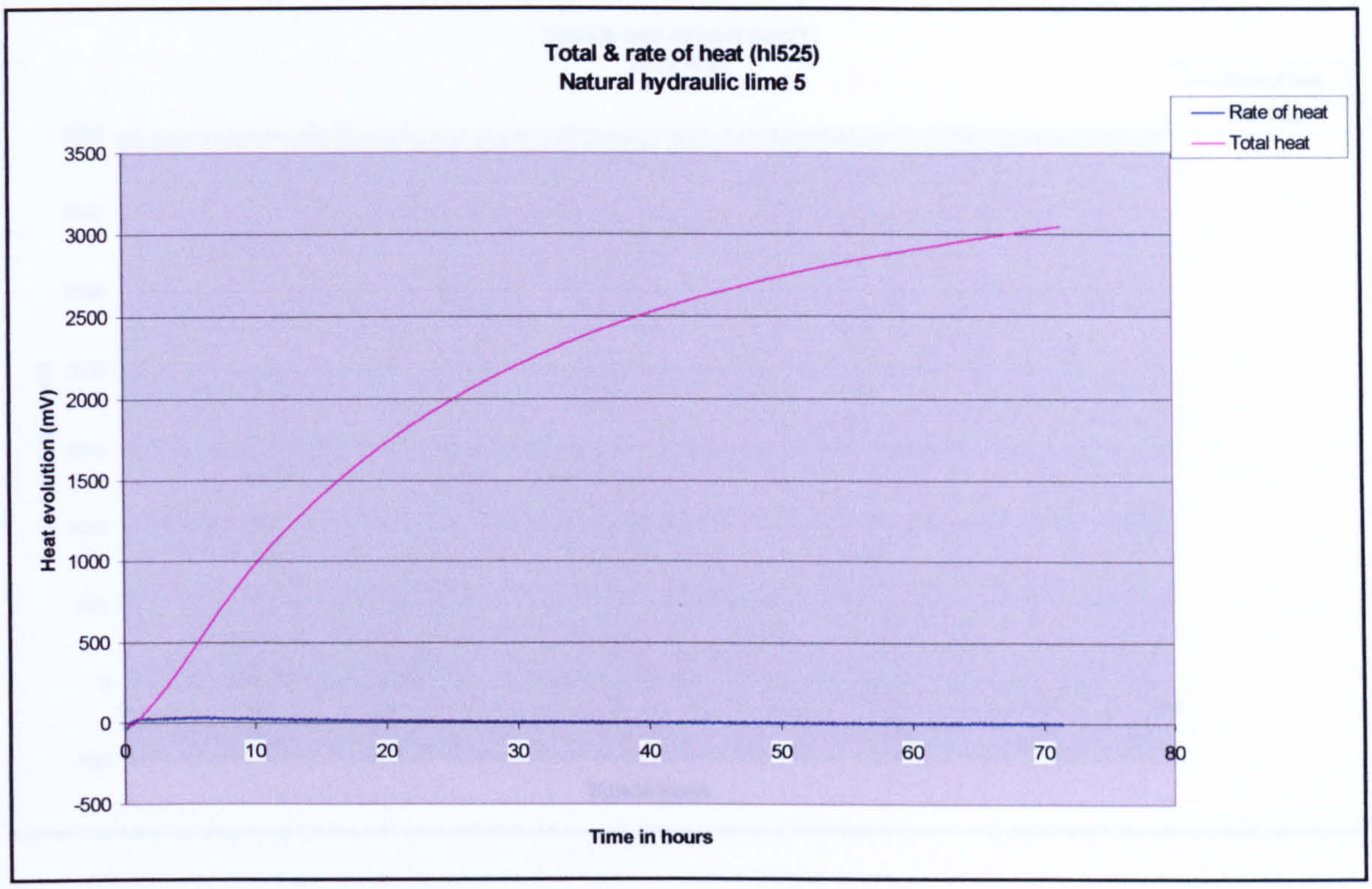

4.2.4 Natural Hydraulic lime: Jura-Kalk samples

The Jura-Kalk hydration plots show primary and secondary hydration peaks that occur some 13 hours apart. The initial peak of 65.75 W/kg is followed by a minimum value of 29 W/kg and a second peak of 58 W/kg, after which the graph flattens to zero. The total heat was 3054 kJ/kg.

Figure 51 : Rate of heat for Jura Kalk sample (72 hours)

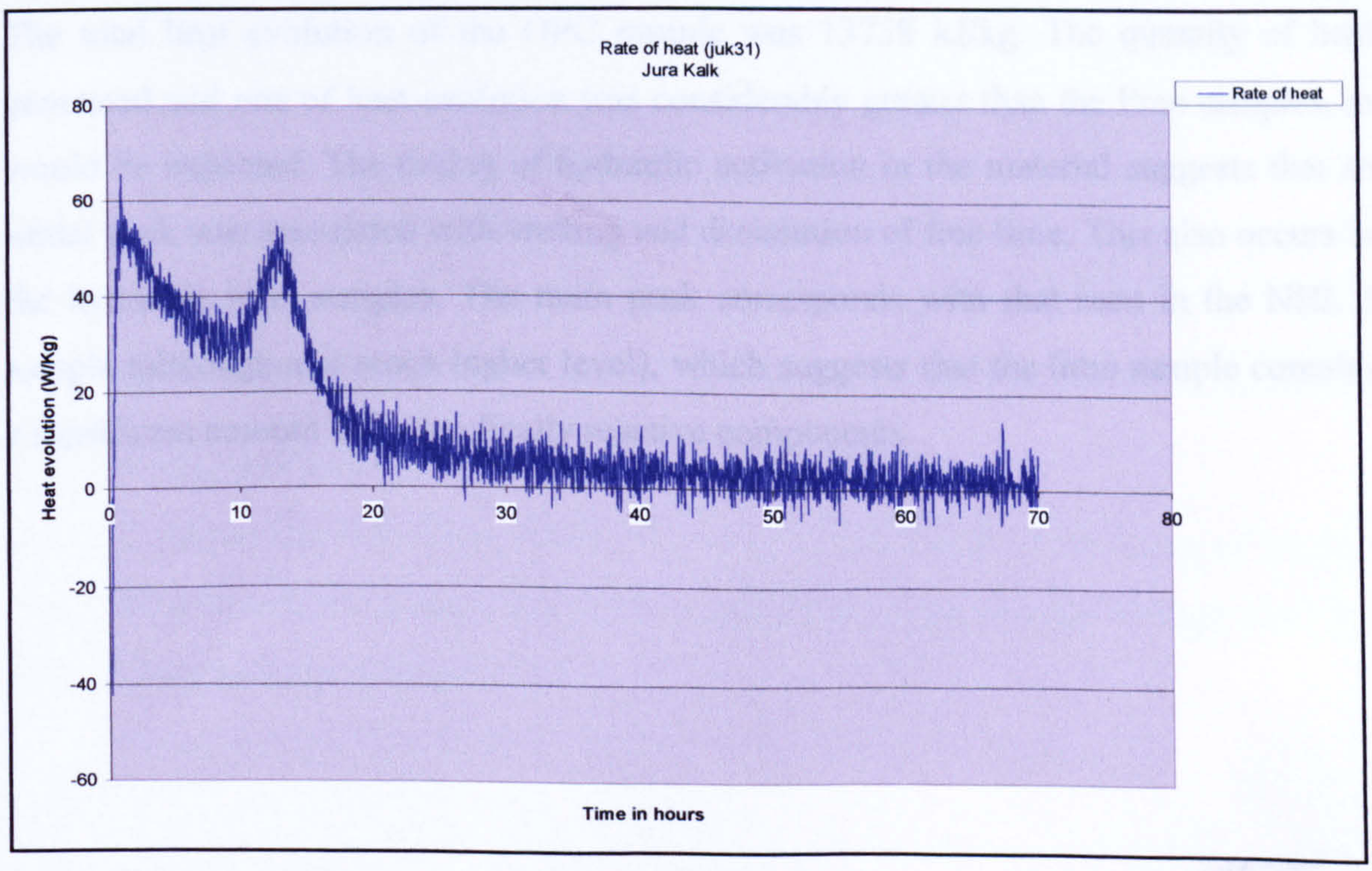

Figure 52 : Total and rate of heat for Jura Kalk sample (72 hours)

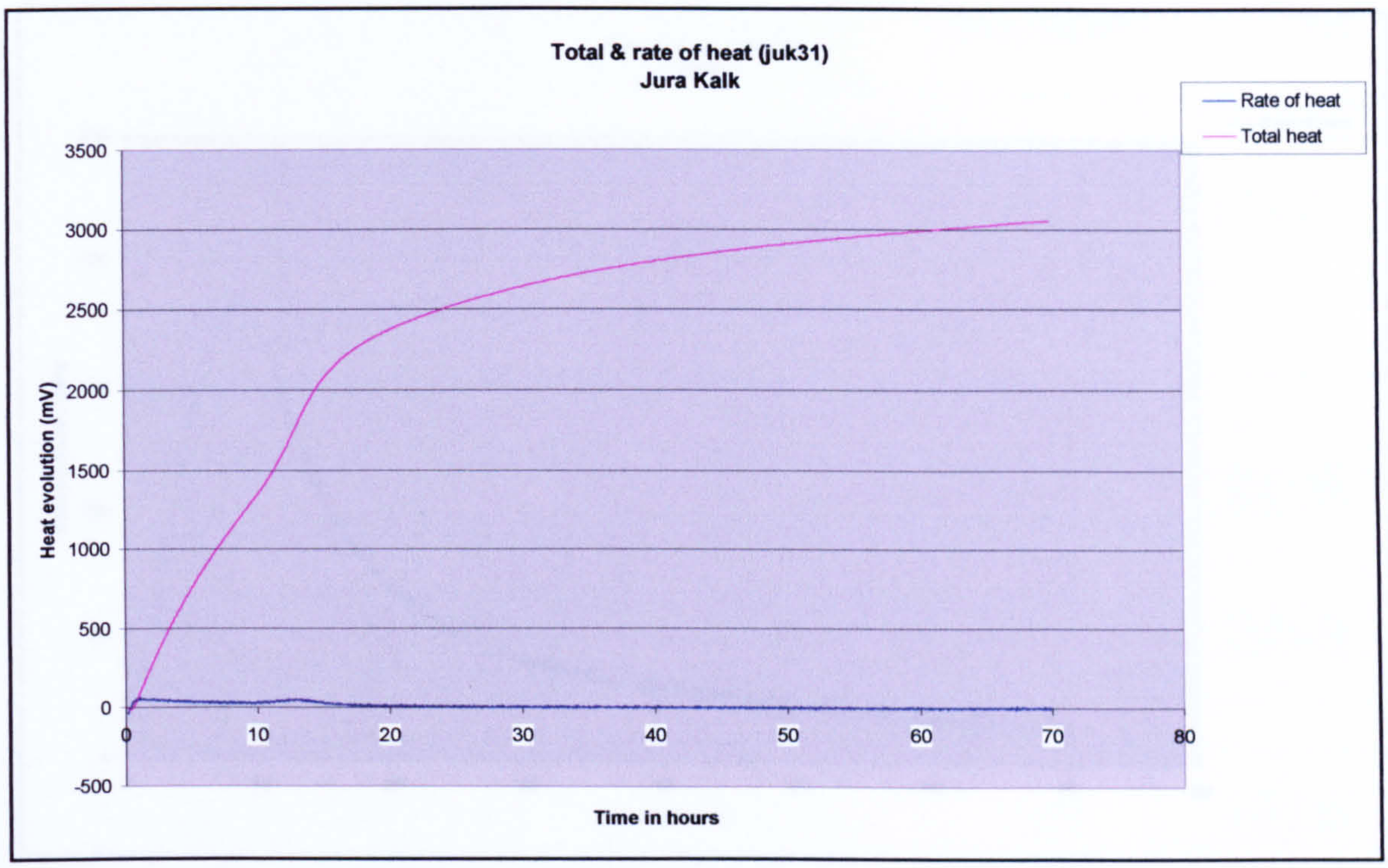

4.2.5 Ordinary Portland cement samples

Portland cement hydration is characterised by an initial heat peak developing almost instantaneously (within the first hour) after the wetting phase, which decreases almost as fast as its formation. From this point the development of a secondary heat evolution phase, normally attributed to C_3S hydration is seen with the traditional shoulder formation occurring. A maximum rate of heat of 188.4 W/kg at 8.9 hours was noted (figure 53). The decline in the heat evolution from this shoulder is relatively gradual with a period of approximately 50 hours taken prior to relative dormancy been seen. The total heat evolution of the OPC sample was 13738 kJ/kg. The quantity of heat generated and rate of heat evolution was considerably greater than the lime samples, as would be expected. The timing of hydraulic activation in the material suggests that an initial peak was associated with wetting and dissolution of free lime. This also occurs in the hydraulic lime samples. The main peak corresponds with that seen in the NHL 5 sample (although at a much higher level), which suggests that the lime sample contains a significant amount of hydraulically reactive components.

Figure 53 : Rate of heat for Portland cement sample (72 hours)

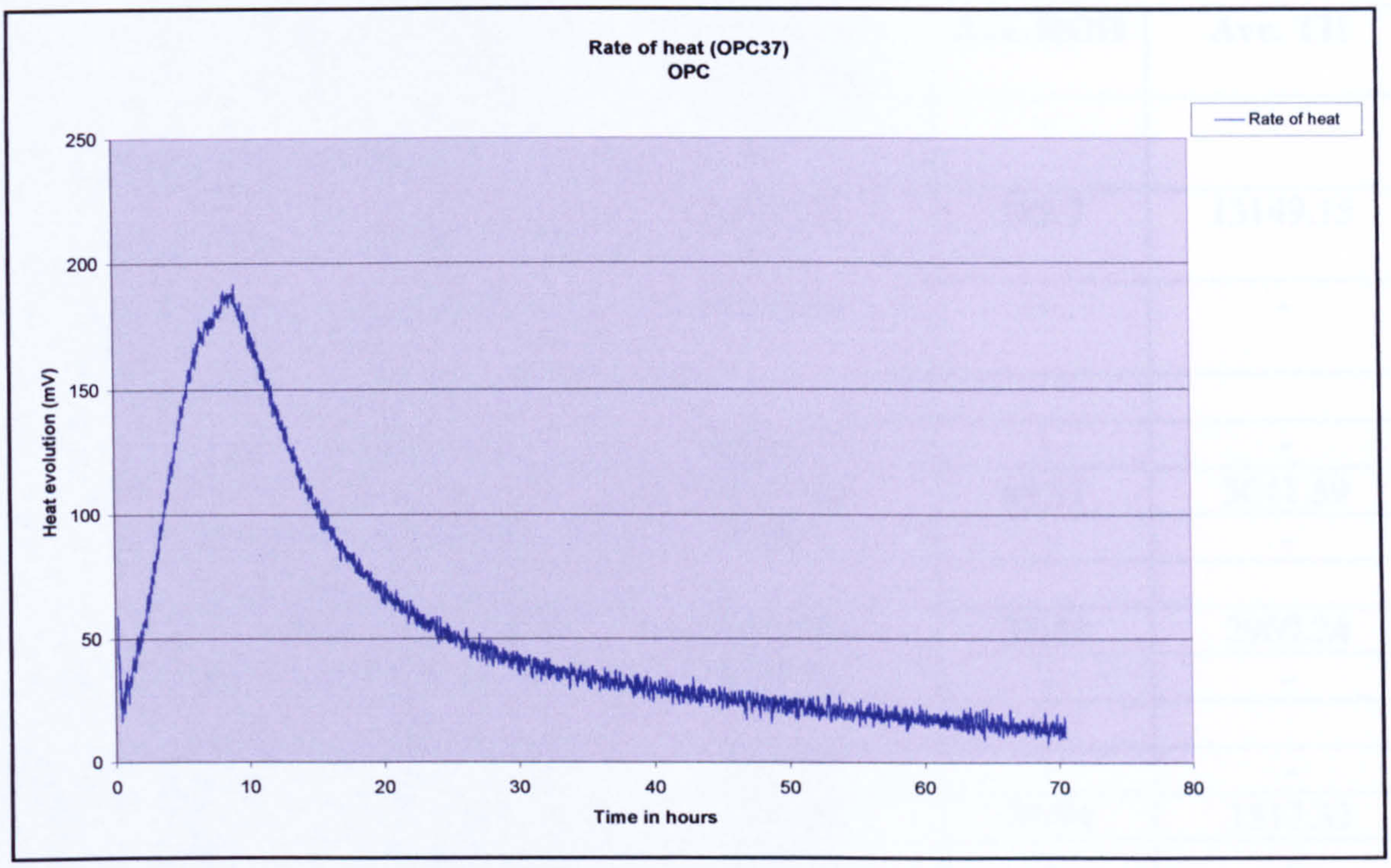

Figure 54 : Total and rate of heat for Portland cement

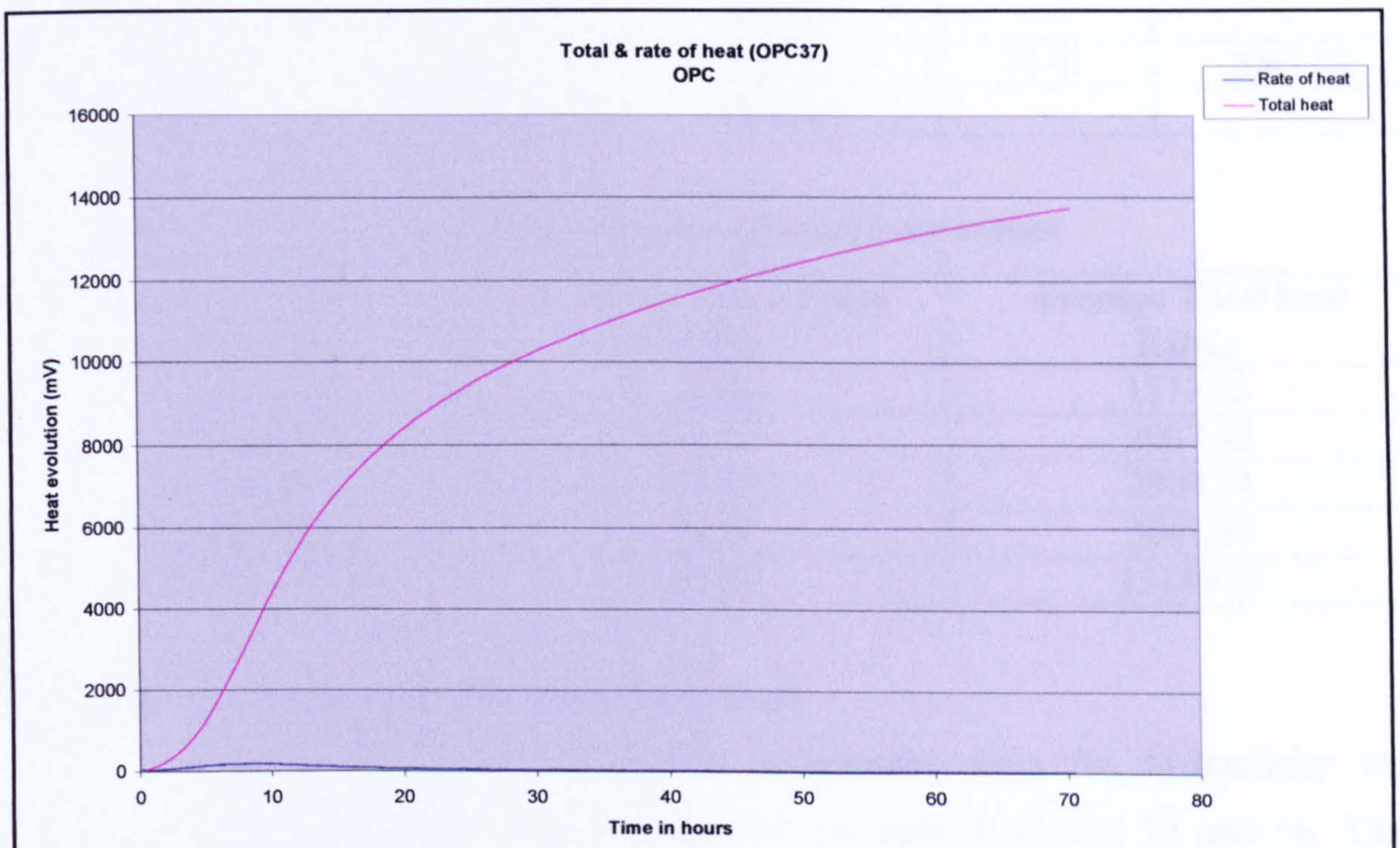

4.2.6 Average values of 72 hour conduction calorimetry test

Table 25 shows the individual rates of heat and the total heat of the range of binders. Table 26 indicates the average rate of heat (ROH) in W/Kg and the average total heat (ΣH) in Kj/Kg for the binders.

Table 25 : Maximum rate of heat and total heat values

Ref No.	Rate Of Heat Max (W/kg) & Times	Total Heat (Kj/kg) Max	Ave. ROH	Ave. TH
Portland cement 23	191.1 @ 8.18	13046.73	-	-
Portland cement 27	189.7 @ 8.08	12662.08	189.7	13149.15
Portland cement 37	188.4 @ 8.9	13738.63	-	-
Jura 31	65.75 @ 1.05	3054.17	-	-
Jura 33	60.77 @ 1.37	2971.503	64.31	3041.59
Jura 34	66.4 @ 0.99	3099.1	-	-
NHL5 25	38.17 @ 6.45	3044.946	37.41	2909.24
NHL5 28	36.65 @ 5.73	2773.53	-	-
NHL3.5 22	19.29 @ 1.78	1083.47	-	-
NHL3.5 29	17.04 @ 0.73	1234.88	24.94	1517.33
NHL3.5 39	27.73 @ 0.86	1828.53	-	-
NHL3.5 40	35.68 @ 0.72	1922.42	-	-
NHL2 26	27.86 @ 1.68	2054.16	-	-
NHL2 35	28.01 @ 2.58	2122.71	31.41	2067.02
NHL2 36	38.37 @ 1.82	2024.19	-	-

Table 26 : Summary of max rate of heat and total heat values

Sample type in order of hydraulicity	Average Rate of heat W/Kg	Average Total heat Kj/Kg
NHL 3.5	24.94	1517.33
NHL 2	31.41	2067.02
NHL 5	37.41	2909.24
Jura-Kalk	64.31	3041.59
Portland cement	189.7	13149.15

4.2.7 Longer term conduction calorimetry tests

A small number of 30 day conduction calorimetry tests for hydraulicity were undertaken. An example of one data set may be seen in figures 55 and 56. These indicate the rate of heat and total heat for NHL 3.5.

Figure 55: Rate of heat for NHL3.5

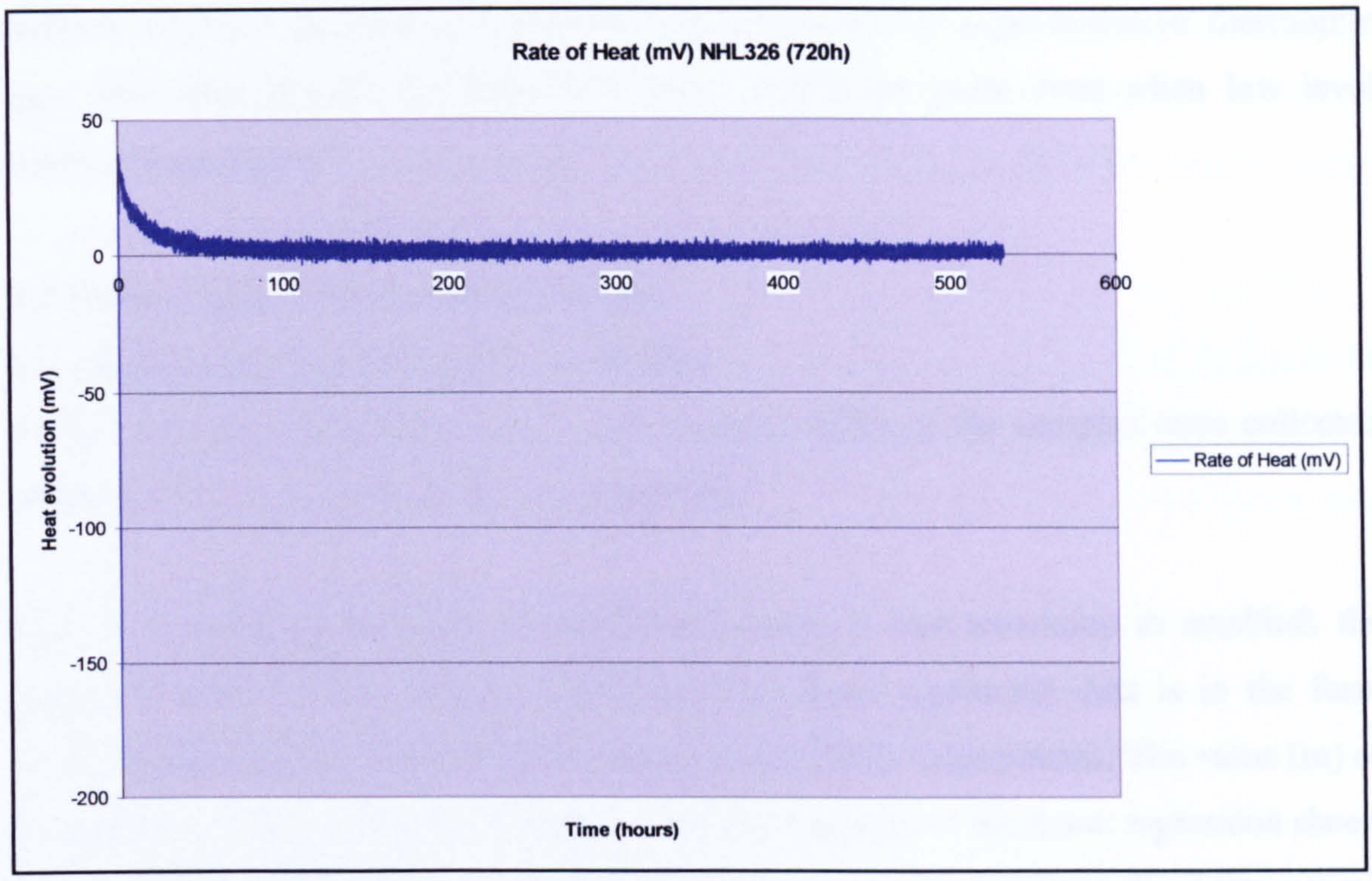

Figure 56: Total heat for NHL3.5

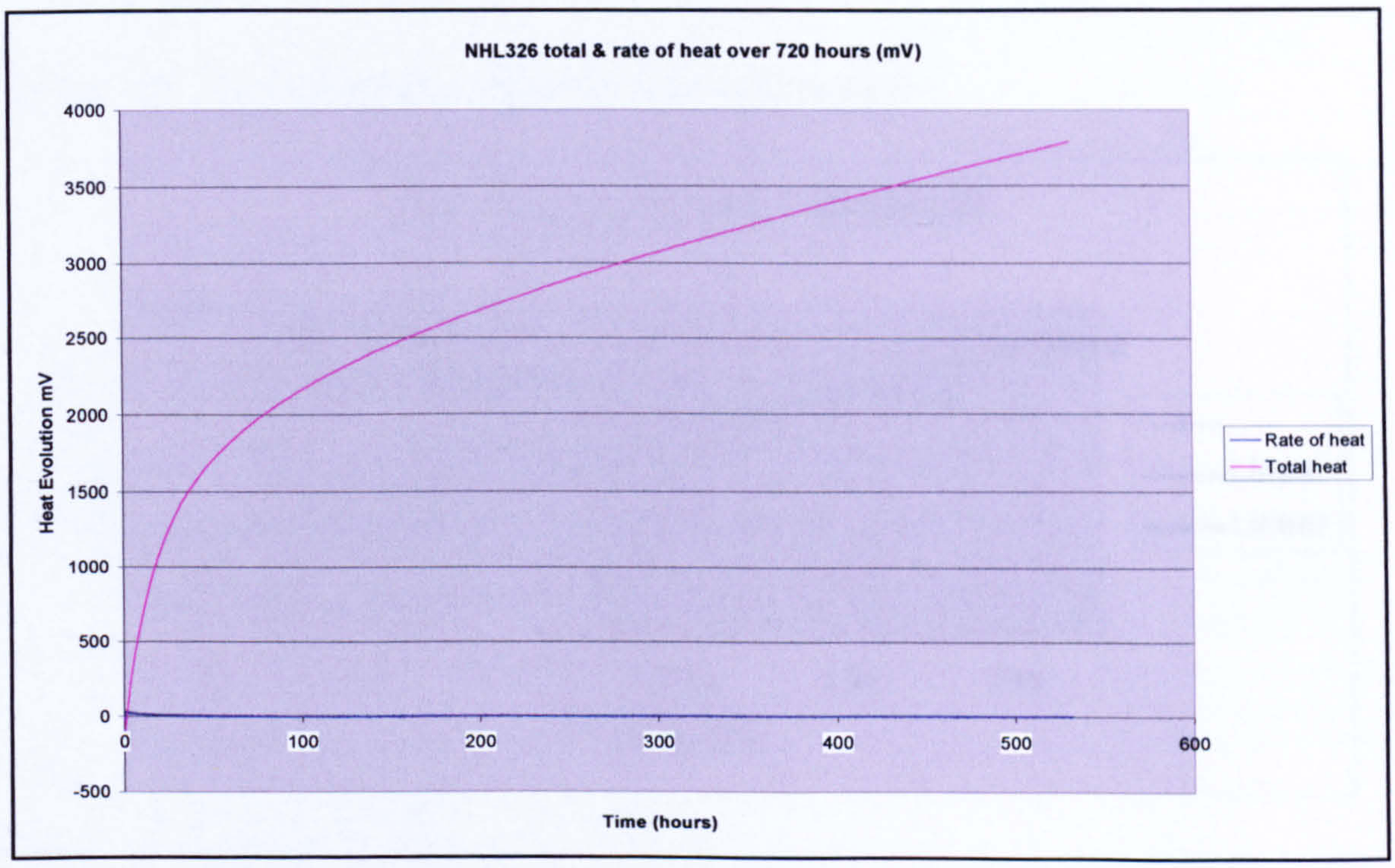

The 30 day tests proved difficult to implement and satisfactory results were difficult to obtain. This may be partially explained by one or a combination of the following reasons. The stability of the instrument over 30 days was problematic and frequently the computer would simply 'crash'. The data that was retrieved was questionable, as the relatively small quantities of heat generated after the first 3 days of hydration are

extremely low when compared with early hydration. Therefore this makes it more difficult to detect the heat of hydration. The adoption of a 'super-sensitive' thermopile may allow the suitable detection of activity within the paste even when low level activity is occurring.

4.3 Water Vapour Permeability Results

4.3.1 Initial data collection and calculations

Values used to calculate the water vapour permeability of the samples were collected adopting a dry cup, desiccant driven experiment.

Prior to calculating the total permeability formula it was necessary to establish the regressed value for the sample under test. The linear regression data is in the form $y=mx+c$ and is taken from the water vapour permeability experiments. The value (m) or the gradient of the line can be attained. A typical example of the linear regression sheets format indicating the gradient and therefore the regressed value from the water vapour permeability is shown in Figure 57. In this case m=0.37.

Figure 57 : Raw data from a permeability experiment

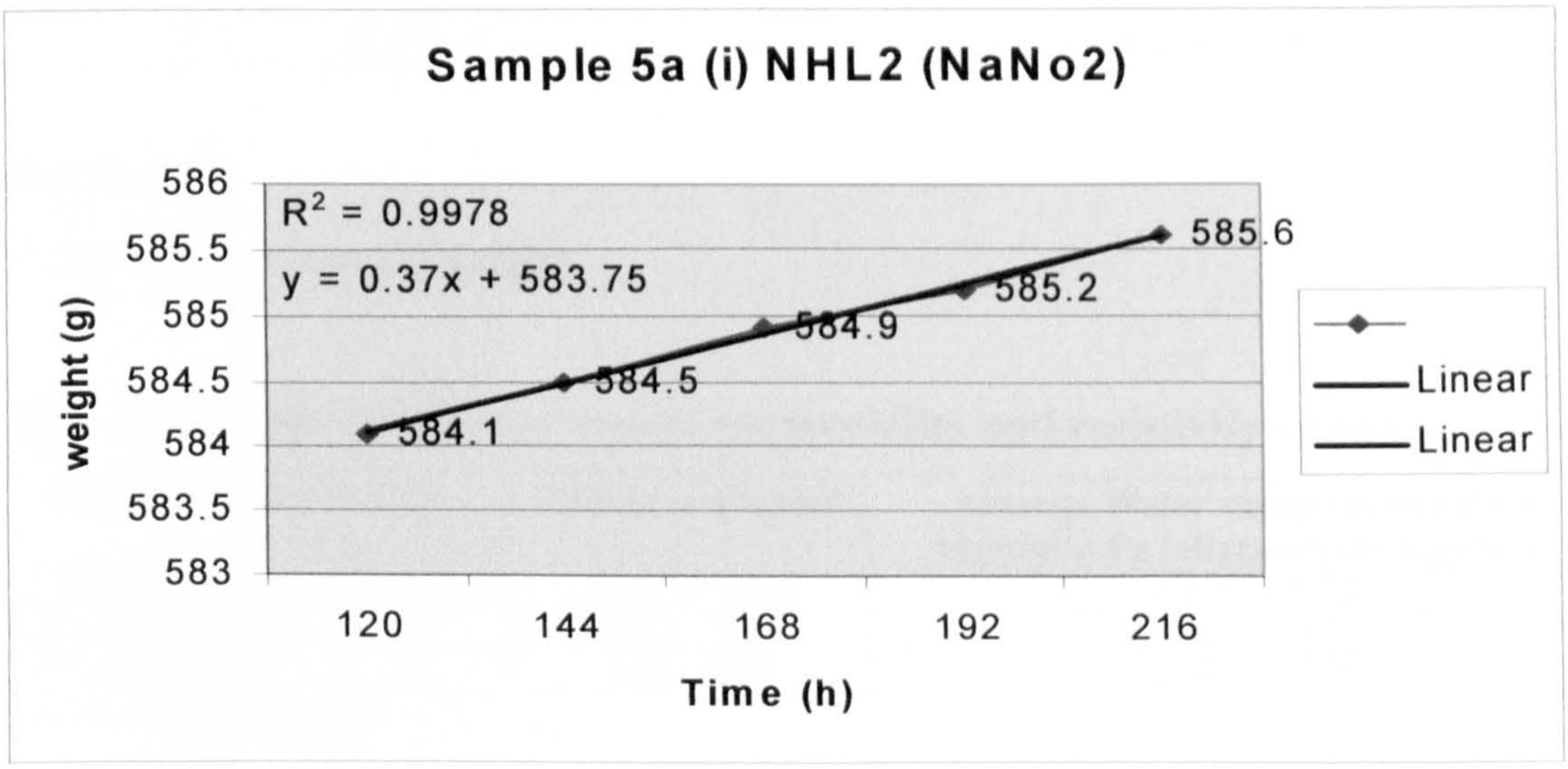

This (m) value can then be adopted along with other variables to calculate the British Standard (BS EN1015-19) method of testing mortar for masonry - part 19: determination of water vapour permeability of hardened rendering and plastering mortars. The regression data integrates specifically with the water flux across the sample. The water flux is a critical element of the total equation and is calculated by adopting change in weight (g) divided by the change in time (h), hence: $\Delta G/\Delta t$. The

sample range is collectively composed of 3 sets of data which upon British Standard calculation may be averaged to attain an average value for the permeance of the mortar sample. This data is consolidated for the 65, 76, and 86% relative humidity conditions which in turn allows for the graphical representation and true fit of the mortar sample averaged over all humidity ranges.

Despite starting before its publication this experiment parallels British Standard for water vapour permeability in cementitious materials. This adopts a suitable calculation for the water vapour permeability of the material. This formula can be seen below with definitions included:

$$\Lambda = 1 / (A\Delta p \ / \ \Delta G/\Delta t - R_A)$$

Where:

Symbol	*Definition*
Λ=	*Permeance kg/m^2.s pa*
A=	*Area of sample in m^2*
Δp=	*Difference in pressure N/m^2 pa*
ΔG=	*Change in weight in kg*
Δt=	*Change in time (h)*
R_A=	*Air resistance*

4.3.2 Results

4.3.2.1 Plaster Board Samples

Table 27 Samples and water vapour permeability and resistivity values

Sample Number & Type	Desiccant adopted	Average Water vapour permeability Kgm/m^2.s.Pa (alternatively KgmN^{-1}s^{-1})
1 – Plaster Board	$NaNO_2$ - 65%	*2.311 x 10^{-10} $*
1 – Plaster Board	NaCl – 76%	*3.2725 x 10^{-10} $*
1 – Plaster Board	KCl – 86%	*2.201 x 10^{-10} $*

$ - two samples only

4.3.2.2 Non-Hydraulic lime, hydraulic lime and Portland cement samples.

Results presented in tables 28 to 33 are given as the average of three specimens, except where noted. In some cases one result had to be discarded because some factors such as a defective mortar bed rendered the result out of agreement with the other two. A measure of the reproducibility achieved in ideal conditions is given by the results for sample 4, the Isle of Man non-hydraulic lime putty. The three values determined from

the sodium nitrite test were 2.20, 1.998 and 2.064 x 10^{-11}Kgm/m^2·s·Pa, averaging 2.09x10^{-11} Kg/m^2·s·Pa. Generally, if one result differed from the other two by more than 10% reason was sought for its exclusion.

Table 28 : water vapour permeability of non-hydraulic limes

Sample Number and Type	Desiccant adopted	Average water vapour permeability Kgm/m^2.s.Pa (alternatively $KgmN^{-1}s^{-1}$)
2 – Shap, non hydraulic lime putty	$NaNO_2$ - 65%	2.2085 x 10^{-11} $
2 – Shap, non hydraulic lime putty	NaCl – 76%	2.206 x 10^{-11}
2 – Shap, non hydraulic lime putty	KCl – 86%	3.763 x 10^{-11}
3- Blair Athol, feebly hydraulic lime putty	$NaNO_2$ 65%	1.705 x 10^{-11} $
3 - Blair Athol, feebly hydraulic lime putty	NaCl – 76%	1.5816 x 10^{-11}
3 - Blair Athol, feebly hydraulic lime putty	KCl – 86%	2.921 x 10^{-11}
4- Isle of Man, non-hydraulic lime putty	$NaNO_2$ 65%	2.0873 x 10^{-11}
4 - Isle of Man, non-hydraulic lime putty	NaCl – 76%	2.229 x 10^{-11}
4 - Isle of Man, non-hydraulic lime putty	KCl – 86%	3.314 x 10^{-11}

Notes: $ - two samples only

Table 29 : water vapour permeability of NHL2 samples

Sample Number and Type	Desiccant adopted	Average water vapour permeability Kgm/m^2.s.Pa (alternatively $KgmN^{-1}s^{-1}$)
5 – Natural Hydraulic lime (dry hydrate) NHL2	$NaNO_2$ – 65%	1.075 x 10^{-11}
5 – Natural Hydraulic lime (dry hydrate) NHL2	NaCl – 76%	1.531 x 10^{-11}
5 – Natural Hydraulic lime (dry hydrate) NHL2	KCl – 86%	4.545 x 10^{-11} $
10 – Shap, non-hydraulic lime putty : Natural Hydraulic lime (dry hydrate) NHL2	$NaNO_2$ 65%	2.0516 x 10^{-11}
10 – Shap, non-hydraulic lime putty : Natural Hydraulic lime (dry hydrate) NHL2	NaCl – 76%	2.5286 x 10^{-11}
10 – Shap, non-hydraulic lime putty : Natural Hydraulic lime (dry hydrate) NHL2	KCl – 86%	4.146 x 10^{-11}

Notes: $ - two samples only

Table 30 : water vapour permeability of NHL3.5 samples.

Sample Number and Type	Desiccant adopted	Average Water vapour permeability Kgm/m^2.s.Pa (alternatively $KgmN^{-1}s^{-1}$)
6 - Natural Hydraulic lime (dry hydrate) NHL3.5	$NaNO_2$ 65%	1.0955 x 10^{-11} $
6 - Natural Hydraulic lime (dry hydrate) NHL3.5	NaCl – 76%	1.746 x 10^{-11}
6 - Natural Hydraulic lime (dry hydrate) NHL3.5	KCl – 86%	1.844 x 10^{-11} $
11 - Shap, non-hydraulic lime putty : Natural Hydraulic lime (dry hydrate) NHL3.5	$NaNO_2$ 65%	3.007 x 10^{-11}
11 - Shap, non-hydraulic lime putty : Natural Hydraulic lime (dry hydrate) NHL3.5	NaCl – 76%	2.6685 x 10^{-11} $
11 - Shap, non-hydraulic lime putty : Natural Hydraulic lime (dry hydrate) NHL3.5	KCl – 86%	7.3235 x 10^{-11} $

Notes: $ - two samples only

Table 31 : water vapour permeability of NHL5 samples.

Sample Number & Type	Desiccant adopted	Average Water vapour permeability $Kgm/m^2.s.Pa$ (alternatively $KgmN^{-1}s^{-1}$)
7 - Natural Hydraulic lime (dry hydrate) NHL5	$NaNO_2$ – 65%	8.115×10^{-12} $
7 - Natural Hydraulic lime (dry hydrate) NHL5	NaCl – 76%	1.194×10^{-11}
7 - Natural Hydraulic lime (dry hydrate) NHL5	KCl – 86%	1.735×10^{-11}
12 - Shap, non-hydraulic lime putty : Natural Hydraulic lime (dry hydrate) NHL5	$NaNO_2$ 65%	1.41×10^{-11}
12 - Shap, non-hydraulic lime putty : Natural Hydraulic lime (dry hydrate) NHL5	NaCl – 76%	3.829×10^{-11} $
12 - Shap, non-hydraulic lime putty : Natural Hydraulic lime (dry hydrate) NHL5	KCl – 86%	2.047×10^{-10} $

Notes: $ - two samples only

Table 32 : Water vapour permeability of Jura-Kalk samples.

Sample Number and Type	Desiccant adopted	Average Water vapour permeability $Kgm/m^2.s.Pa$ (alternatively $KgmN^{-1}s^{-1}$)
8 - Natural Hydraulic lime (dry hydrate) NHL5 (jura kalk)	$NaNO_2$ – 65%	1.998×10^{-11} #
8 – Natural Hydraulic lime (dry hydrate) NHL5 (jura kalk)	NaCl – 76%	2.6516×10^{-11} $
8 – Natural Hydraulic lime (dry hydrate) NHL5 (jura kalk)	KCl – 86%	6.9675×10^{-11} $
13 – Shap, non-hydraulic lime putty : Natural Hydraulic lime (dry hydrate) NHL10 (jura kalk)	$NaNO_2$ 65%	9.73×10^{-12}
13 – Shap, non-hydraulic lime putty : Natural Hydraulic lime (dry hydrate) NHL10 (jura kalk)	NaCl – 76%	1.88×10^{-11}
13 – Shap, non-hydraulic lime putty : Natural Hydraulic lime (dry hydrate) NHL10 (jura kalk)	KCl – 86%	1.87×10^{-11}

Notes: # - one sample only, $ - two samples only

Table 33 : water vapour permeability of Portland cement samples.

Sample Number and Type	Desiccant adopted	Average Water vapour permeability $Kgm/m^2.s.Pa$ (alternatively $KgmN^{-1}s^{-1}$)
9 - Ordinary Portland cement	$NaNO_2$ – 65%	7.646×10^{-12}
9 - Ordinary Portland cement	NaCl – 76%	8.840×10^{-12}
9 - Ordinary Portland cement	KCl – 86%	1.970×10^{-11}
14 - Shap, non-hydraulic lime putty : Ordinary Portland cement	$NaNO_2$ 65%	1.73×10^{-11}
14 - Shap, non-hydraulic lime putty : Ordinary Portland cement	NaCl – 76%	3.84×10^{-11}
14 - Shap, non-hydraulic lime putty : Ordinary Portland cement	KCl – 86%	4.81×10^{-11}

4.3.2.3 Summary of water vapour permeability results

Figures 58-60 represent the water vapour permeability of the full range of sample types, including gauged batches and modern Portland cement mortars.

Figure 58: Water vapour permeability adopting sodium nitrite as a desiccant

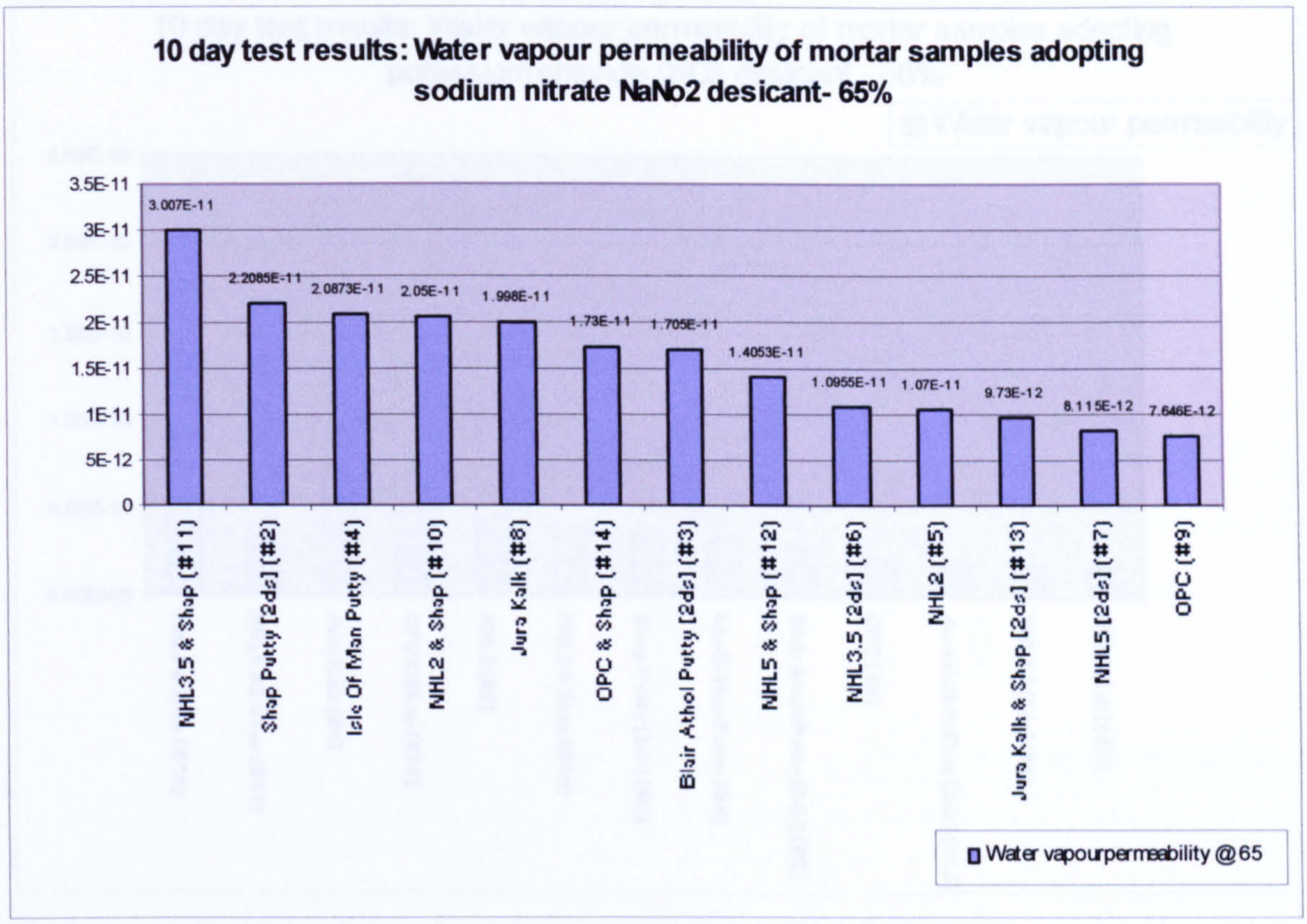

Figure 59 : Water vapour permeability adopting sodium chloride as a desiccant

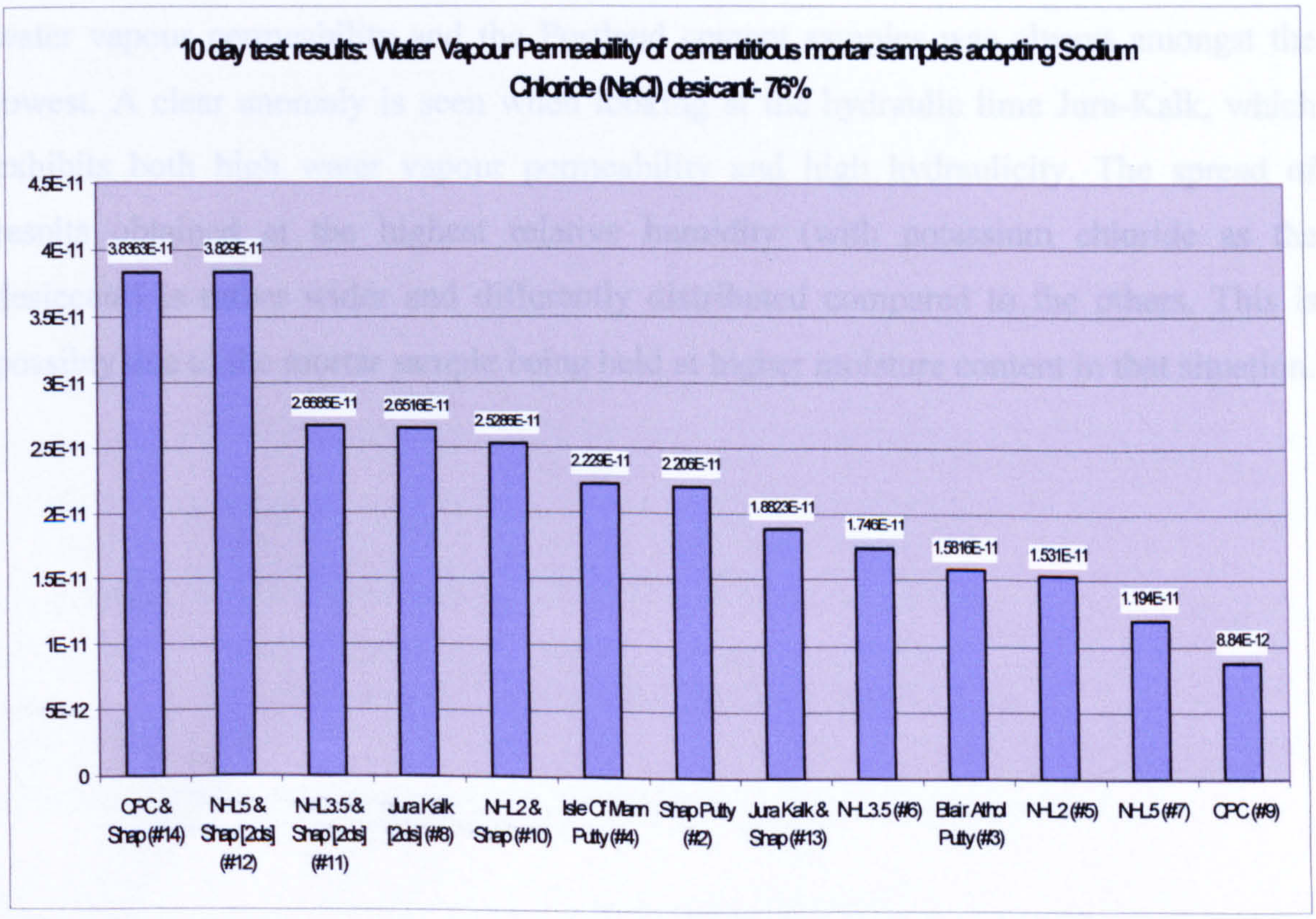

Figure 60 : Water vapour permeability adopting potassium chloride as a desiccant

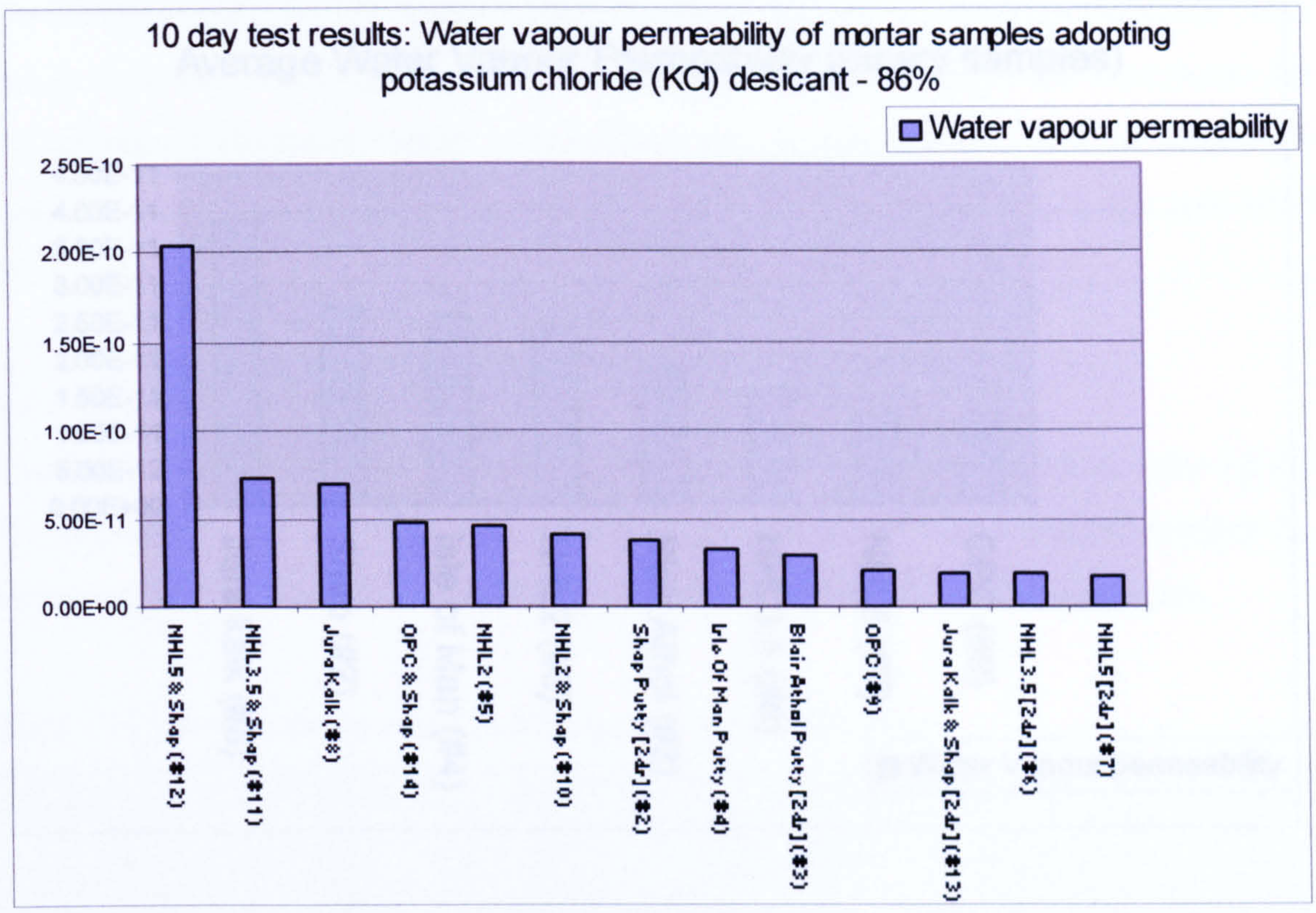

The chart indicates that in those samples with strong hydraulicities a decrease in permeability is generally noted. In general the non-hydraulic limes showed the highest water vapour permeability and the Portland cement samples was always amongst the lowest. A clear anomaly is seen when looking at the hydraulic lime Jura-Kalk, which exhibits both high water vapour permeability and high hydraulicity. The spread of results obtained at the highest relative humidity (with potassium chloride as the desiccant) is rather wider and differently distributed compared to the others. This is possibly due to the mortar sample being held at higher moisture content in that situation.

Figure 61: Average water vapour permeability: binary samples

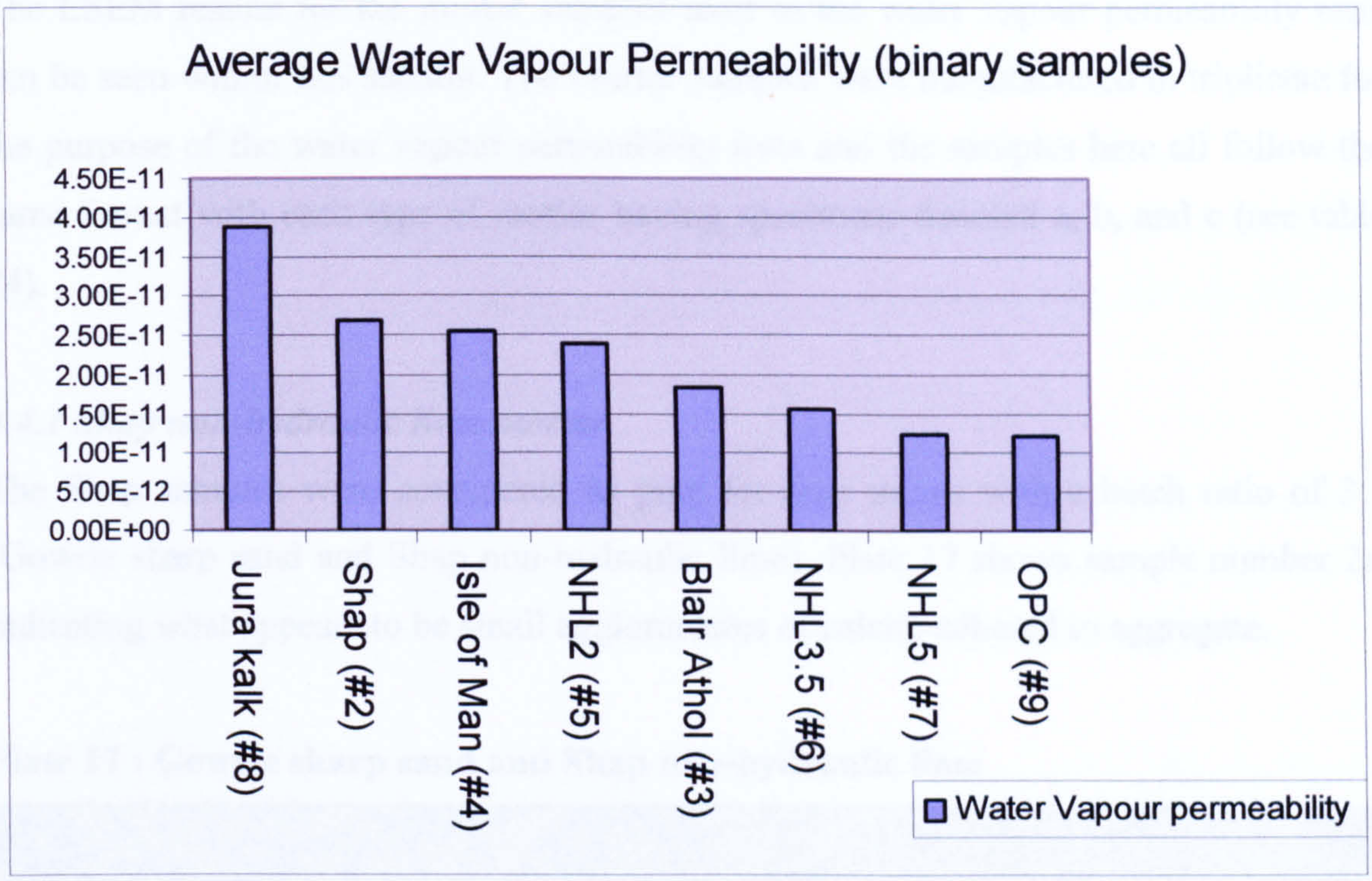

Figure 62: Average water vapour permeability: ternary samples

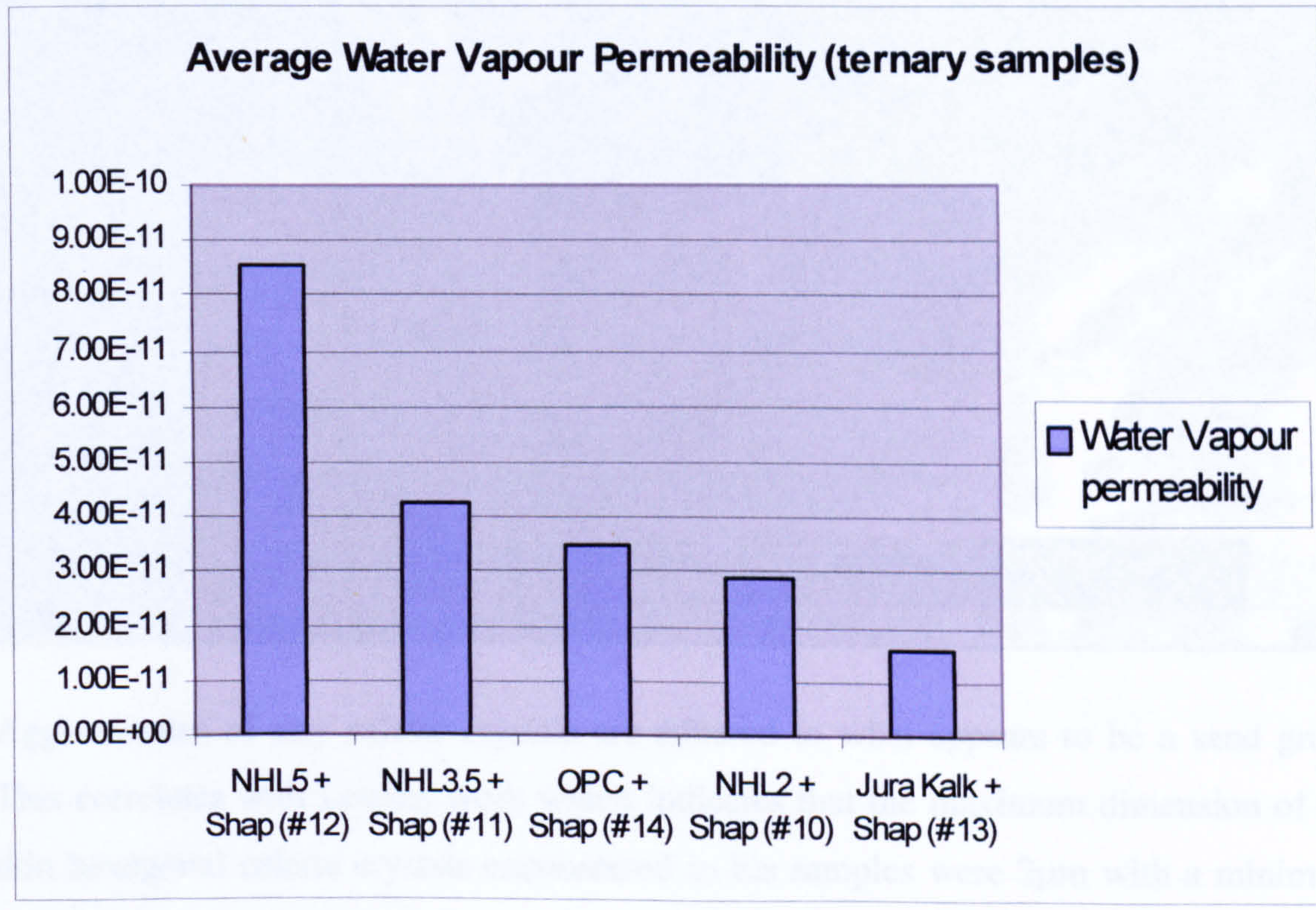

4.4 Environmental Scanning Electron Microscope (ESEM) Results

The ESEM results for the mortar samples used in the water vapour permeability tests can be seen within this section. The mortar samples were manufactured in triplicate for the purpose of the water vapour permeability tests and the samples here all follow the same format with each type of mortar having specimens denoted a, b, and c (see table 24).

4.4.1 Shap non-hydraulic lime mortar

The Shap samples were considered as pure fat lime mixes with a batch ratio of 3:1 (Gowrie sharp sand and Shap non-hydraulic lime). Plate 17 shows sample number 2a, indicating what appears to be small agglomerates of calcite adhered to aggregate.

Plate 17 : Gowrie sharp sand and Shap non-hydraulic lime

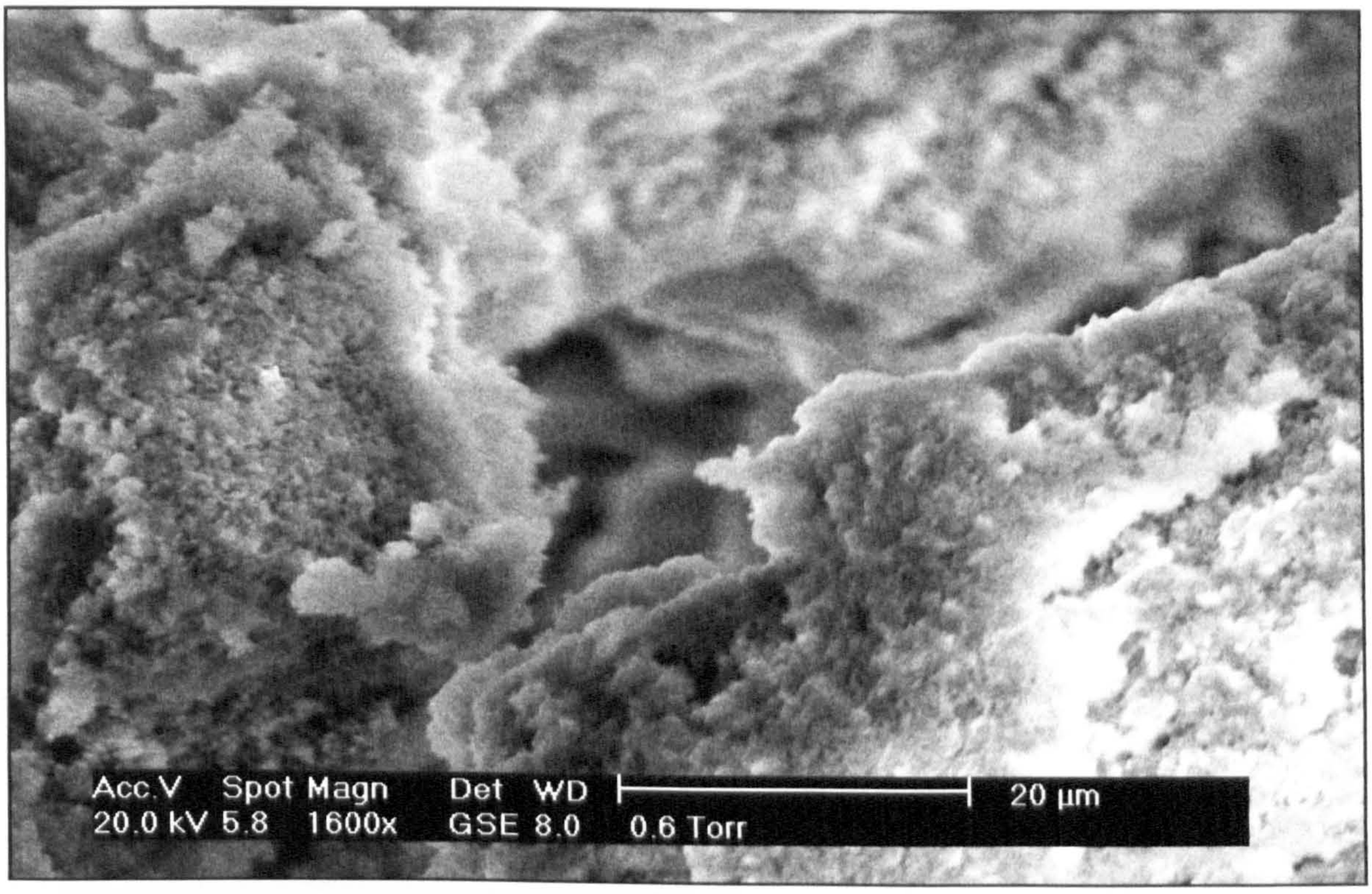

Agglomerates of tiny calcite crystals are adhered to what appears to be a sand grain. This correlates with Lewins work which indicates that the maximum dimension of the thin hexagonal calcite crystals encountered in his samples were 2µm with a minimum value of 0.07µm which compare favourably with those seen upon the sand grain.

Under EDX analysis, sample 2a-1 exhibited an elemental composition that was high in calcium (Ca). The peaks consisted of a high Kα-peak representing calcium at 3.9KVe and a secondary peak that was considerably lower at 4.1Kve however, this is the Kβ-

peak and is generally discounted from EDX analysis. The large Ca peak may be associated with the formation of $Ca(OH)_2$ crystallites which have converted into calcite crystals. A Kα-peak associated with silica (Si) was seen at 1.8KVe, and a small Kα-peak associated with aluminium (Al) at 1.7KVe. The Si Kα-peak may have been associated with the Gowrie aggregate found within the mortar, rather than C-S-H crystal types, however, the Al Kα-peak is more likely to be associated with low level C-A-H crystal formation.

Plate 18 shows sample number 2b, indicating what appear to be masses of irregular calcite crystals. This is most dense upon the left of the plate, whilst to the right of the plate, appears to be a piece of aggregate with calcite poorly bonded to the surface.

Figure 63: EDX plot indicating chemical elements and concentration for the binary Shap non-hydraulic lime mortar samples

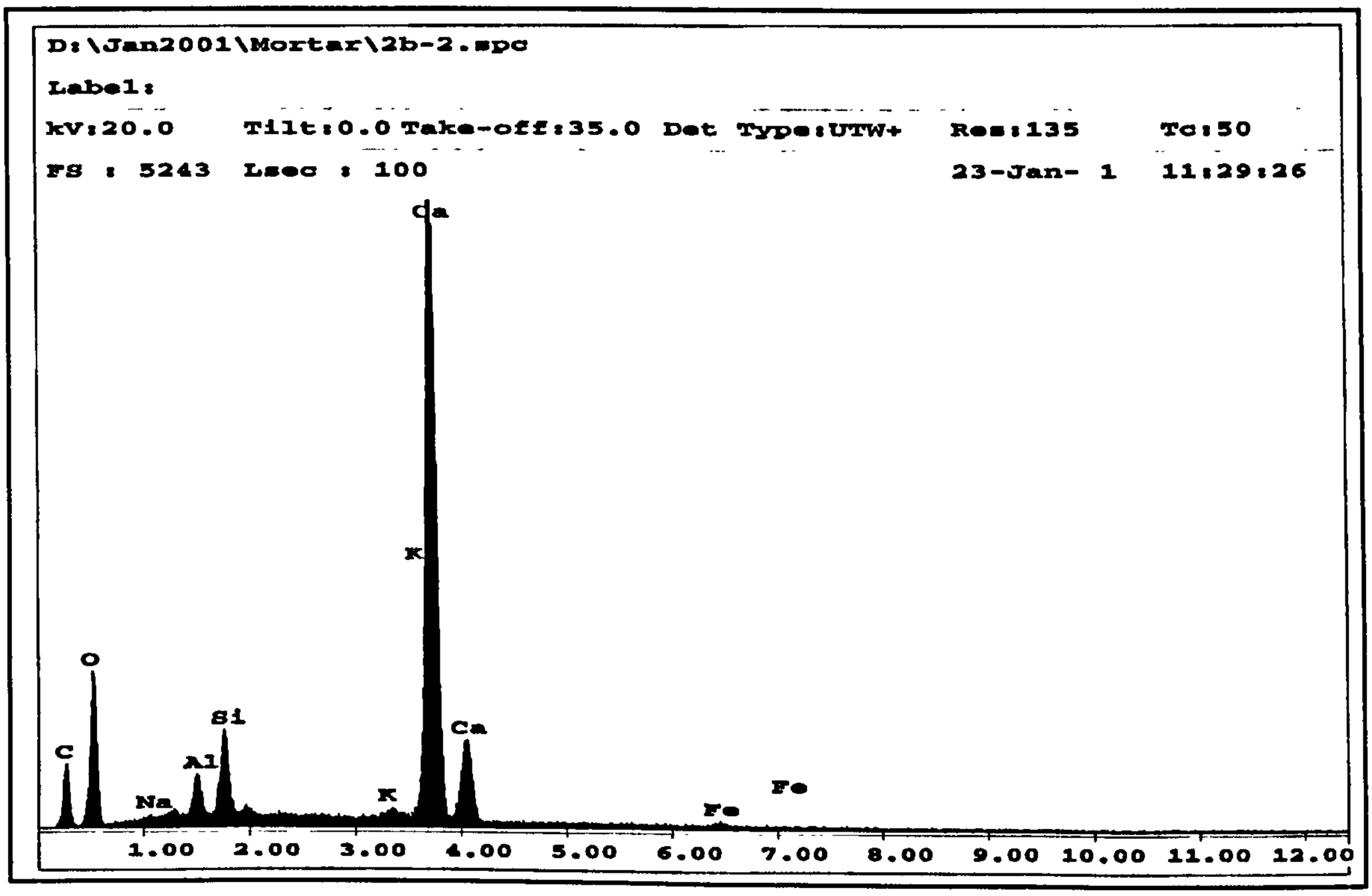

In addition to the aforementioned primary components, trace element of iron (Fe), potassium (K) and sodium (Na) were seen.

Plate 18 : Gowrie sharp sand and Shap non-hydraulic lime

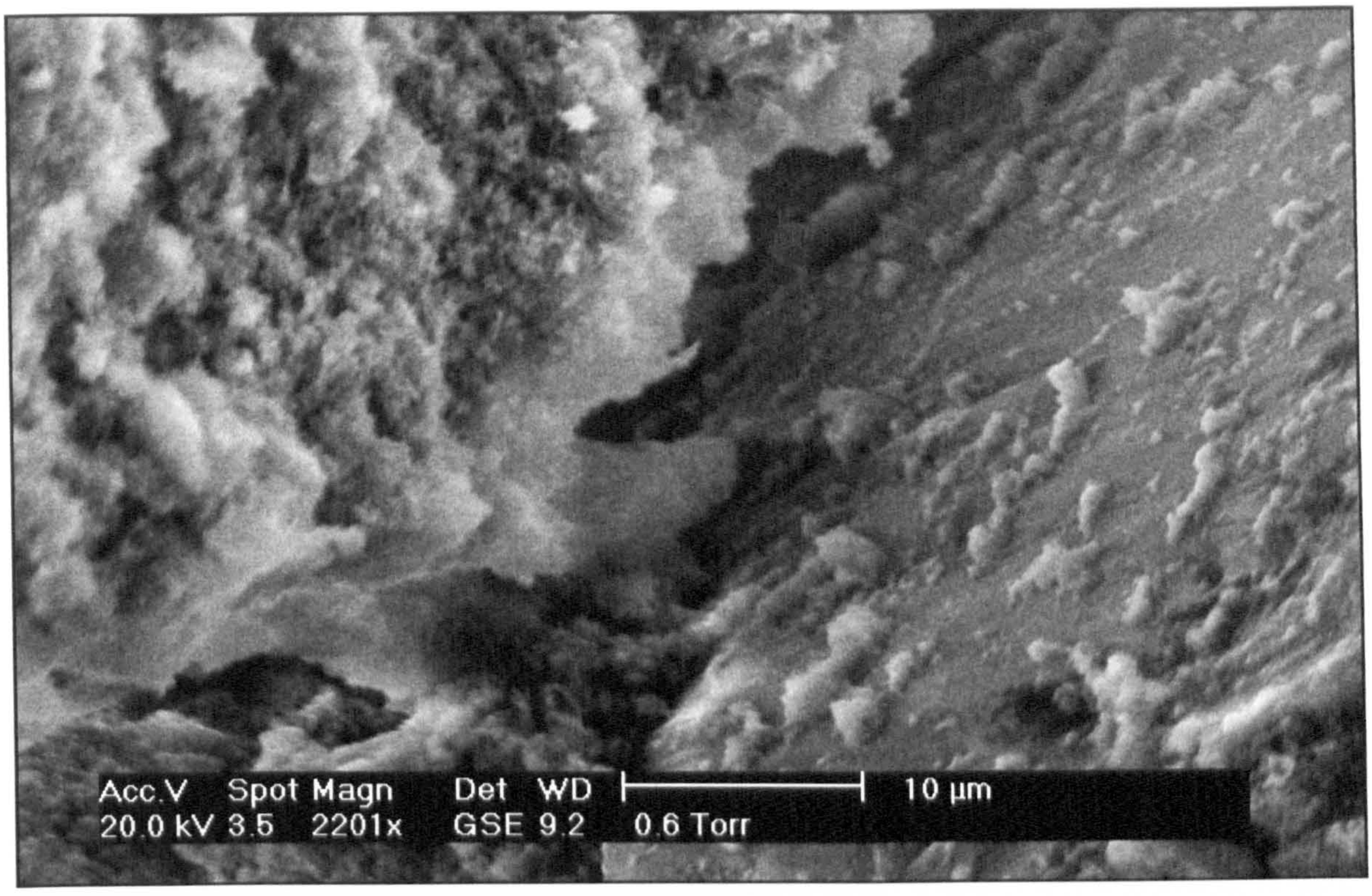

4.4.2 Blair Athol non-Hydraulic Lime

The Blair Athol samples were initially considered as a pure fat lime mixes with a batch ratio of 3:1 (Gowrie sharp sand and Blair Athol non hydraulic lime). Plate 19 shows sample number 3b, indicating what appear to be agglomerates of calcite crystallites.

Several needle-like crystal forms appear to be protruding from the surface. These may be C-S-H forming from traces of reactive silicate particles. This would lead us to believe that the Blair-Athol lime has a slightly hydraulic component and should possibly be reclassified as a feebly hydraulic lime.

EDX analysis indicates primary Kα and secondary Kβ- Ca peaks at approximately 3.7KVe and 4.2KVe as before (figure 64). The presence of a silica Kα-peak at 1.8KVe would tend to indicate the presence of aggregate, however, a certain amount of C-S-H may have formed generating a silica trace. This would tend to correlate with the ESEM image, which does not discount the possibility of C-S-H and C-A-H crystal formation.

Very small Kα-peaks for carbon, magnesium and aluminium are seen in roughly similar quantities to each other. The respective KVe were 0.4, 1.4 and 1.6. Both the Al and the Mg Kα-peaks could be associated with variations in exhibited crystal types seen in the

ESEM plate. In addition to the small quantities of compounds aforementioned, trace element of Fe was also noted with a Kα-peak at 6.6KVe.

Plate 19 : Gowrie sharp sand and Blair Athol non-hydraulic lime

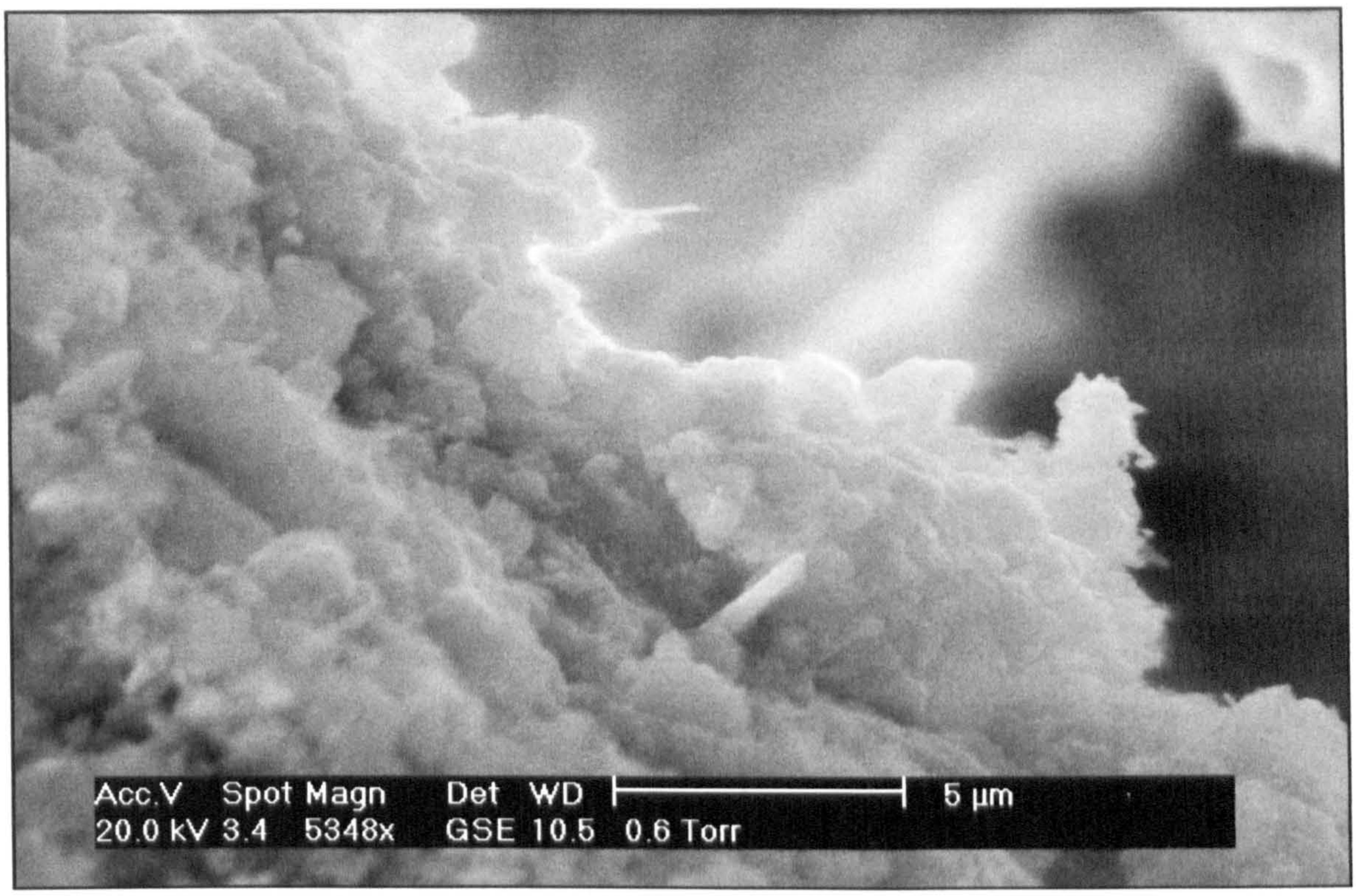

Plate 20 shows sample number 3c, indicating what appears to be an irregular mass of calcite crystallites. This would correlate with the Ca Kα-peak seen in the EDX analysis.

As in plate 19, the presence of tiny rod like crystals cannot be disregarded. Small quantities of carbon, magnesium, aluminium and silica are seen in Kα-peaks at 0.4KVe, 1.4KVe, 1.6KVe and 1.8KVe respectively. Both the aluminium and silica components may be responsible for the presence of C-S-H and / or C-A-H crystal types within the plate, however, the Silica Kα-peak in the EDX could possibly be easily associated with small grains of aggregate which have calcite covering it and thereby hiding its presence.

Figure 64: EDX plot indicating chemical elements and concentration for the binary Blair-Athol non-hydraulic lime mortar samples

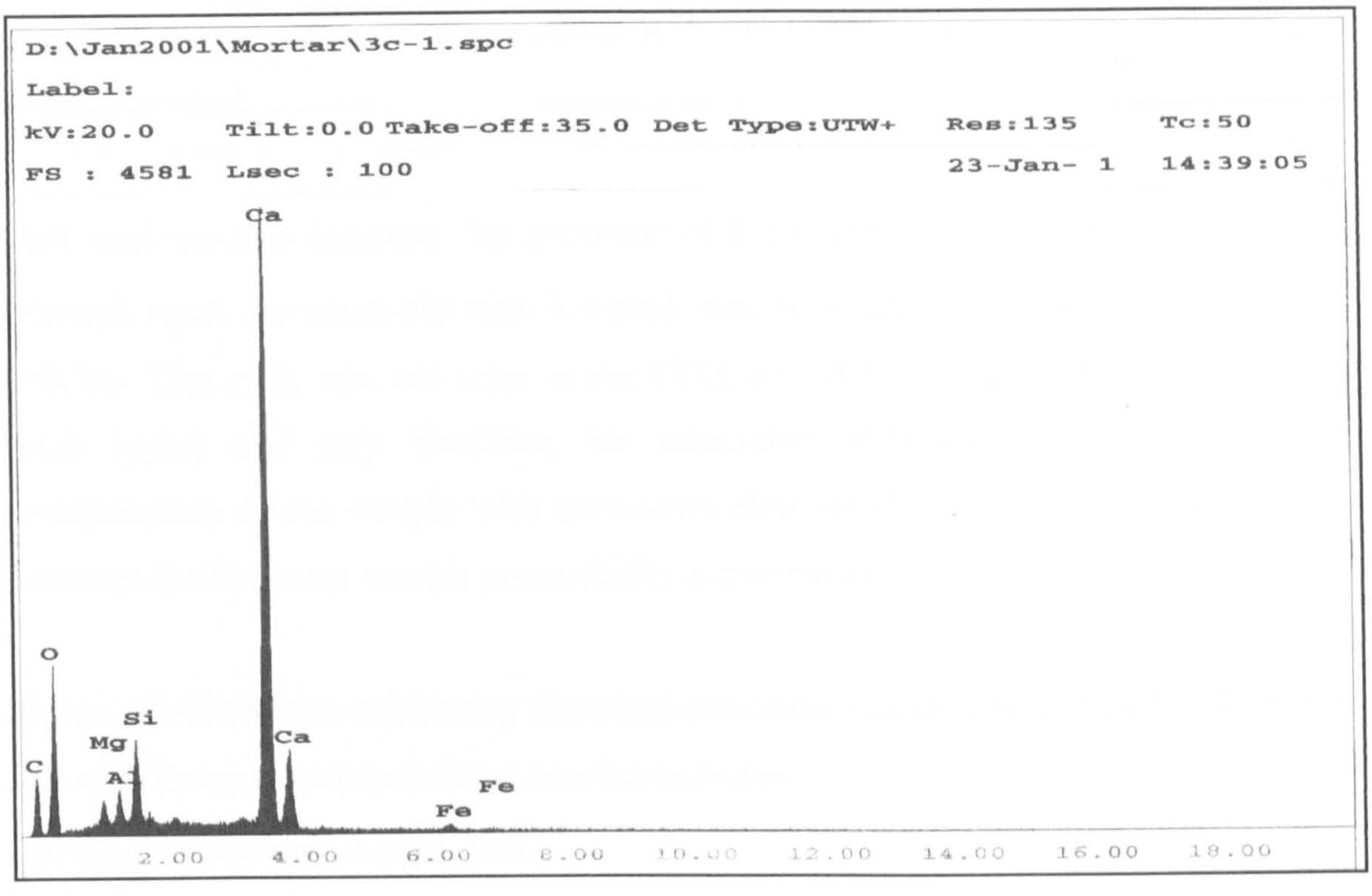

Plate 20 : Gowrie sharp sand and Blair Athol non-hydraulic lime

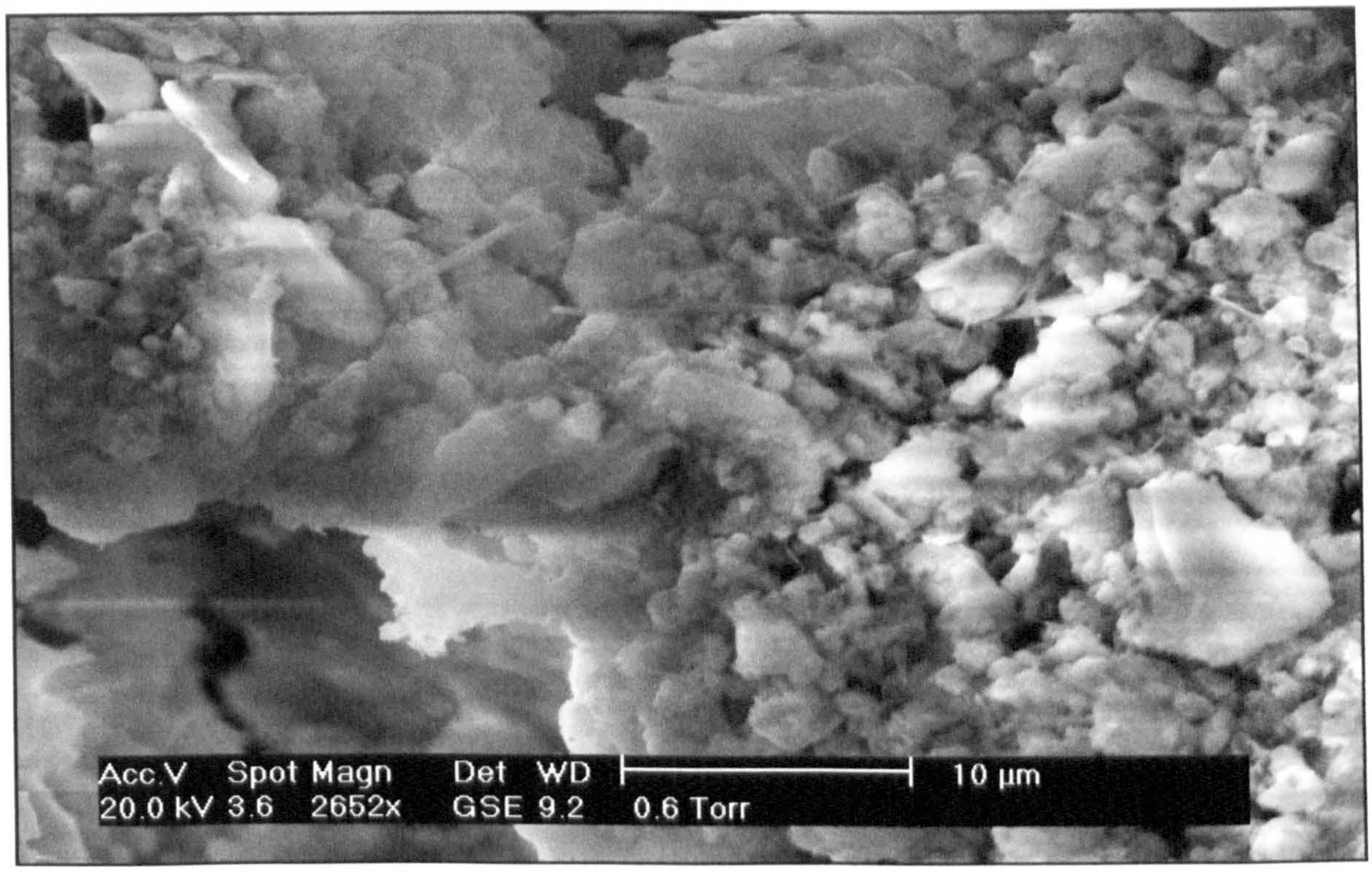

4.4.3 Isle of Man non-hydraulic lime

The Isle of Man samples were initially considered to be pure fat lime mixes with a batch ratio of 3:1 (Gowrie sharp sand and Isle of Man non-hydraulic lime). Plate 21 shows sample number 4a, indicating what appears to be agglomerates of calcite. These are

found in irregular masses throughout the sample. A Kα-peak for Ca was present under EDX, (figure 65). It is possible that both forms of Ca are occurring simultaneously, namely portlandite and calcite, however, it is more likely that the $Ca(OH)_2$ would have fully carbonated.

EDX analysis also indicates the presence of Kα-peaks for C, Na, Mg, S, K and Fe, although trace. An unusually high Kα-peak was also seen for potassium and is seen at 3.9KVe. This peak was not seen in the EDX results for sample 4b and 4c (identical batch types) and may therefore, be associated with possible, though unlikely, contamination of the sample with potassium chloride (KCl), which was adopted as a desiccant for the water vapour permeability experiments.

Figure 65: EDX plot indicating chemical elements and concentration for the binary Isle of Man non-hydraulic lime mortar samples

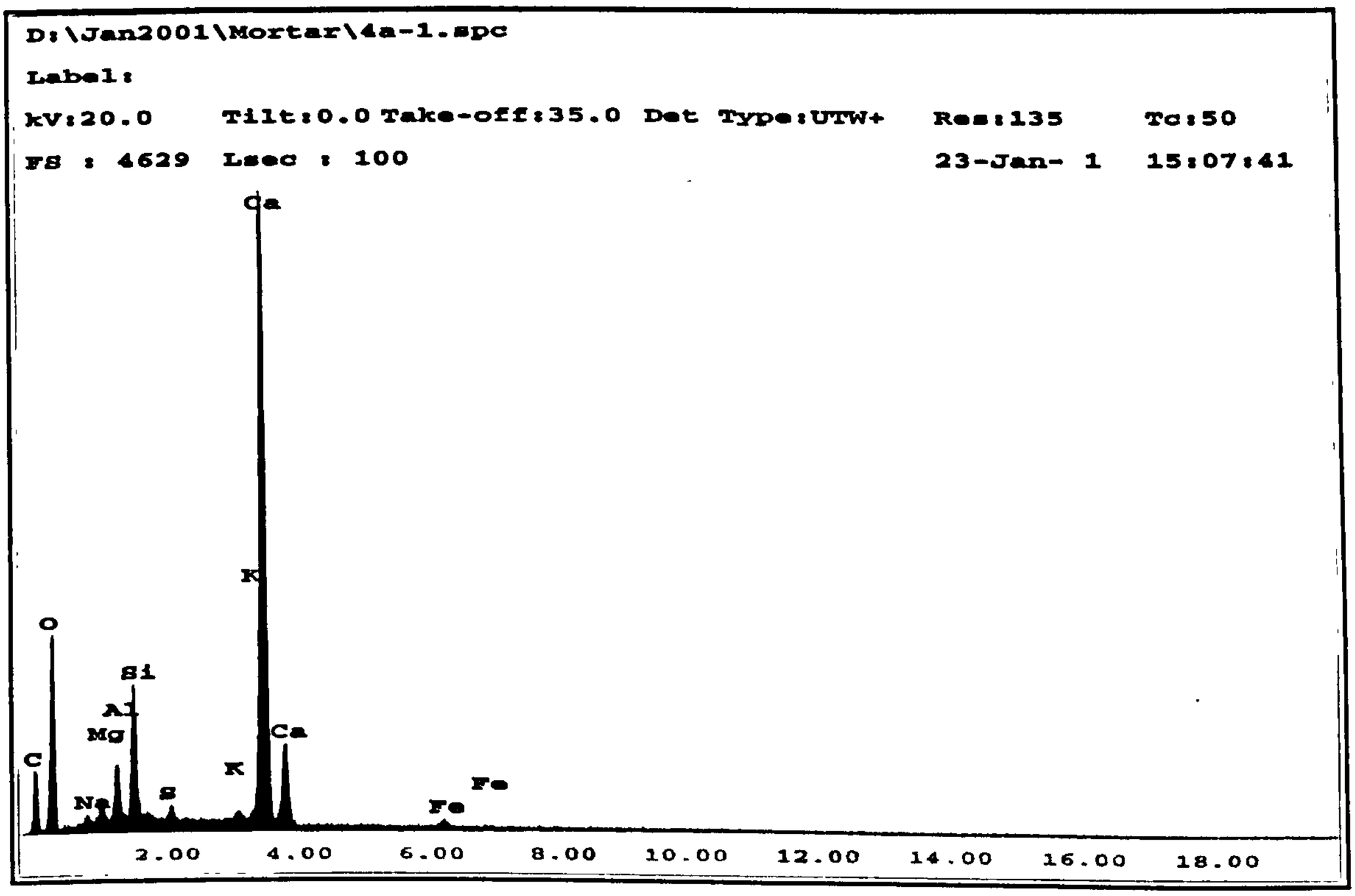

Plate 21 : Gowrie sharp sand and Isle of Man non-hydraulic lime

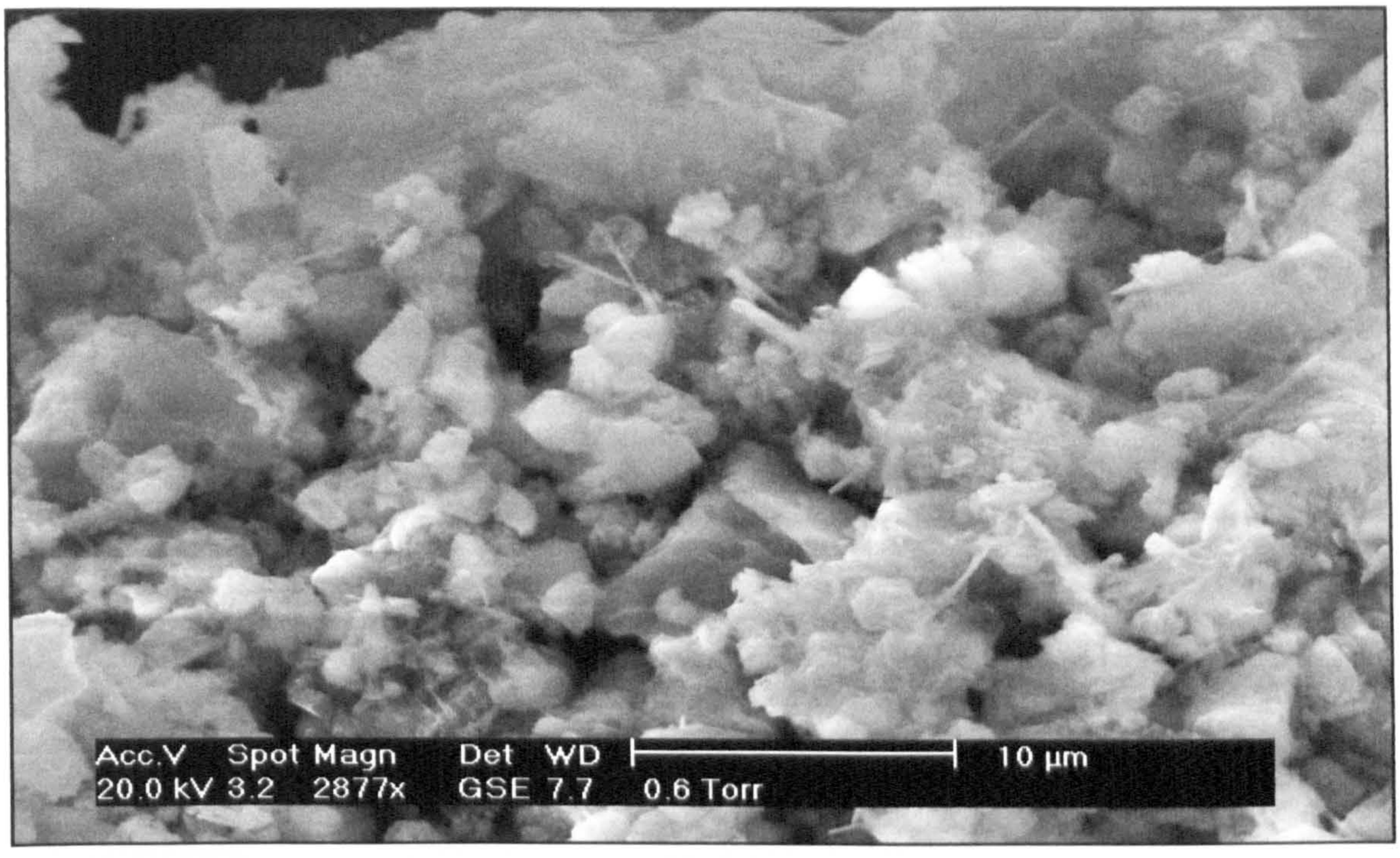

A very small quantity of rod type crystals may also be seen within the irregular crystallite mass. This correlates with a moderate level of silica and aluminium that are known to be present within the sample due to EDX analysis. This would tend to indicate that the presence of C-S-H and C-A-H are present within the matrix.

Plate 22 shows sample number 4a, indicating what appear to be agglomerates of calcite crystals.

Plate 22 : Gowrie sharp sand and Isle of Man non-hydraulic lime

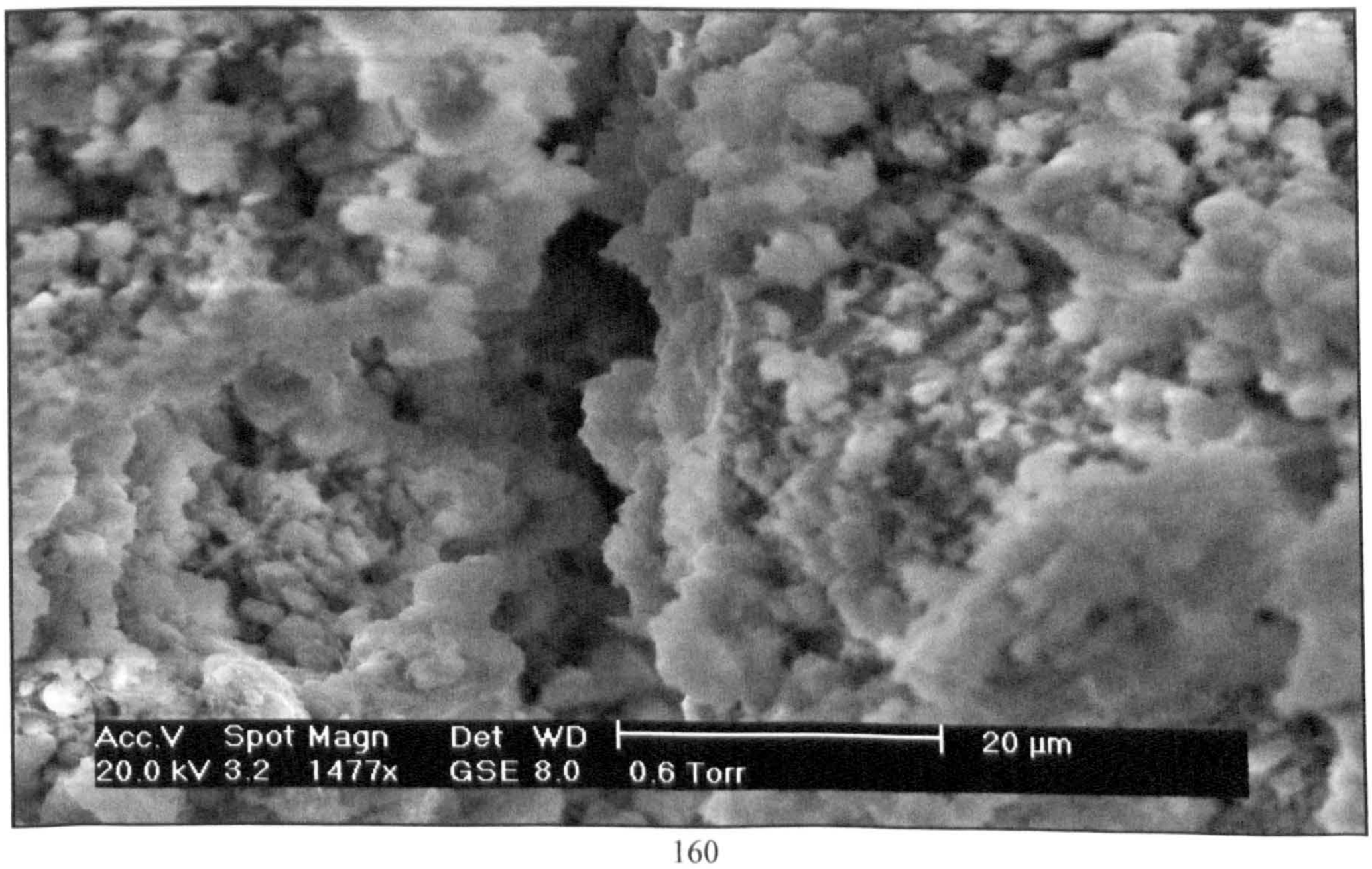

4.4.4 Natural Hydraulic Lime 2 (NHL2)

The NHL2 samples are considered to be feebly hydraulic lime mixes with a batch ratio of 3:1 (Gowrie sharp sand and NHL2 hydraulic lime). Plate 23 shows sample number 5a, indicating what appears to be agglomerates of calcite and smaller C-S-H rod like crystals. The well developed calcite crystals range in size, and are wide spread across the sample.

Throughout the plate agglomerates of tiny calcite crystals are adhered to what would appear to be aggregate. The EDX analysis (see figure 66) indicates a large Kα-peak which may be associated with calcite.

Plate 23 : Gowrie sharp sand and NHL2 hydraulic lime

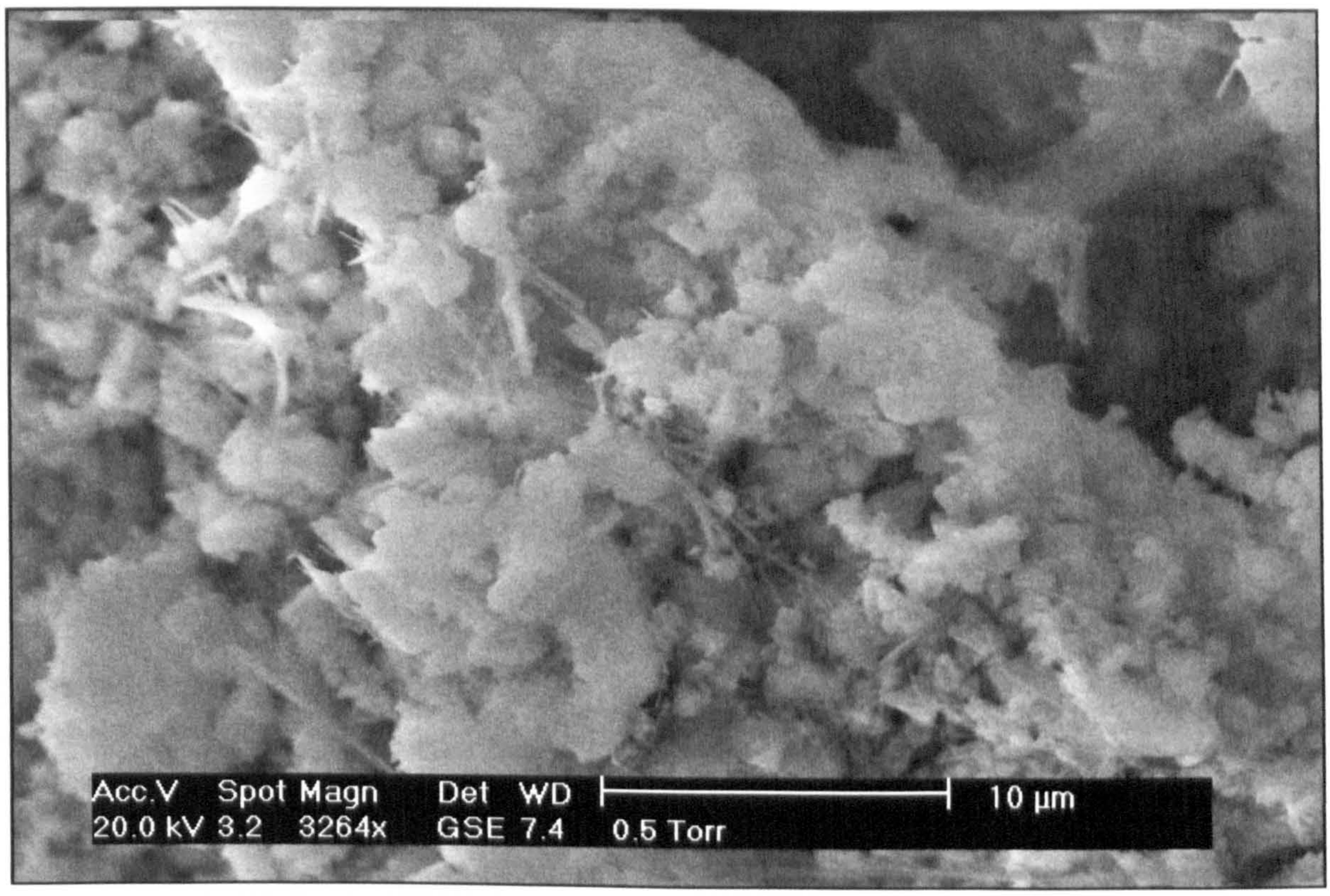

The image appears to show a certain degree of needle or rod like crystal types, that are knitting across the material.

Figure 66: EDX plot indicating chemical elements and concentration for the binary NHL2 mortar samples

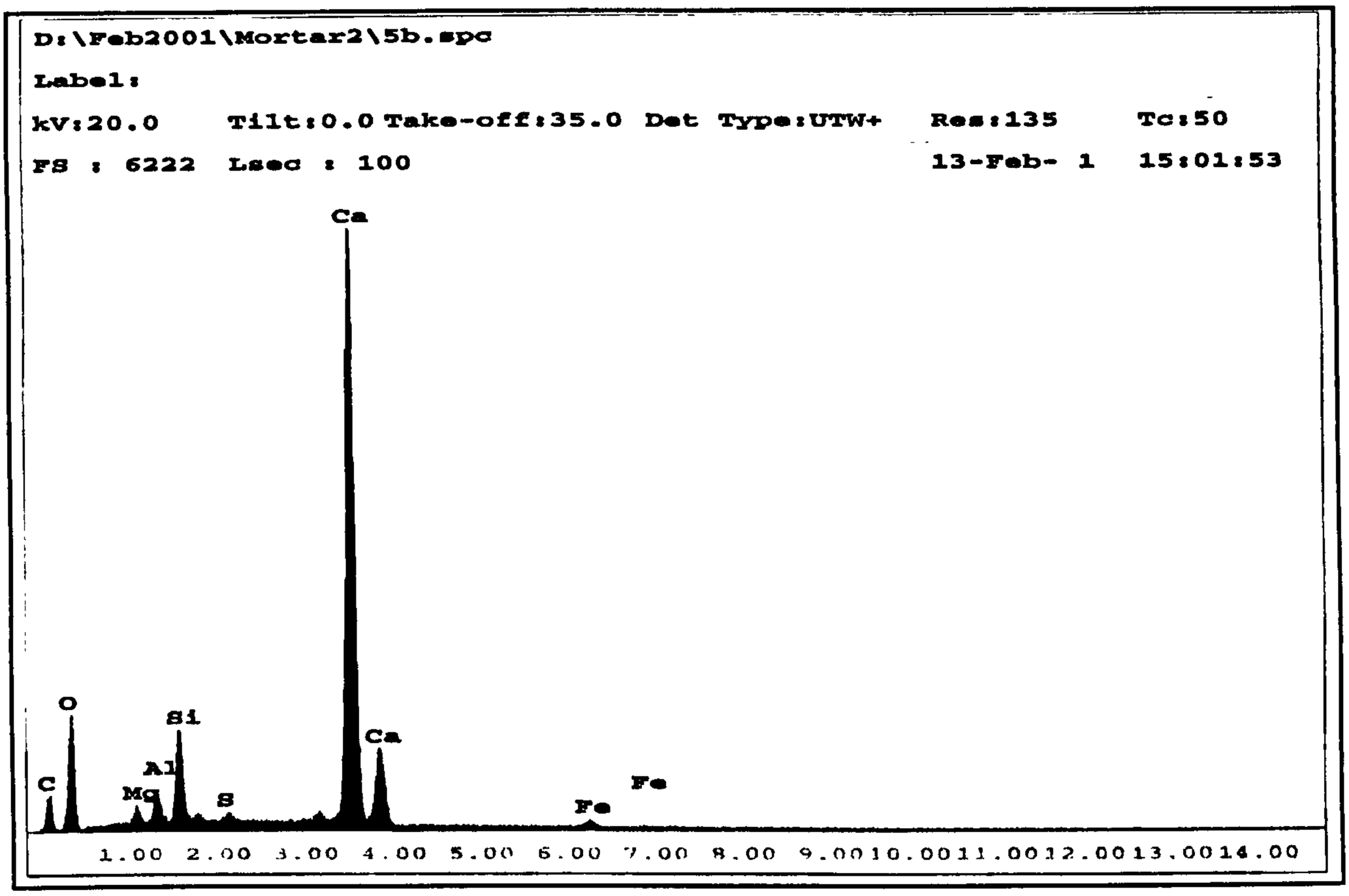

The EDX analysis indicates the presence of moderate / low quantities of aluminium and silica which may be responsible for small quantities of C-S-H and C-A-H. This is to be expected within a feebly hydraulic lime mortar with known hydraulic set characteristics. In addition, EDX analysis revealed the presence of small quantities of C, Mg and S.

Plate 24 shows sample number 5a, indicating what appears to be tiny calcite crystal formation with a significant amount of C-S-H needle like crystal formation also exhibited.

Plate 24 : Gowrie sharp sand and NHL2 hydraulic lime

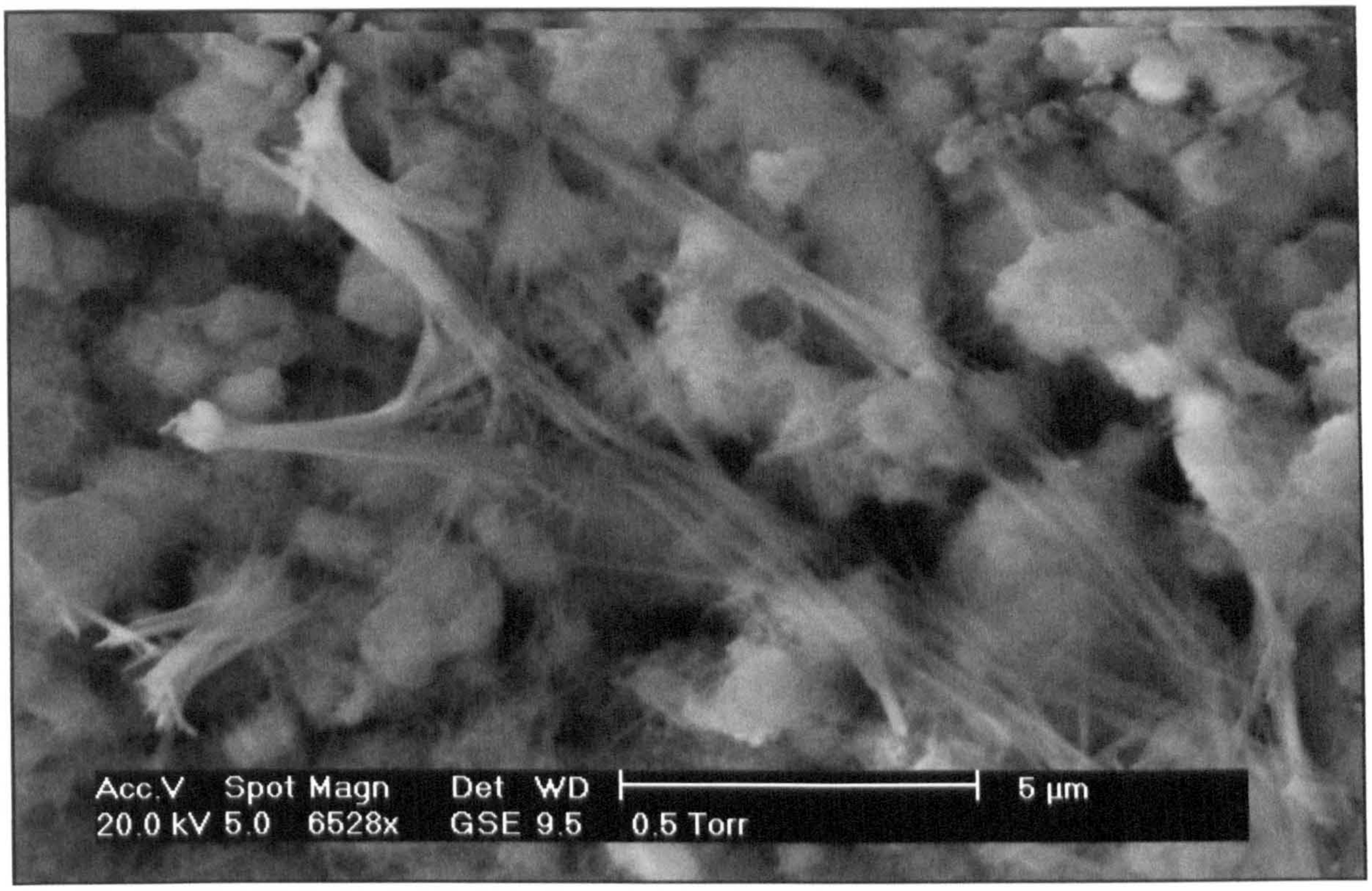

The C-S-H crystalline formations have developed into a relatively loose mat-like network. The rods are bundled at mid - end of the crystal chain, and appear to develop from larger calcite crystals, which are acting as a primary framework for the C-S-H structure.

4.4.5 Natural Hydraulic Lime 3.5 (NHL3.5)

The NHL3.5 samples are considered to be moderately hydraulic lime mixes with a batch ratio of 3:1 (Gowrie sharp sand and NHL3.5 hydraulic lime)

Plate 25 shows sample number 6a, indicating what appears to be a network of C-S-H rods. These are formed throughout the sample and resemble a mat or hyphae effect with a texture noticeably less porous than that of the non-hydraulic limes - for example in Plate 21 or 22. The C-S-H crystallites can clearly be seen bridging the pore structure in several regions.

Plate 25 : Gowrie sharp sand and NHL3.5 hydraulic lime

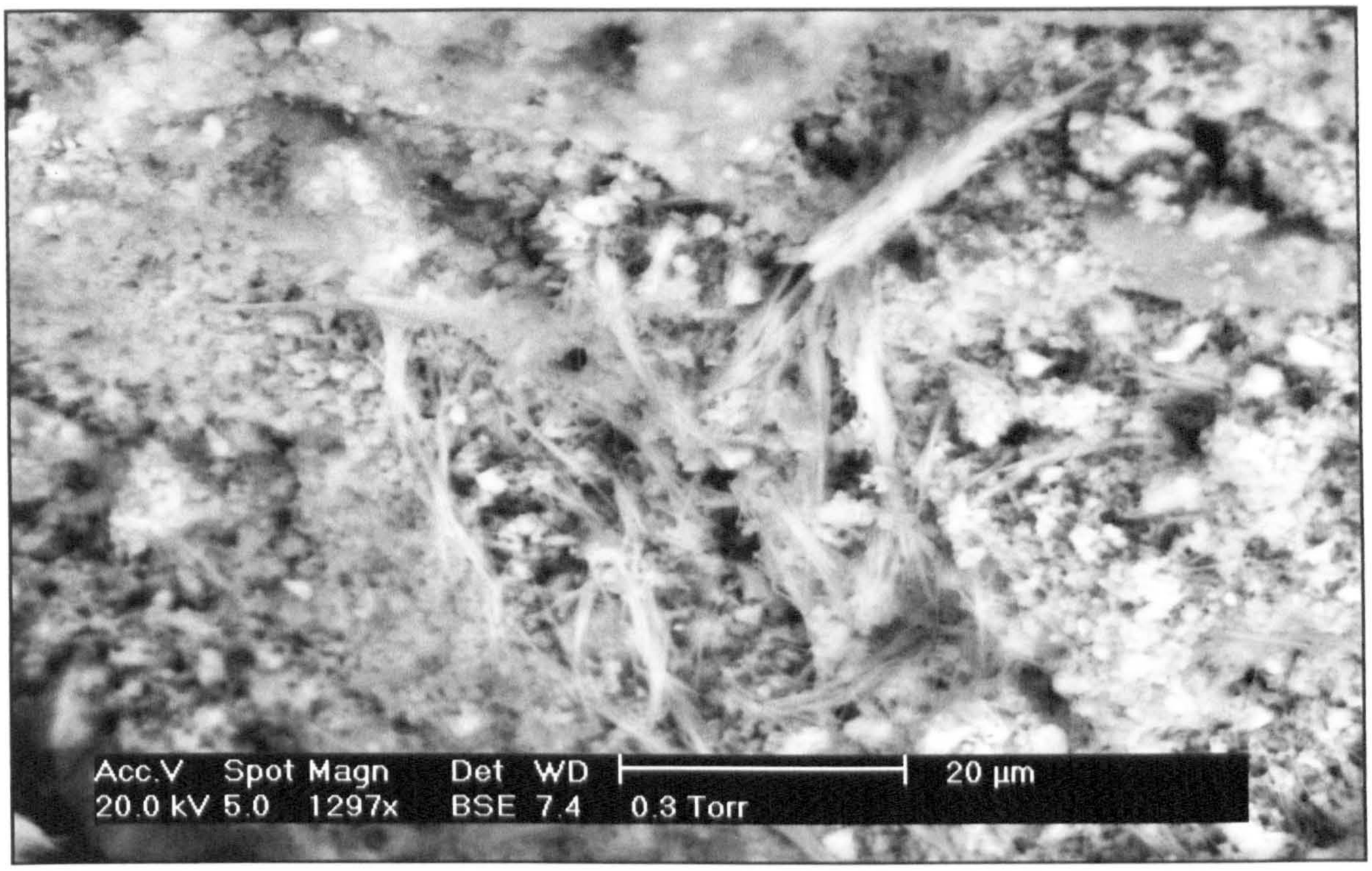

There is a widespread irregular mass of calcite crystals beneath, consistent with the Ca Kα-EDX peak (figure 67). Moderate to low traces of silica and aluminium are also present and are attributable to the C-A-H and C-S-H formation. EDX analysis also highlights the presence of Kα-peaks for C, Mg, S, and Fe, although they appear in such small quantities that they may be considered as trace only.

Figure 67: EDX plot indicating chemical elements and concentration for the binary NHL3.5 mortar samples

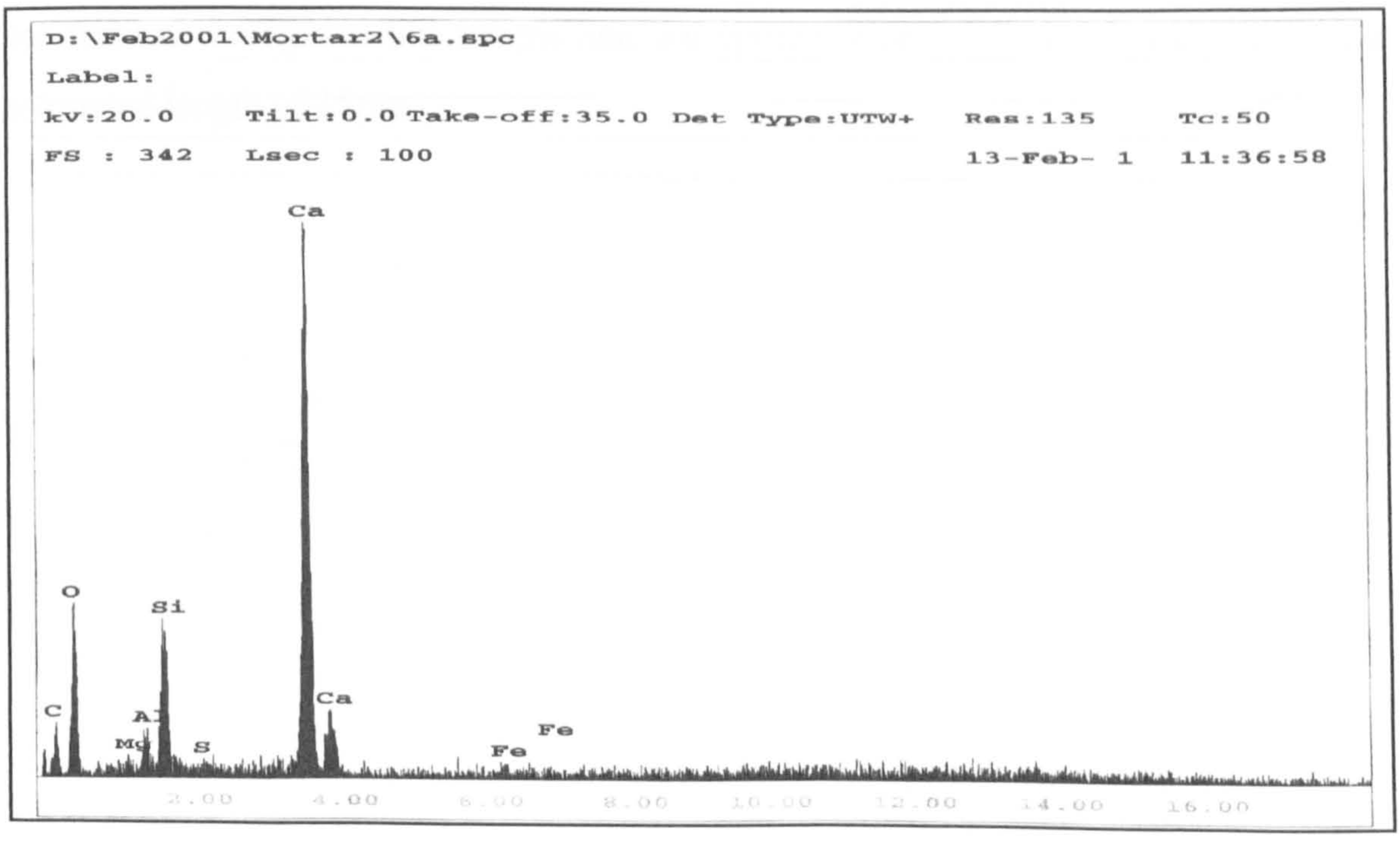

Plate 26 shows sample number 6b, indicating what appears to be a network of C-S-H rods / filaments, that are inter-dispersed within a substrate of irregular calcite crystallites. The C-S-H needles can be seen bridging the pore structure of the material knitting the mortar together. As aforementioned the presence of C-A-H cannot be discounted and several larger tabular crystals may be seen inter-dispersed throughout the sample. (see plate 27)

Plate 26 : Gowrie sharp sand and NHL3.5 hydraulic lime

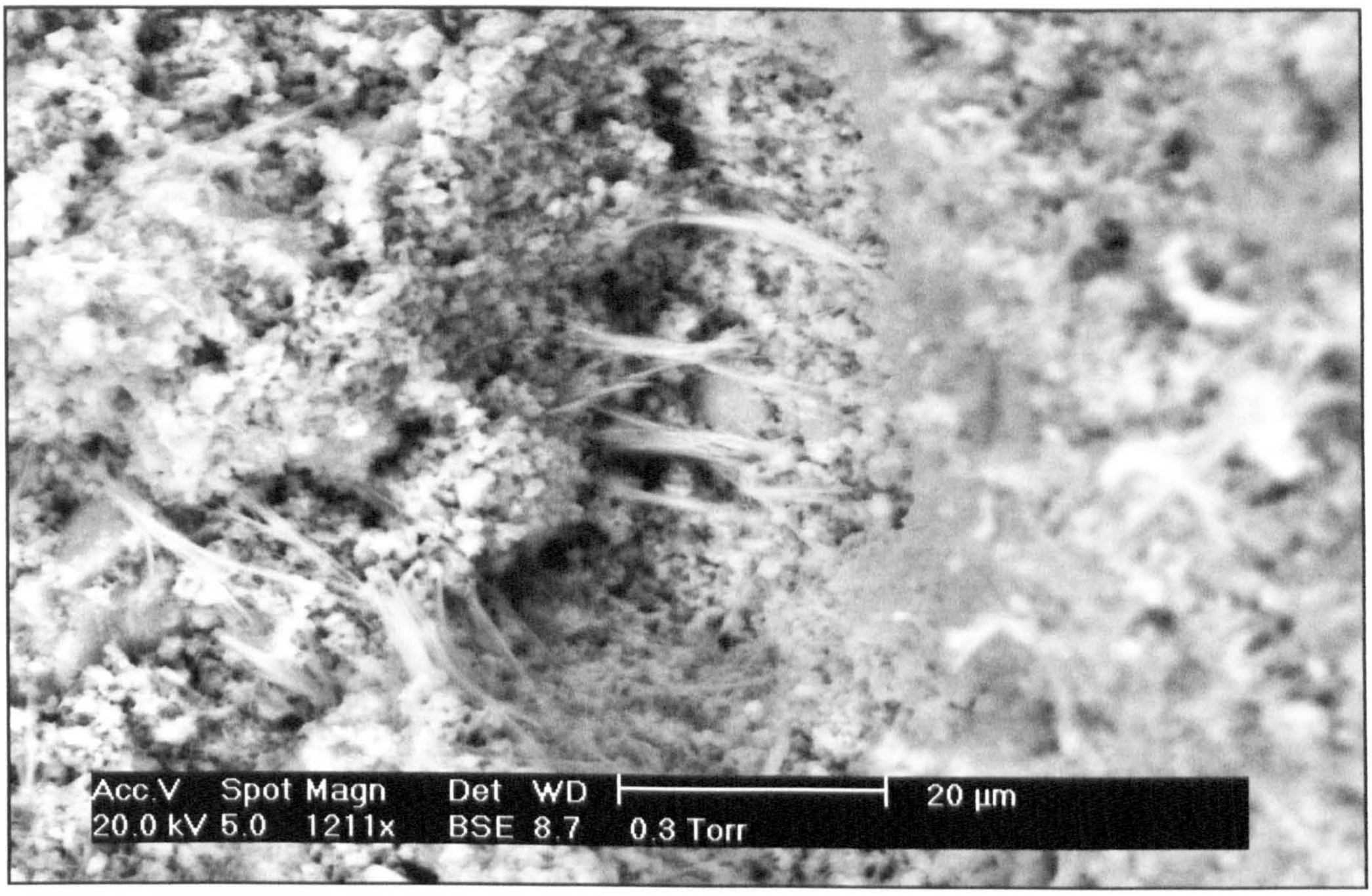

Plate 27 shows sample number 6b, at higher magnification. The C-S-H rods / filaments are formed throughout the sample and are approximately 0.5µm in diameter with an estimated length of 15µm.

Plate 27 : Gowrie sharp sand and NHL3.5 hydraulic lime

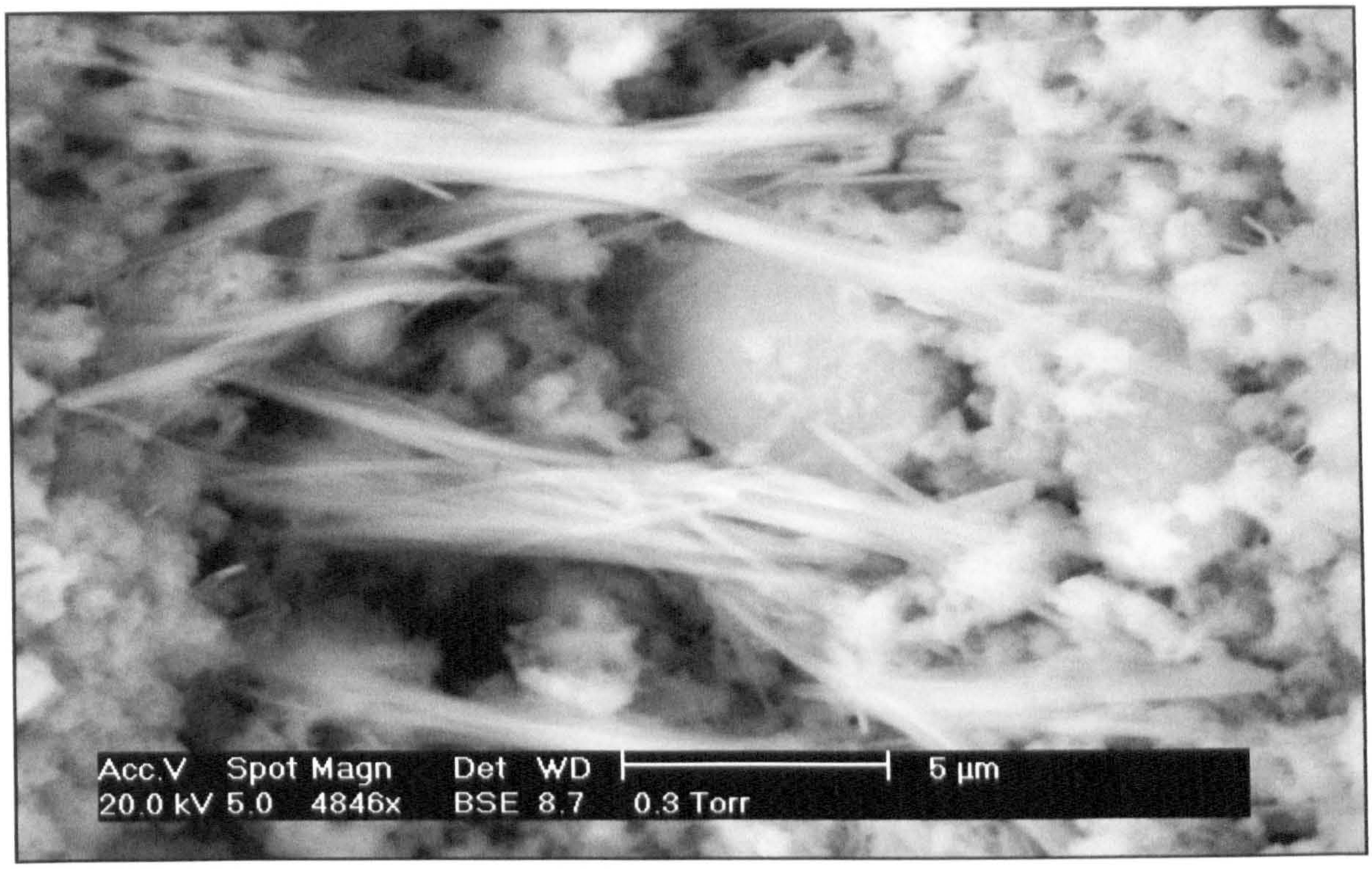

4.4.6 Natural Hydraulic Lime 5 (NHL5)

Plate 28 shows sample number 7b, indicating what appears to be a network of C-S-H rods and plates. These are formed throughout the sample.

Plate 28 : Gowrie sharp sand and NHL5 hydraulic lime

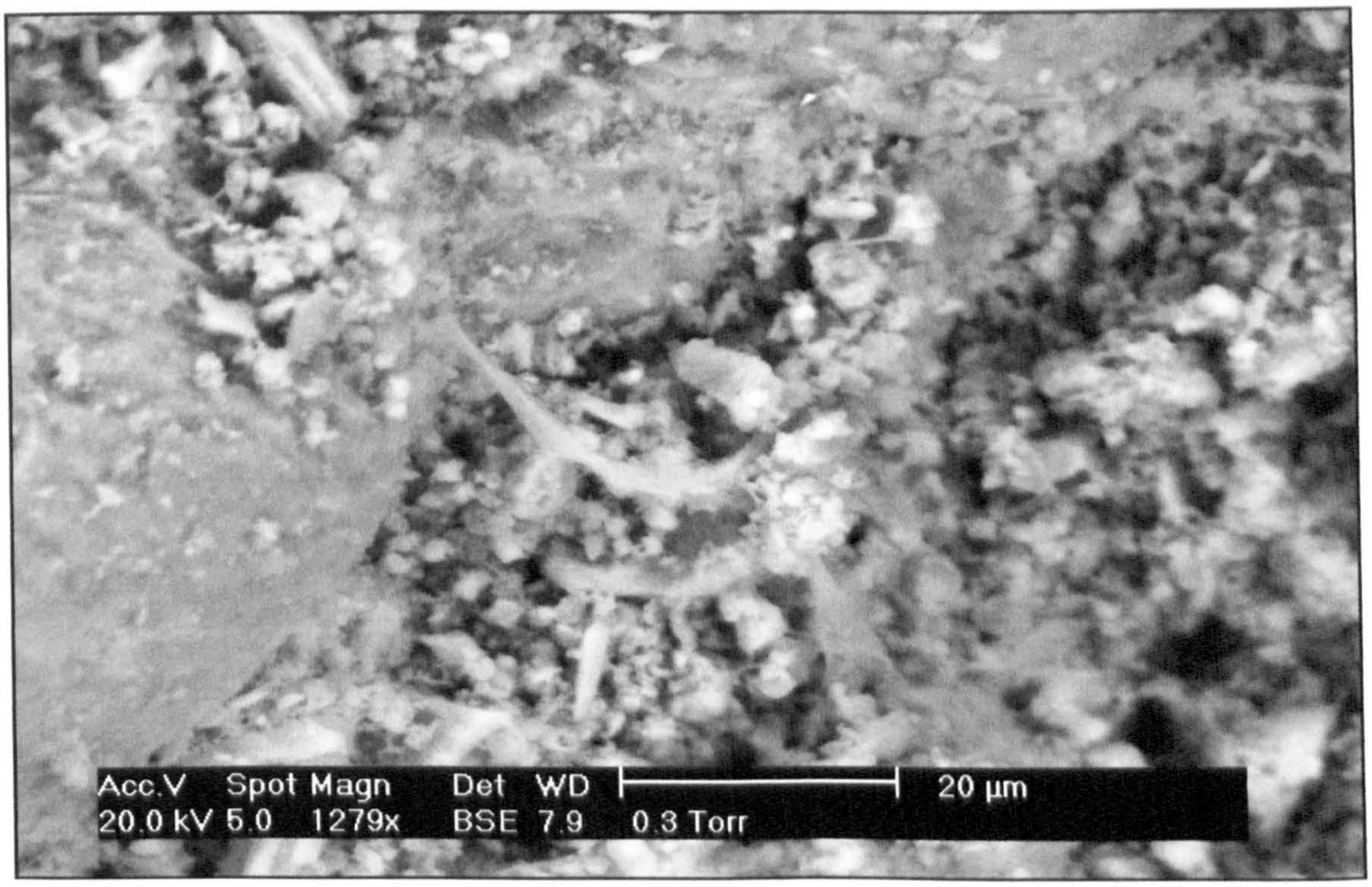

The presence of calcite crystals can be seen in irregular agglomerate masses with the C-S-H and C-A-H crystals dispersed across the surface of the material. The large relatively barren region within the upper left of the plate may be associated with aggregate.

The C-S-H and C-A-H can be correlated with the EDX analysis which indicates the presence of a moderate Kα-peak of silica and a lower peak of aluminium. In addition the EDX plot (figure 68) indicates a large Kα-peak for Ca, this is associated with calcite agglomerations.

Figure 68: EDX plot indicating chemical elements and concentration for the binary NHL5 mortar samples

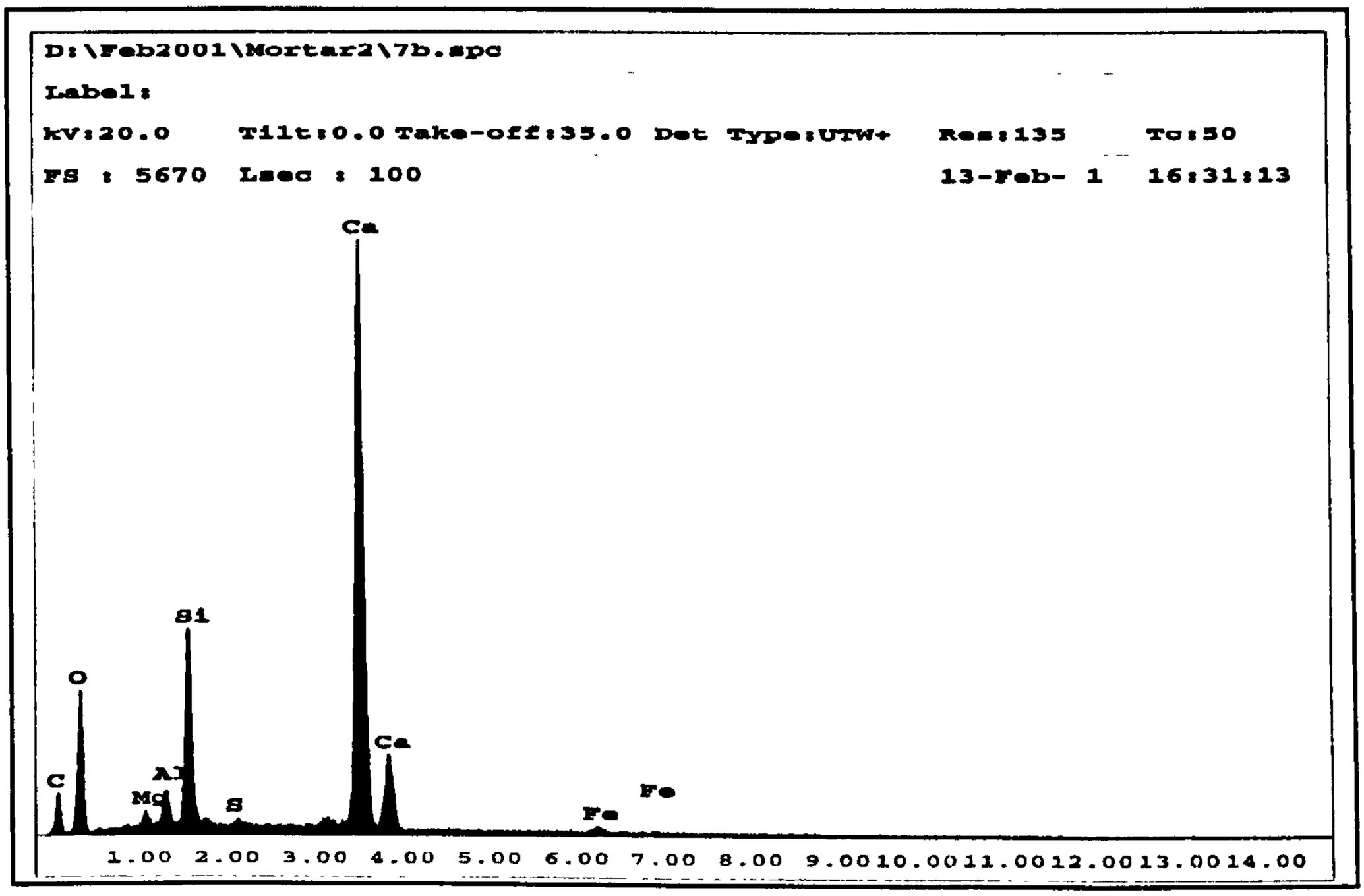

Plate 29 shows sample number 7b, indicating what appears to be a network of C-S-H rods and plates. These are formed throughout the sample.

Plate 29 : Gowrie sharp sand and NHL5 hydraulic lime

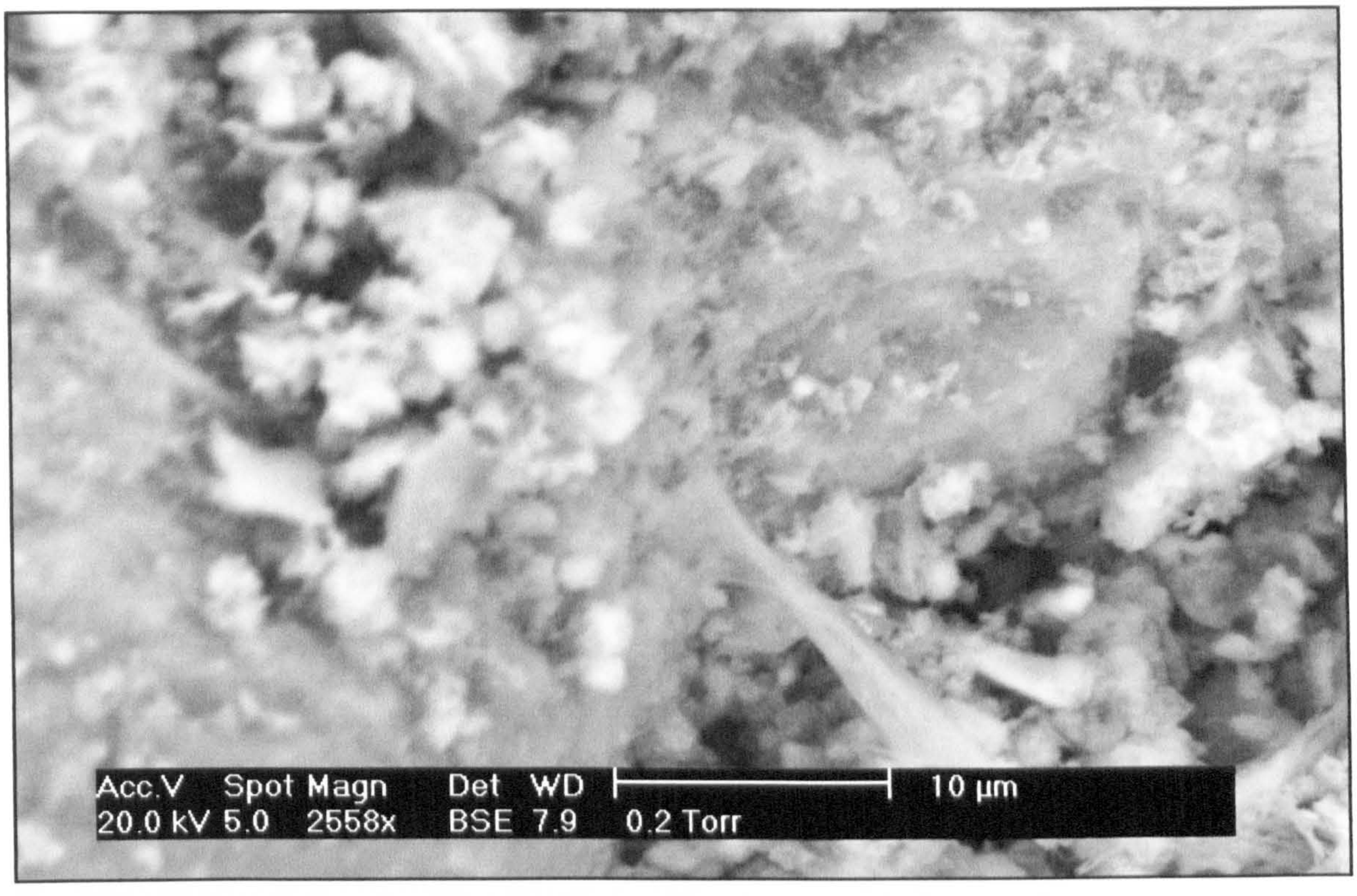

Plate 30 shows sample number 7b, indicating what appears to be a network of C-S-H rods and plates. These are formed throughout the sample.

Plate 30 : Gowrie sharp sand and NHL5 hydraulic lime

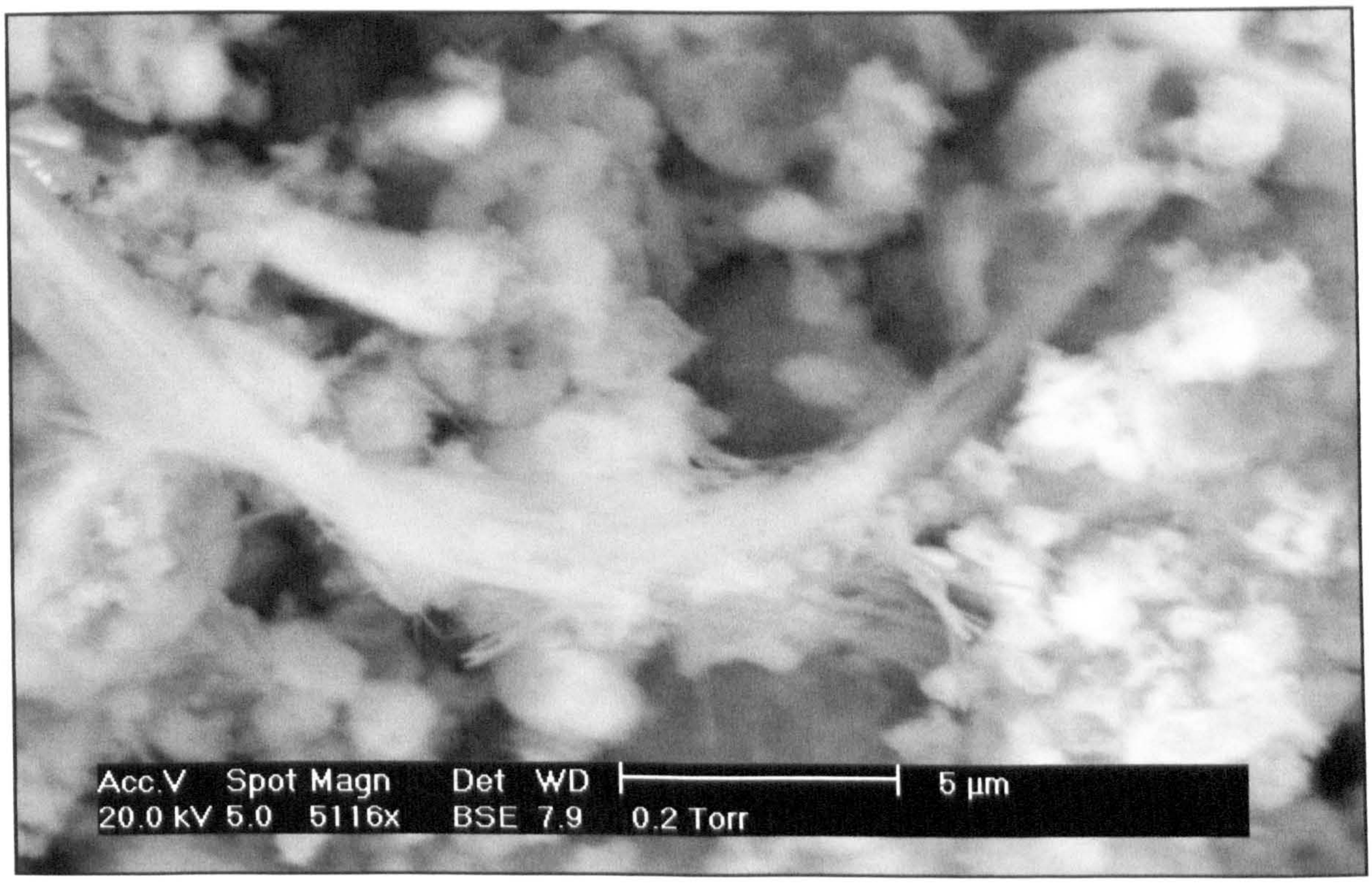

4.4.7 Natural Hydraulic Lime Jura-Kalk (NHL5)

Plate 31 shows sample number 8c, where the network of C-S-H rods and plates are visible but less pronounced.

Plate 31 : Gowrie sharp sand and Jura-Kalk hydraulic lime

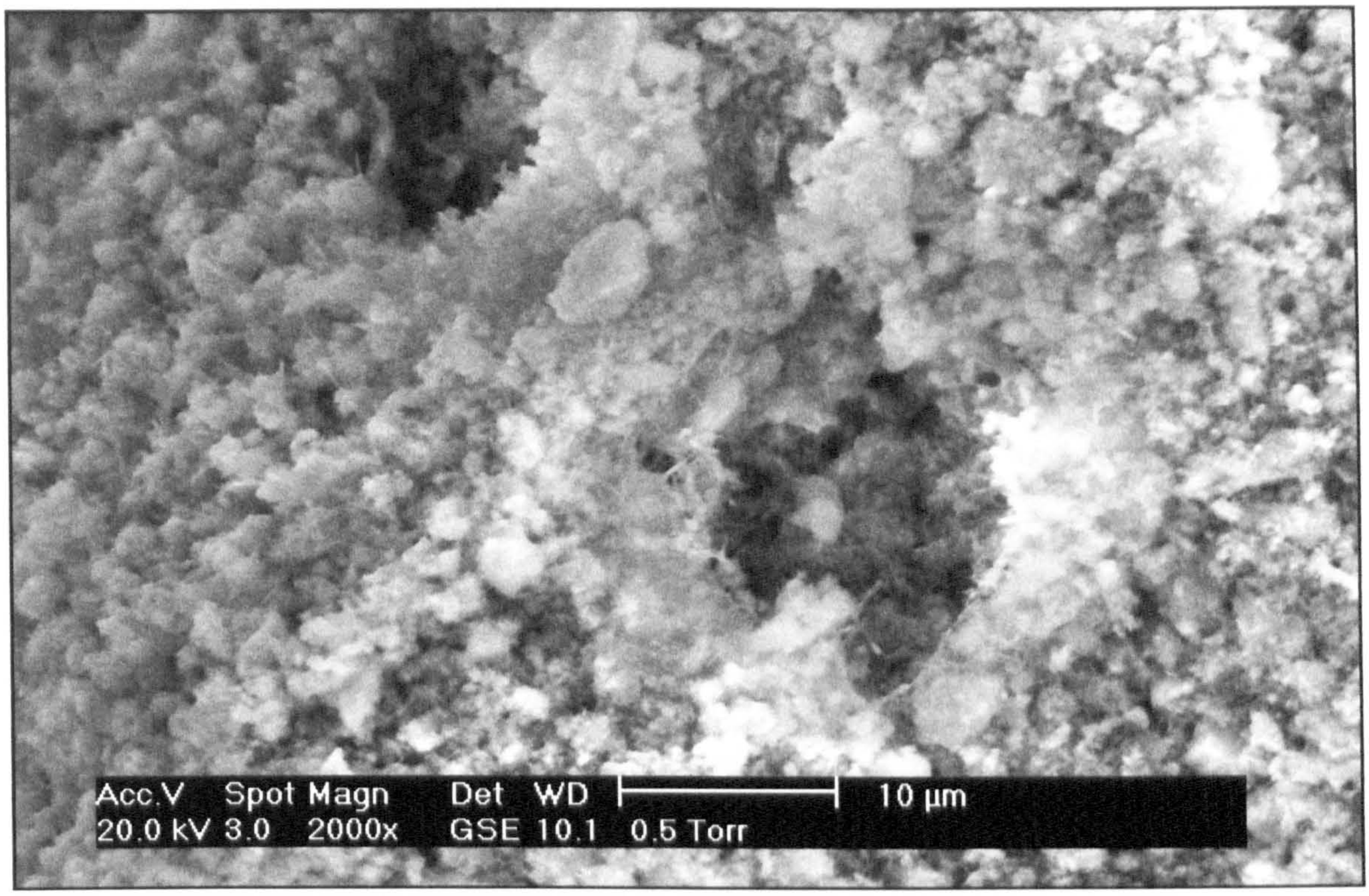

C-S-H appears to be protruding from a substrate of calcite crystallites. It is possible that portlandite crystals may be present due to the materials relatively dense matrix, preventing CO_2 from penetrating the mortar and therefore prohibiting full conversion of calcite from occurring. These calcium-based crystals were characterised by a Kα-peak at 3.6KVe (figure 69).

Figure 69: EDX plot indicating chemical elements and concentration for the binary Jura-Kalk mortar samples

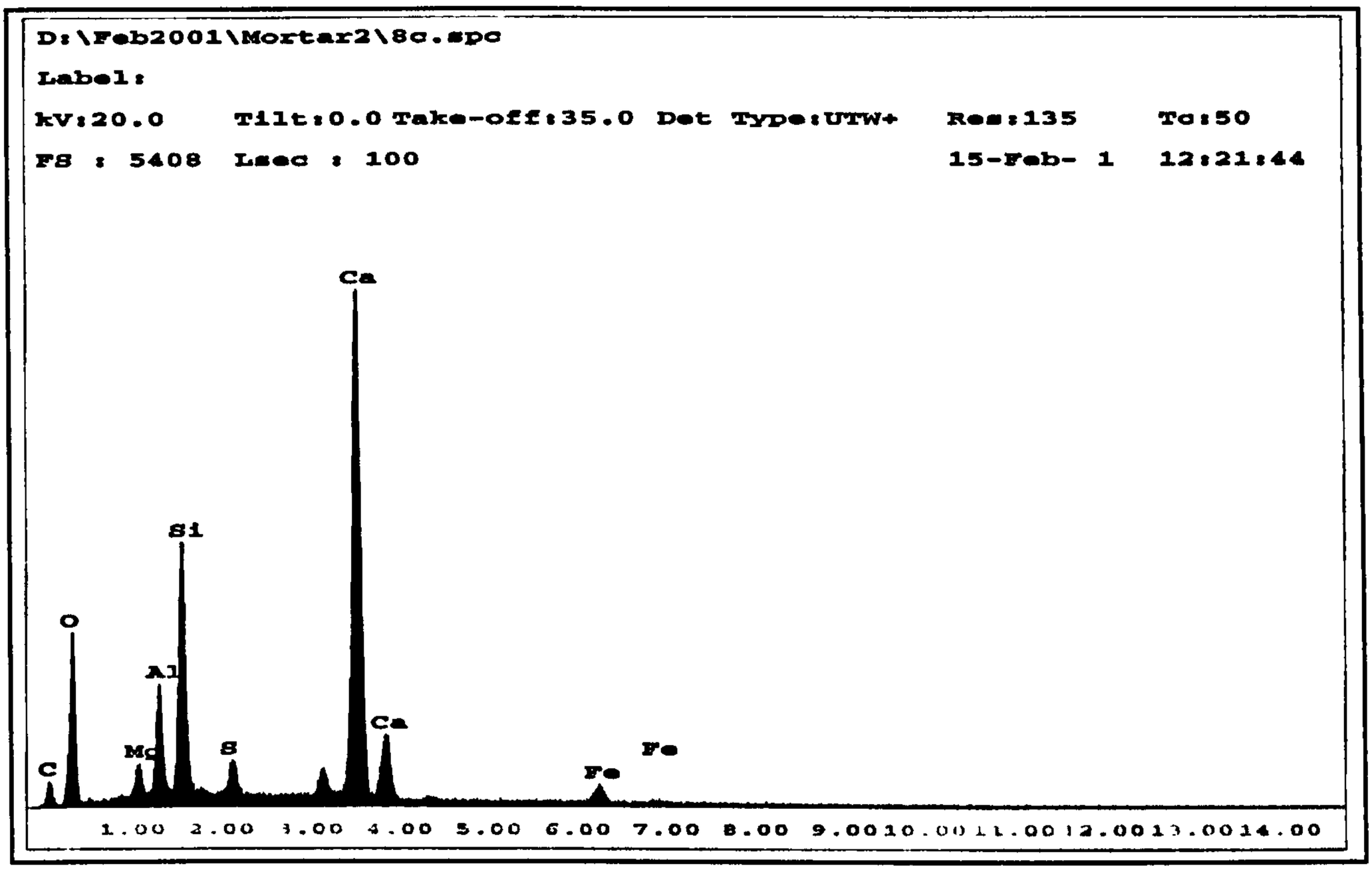

The larger regular hexagonal crystal types may be associated with portlandite or C-A-H. The presence of moderate levels of C-S-H and lower levels of C-A-H are expected when assessing the EDX analysis. This is reinforced in the EDX plot seen in figure 69. Moderate to high levels of Si at 1.8KVe where exhibited, lower, yet still significant levels of Al at 1.6KVe also being present.

Plate 32 and 33 show sample number 8c, at different magnifications.

Plate 32 : Gowrie sharp sand and Jura-Kalk hydraulic lime

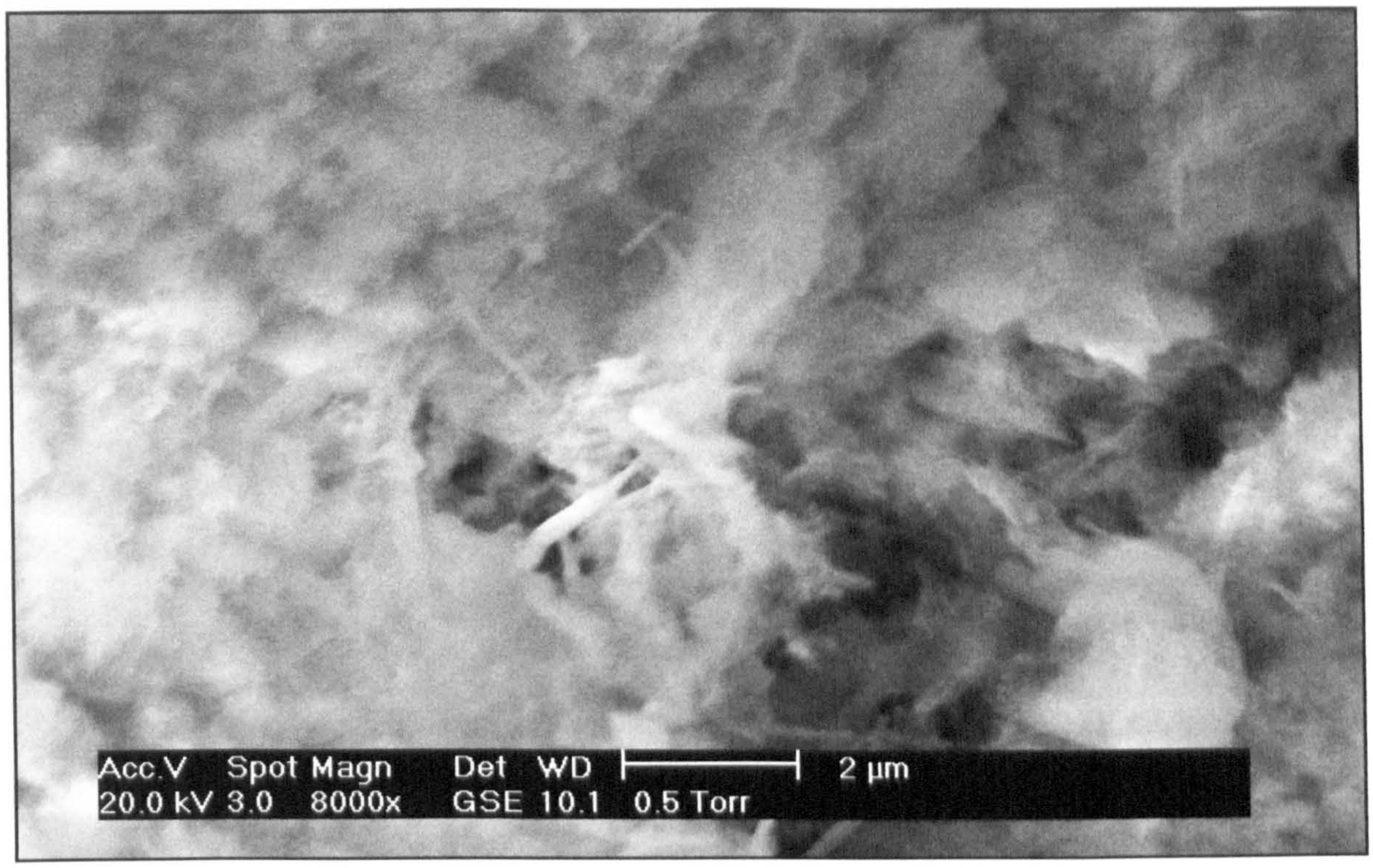

Plate 33 : Gowrie sharp sand and Jura-Kalk hydraulic lime binary mortar sample

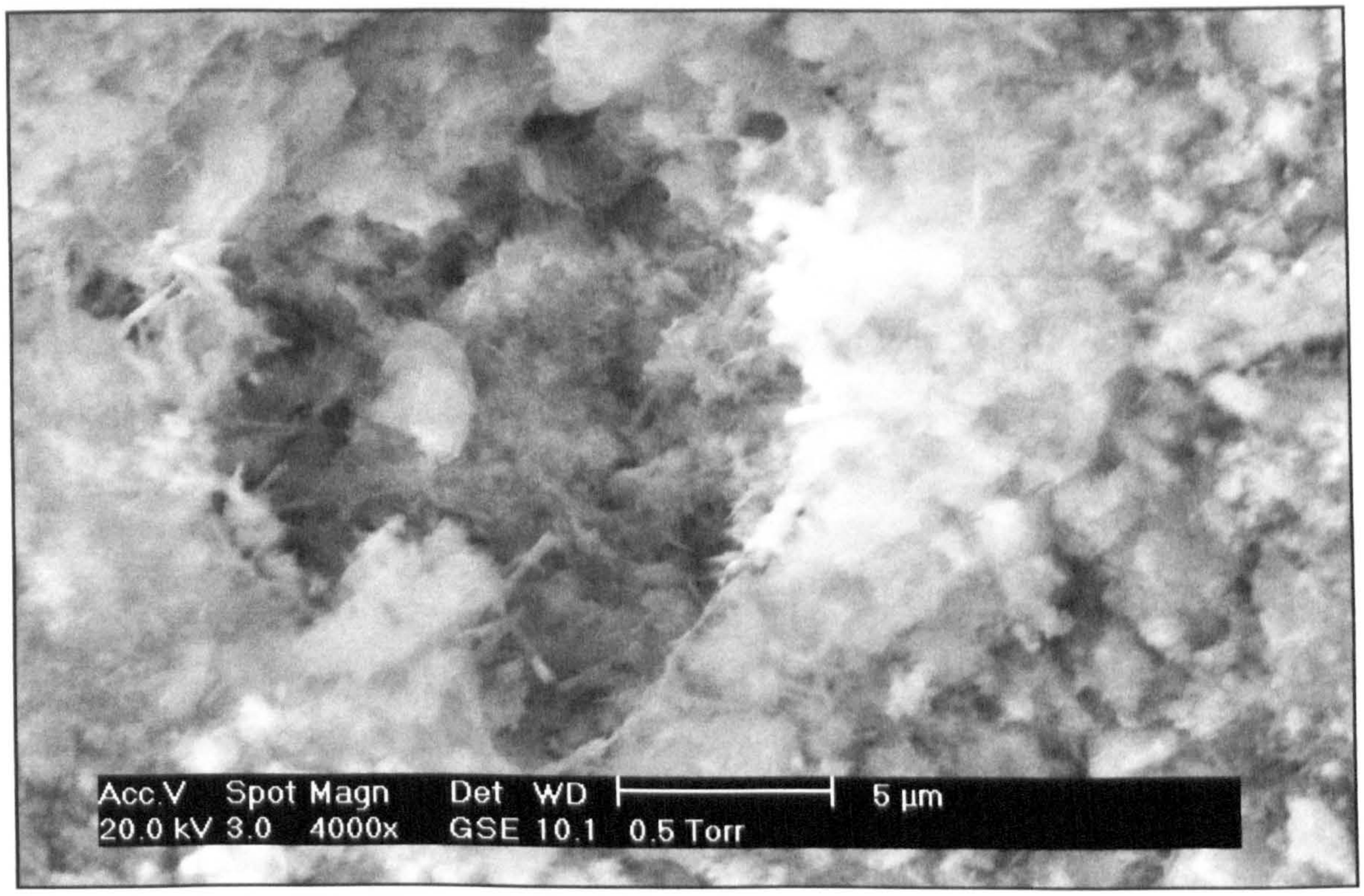

4.4.8 Ordinary Portland cement binary mortar sample

Plate 34 shows sample number 9b, a network of C-S-H and C-A-H rods and plates and tabular crystals of $Ca(OH)_2$.

Plate 34 : Gowrie sharp sand and ordinary Portland cement binary mortar sample

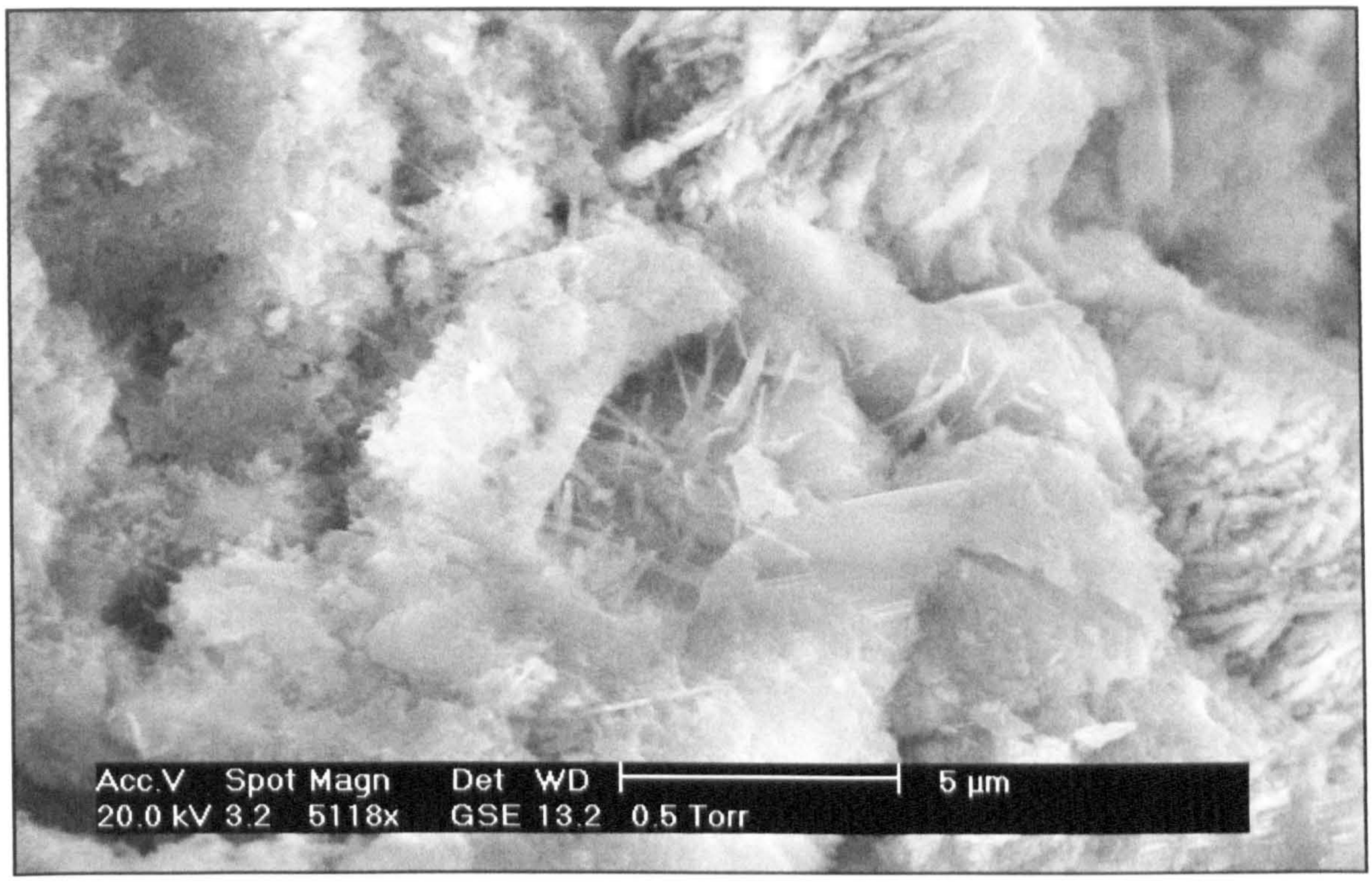

EDX analysis seen in figure 70, shows a much larger Si Kα-peak than the previous analyses, consistent with the Portland cement samples. The silicate and aluminium phases assessed under EDX have Kα-peaks of approximately 1.8KVe and 1.6KVe respectively. The concentration of silicate phase is larger than the aluminate phase by approximately a factor of 4.

Figure 70: EDX plot indicating chemical elements and concentration for the binary Ordinary Portland Cement mortar samples

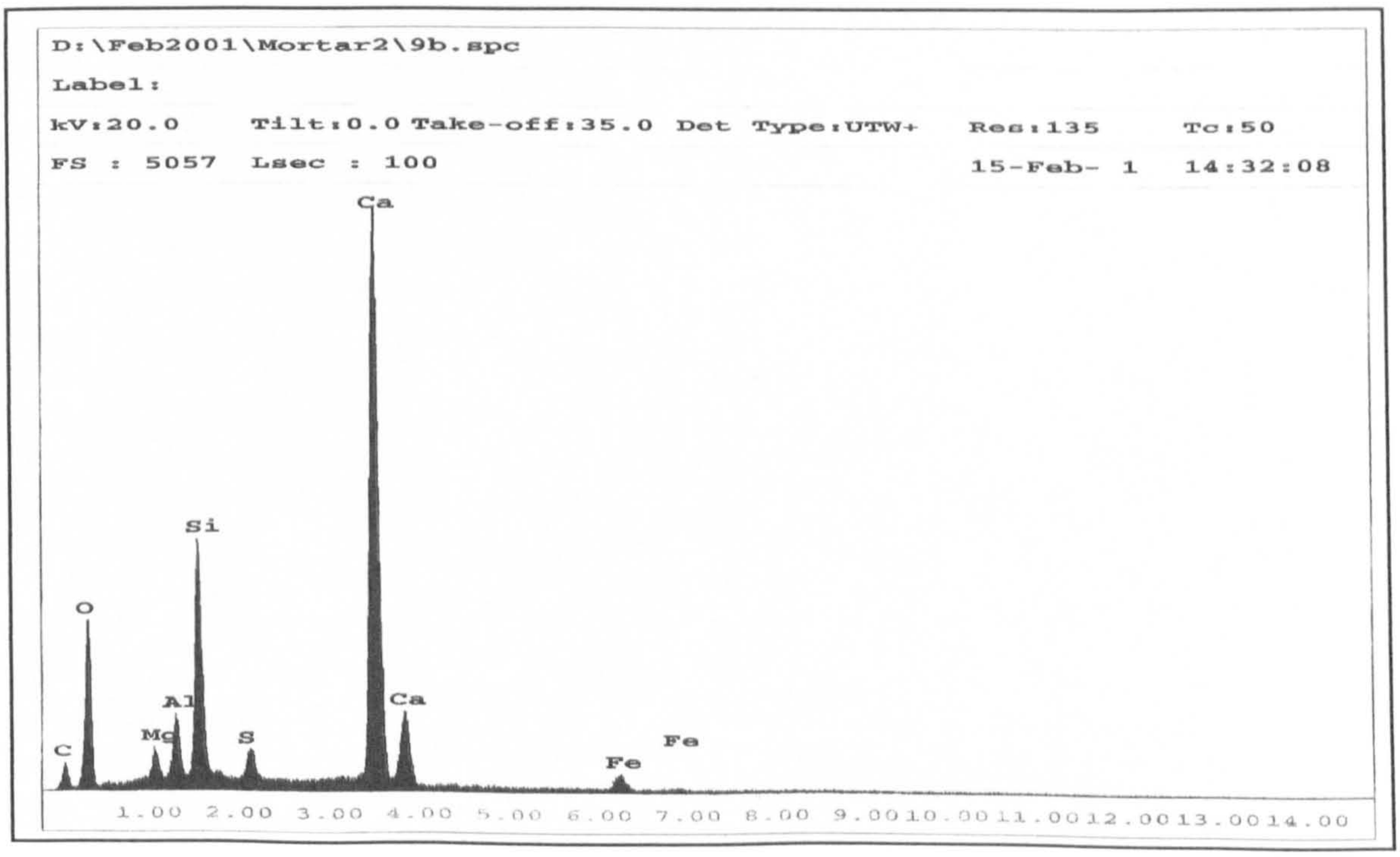

Plate 35 and 36 shows sample number 9a, at different magnifications.

Plate 35 : Gowrie sharp sand and ordinary Portland cement binary mortar sample

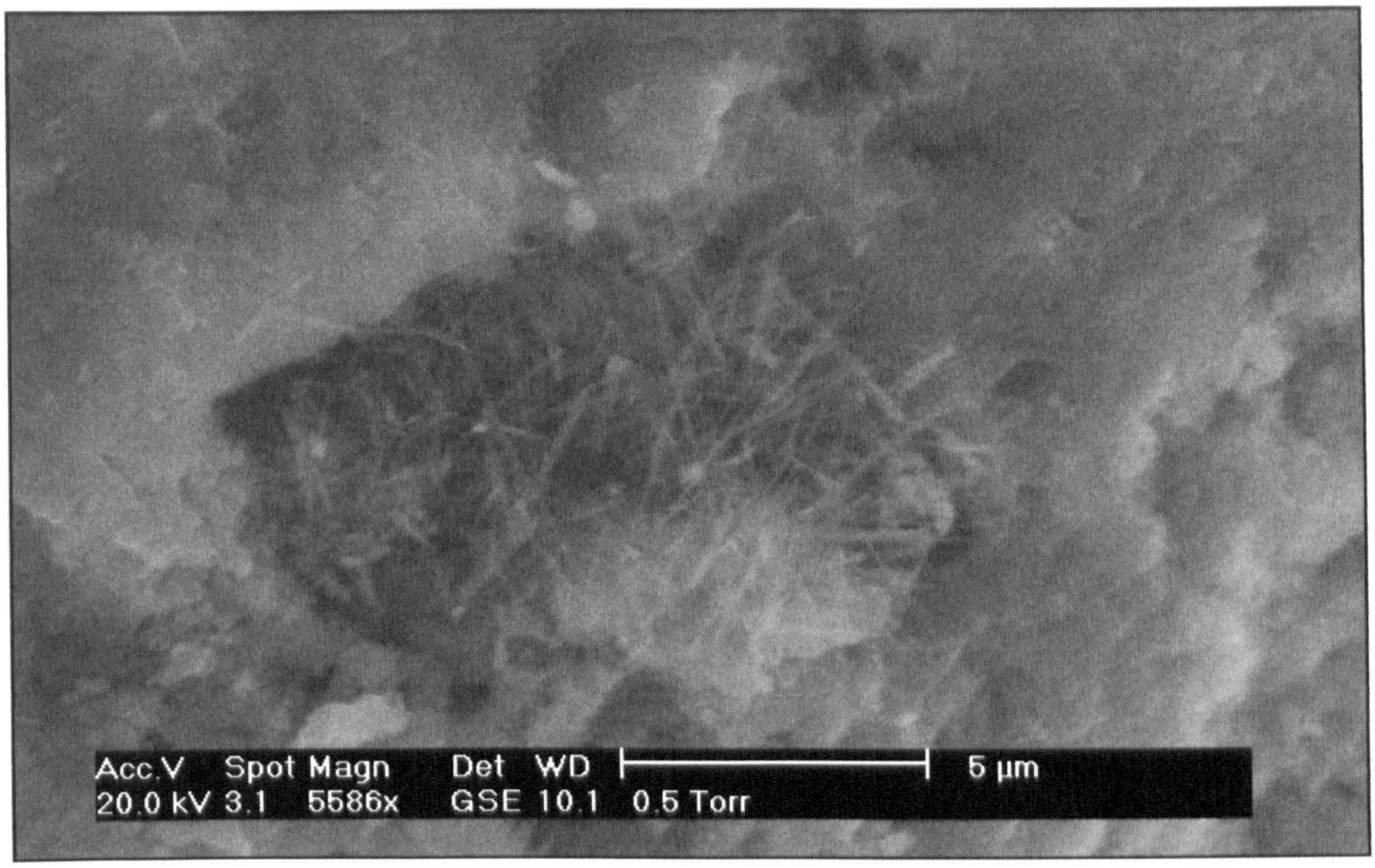

Plate 36 shows sample number 9a, indicating what appears to be a crystalline network of C-S-H rods and confirms the extent to which C-S-H can form relatively impenetrable dense matrix / network which is essential for the strength of O.P.C. It is noticeable that the Portland cement specimens have a much closer texture than the lime specimens.

Plate 36 : Gowrie sharp sand and ordinary Portland cement binary mortar sample

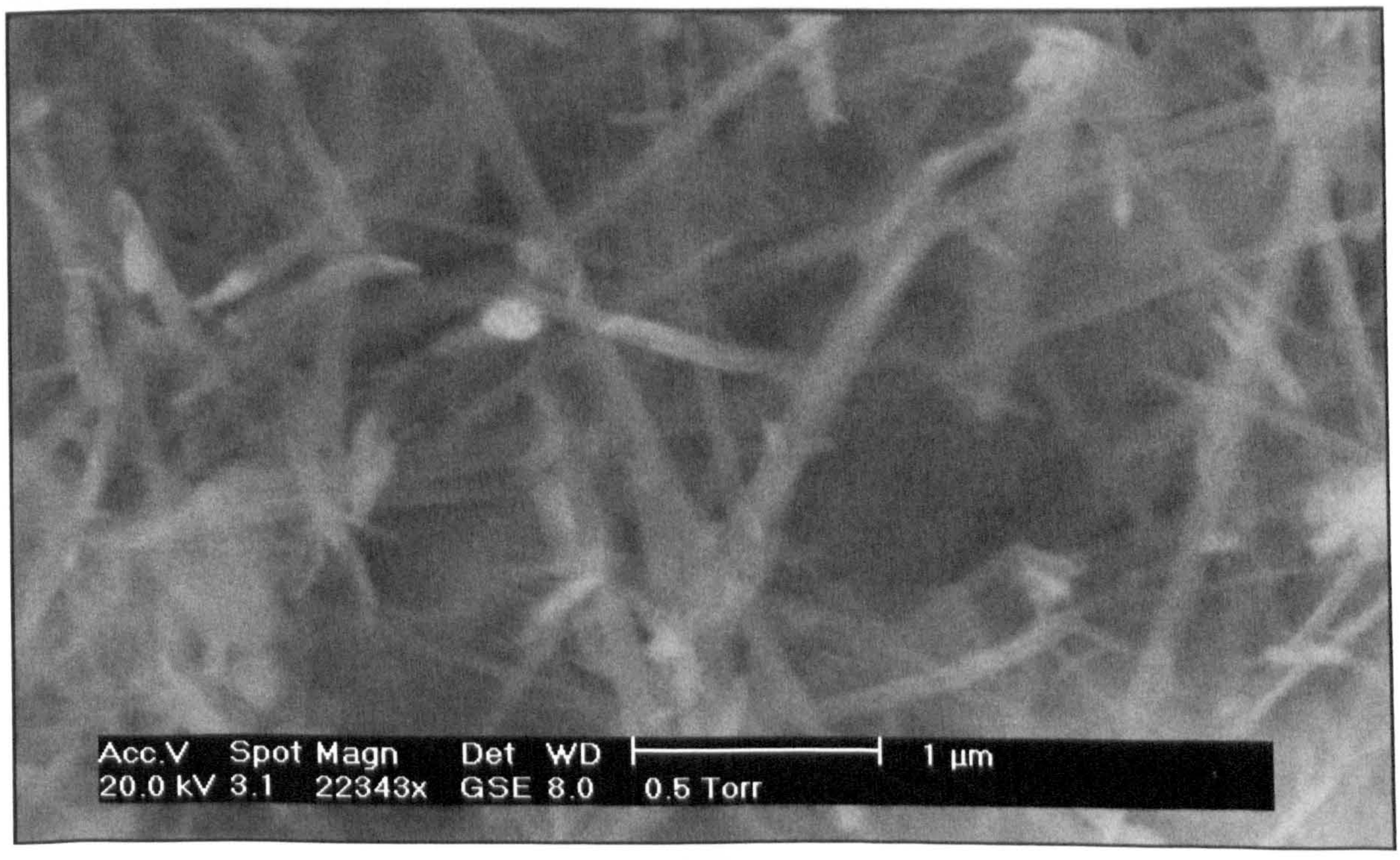

4.4.9 Shap non-hydraulic lime and NHL2 gauged sample

Plate 37 shows sample number 10a, indicating the network of C-S-H rods. Small agglomerates of calcite crystals can be seen throughout the image.

Plate 37 : Gowrie sharp sand and blended Shap non-hydraulic lime and NHL2

The C-S-H crystals are abundant, however, they appear to be most densely packed at the aggregate interface (the darker region of the image) and in an agglomerated form.

EDX analysis seen in figure 71, reveals a high Kα-peak level for Ca at 3.6Kve. This is associated with mass calcite agglomerates. A relatively small Kα-peak is associated with the quantity of silica and therefore correlates with the formation of C-S-H. An aluminium Kα-peak is present at 1.6KVe, this is approximately half the concentration of silica. Although no visual evidence exists for C-A-H crystal types it does not mean that their presence may be discounted as they may occur within the tightly packed C-S-H forms.

The C-S-H needles are clearly visible in plates 38 and 39.

Figure 71: EDX plot indicating chemical elements and concentration for the ternary NHL 2 & Shap non-hydraulic lime mortar samples

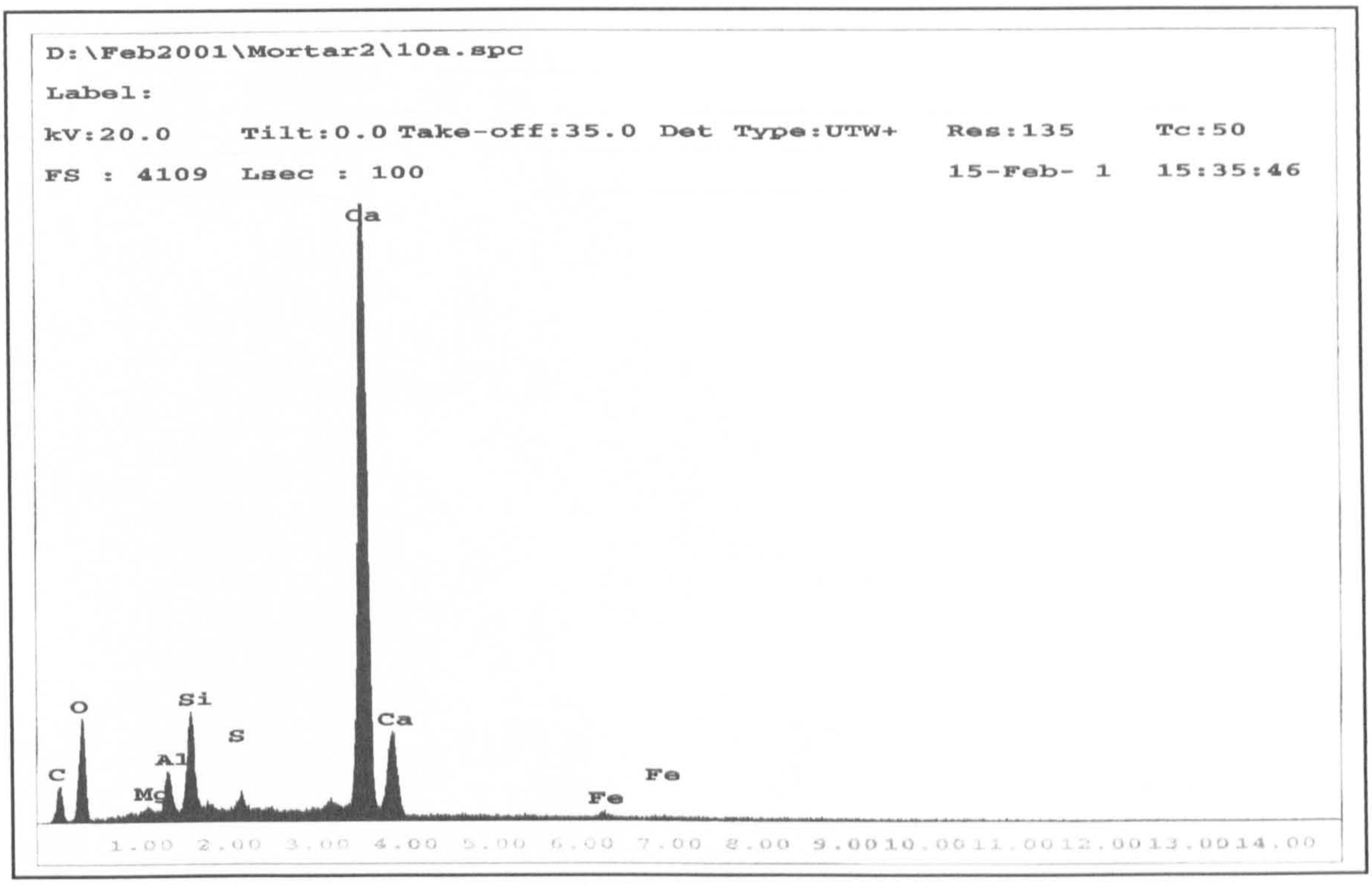

Plate 38 : Gowrie sharp sand and blended Shap non-hydraulic lime and NHL2

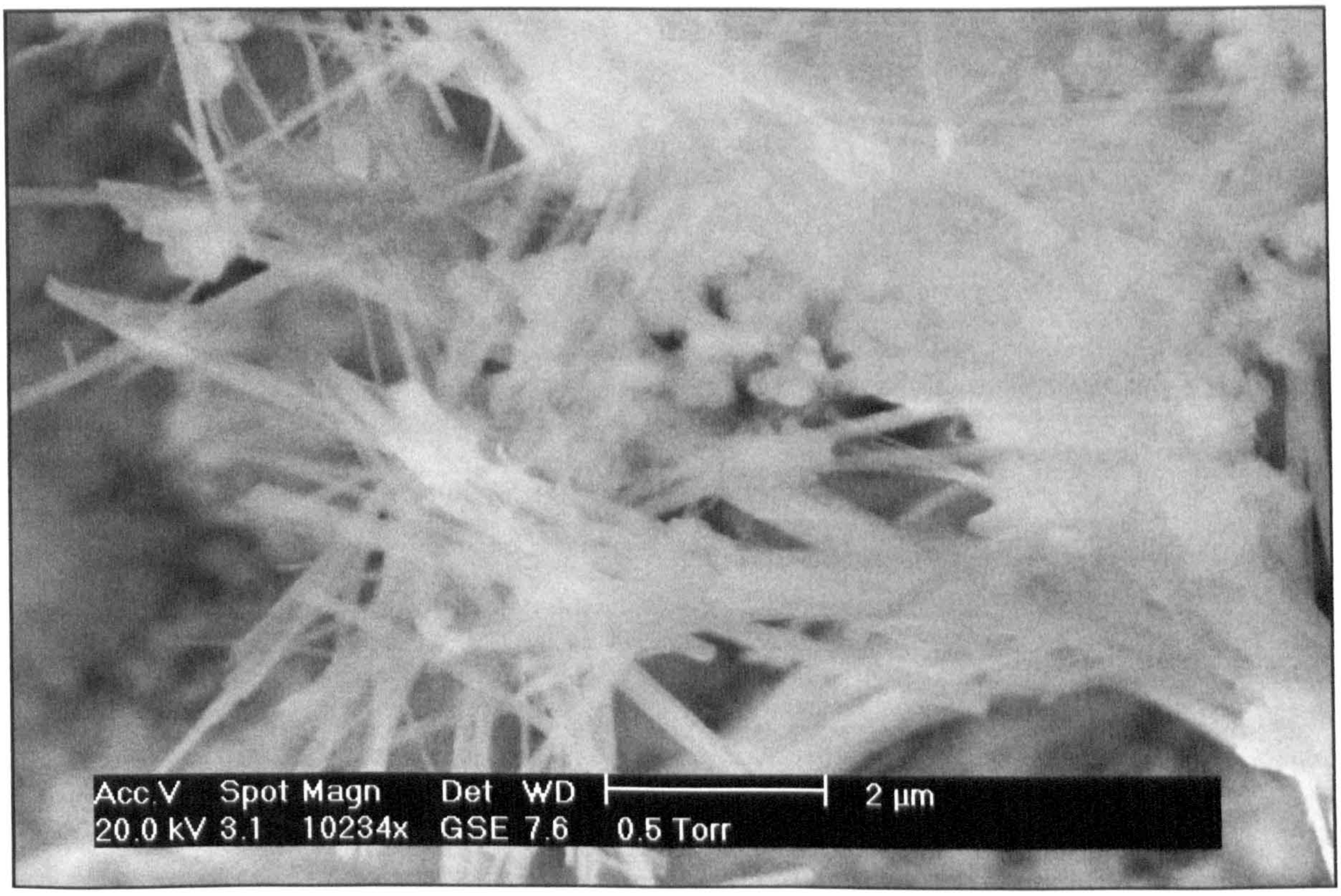

Plate 39 : Gowrie sharp sand and blended Shap non-hydraulic lime and NHL2

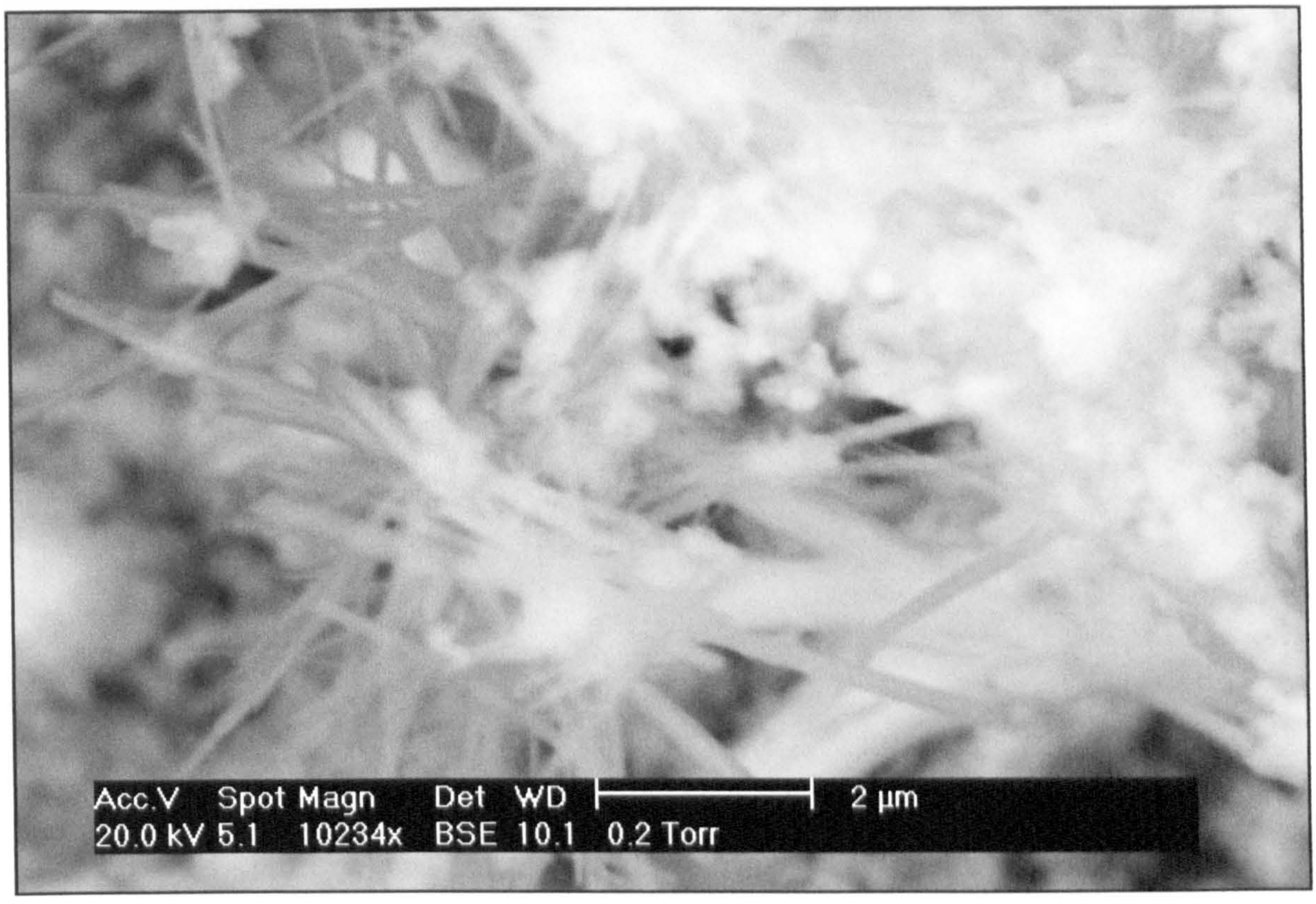

It is evident that the C-S-H is developing from the calcite deposition, which is widespread throughout the mortar matrix.

4.4.10 Shap non-hydraulic lime and NHL3.5 gauged sample

Plate 40 shows sample number 11a, indicating a less abundant network of C-S-H rods and plates. These are formed from the substrate of calcite which are characterised by their rather chunky hexagonal crystal type. The texture is relatively "grainy".

Although difficult to assess (β-C_2S) beta di-calcium silicate plate crystals may be present and are not to be confused with C-S-H rod type formation which are smaller. These hydration products are clearly seen to be bridging the pore structure of the mortar, particularly in plates 41 and 42 which are at higher magnification.

Plate 40 : Gowrie sharp sand and blended Shap non-hydraulic lime and NHL3.5

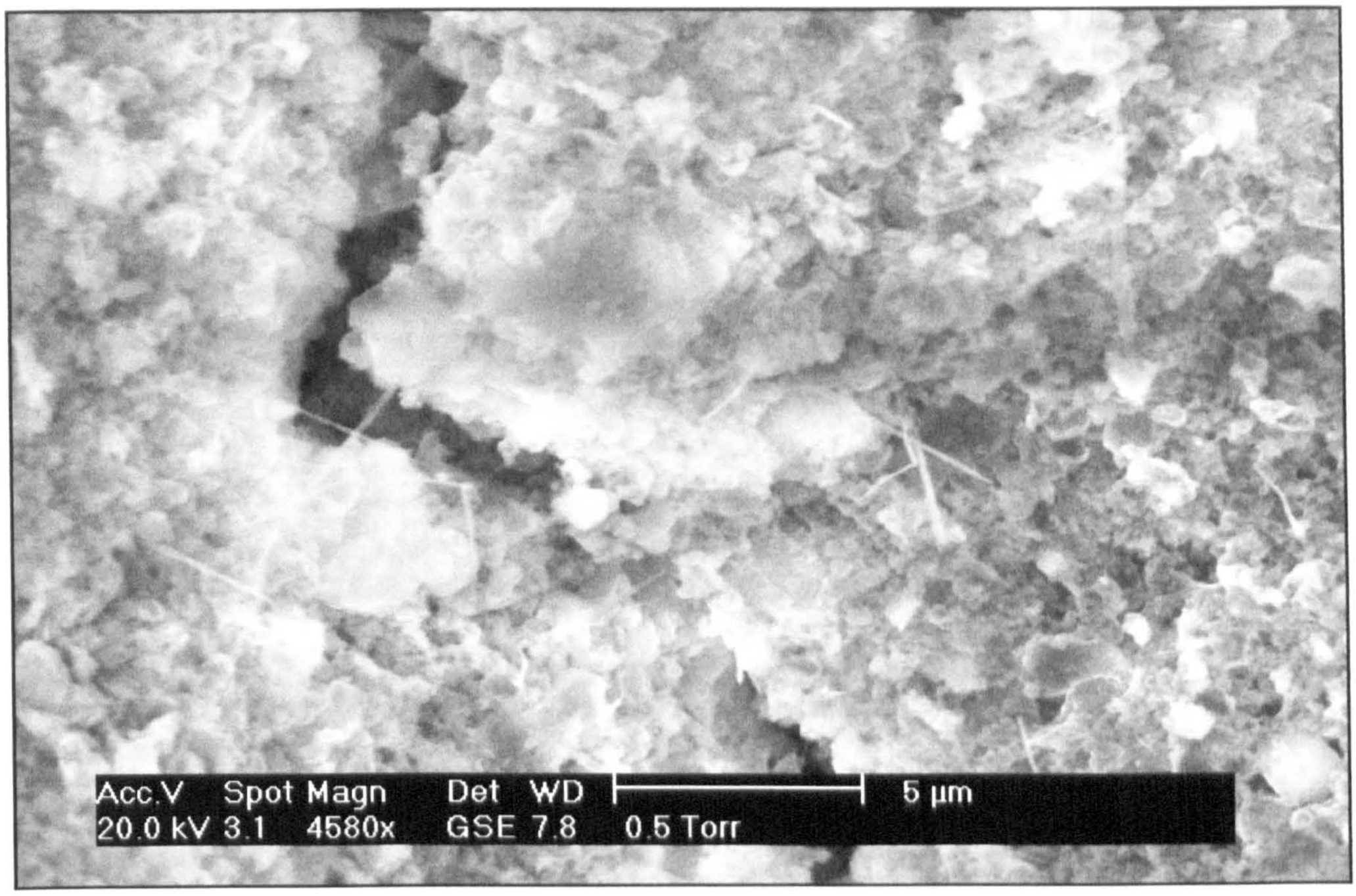

EDX analysis seen in figure 72 indicates a large Kα-peak for Ca at 3.6KVe. This is associated with calcite formation. A moderate Kα-peak associated with silica is also seen at 1.8KVe and may be associated with C-S-H and/or aggregate. Aluminium is exhibited by a very small Kα-peak at 1.6KVe and may be correlated with C-A-H crystal types that generally follow tabular crystal growth.

Traces of carbon, magnesium, sulphur and iron are also seen with Kα-peaks at approximately 0.4KVe, 1.4KVe, 2.2KVe and 6.5KVe respectively. Therefore, low level formation of binary or ternary crystal forms associated with these elements cannot be ruled out.

Figure 72: EDX plot indicating chemical elements and concentration for the ternary NHL 3.5 & Shap non-hydraulic lime mortar samples

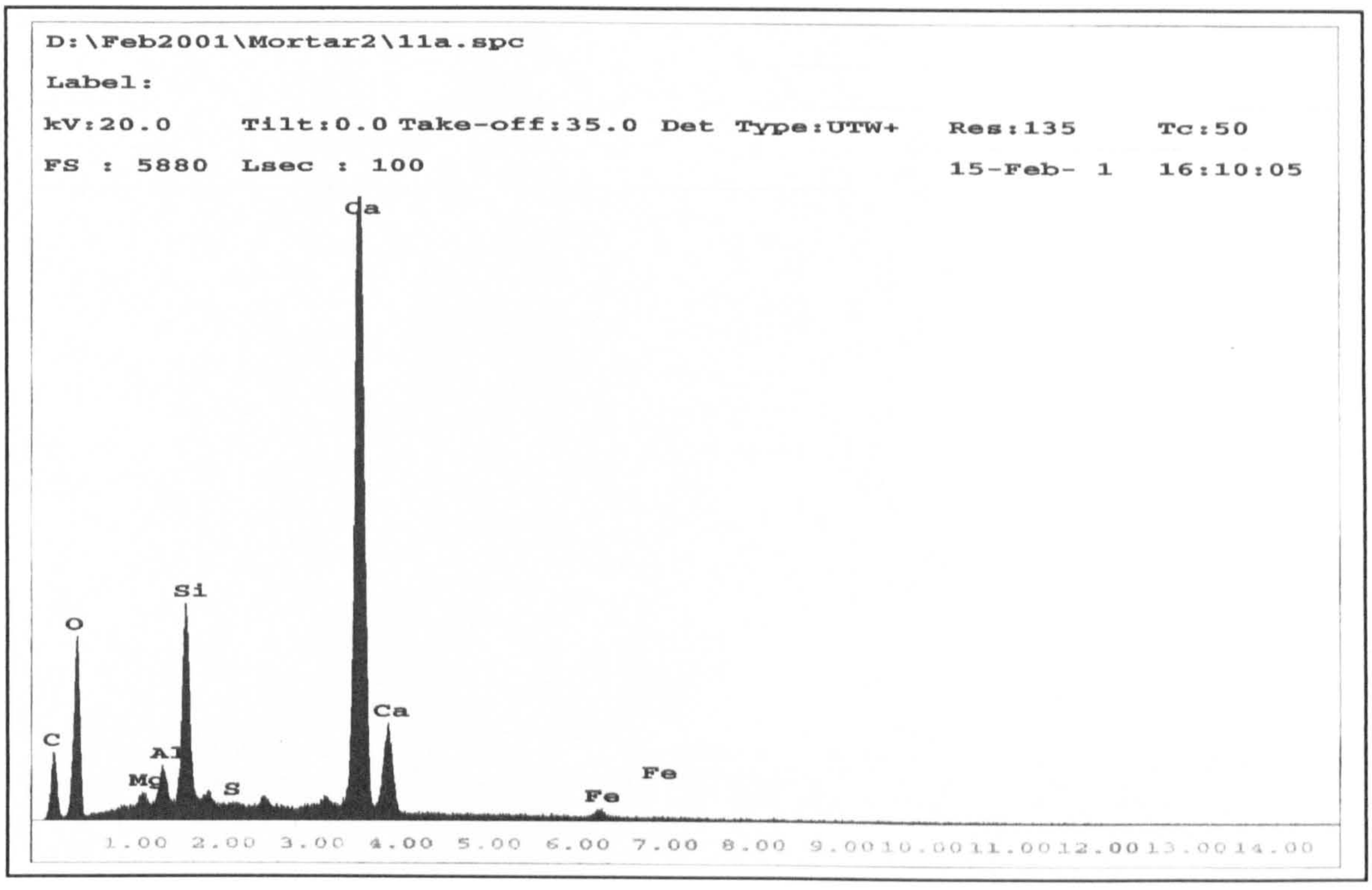

Plate 41 : Gowrie sharp sand and blended Shap non-hydraulic lime and NHL3.5

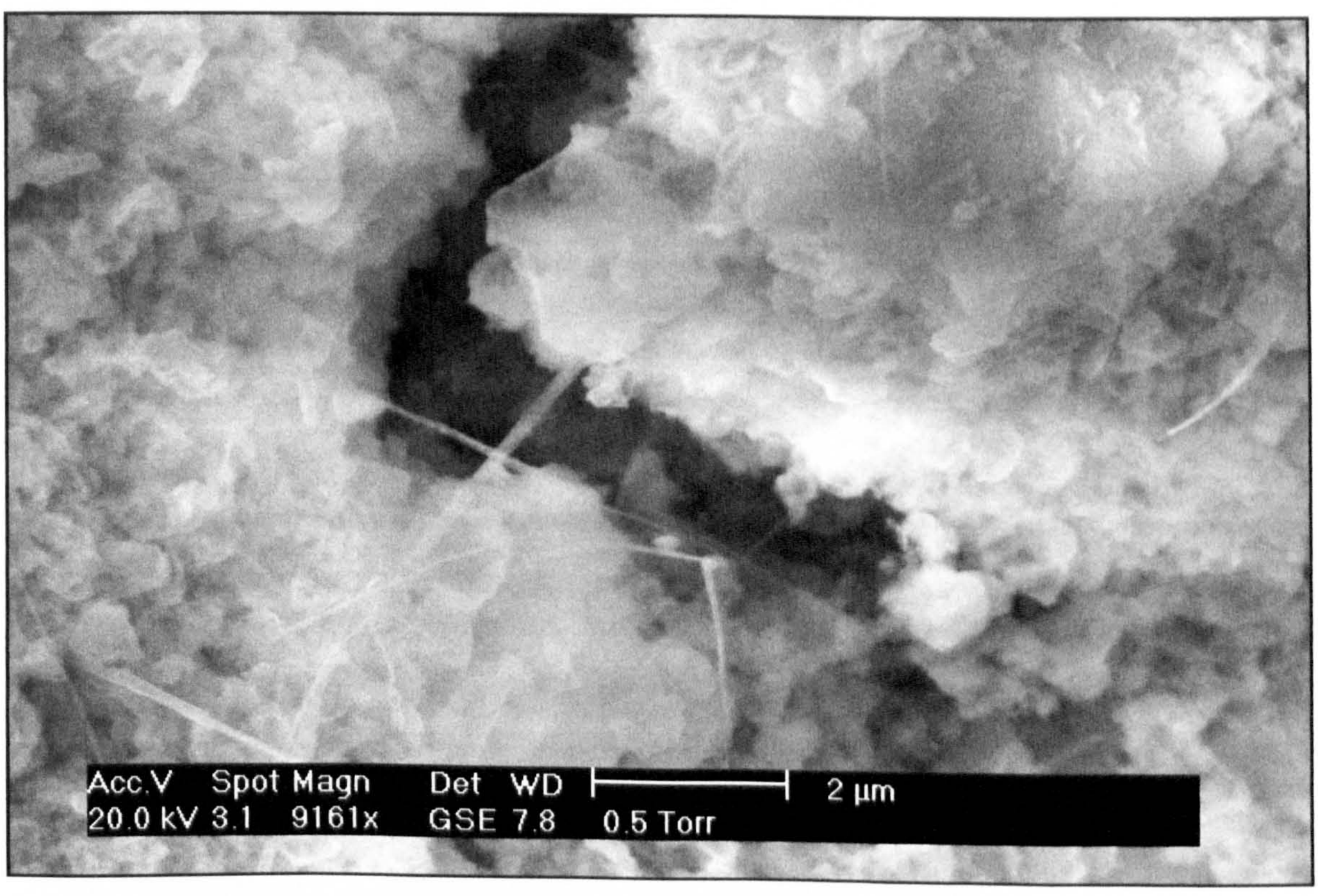

Plate 42: Gowrie sharp sand, Shap non-hydraulic lime and NHL3.5 ternary gauged mortar

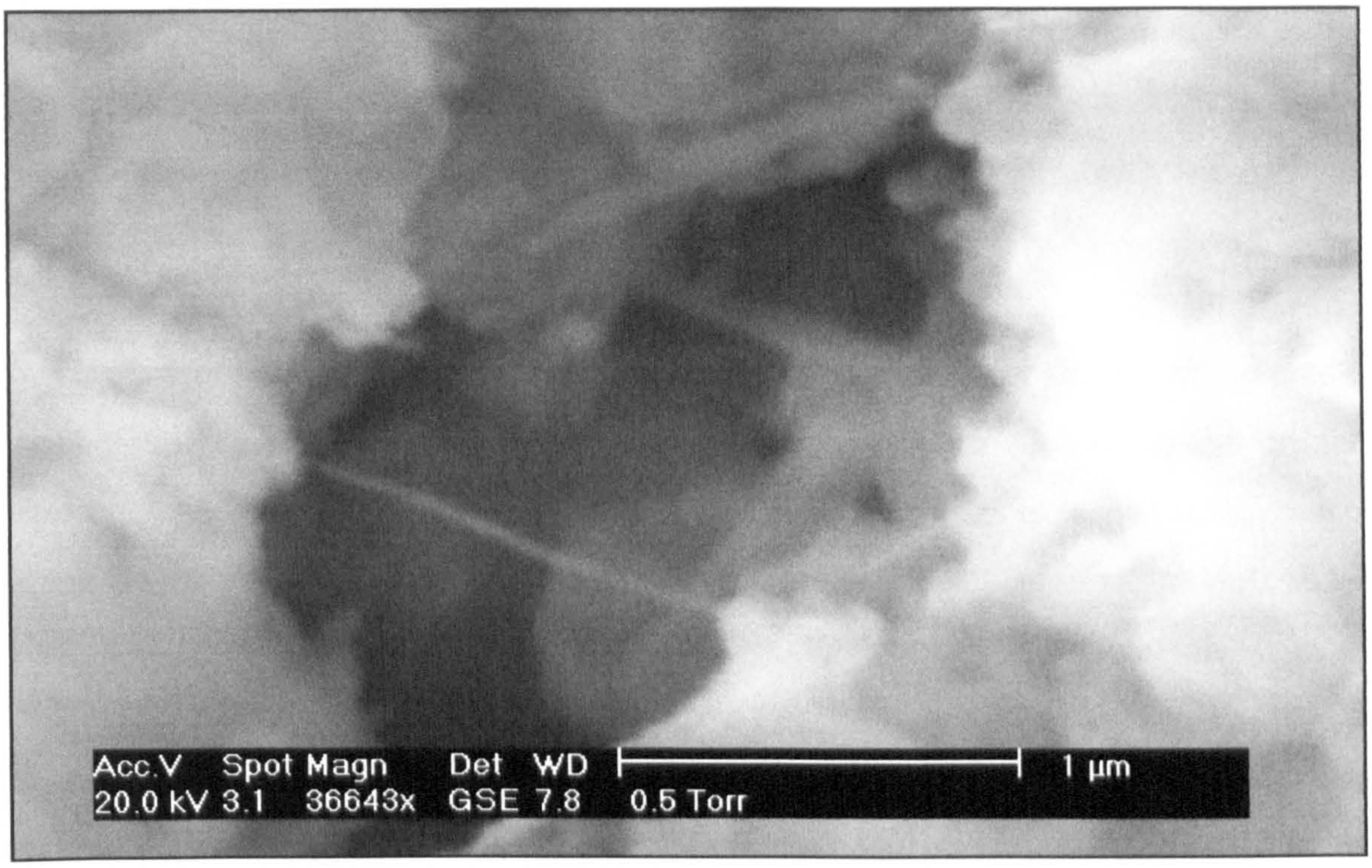

4.4.11 Shap non-hydraulic lime and NHL5 ternary gauged mortar sample

Plate 43 shows sample number 12a, with a small quantity of C-S-H rods. These are formed from the substrate of calcite which are characterised by their rather chunky hexagonal crystal type.

Plate 43 : Gowrie sharp sand, Shap non-hydraulic lime and NHL5 ternary gauged mortar

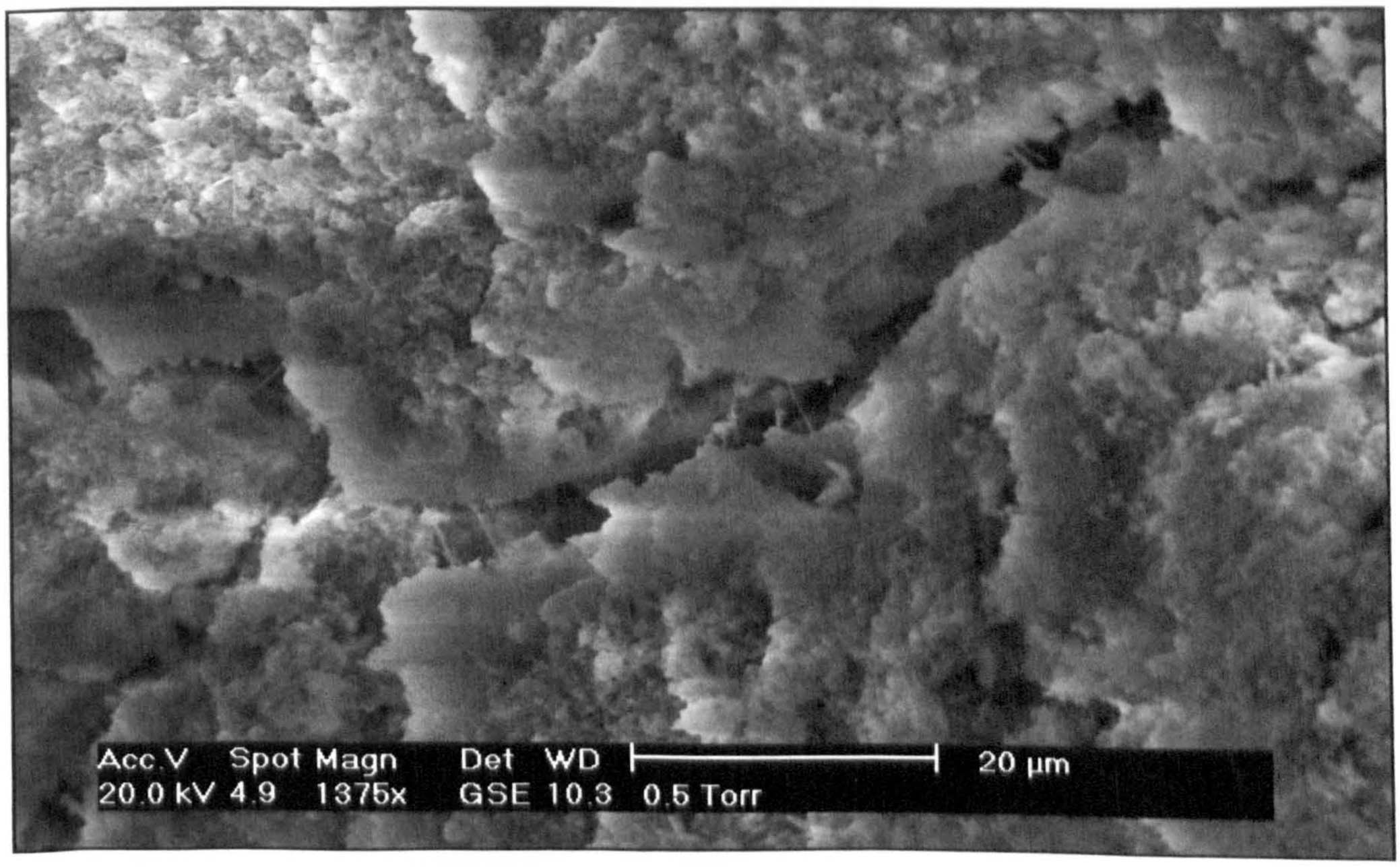

Plate 44 shows hydration products bridging the pore structure of the mortar.

EDX analysis indicated in figure 73 shows a Kα-peak for Ca at approximately 3.6KVe. This is associated with calcite. Both Al and Si have relatively high Kα-peak concentrations at approximately 1.6KVe and 1.8KVe respectively, with the Al being only slightly lower than the silica concentration.

The concentration of Si is only just below that of the Kα-peak for Ca and would tend to be chemically indicative of C-S-H component formation. In addition to the primary components a moderate Kα-peak associated with Ferrite phases is seen at 6.5KVe. Kα-peaks for carbon, magnesium, potassium where exhibited at approximately 0.4KVe, 1.4KVe, 2.1Kve and although very low in concentration cannot be discounted.

Figure 73: EDX plot indicating chemical elements and concentration for the ternary NHL 5 & Shap non-hydraulic lime mortar samples

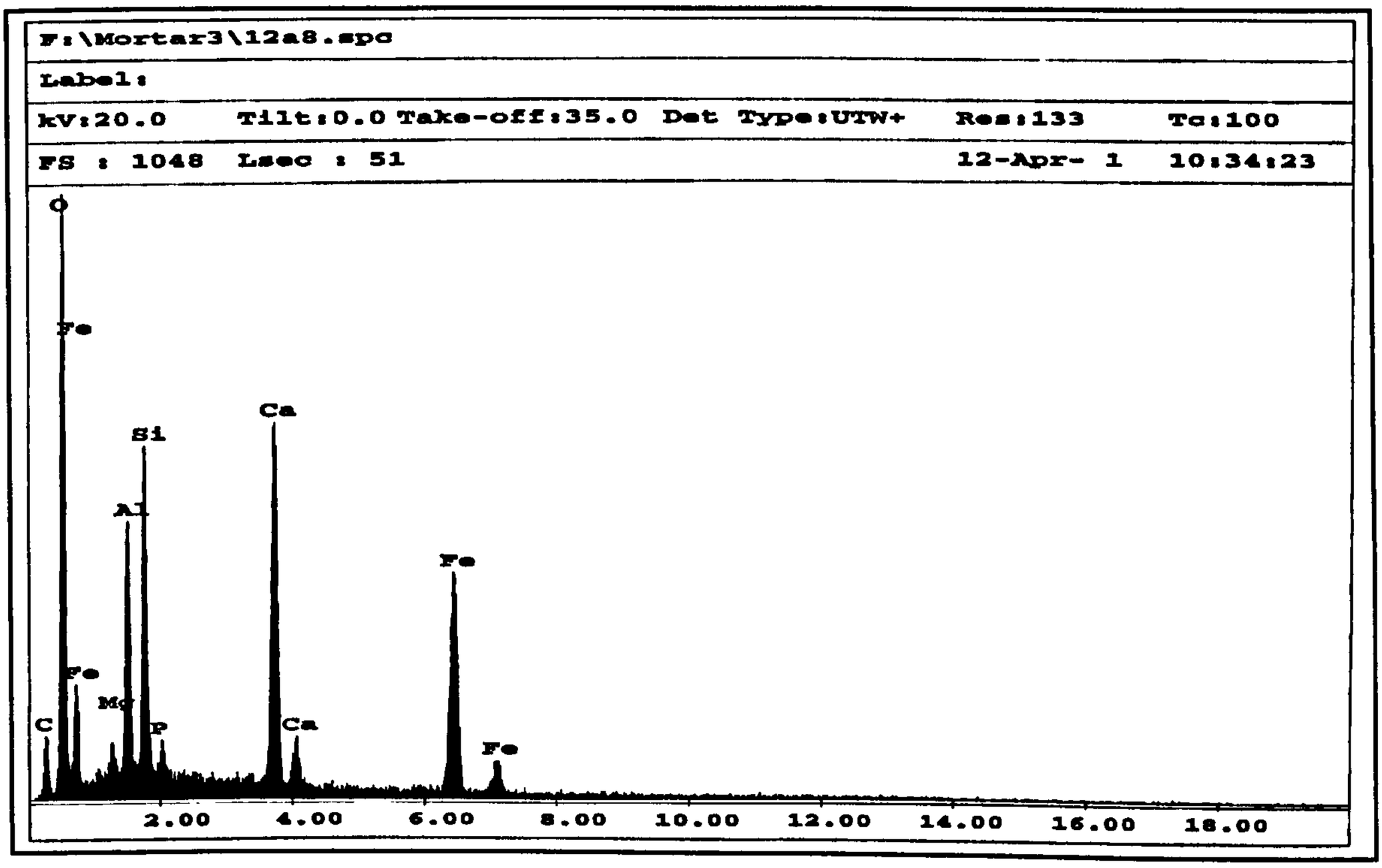

Plate 44: Gowrie sharp sand, Shap non-hydraulic lime and NHL5 ternary gauged mortar

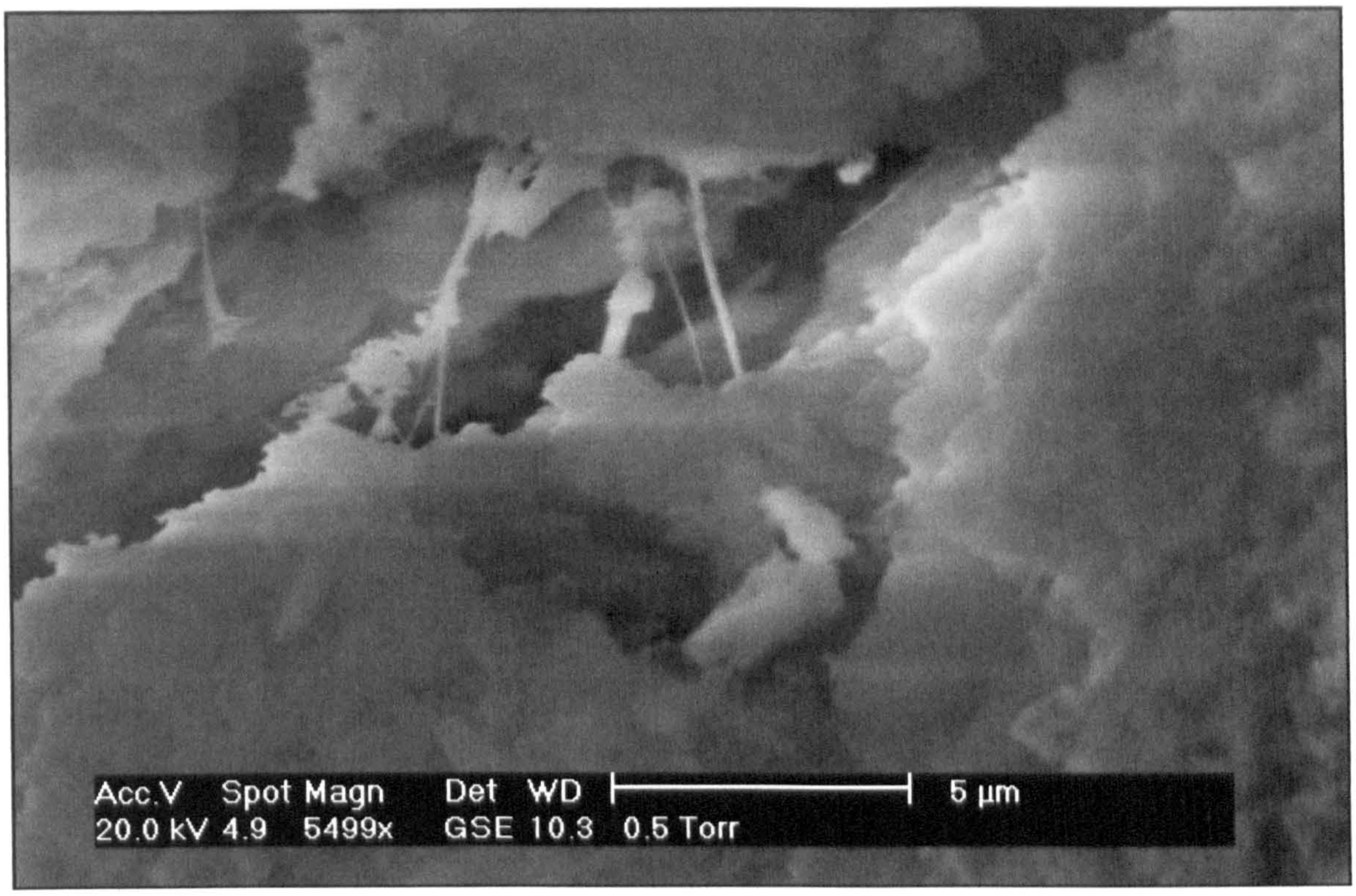

4.4.12 Shap non-hydraulic lime and Jura-Kalk ternary gauged mortar

Plate 45 and 46 show sample number 13a, indicating the network of C-S-H rods and plates. These are formed from the substrate of agglomerated calcite / unconverted portlandite which are characterised by their rather chunky hexagonal crystal type. The presence of widespread C-S-H crystals can also be seen within the plate. The C-S-H crystals are rod like in form and appear to be growing from the calcite agglomerated substrate. Bridging of the pore structure by the C-S-H is clearly seen.

The EDX analysis shown in figure 74 indicates a large Ca Kα-peak for 3.6KVe. This is most probably associated with calcite and portlandite. A moderate Kα-peak associated with Si is seen at approximately 1.8KVe and therefore may be associated with C-S-H mineralogical types. A moderate Kα-peak for Al at approximately 1.6KVe is also seen and may be associated with C-A-H formation.

Kα-peaks for carbon, magnesium, sulphur and iron are also seen at approximately 0.4KVe, 1.4KVe, 2.2KVe and 6.5KVe respectively, however it must be emphasised that they only occur in trace concentration.

Figure 74: EDX plot indicating chemical elements and concentration for the ternary Jura-Kalk & Shap non-hydraulic lime mortar samples

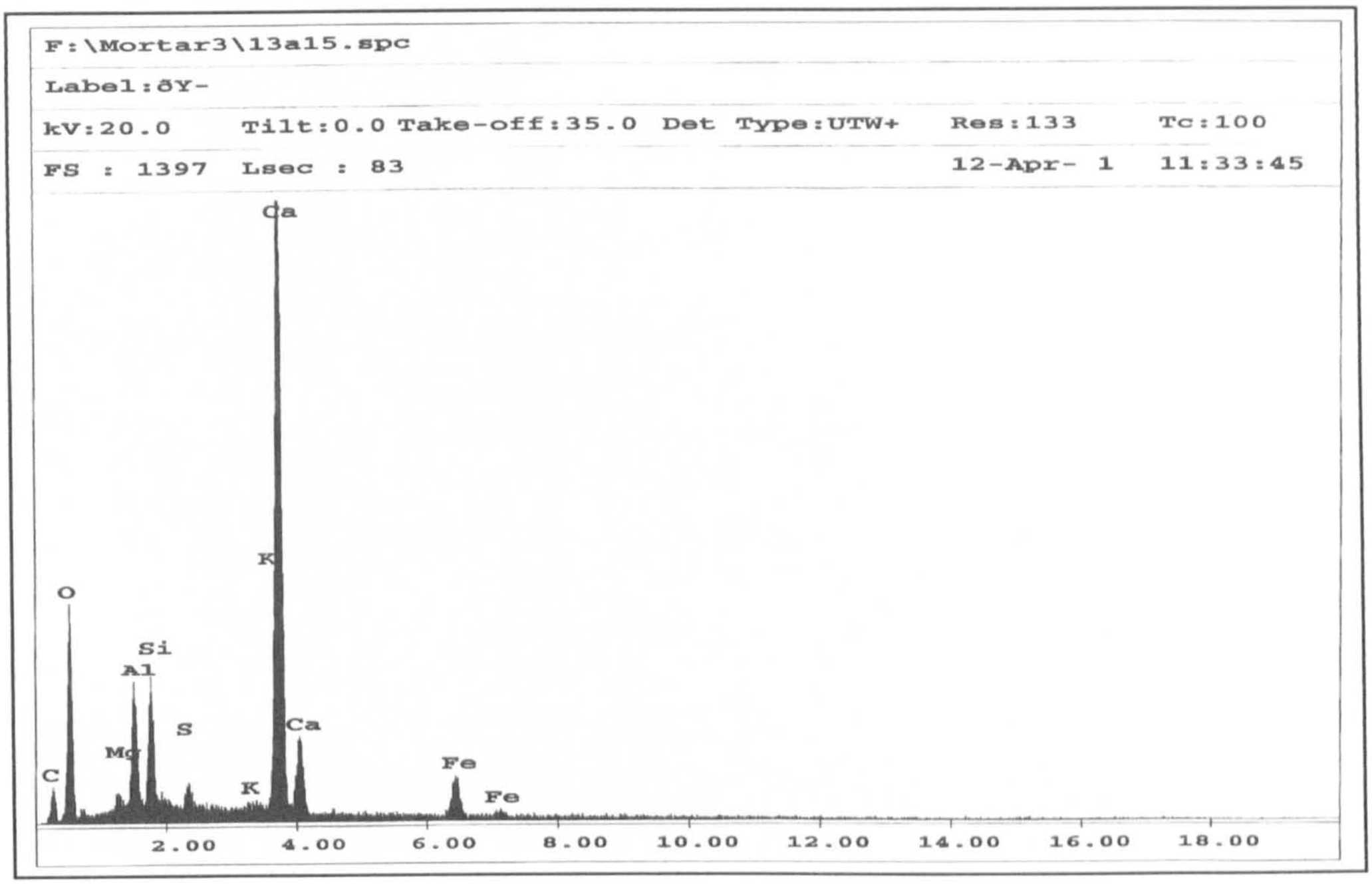

Plate 45 : Shap non-hydraulic lime and Jura-Kalk ternary gauged mortar

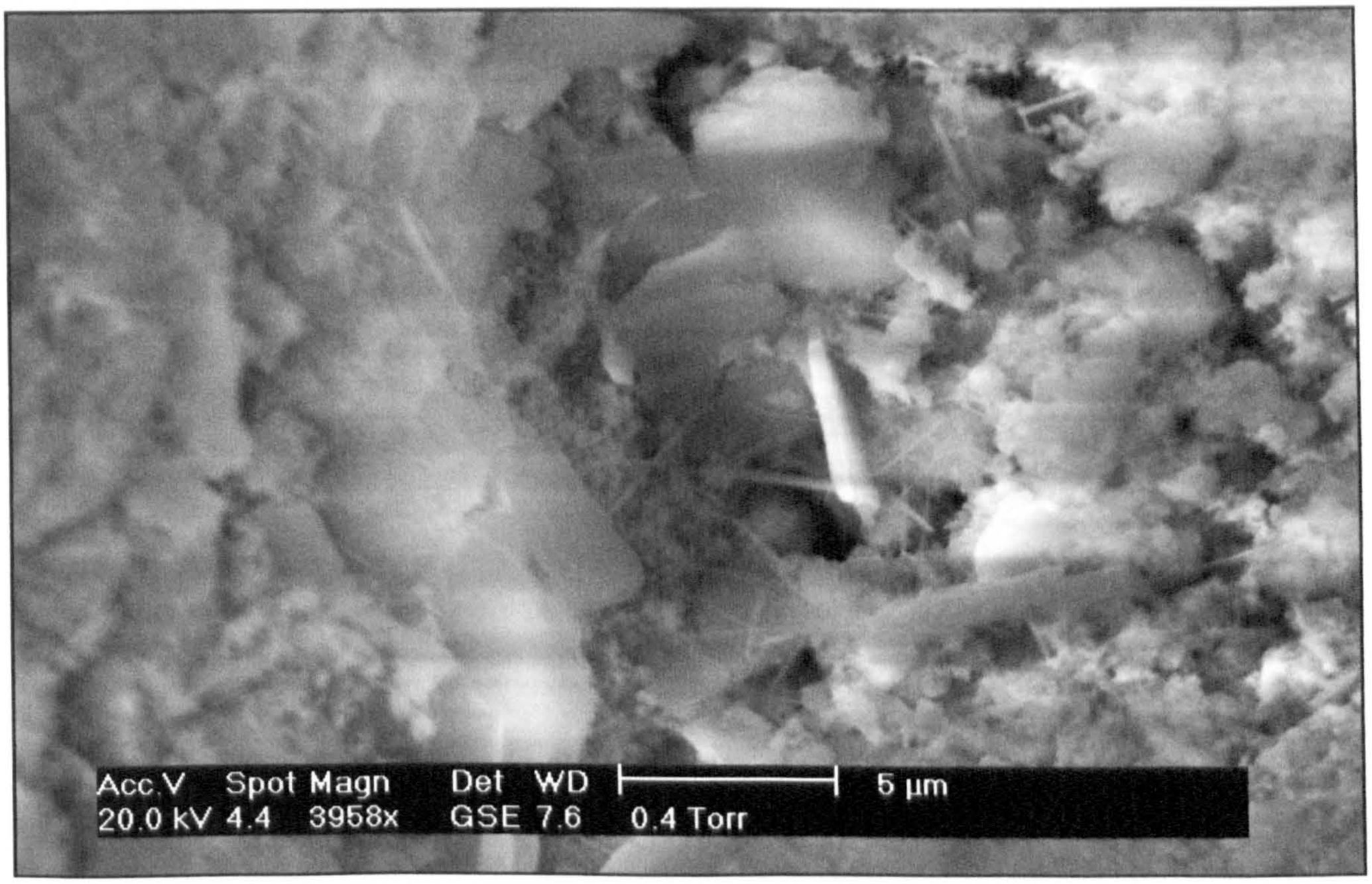

Plate 46 Shap non-hydraulic lime and Jura-Kalk ternary hybrid mortar

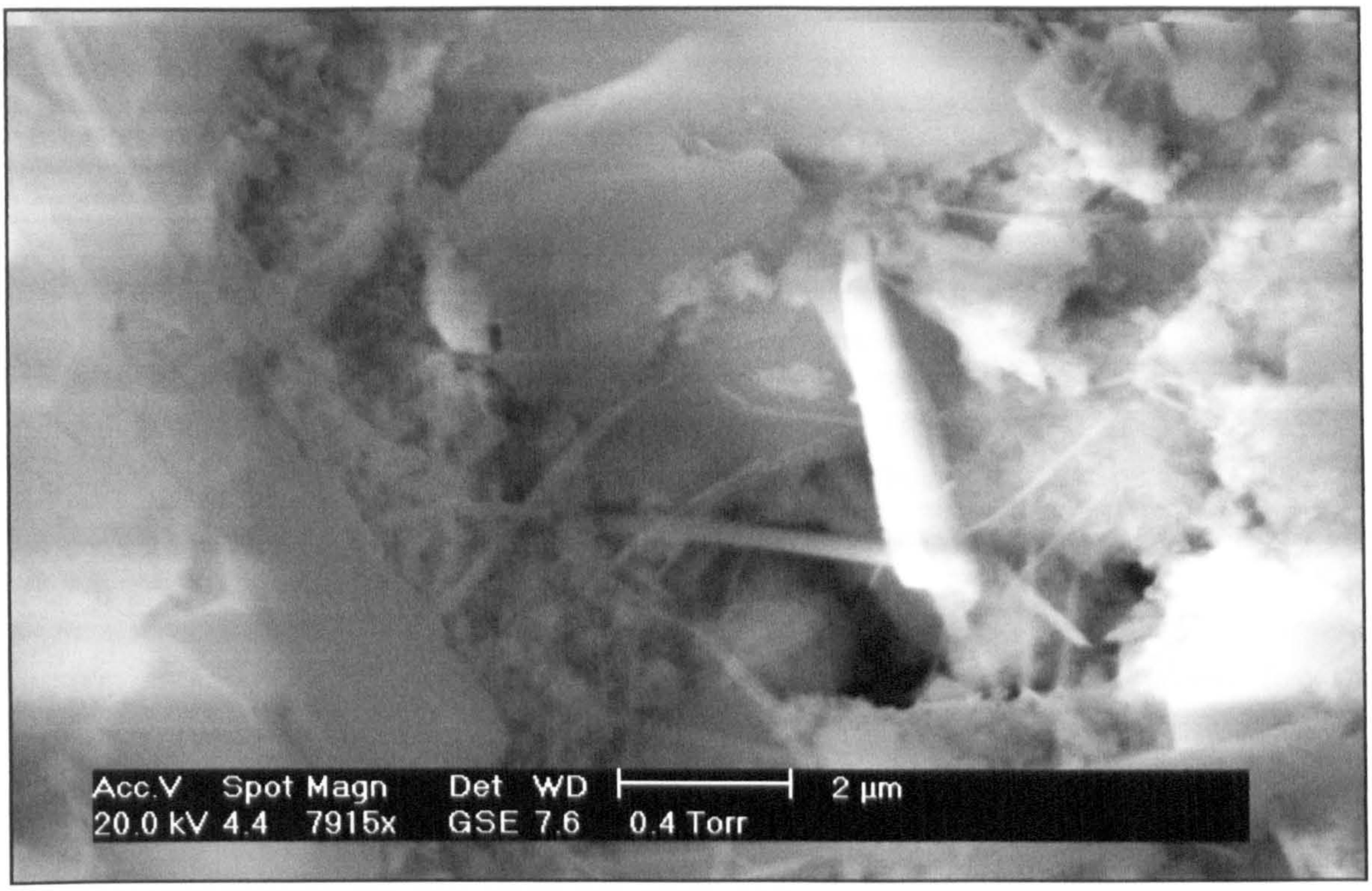

4.4.13 Shap non-hydraulic lime and OPC gauged sample

Plate 47 and 48 show sample number 14a, with a markedly different texture including C-S-H rods and plates. The substrate would appear to be a piece of aggregate with relatively large crystals (approximately 10µm in length) developing from the etched surface.

Plate 47 Shap non-hydraulic lime and O.P.C ternary hybrid mortar

The EDX mortar analysis shown in figure 75 indicates a Kα-peak for Ca at 3.6KVe. This may be associated with calcite and portlandite formation.

An extremely high Kα-peak for Si is exhibited at 1.8KVe. This is indicative of the high concentration of C-S-H within O.P.C. A moderate to low Kα-peak associated with Al is seen at approximately 1.6KVe and is obviously related to C-A-H formation albeit at a much lesser degree than the C-S-H mineralogical forms.

Traces of carbon, magnesium, potassium and iron were seen with Kα-peaks at 0.4KVe, 1.4KVe, 2.1KVe and 7.0KVe respectively.

Figure 75: EDX plot indicating chemical elements and concentration for the ternary OPC & Shap non-hydraulic lime mortar samples

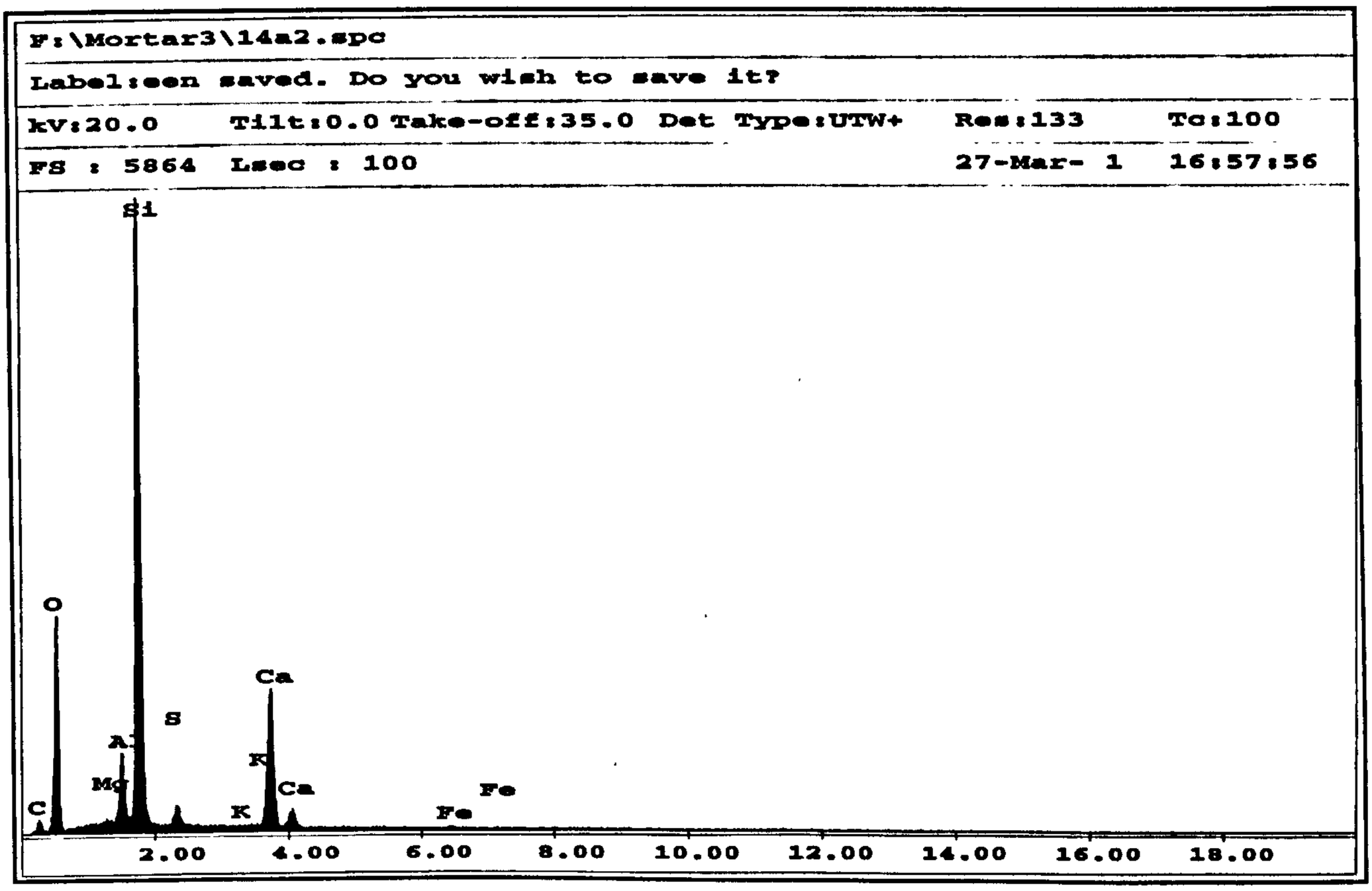

Plate 48 Shap non-hydraulic lime and O.P.C ternary gauged mortar

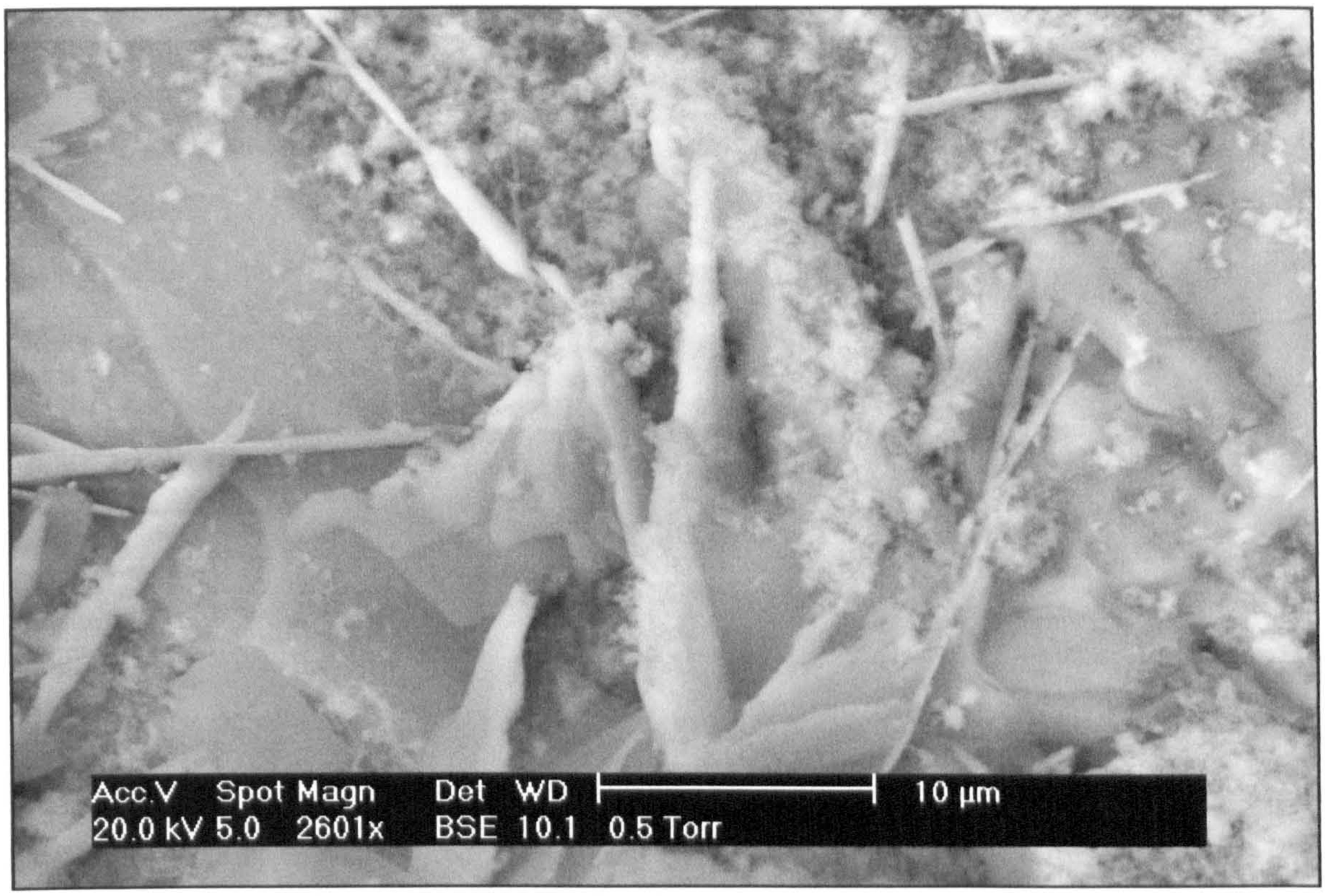

4.5 Concluding comments

Conduction calorimetry, water vapour permeability and ESEM investigations have been carried out on a range of lime mortars. A number of novel features have been recorded and these will be discussed in the next chapter.

Chapter 5: Discussion

5.1 General hydration theory of binders

The hydration of the full range of binary and ternary mortar samples gave an invaluable insight into the different hydration reactions and products formed. The formation of C-S-H / C-A-H, C-A-S-(H) and / or portlandite / calcite crystals types will ultimately affect the binding characteristics of the mortar. In addition the presence of polymorphs of the hydrates aforementioned cannot be ruled out. The binders used were; non-hydraulic lime putty (Shap, Cumbria), non-hydraulic lime putty (Isle of Man) and finally, feebly hydraulic lime putty (Blair-Athol), NHL2 dry hydrate, NHL3.5 dry hydrate, NHL5 dry hydrate, Jura-Kalk dry hydrate and finally, O.P.C.

The binders used fell into 4 broad categories, namely: non-hydraulic limes, natural hydraulic limes, natural cements and artificial cements. The non-hydraulic limes should theoretically manufactured from limestone that is considered to be pure $CaCO_3$ (99.9%), whereas the NHL's, natural and artificial cements have varying degrees of clayey impurities present. The concentration of clay can range from trace element, up to 40%, and upon calcination, the silica, aluminium and iron that compose the clay alter their structure and produce complex phase systems (most importantly $CaO\text{-}SiO_2$). When hydration occurs they lead to the formation of complex crystalline calcium silicate hydrates (C-S-H), calcium aluminate hydrates (C-A-H) and alumino-silicates [C-A-S-(H)].

Despite being classified as non-hydraulic limes, the Isle of Man and Blair-Athol samples were found to contain a proportion of what appeared to be silicate crystalline phases (determined via ESEM analysis). This would lead us to believe that the limes were in fact slightly hydraulic and must therefore be re-assessed accordingly. Shap non-hydraulic lime is commercially produced and uses only very pure $CaCO_3$, in a highly refined calcination and manufacturing processes. Blair-Athol and Isle of Man limes are not commercially produced and are today generally produced only for developing our understanding of the physical and chemical properties of traditional small scale burnt limes.

The discrepancy between traditional classification of limes and cements and the actual level of hydraulicity is unfortunately not limited to this situation. This is reflected in

studies undertaken by Hughes and Swann [21] who believe that confusion prevails when adopting the use of Vicat's, DD-ENV's, CI's and manufacturer's description methods for assessing hydraulicity. This confusion is highlighted in table 34.

Table 34: Classifications according to different systems (author after Hughes) [21]

Limes	Vicat	DD ENV 459-1□	Cementitious Index	Distributor's description
St Astier NHL 2	Em+	NHL 2	F/m	F
St Astier NHL 3.5	Em+	NHL 3.5	Em	M
St Astier NHL 5	Em+	NHL 5	Em	Em
Jura-Kalk	Em+	NHL 5	Natural cement	Em
Bio-E	Em+	-	Em	-
Chaux de Paviers	Em+	-	<f	-

□ **Manufacturers claim** **Notes: f, feebly, m, moderately, em, eminently**

Due to this situation the assessment of hydraulicity was based upon the results of conduction calorimetry.

The set propagation of hydraulic limes are derived from twin processes, namely, carbonation and hydration. Although the hydration products are important the primary set in hydraulic limes is generally derived from carbonation processes, however it must be emphasised that carbonation and hydration within natural hydraulic limes may vary significantly.

The assessment of secondary 'side reactions' (a relatively rapid hydraulic setting process) within natural hydraulic limes cannot be underestimated, with limes hydraulic reactivity being primarily related to the quantity of soluble silica, aluminium, iron and trace element of other chemicals within the material. Therefore, a lime with low quantity of soluble silica and other hydraulically reactive compounds would be deemed to have a low-level side reaction, and vice versa.

The reactive silicates and aluminates consume a proportion of the calcium within the hydrate and by doing so allow the growth of C-S-H, C-A-H and C-A-S (H) hydration products. Without the presence of Ca components the aforementioned hydration products could not occur. Hence, the consumption of calcium within a binder will ultimately affect the carbonation requirements of the matrix. Therefore, the lower the level of remaining free lime within the material the lower the amount of portlandite and calcite crystal formation that will ultimately occur. An increase in the amount of hydraulic constituents within a lime will ultimately lead to a reduction in the portlandite

concentration. The level of portlandite within the material plays an integral role in the development of C-S-H, C-A-H and C-A-S-(H) as it acts as the primary framework upon which these hydration products grow. It must also be emphasised that the carbonation requirements of the material will vary depending upon the amount of portlandite present within the matrix. The ability of the lime to reabsorb carbon dioxide into the mortar is integral to the final set characteristics and long term strength development and is also correlated with the relative humidity and temperature to which the material is subjected.

The primary hydration products associated with hydraulic limes and cements alter with variation in the calcination temperature, i.e. spurrite ($2C_2S.CaCO_3$) formation at approximately 800-1000°C due to the reaction of silica and carbonate, and gehlenite (C_2AS) formation within a temperature range between 1000 -1200°C [21].

This is particularly interesting when placed in context of hydration rates. For example traditionally the formation of belite (C_2S) was believed to occur primarily post 28 days, however, new research by Lawrence [5] has lead to a reassessment of the speed of reactivity of this component. He believes that low temperature calcination twinned with altered cooling rates may lead to the attainment of stable modified forms of belite which have higher reactivity pre 28 day.

When assessing the differences between NHL and OPC strategic components (adopting St Astier data), it is evident that substantial differences occur within the 2 materials. This is most markedly seen in terms of sulphates, aluminates and other minor components. The difference in concentration may be seen in table 35, and although this is not a holistic list it is still useful for an assessment of hydration performance and set characteristics.

Table 35: hydration products in OPC and hydraulic limes (author after St Astier) [27]

Hydraulic component	OPC	NHL
C_3A	3-10+ %	< 1%
C_4AF	8-10%	Nil
Sulphates SO_3	2-7%	0.4-0.6%
Alkali Na_2O/K_2O	1-3%	> 0.1%
Gypsum $CaSO_4$	2-4%	Nil

The primary hydration products associated with hydraulic limes include, mono-calcium silicate (CS), di-calcium silicate (C_2S), calcium aluminate (CA) and di-calcium alumino-ferrite (C_2AF).

The St Astier [27] range of natural hydraulic limes are calcined within a temperature range of 900-1000°C. This affects the types of hydration products exhibited within the material as shown above. Generally an increase in calcination temperature will lead to an increase in the quantity of combined (soluble) silica, with stage development of silicates following mono, di and tri calciums at increasing temperatures. The resultant combination of CaO and soluble silica has an approximate ratio of 1:3 at 900°C with St Astier believing that one of the most important factors to consider when assessing the hydraulicity of a lime is to scrutinise the degree of soluble silica within the material. They also emphasise that the assessment of soluble silica is 'by far the most reliable method of classifying hydraulicity', continuing to be quite categorical in stating 'the principle is simple but indisputable' [27]. The soluble silica has a relationship with the material's compressive strength as shown in table 36.

Table 36: Percentage of combined silica in binders and its relationship to setting time and compressive strength (author after St Astier) [27]

Binder	Setting time	Soluble silica concentration	Compressive strength N/mm^2
Lime Putty	Days +	1-4%	<1 N/mm^2
NHL 2	6-10 hours	4-8%	2-7 N/mm^2
NHL 3.5	4-6 hours	8-12%	3.5-10 N/mm^2
NHL 5	2-4 hours	12-16%	5-15 N/mm^2
Natural Cements	1-2 hours	16-20%	≈20 N/mm^2
OPC	1 hour or less	>20%	>20 N/mm^2

The setting times are a function of both pozzolanic / hydration reactions and or carbonation derived products that ultimately lead to the complex crystalline formations under assessment. Table 37 indicates the initial and final set times for the range of hydraulic limes.

Table 37: Setting times in natural hydraulic limes (author after Hughes) [21]

Limes	W/l ratio	Initial Set	Final Set
St Astier NHL 2	0.526	4 hrs 30 mins	16 hrs 15 mins
St Astier NHL 3.5	0.436	4hrs 25 mins	11 hrs 00 mins
St Astier NHL 5	0.388	4 hrs 40 mins	8 hrs 30 mins
Jura-Kalk	0.300	3 hrs 05 mins	5 hrs 45 mins

The silica concentration in pure limestones is less than 4% and therefore will not produce a hydraulic lime. St Astier lime producers indicate that 'from 4% (soluble silica) and above hydraulicity will be generated in direct proportion to the combined amount between available silica and CaO' [27]. This reinforces the importance of understanding the aforementioned CaO-SiO phase system. In addition they also indicate that the St Astier lime deposits have no aluminium, low sulphates concentration and only traces of alkali namely, potassium and sodium. This will obviously reflect in the very low levels of C_3A found within their NHL products and will ultimately have an effect upon the materials performance.

5.2 Conduction calorimetry

The calorimetry results for the hydraulic lime and O.P.C samples confirmed that the rate of heat evolution alters over time, from early wetting through to full hydration. The samples exhibited different characteristics associated with their respective hydration development and certain general 'foot prints' could be seen to develop from the individual binder types. Table 38 summaries these.

Table 38: Assessment of hydration adopting heat of hydration graphs (72 hours)

Binder	Hydration 'foot print' form	Comments	Conduction calorimetry classification	Traditional hydraulicity classification
NHL2	**Single peak** (low level hydraulic activity)	Hydration heat peak followed by a slow yet steady decrease in activity	Low hydraulic activity	Feebly hydraulic
NHL3.5	**Single peak** (low level hydraulic activity)	Hydration heat peak followed by a slow yet steady decrease in activity	Low hydraulic activity	Moderately hydraulic
NHL5	**Single shoulder** (moderate-high hydraulic activity)	Hydration heat peak slowly forms a shoulder then slowly decrease in activity	Moderate hydraulic activity	Eminently hydraulic
Jura-Kalk	**Double peak** (high hydraulic activity)	First hydration heat peak encapsulates maximum rate of heat then reduces in activity until heat peak 2 starts. Second heat peak is rapidly formed, then slowly decreases in activity	Moderate - high hydraulic activity	Eminently / Natural cement
O.P.C.	**Large single shoulder** (extremely high hydraulic activity)	First peak associated with wetting phase. Second heat peak forms into a shoulder then slowly decrease in activity	High hydraulic activity	Eminently and above / cements

The footprints described in table 38 may be graphically represented with the idealised hydration 'foot-prints' commonly associated with the range of cementitious binders falling into one of three groups. Figure 76 indicates the 3 most common heat evolution footprints (W/Kg) with a basic description of the common hydration activity. As emphasised previously, the rate of exothermic heat evolution in graphical form may be correlated with change or dormancy within the hydration activity of the sample.

Figure 76: Idealised conduction calorimetry hydration graphs or 'Foot prints'

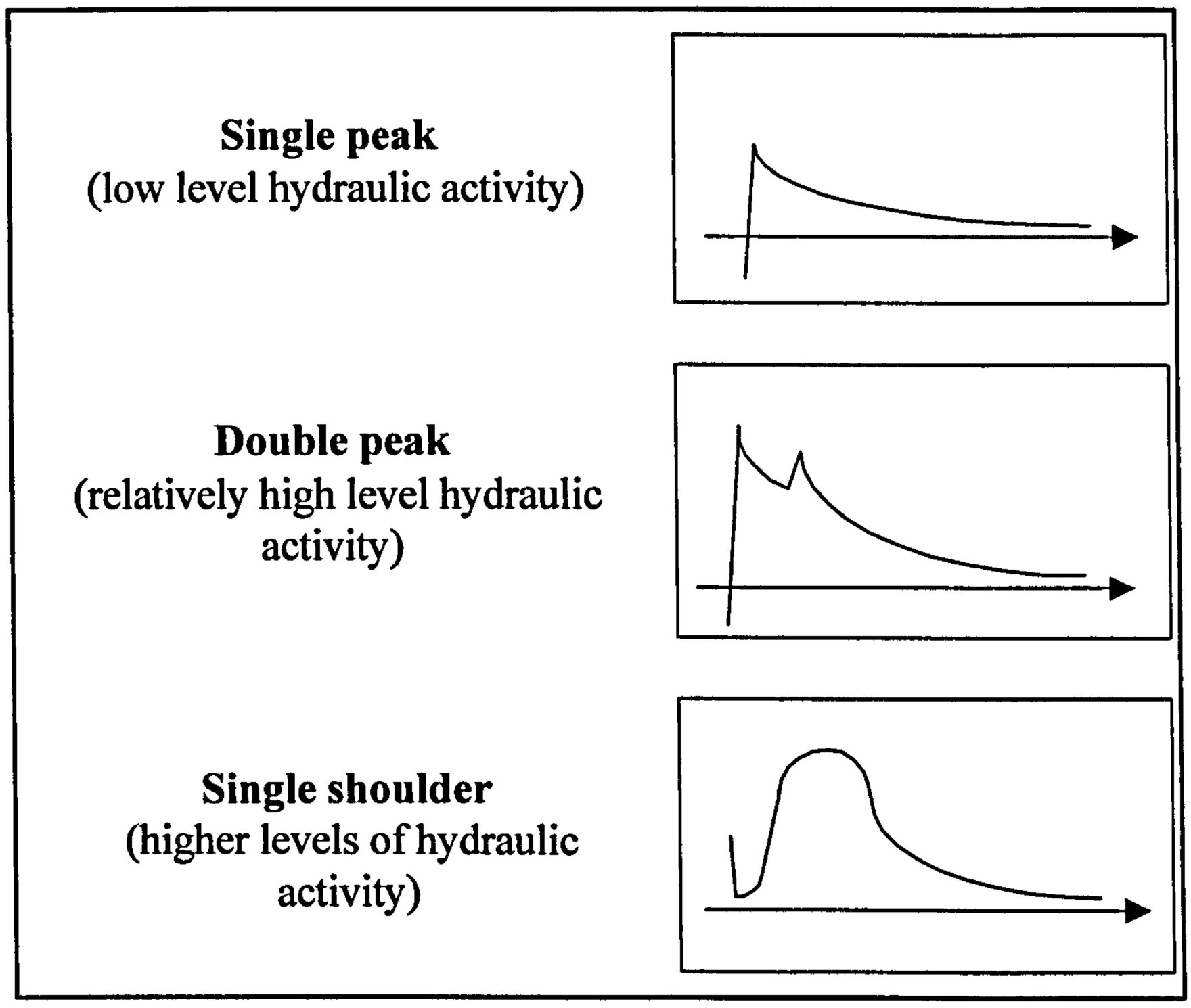

The 'Single-peak' type hydration 'footprint' was associated with St Astier NHL2 and NHL3.5. These would traditionally be classified as feebly and moderately hydraulic limes respectively. It could therefore be assumed that the 'Single-peak' type hydration 'footprint' best represents the feebly and feebly-moderately hydraulic range of limes tested and reflects their relatively low levels of hydraulic activity. It must be emphasised that although the footprint shapes may be similar, it must always be assessed in conjunction with the rate of heat and total heat outputs.

The hydraulic materials that fell within the 'single shoulder' type of hydration 'footprint' were NHL5 and OPC. These would traditionally be classified as eminently hydraulic lime and cements. The shape of the rate of heat graphs for NHL 5 and OPC are similar,

however, the hydration average rate of heat (AvROH) and total heat (ΣH) for the 2 samples vary greatly, with (AvROH) 37 W/kg for NHL5 and 186 W/kg for OPC and (ΣH) 2909 Kj/Kg for NHL5 and 13149 Kj/Kg for OPC. It could therefore be assumed that the 'single shoulder' type hydration 'footprint' best represent eminently hydraulic range of limes through to OPC. As before it must be emphasised that although the 'footprint' shape may be similar the data must also be assessed in conjunction with the rate of heat and total heat outputs.

Jura-Kalk showed the 'double-peak' type of hydration 'footprint' and is traditionally classified as NHL5 (but under CI tends to act like natural cement). O.P.C. can also exhibit a second peak but it depends upon the amount of aluminium and SO_3 present within the material. These would traditionally be classified as eminently hydraulic limes / natural cements. It could therefore be assumed that the 'double peak' type hydration 'footprint' twinned with an assessment of the higher level of total heat and rate of heat would best represent those limes and cements with a higher level of SO_3.

When assessing the range of hydraulic materials via heat evolution (72 hours) it became clear that generally the materials performed as expected, however, the NHL3.5 did have a lower than expected average rate of and total heat. However, alternatively the NHL2 may have exhibited a higher than expected heat of hydration over the same period. It is therefore reasonable to assume that within the first 72 hours of hydration both NHL 2 and 3.5 may be classified as feebly hydraulic limes. However, post 72 hours the NHL3.5 may increase in its hydraulic activity and perform as traditionally expected or the NHL2 will reduce in its hydraulic activity and possibly be overtaken by the NHL3.5.

The alteration in the heat of hydration over time is obviously indicative of the level of hydraulic activity. The formation of individual hydration products may occur individually and or simultaneously. In the case of O.P.C, alite (C_3S) and belite (C_2S) form at significantly different stages in the hydration process. Taylor [17] believes that the aluminate phases and the majority of alite is consumed pre-90 days, and the majority of the belite develops at a slower rate. Table 39 indicates the differential setting rates of belite (C_2S) and alite (C_3S).

Table 39: Setting rates of C_2S and C_3S (author after Eckels)

-	7 days	28 days	180 days	365 days
C_3S	322	466	512	584
β-C_2S	24	42	194	325

Strength (Kg/cm^2) development of pure compounds [15]

Although this is true of O.P.C, it is believed by Lawrence [5] that low temperature alternative cements may have belite (βC_2S) that has faster hydration times than the aforementioned. If this is the case then the reactivity of belite (βC_2S) yielding compounds in hydraulic limes may also be expected to be different, with hydration occurring pre 28 days as opposed to post 28 days.

The primary hydrates associated with St Astier hydraulic limes can be seen in table 40. It also indicates the chemical and mineralogical components in NHL, including the primary hydration products, namely, free lime, C_2S and secondary components, C_4AF and $CaSO_4$.

Table 40: Chemical and consequent mineralogical components found in St Astier natural hydraulic limes (author after St Astier) [27]

Composition	**Chemical (%)**			**Mineralogical (%)**			
	NHL 5	NHL 3.5	NHL 2	NHL 5		NHL 3.5	NHL 2
Loss on ignition	16	18	20	-		-	-
Calcimetry CaO_2	10	11	6	-		-	-
Insoluble components	5.6	9.6	8	5.6		9.6	8
CaO	59	56	63	Free lime $Ca(OH)_2$	22	25	58
				$CaCO_3$ unburnt	23	25	13
SiO_2 (comb)	15	12	6	C_2S	43	35	17
Al_2O_3	1.92	1.66	1.3	C_3A	0.7	0.5	0.4
NB: Al combination also with C_2AS & C_4AF				C_2AS	1.3	1.0	0.8
Fe_2O_3	0.57	0.99	0.4	C_4AF	0.7	0.5	0.4
SO_3	0.41	0.45	0.31	$CaSO_4$	0.7	0.8	0.5
MgO	1.01	0.98	0.75	The quantities of these components are so small that their mineralogical presence is too minute to be relevant. Very significant for the alkalis (K_2O/Na_2O) which, even in small quantities (1.5/2% as in ordinary cement) can produce ALKALI SILICA reactions			
MnO	0.02	0.01	>0.01				
TiO_2	0.18	0.16	0.12				
K_2O	0.21	0.16	0.12				
Na_2O	0.07	0.06	0.04				

The identification and assessment of the strategic components of the lime samples, that is to say the primary calcium silicate crystal types has been essential in developing a

sound understanding of the materials binding characteristics and consequently its effect upon moisture transportation characteristics.

The primary hydraulic set of natural hydraulic limes is derived by C_2S, which generally develops post 28 days. The level of C_2S in the St Astier limes is claimed to be 17% in NHL2, 35% in NHL3.5 and 43% in NHL5, and therefore generally reflects in the heat of hydration. This explains the slower strength development in hydraulic lime when compared with OPC. Although the hydration of C_2S is slow it cannot be eradicated from the assessment of heat of hydration post wetting as seen in the conduction calorimeter hydration plots. The fundamental difference between OPC and hydraulic lime is the presence of alite (C_3S) and ettringite (C_3A), which unlike belite (C_2S) hydrates pre 28 days. Hence C_3S is responsible for the earlier more rapid strength development in OPC.

This can clearly be seen in figure 77 in which the alite (C_3S) has developed approximately 50% of its total strength in 28 days, whereas the belite (C_2S) has a very low strength development at the same stage.

Figure 77: Belite (βC_2S) and alite (C_3S) crushing strength Kg/M_2 (Author after Eckels)

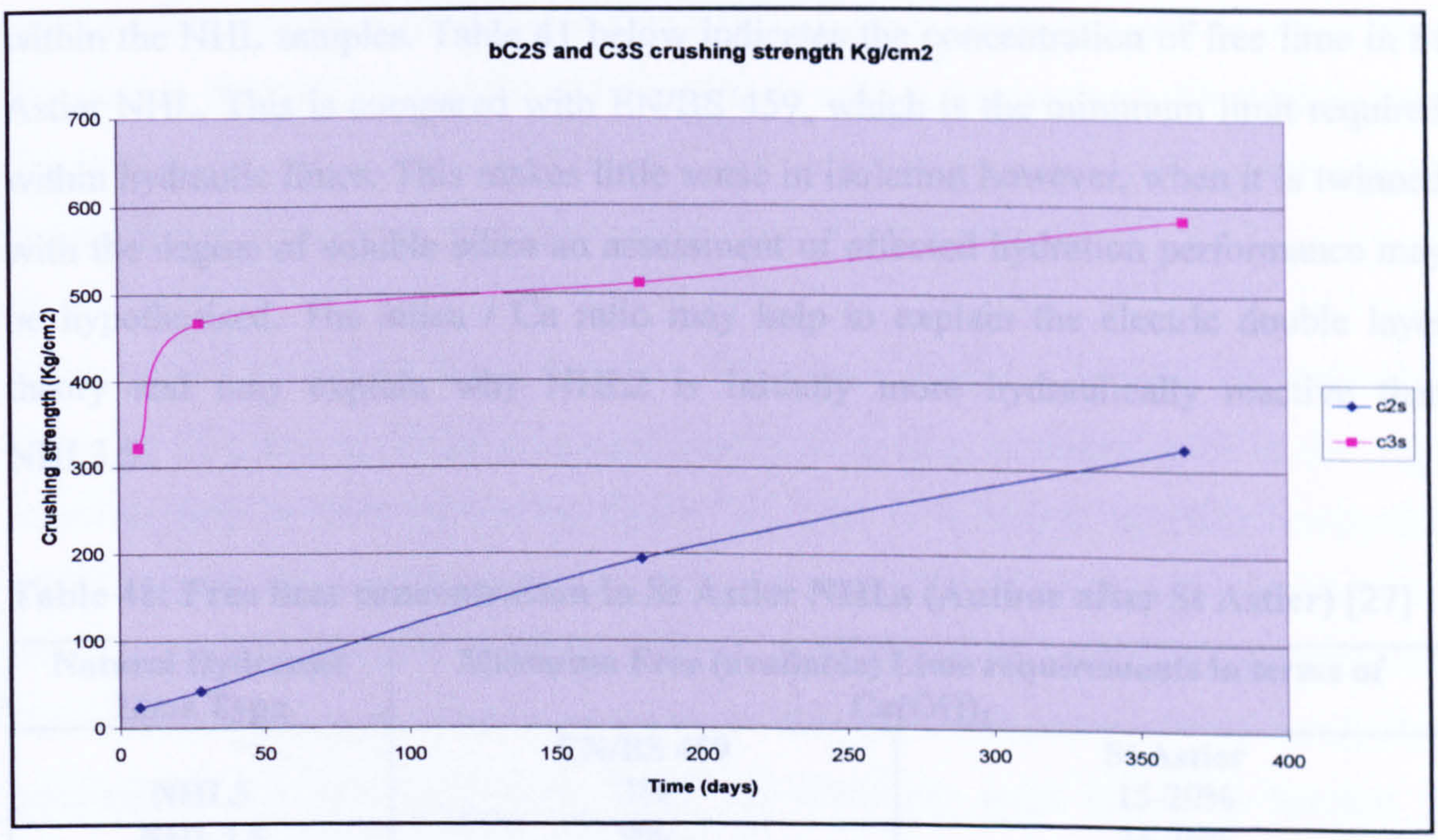

When Taylor [17] had undertaken tests via XRD analysis upon O.P.C he found that calcium hydroxide (CH) growth occurred within a few hours, with noticeable

dominance up to and post a few days. This is of obvious importance for the subsequent, heat of hydration and the formation of C-S-H products.

The early heat evolution associated with the NHL's is most likely to be attributed with continued $Ca(OH)_2$ / portlandite, mono-calcium and di-calcium silicate hydration (although at a low level).

The activation of hydraulically reactive components that lead to the consequent heat of hydration may differ considerably in terms of speed of reaction and heat evolution, with various factors that may affect them. These include:

- Temperature
- Water ratios
- Particle size and distribution
- Impedance to hydration, including; over saturation of Ca in the water for hydration, leading to electrical double layers and other hypothesised impedance mechanisms

The last factor upon this list is affected by the concentration of the free lime within the anhydrous material. It is therefore necessary to assess the concentration of free lime within the NHL samples. Table 41 below indicates the concentration of free lime in St Astier NHL. This is compared with EN/BS 459, which is the minimum limit required within hydraulic limes. This makes little sense in isolation however, when it is twinned with the degree of soluble silica an assessment of affected hydration performance may be hypothesised. The silica / Ca ratio may help to explain the electric double layer theory and may explain why NHL2 is initially more hydraulically reactive than NHL3.5.

Table 41: Free lime concentration in St Astier NHLs (Author after St Astier) [27]

Natural Hydraulic Lime Type	Minimum Free (available) Lime requirements in terms of $Ca(OH)_2$	
	EN/BS 459	**St Astier**
NHL5	3%	15-20%
NHL3.5	9%	24-26%
NHL2	15%	Over 50%

The importance of $Ca(OH)_2$ in the early stages of hydration has already been partially expressed, with the wetting phase being generally associated with portlandite formation without this, C-S-H and other associated hydration products could not develop

Although the graphical representation of the heat of hydration cannot indicate the individual hydrated crystal forms it may be linked with known hydration theory to allow a good estimate of the binders activity to be ascertained (omitting the carbonation process).

5.3 Individual analysis of conduction calorimeter results and correlation

5.3.1 Natural hydraulic lime NHL2 classification 2

The conduction calorimetry data for the NHL2 samples may be schematically represented indicating the significant hydration phases, seen in figure 78. This representation was developed from test data such as that seen in figure 45 in chapter 4, and reflects the actual changes that are taking place within the early - mid hydration phases of the NHL 2.

The level of $Ca(OH)_2$ in NHL2 is significantly higher than NHL3.5. The effect upon the heat of initial wetting and continued $Ca(OH)_2$ formation / hydration will be higher than that seen in the NHL3.5 sample, and this will be reflected in the heat of hydration. This does not necessarily mean that NHL 3.5 will exhibit constantly low heat throughout hydration and may alter its hydration rate in the medium to long term.

Although not shown in the conduction calorimetry results it is believed, following Forrester [26] that an initial heat peak would have been exhibited prior to the large negative drop in heat shown in figure 78. This is common in OPC conduction calorimetry and is generally associated with early wetting of $Ca(OH)_2$. The sudden drop in heat evolution from this point is common to all hydration graphs and concurs with Forrester [26] research. This is associated with the stabilisation of the conduction calorimeter with the water bath. Once the minimum point has been reached at approximately 2 hours, the induction of heat peak 'A' may begin. This is caused by the continued production of $Ca(OH)_2$, reactive silicates, ferrites and to a lesser degree the aluminate phases.

Figure 78: Schematic interpretation of the rate of heat development in St Astier NHL2 pastes

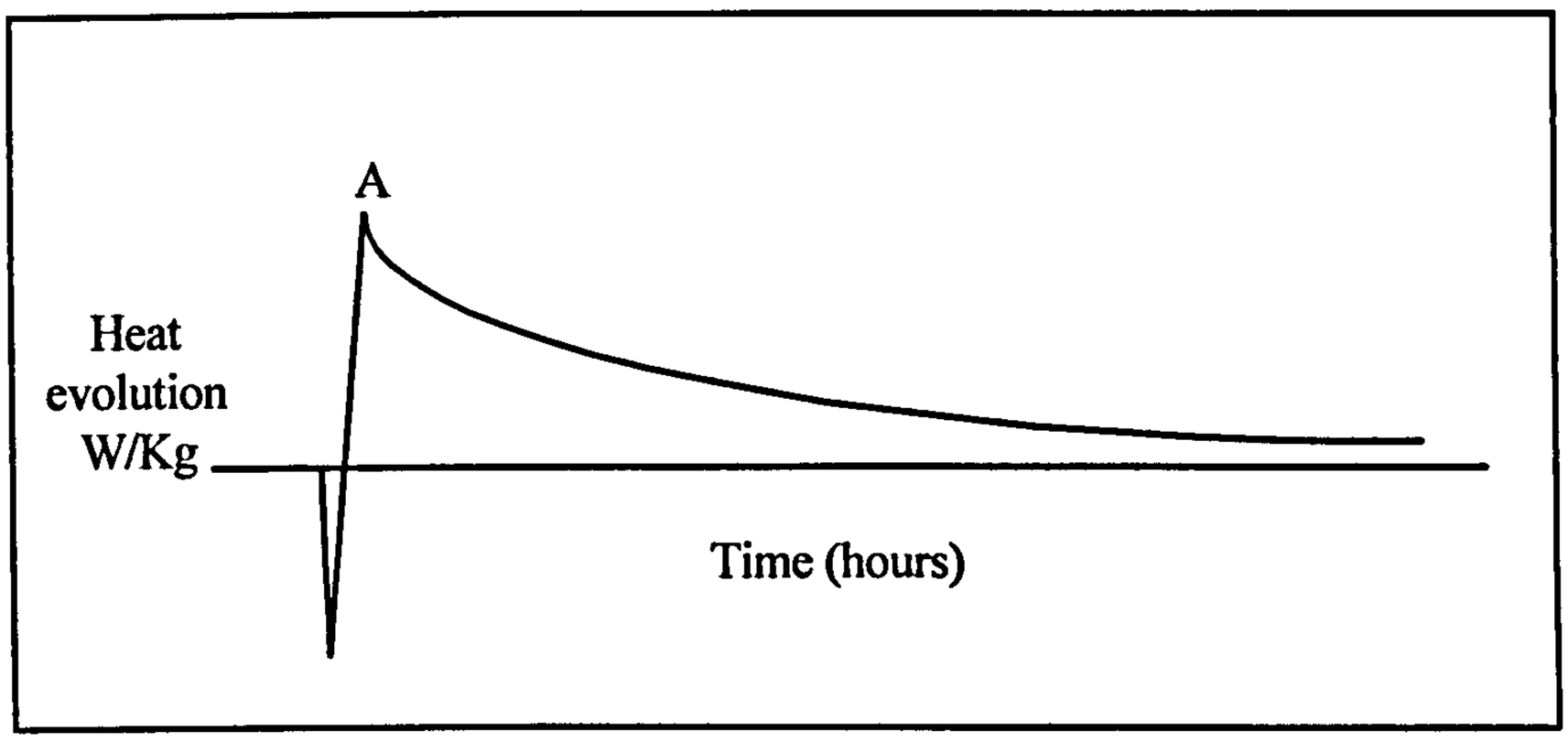

The authors' research would tend to correlate with the manufacturers' data with respect to ettringite formation, which should not theoretically occur in NHL2 due to the very low levels of SO_3 within the material. However the concentration of SO_3 cannot be discounted from the total heat of hydration of the NHL 2 sample. The continuation of hydration post maximum heat peak 'A' occurs due to the hydration of the aforementioned formation of C-S-H, C-A-H and minor AFm / AFt phases. These can be more specifically identified and quantified as C_2S with 17%, C_3A with 0.4%, C_2AS with 0.8%, C_4AF with 0.4% (based upon St Astier mineralogical components).

The NHL2 paste would be expected to have the lowest level of hydraulic activity and theoretically the lowest heat of hydration. This was reinforced by Livesey's assessment of the C_2S content within hydraulic limes in which he believed that it was 'major in class 5 lime, significant in class 3.5 lime and minor in class 2 lime.' [20]. However, when assessing the full range of pastes, it was clear it was not the case with an anomaly occurring, namely that of NHL3.5, which had an initially lower heat of hydration than the NHL2. This anomaly may possibly be explained via the mass heat of hydration that occurs in the NHL2 upon initial wetting, (pre-72 hours) associated with the high concentration of $Ca(OH)_2$ (approximately 43%) coming in contact with water. This will form into crystalline portlandite and eventually develop into mineral calcite [mineral $Ca(CO)_3$] if carbonated. The rate of $Ca(OH)_2$ crystallite formation increases with an increase in the temperature (due to solubility of lime in water) and consequently the rate of portlandite development will be rather rapid especially when C-S-H hydration does occur simultaneously, pushing the hydration temperature up even further. The development of portlandite is inter-dispersed and may also possibly engulf the C-S-H as

the dissolution and precipitate phase continues. The phenomena may be seen in Figure 79, depicting C-S-H interaction with portlandite, and although it represents C_3S hydration in OPC the principle may be similar to C_2S hydration in hydraulic limes.

Figure 79: Hydration of C_3S grain indicating engulfing of $Ca(OH)_2$ crystals [18]

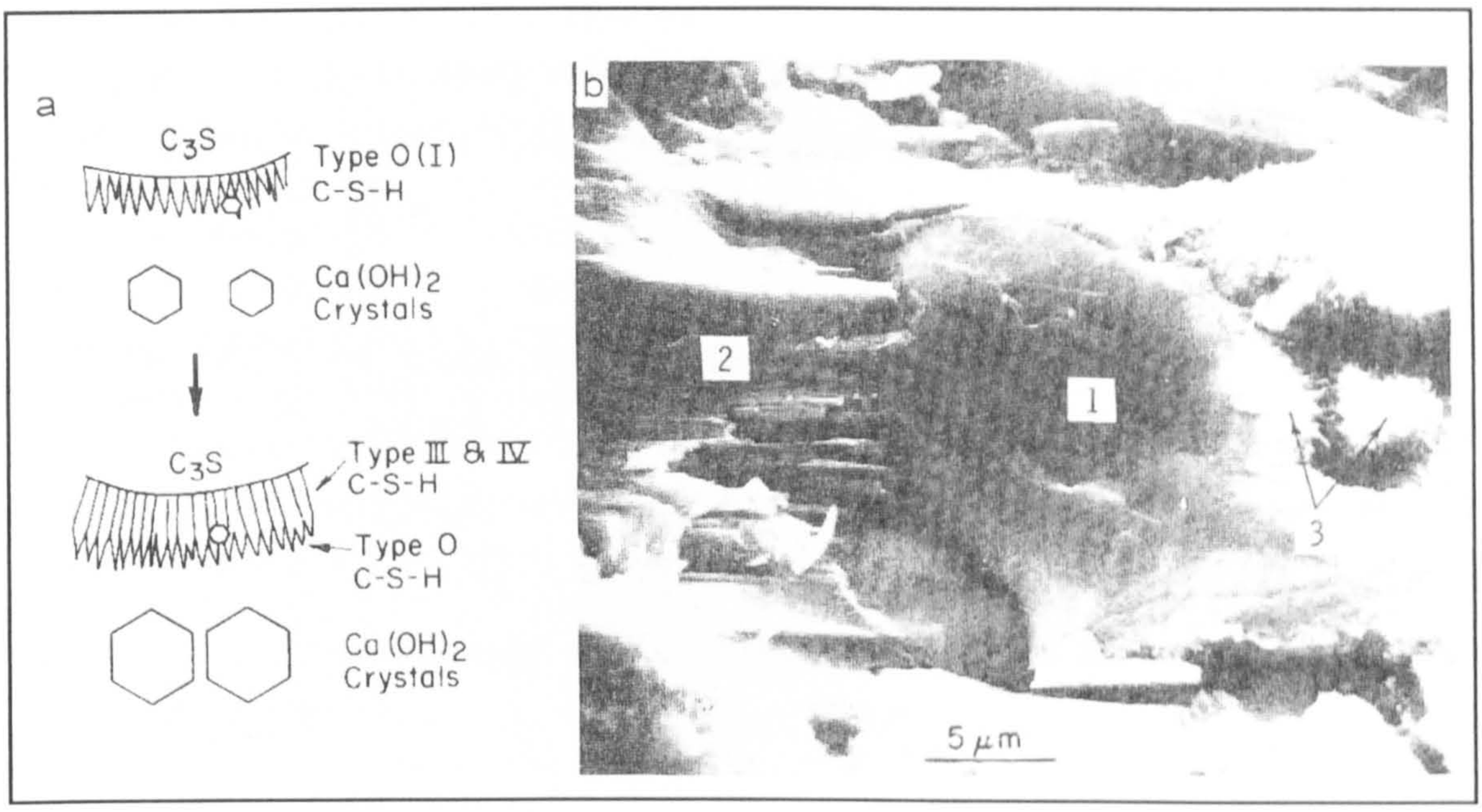

The high level of heat of hydration associated with initial wetting may also be affected by the relatively small particle size of the NHL2. This may be seen in table 42 indicating particle size and respective water requirements for the range of materials. The particle size is approximately half the size of that of the NHL3.5 and it is well accepted that a general reduction in particle size will increase the rate of hydration in the material due to a relative increase in surface area coming in contact with the water. This will have a positive affect upon the heat of hydration measured in the material.

Table 42:Rank order of water demand (author after Hughes) [21]

Limes	W/l ratio	D_{50}(mm)	D_{70}(mm)	$Ca(OH)_2$ (%)
St Astier NHL 2	0.526	5.34	16.28	43
St Astier NHL 3.5	0.436	11.64	27.51	28
St Astier NHL 5	0.388	18.49	39.16	23
Jura-Kalk	0.300	23.84	53.30	2

When the $Ca(OH)_2$ concentration is assessed against the other NHL's it is clear that NHL2 has approximately double that of NHL3.5. However, the concentration of soluble silica has been identified in NHL2 limes as being very low and this reflects upon the C-S-H development [21]. This emphasises the reliance upon heat of hydration derived from the formation of portlandite in generating early stage heat evolution. In addition

the concentration of Ca within a solution will greatly effect the rate of hydration of silicates and aluminates and may slow the initial hydration reaction down due to the development of a theoretical impermeable layer of Ca rich water surrounding the silicate particles. This impeding thermodynamic barrier may follow general neucleation theory of C-S-H [5]. However, further research is required in this area.

This is reinforced by Bergoin [16], indicating that the energy required for the dissolution of an NHL2 is greater than that of NHL3.5, due to the $Ca(OH)_2$ concentration and particle size.

5.3.2 Natural hydraulic lime NHL classification 3.5

The conduction calorimetry data for the NHL3.5 samples may be schematically represented indicating the significant hydration phases, seen in figure 80. This representation was developed from test data such as that seen in figure 47, in chapter 4 and reflects the actual changes that are taking place within the early - mid hydration phase of NHL3.5.

Figure 80: Schematic interpretation of the rate of heat development in St Astier NHL3.5 pastes

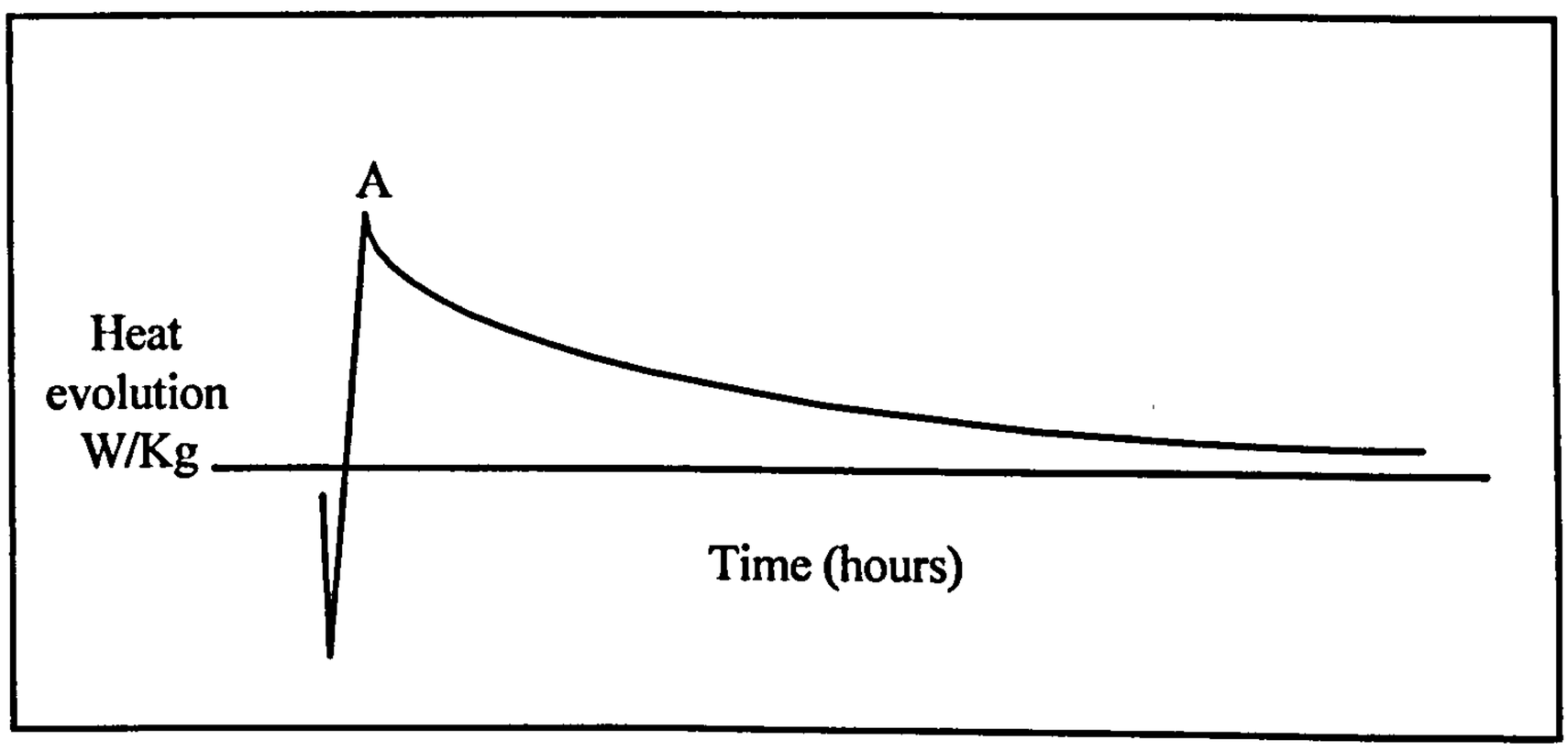

Although not shown in the conduction calorimeter results it is believed, following Forrester [26], that an initial heat peak would have been exhibited prior to the large negative drop shown in figure 80. This is common in OPC conduction calorimetry and is generally associated with early wetting of $Ca(OH)_2$ / freelime. The formation of the silicate, ferrite and low level aluminate phases are associated with heat peak 'A' however, it must be emphasised that a certain percentage of continued hydration of free lime will react contributing to the heat of hydration. The subsequent decreasing

hydraulic activity, post maximum value 'A', reflects in the continued consumption of the hydraulic compounds until relative dormancy occurs at approximately 70 hours.

As aforementioned, the level of $Ca(OH)_2$ in NHL3.5 is significantly lower than NHL2 and has an effect upon the heat of initial wetting and continued $Ca(OH)_2$ formation. The early heat of hydration will therefore be lower than that seen in the NHL2 sample, and this will be reflected in the heat of hydration. This does not necessarily mean that NHL 3.5 will exhibit constantly low heat throughout hydration and may alter its hydration rate in the medium to long term. In addition the particle size of NHL3.5 is greater than the NHL2 and therefore a slight reduction in the hydration rate would be expected as an increase in the relative surface area in contact with water is exhibited.

One partial explanation for the aforementioned may be that the formation of belite (C_2S) is most prevalent post 28 days in traditionally tested OPC. However, as discussed in the literature review low fired, highly reactive forms of belite (C_2S) yielding oxides may be created in low temperature calcination manufacture processes such as those associated with hydraulic limes. In addition the high levels of $Ca(OH)_2$ and subsequent formation of portlandite may be rapid, with limes that have high Ca contents exhibiting high initial heat evolution. However, it must be emphasised that this may be a delicate balance between the level of Ca, soluble silica and other hydraulically active components present within the material. The difference between NHL3.5 and certain types of NHL2 may be associated with the level of soluble silica, aluminium, iron and lower calcium content. Hughes and Swann [21] have shown that medium levels of soluble silica are known to be present within NHL3.5 limes (assessed via XRD and TG) and it could be hypothesised that the ratio of reactive silica / $Ca(OH)_2$ could have an impeding or over powering effect upon the initial and early formation of the aforementioned C-S-H. In those materials with a greater degree of hydraulicity a higher level of ca consumption will be seen to enable C-S-H formation. This leaves less lime to form portlandite, which generates heat upon hydration, and may partially explain the initially higher level of heat of hydration in the NHL2 sample.

The relatively low total heat of hydration value of NHL3.5 (at 72 hours) may also be explained by the possibility of the formation of one of the aforementioned hydration impedance theories.

Bergoin believes that a fundamental difference between St Astier NHL3.5 and the other NHL's is the proportion of soluble silica to the quantity of $Ca(OH)_2$. He believes that the quantity of soluble silica is proportional to the hydraulicity, emphasising that for 1% increments of combined silica (SiO_2), a 3 fold increase in hydraulicity seen in terms of belite (C_2S), however he is non-specific with respect to other hydraulically reactive components. It must also be noted that the relationship between soluble silica and free lime may affect the materials ability to rapidly hydrate as saturation of the liquid phase may occur relatively quickly.

5.3.3 Natural hydraulic lime NHL classification 5

The conduction calorimetry data for NHL5 may be schematically represented. This is seen in figure 81, indicating the significant hydration phases. This representation was developed from test data such as that seen in figure 49 in chapter 4 and reflects the actual changes that are taking place within the early - mid hydration phases in NHL 5.

Figure 81: Schematic interpretation of the rate of heat development in St Astier NHL5 pastes

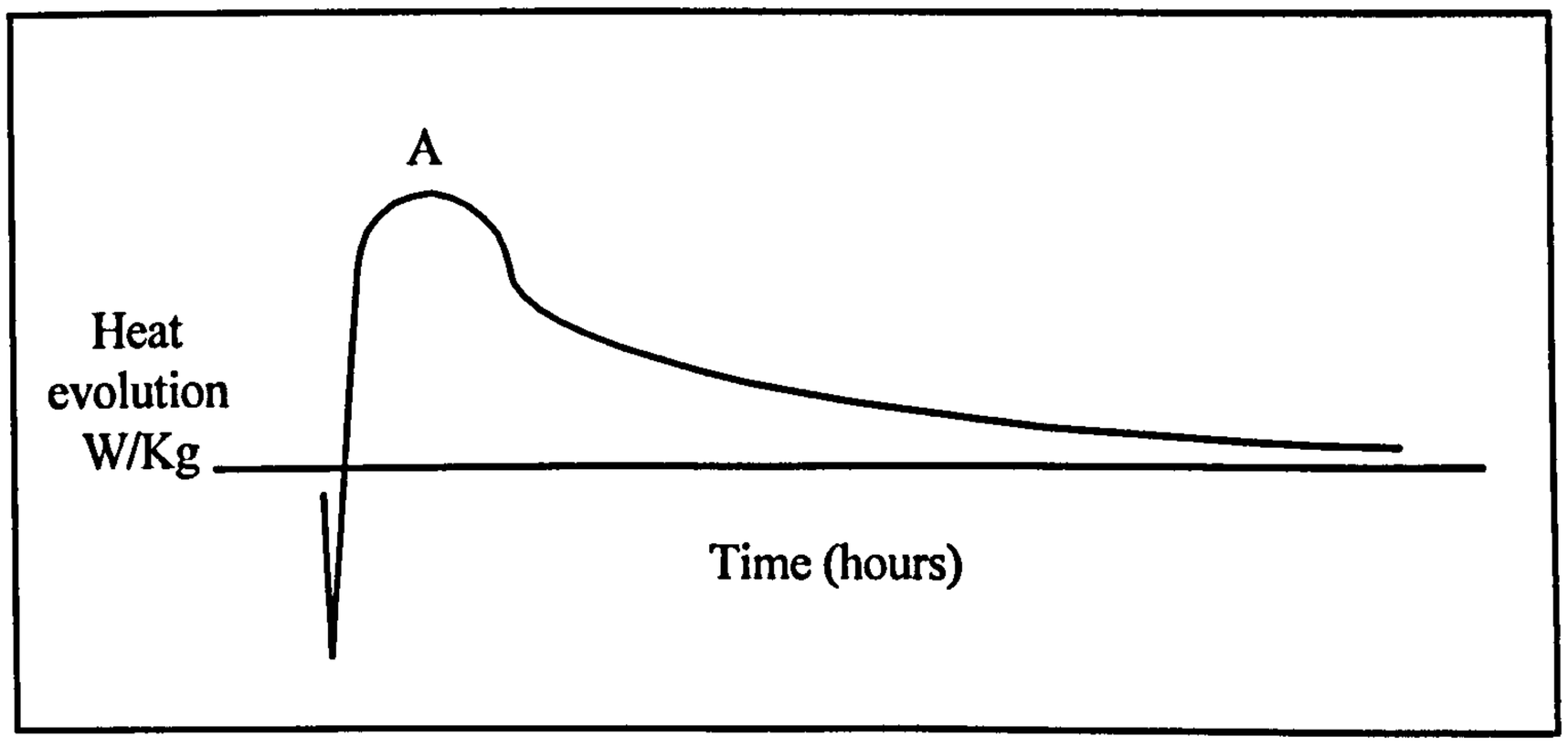

Although not shown in the conduction calorimeter results it is believed, following Forrester [26], that an initial heat peak would have been exhibited prior to the large negative drop in heat shown in figure 81. This is common in OPC and is generally associated with early wetting of $Ca(OH)_2$ / free-lime and generally occurs within the first 1-2 hours of hydration. The development of heat peak 'A' begins after the stabilization of the conduction calorimeter and water bath has occurred. It is associated with the formation of silicate, low level aluminate and ferrite hydration products. As would be expected the NHL5 shoulder is not as high in terms of heat of hydration as that of OPC. In addition the shoulder is not sustained for as long as those seen in the

Portland cement and Jura-kalk hydration plots, and follows with a slow, yet steady decrease in the exothermic heat evolution. This period concurs with Forrester's [26] work in which he emphasises that maximum point 'A' occurs at approximately 10-14 hours after initial wetting. On average, a state of relative dormancy prevails at the 70 hours stage, with an expected flattening of the graph exhibited.

When examining the hydration of the pastes in further detail it is clear that in the hydraulic materials above NHL5 designation tend to follow the more traditional conduction calorimetry graphical forms associated with Portland cement although the peak rate of heat evolution is much lower. That is to say it would appear that the greater the degree of hydraulicity seen within a cementitious material then the more the material will tend to generate the higher level chemical reactions associated with Portland cement hydration, with the exception of certain strategic components such as alite (C_3S). This is reflected in table 38 from St Astier manufactures data.

5.3.4 Natural hydraulic lime, Jura-Kalk (NHL5)

The conduction calorimetry data for Jura-Kalk may be schematically represented and is seen in figure 82, indicating significant hydration phases. This representation was developed from test data such as that seen in figure 51 in chapter 4 and reflects the actual changes that are taking place within the early - mid hydration phases in Jura-Kalk.

Figure 82: Schematic interpretation of the rate of heat development in Jura-Kalk pastes

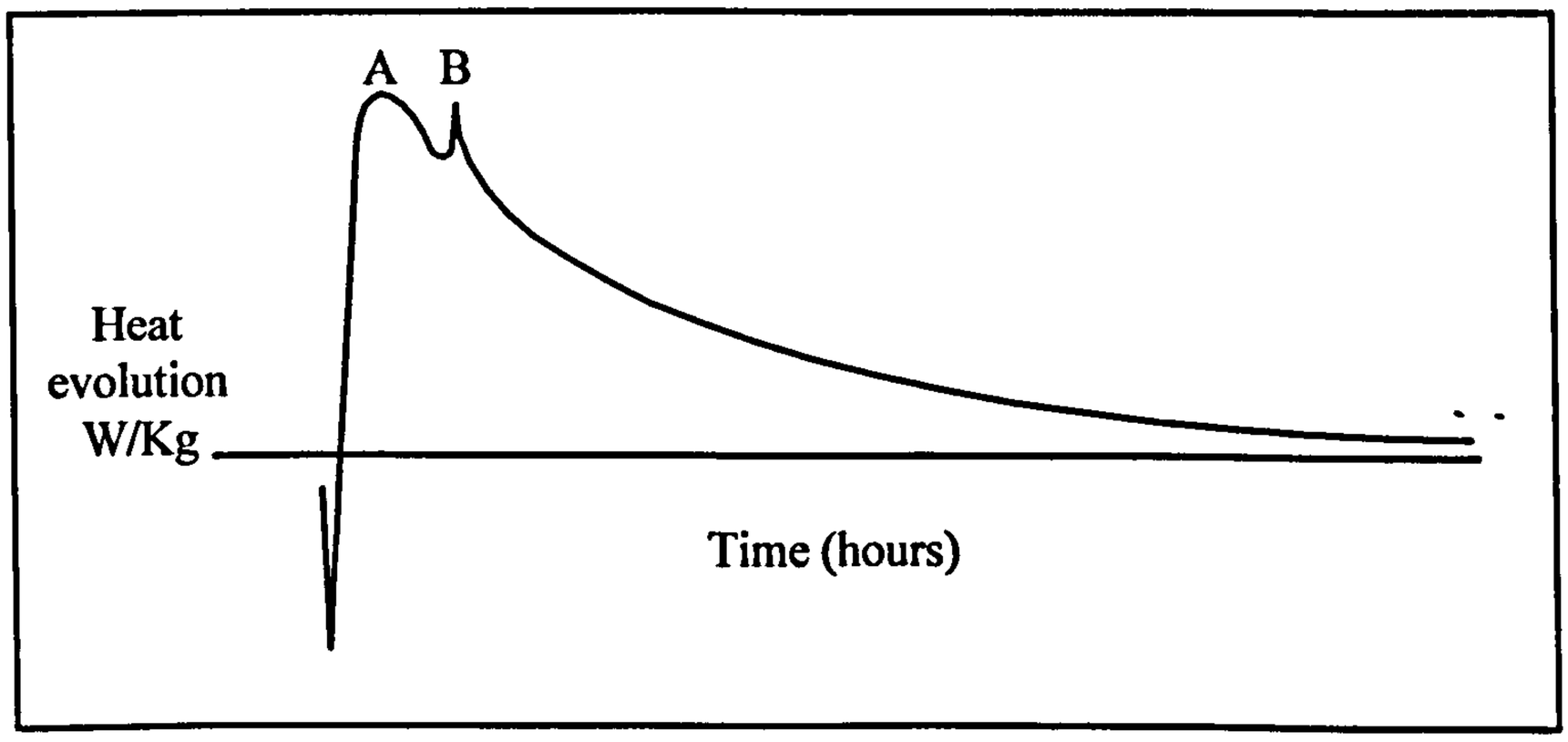

The Jura-Kalk hydration plots show primary and secondary hydration peaks, A and B respectively, that occur some 20 hours apart. Heat peak A is associated with the

formation of silicates, aluminates and ferrites. Generally this phase would continue until a relatively low background level of hydration occurs (as seen in OPC / NHL series). The Jura-Kalk samples differ by having the presence of a punctuation in the heat of hydration peak 'A', by the supplementary heat peak 'B'. This is associated with the formation of ettringite (excessive C_3A and sulphates [SO_3]) / monosulphoaluminate. This correlates with Forresters' [26] work and with manufactures data which indicate that Jura-Kalk has a higher level of gypsum than the St Astier range. On average relative dormancy prevails at the 70 hours stage, with an expected flattening of the graph exhibited.

It is interesting to note that when Hughes & Swann [21] assessed the work undertaken by Eckels it led to the belief that Jura-Kalk should be reclassified as an 'imperfectly burned natural cement'. This comment may be valid when assessing the early hydration phases in Jura-Kalk with the level of heat generated in terms of rate of heat (ROH) being 64 W/Kg. This is approximately double that associated with NHL5 which is supposedly placed within the same category. It would be interesting to assess the hydration via conduction calorimetry for the first 3 months to ascertain the medium-long term hydration of the material.

When assessing Jura-Kalk (NHL5) which has 2% $Ca(OH)_2$ concentration it is clear that it is far surpassed by the NHL 3.5 with a $Ca(OH)_2$ concentration of 43% [21]. This may suggest that the formation of an impermeable hydrate layer in Jura-Kalk would be improbable and may partially explain the materials relatively rapid hydration and consequent fast setting times.

5.3.5 Portland cement Samples

The conduction calorimetry data for OPC may be schematically represented and is seen in figure 83, indicating significant hydration phases. This representation was developed from test data such as that seen in figure 53 in chapter 4 and reflects the actual changes that are taking place within the early - mid hydration phases in OPC.

Figure 83: Schematic interpretation of the rate of heat development in O.P.C pastes

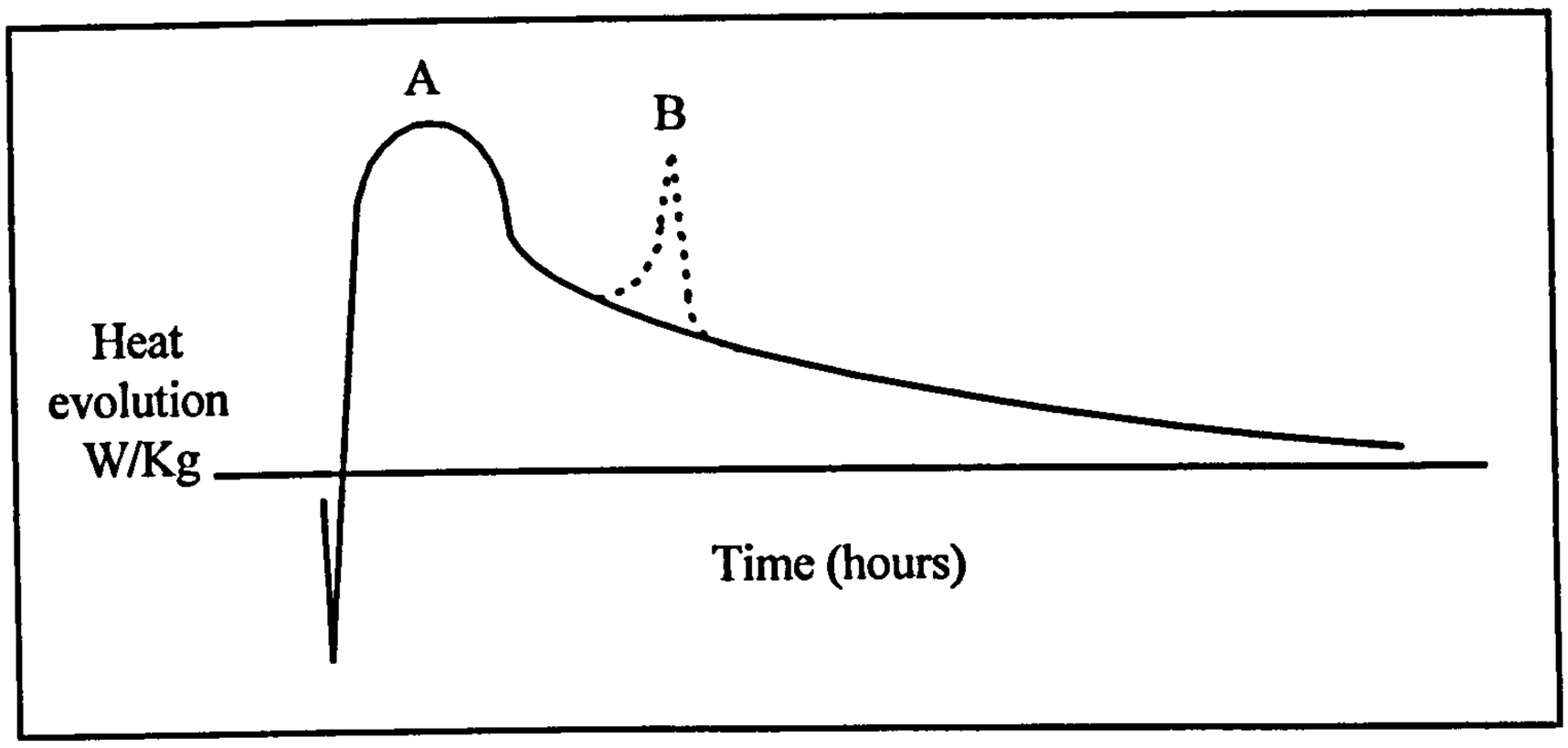

Although not shown in the conduction calorimeter results it is believed, following Forrester [26], that an initial heat peak would have been exhibited prior to the large negative drop in heat shown in figure 83. This is common in OPC and is generally associated with early wetting of $Ca(OH)_2$ / free-lime and generally occurs within the first 1-2 hours of hydration. After this point the development of a secondary heat peak 'A' is seen. This is associated with the hydration of early C_3S (alite), C_3A, and the other hydraulic components. The maximum point 'A' is attained at approximately 10 hours, this concurs with Forresters' work [26] in which his sample range attained maximum peak 'A' after approximately 10-14 hours, however, it must be emphasised that this is affected by the W/C ratios adopted. The decline in the heat evolution from this shoulder is relatively gradual with a period of approximately 50 hours taken prior to relative dormancy. There was no evidence of heat peak 'B' as seen in the Jura-Kalk samples, which is indicative of the SO_3 concentration within the material that must be present in insufficient quantities to form monosulphoaluminate.

The OPC samples followed the basic hydration model set down by Odler [5], in which he believed that 4 primary stages are generally exhibited in cementitious materials (see figure 84). These are stage 1, which indicates early reaction and exothermic wetting. Followed by the induction period lead up to stage 2 which is the main peak associated with the middle stage reaction. This phase is associated with the main C-S-H component formation. Stage 3 indicates a gradually decreasing rate of heat evolution and corresponds to a reducing level of C-S-H formation. Finally, stage 4 indicates a reduction in the hydraulic components with low-level activity being exhibited until relative dormancy occurs.

Figure 84: Theoretical hydration plot for Portland cement

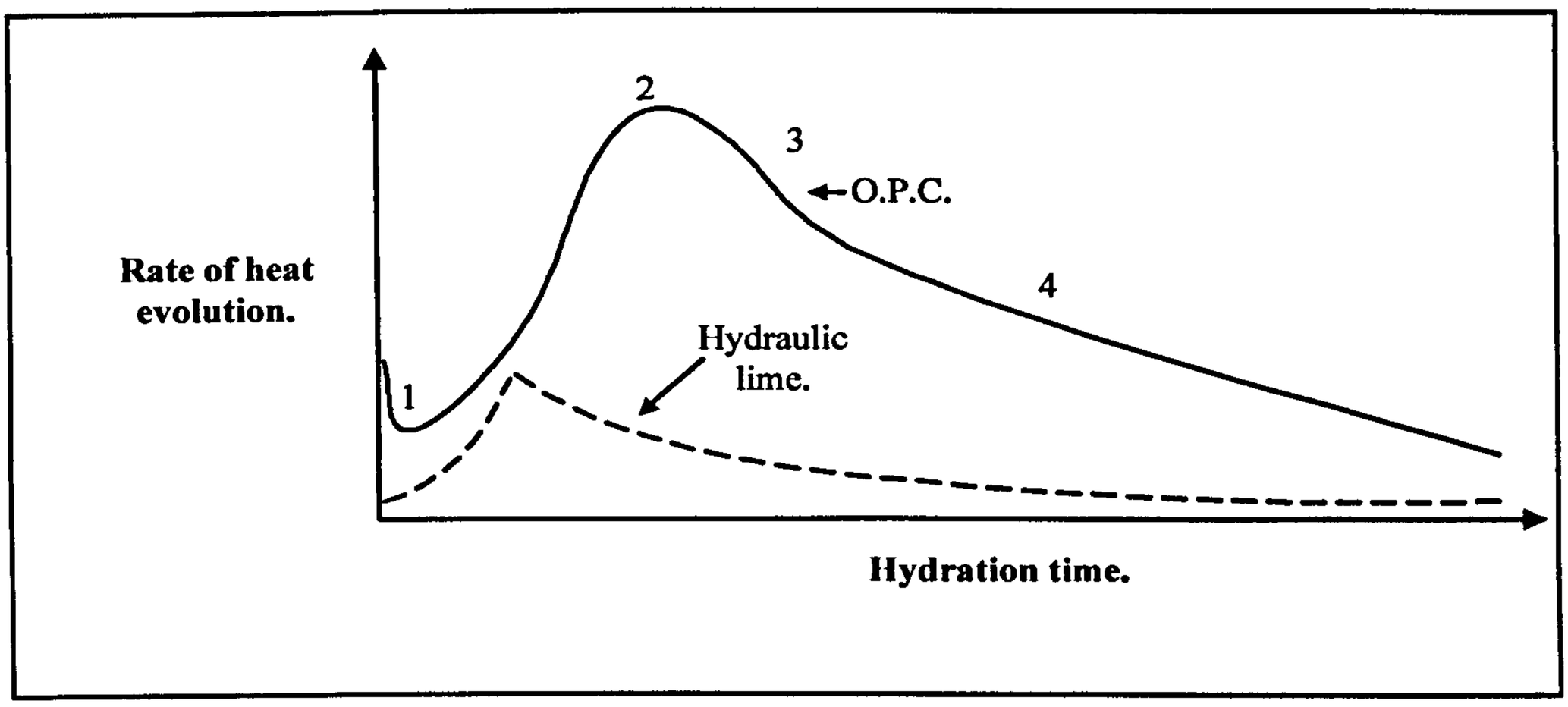

Those hydraulic components that contribute to OPC set characteristics have been shown by Anderson et al [50] indicating the primary hydration products and their respective hydration rate, heat of hydration and other salient factors in table 43.

Table 43: Characteristics and significance of the main constituents of cement [50]

Approximate chemical composition	**$3CaO{\cdot}SiO_2$ (C_3S)**	**$2CaO{\cdot}SiO_2$ (C_2S)**	**$3CaO{\cdot}Al_2O_3$ (C_3A)**	**$4CaO{\cdot}Al_2O_3{\cdot}Fe_2O_3$ (C_4AF)**
Rate of hydration	Rapid	Slow	Very Rapid	Rapid
Rate of strength development	Rapid	Slow	Rapid	Medium
Ultimate strength	High	High	Low	Low
Heat of hydration	Medium	Low	Very High	Medium
General comments	Proportion increases in rapid hardening cement, reduced in low heat cement	Responsible for the continued hardening of cement over long time	Proportion reduced in low heat and sulphate resisting cements	Gives grey colour to cement. Proportion increases in sulphate resisting cement

This table reinforces the analysis of those hydration products that have been attributed to the formation of O.P.C conduction calorimetry results.

5.4 Summary of hydration

Generally the cementitious materials under test performed as expected within the first 3 days of hydration. The only exception to this was the early hydration of St Astier NHL3.5, generating a lower than expected heat of hydration. This may be theoretically attributed with the 'doping' of silicates leading to retarded hydration. This is believed to occur in OPC hydration and relates to the super saturation of $Ca(OH)_2$ within the liquid

phase. Alternatively, the St Astier NHL 2 samples may in actual fact have higher than expected heat of hydration when compared with NHL 3.5. This may be partially due to the higher levels of free lime within the material.

The total heat of hydration (Σ.H) and average rate of heat (Av.R.O.H) for the range of pastes can be seen in table 44.

Table 44: Conduction calorimetry results for hydraulic lime and cement pastes (72hours)

Sample type in order of hydraulicity (determined via calorimetry)	Average Rate of heat (ROH) W/Kg	Total heat (ΣH) Kj/Kg
NHL 3.5	24W/Kg	1517Kj/Kg
NHL 2	31 W/Kg	2067 Kj/Kg
NHL 5	37 W/Kg	2909 Kj/Kg
Jura-Kalk	64 W/Kg	3041 Kj/Kg
Portland cement	189 W/Kg	13149 Kj/Kg

Those materials with a lesser degree of hydraulic reactivity (namely NHL 2 and NHL 3.5) have a tendency to perform differently to the other samples, exhibiting a rapid increase in exothermic heat evolution within the first hour of hydration known as the wetting phase. Although this is not shown in the conduction calorimeter results it was shown in work by Forrester [26]. After this phase the development of heat peak 'A' occurs exhibiting rather rapid heat evolution. A consequent steady decrease in hydraulic activity after this point is noted.

The hydraulic limes that have higher levels of reactive silicates, have a propensity to sustain a shoulder forming to peak 'A' and this is indicative of higher levels of hydraulic activity. The conduction calorimeter results were also informative in detecting other components such as the SO_3 concentration exhibited in the Jura-Kalk sample.

The OPC samples differed from the hydraulic lime as their set characteristics are primarily derived from the hydration of C_3S (alite), with long-term strength development been associated with C_2S (belite) (post approximately one month). As a consequence the majority of free lime or portlandite [$Ca(OH)_2$] is consumed or combined in the formation of the C-S-H.

The high heat of hydration in OPC is attributable to the formation of C_3S, C_3A and other common hydration products. The high level of heat evolution is due to the presence of C_3S.

Hydraulic lime differs from cement due to several factors, such as the absence of C_3S, due to only lower level silicates being present (ie: mono calcium silicates and di-calcium silicates) and secondly, higher levels of portlandite [$Ca(OH)_2$] ultimately leading to calcite development, if exposed to CO_2. As less calcium is consumed in the hydration of hydraulic limes a greater level of portlandite and subsequent chunky calcite crystals form develop as opposed to the rod and flake crystals associated with C-S-H, and this obviously has a significant bearing upon the physical characteristics of the paste or mortar.

Generally those hydraulic limes with greater levels of hydraulicity tended to perform in a graphically similar manner to the OPC hydration plots. However, the hydraulic activity was dwarfed in comparison to the OPCs reactivity.

It must be emphasised that the level of hydraulic activity is always greatest in the earlier stages of the materials life. However, once this level has been ascertained it may be used as an indicator of expected longer-term hydration. An indication of these changes in the maturing of cement can be seen in table 45.

Table 45: Results of statistical analysis of heat of hydration of cement (21°C) (author after Verbeck & Foster) [19]

Period of hydration	Calculated heat evolution (in cement paste) expressed as calories per 0.01 gramme of compound			
	C_3S	C_2S	C_3A	C_4AF
3 Days	0.58	0.12	2.12	0.69
7 Days	0.53	0.10	3.72	1.18
28 Days	0.90	0.25	3.29	1.18
3 Months	1.04	0.42	3.11	0.98
1 Years	1.17	0.54	2.79	0.90
6 $^1/_2$ Years	1.17	0.53	3.28	1.11

Note: 1 cal / 0.01g = 418KJ/Kg

In conclusion, the hydration plots give an excellent indication of the performance of early stage hydration in hydraulic limes, an area that has previously been little researched. This gives us an insight into the hydration mechanisms in hydraulic limes and a better picture of initial hydraulic activity (up to 72 hour).

If conduction calorimetry tests were undertaken for the assessment of hydration phases, twinned with extremely high levels of thermopile sensitivity, the change in the crystallography seen in the components in table 43 should in theory be identified (with the exception of C_3S). This would allow cross correlation to be established between heat evolution and actual visual identification of the hydration products.

5.5 General water vapour permeability

When assessing the authors results pertaining water vapour permeability for the plaster board samples it was evident that they compared favourably with work undertaken by and Batty, W J [53] and McClean et al [54]. These may be seen in tables 46 and 47.

Table 46 : Water vapour permeability values

Material	*Permeability*	*Thickness (where applicable)*	*Units*	*Source*
Plaster-board	Water Vapour Permeability $2.31x10^{-10}$ @ 65% 2.97x10-^{11} @ 76% $2.81x10^{-10}$ @ 86%	12mm	Kgm/m^2.s. Pa Or $KgmN^{-1}s^{-1}$	This work
Plaster-board	Water Vapour Permeability $2.5x10^{-11}$Kgm $N^{-1}s^{-1}$	-	Kgm $N^{-1}s^{-1}$	Batty / Cranfield [53] – vapour diffusion and condensation

Table 46 takes into consideration the differences in relative humidity across the sample as with the author's research techniques.

Table 47: Permeability of plasterboard (author after McLean et al) [54]

Material	*Temperature*	*RH difference across the sample 0-60*	*Average permeability test results Kgm/Ns x 10^{11}*
Plaster-board (1)	20°C	0-60	2.13
Plaster-board (1)	25°C	0-60	2.10
Plaster-board (2)	20°C	0-60	2.37
Plaster-board (2)	25°C	0-60	2.33

This has been further reinforced by unpublished data by Galbraith, G.H, in which he tested a wide range of building materials, including mortars. It was interesting to note that all of the binary materials tested fell within a water vapour permeability range of 0.8-5.0 x 10^{-11}Kgm/m^2·s·Pa. When looking more specifically at Galbraiths' results it was noted that the measured permeability's of plaster board were 2.3-4.8 x 10^{-11}Kgm/m^2·s·Pa and for cement mortars they ranged from 0.9 - 2.5 x 10^{-11}Kgm/m^2·s·Pa. The authors

results for the full spectrum of mortar samples ranged from 7.65×10^{-12} through to 2.05×10^{-10} Kgm/m^2·s·Pa.

When assessing the average values for the spectrum of mortar samples it was evident that with an increase in relative humidity an increase in water vapour permeability was seen. This also concurs with work by Galbraith.

The individual binary and ternary mortar samples will be discussed to develop understanding of their performance (in rank order of water vapour permeability). This evaluation is based upon the average water vapour permeability across the 3 desiccant ranges. See figures 61 and 62 in chapter 4.

5.5.1 Binary Jura-Kalk (NHL5) lime mortar samples

When assessing the average water vapour permeability of the Jura-Kalk mortar samples it was evident that this mortar type had the highest capability to transmit water vapour from the sample range (8 in all) with an average value of 3.87×10^{-11} Kgm/m^2·s·Pa. This would not be expected when assessing the material via hydraulicity, as Jura-Kalk has a high level of hydraulic reactivity and would be expected to perform more like NHL5 or OPC. However, when the Jura-Kalk mortar samples were tested for water vapour permeability over the 3 different driving pressures it was clear that it was performing in a similar manner to the others, exhibiting an increase in water vapour permeability with an increase in relative humidity.

The Jura-Kalk eminently hydraulic lime mortar did not follow the hypothesis in so much as, with high level hydraulicity of the binder a high water vapour permeability was attained.

5.5.2 Binary Shap non-hydraulic lime mortar samples

When assessing the average water vapour permeability the Shap non-hydraulic mortar samples it was evident that this mortar type had the second highest capability to transmit water vapour from the sample range (8 in all). The average water vapour permeability value was 2.69×10^{-11} Kgm/m^2·s·Pa. This would be expected when assessing the limited information pertaining water vapour permeability of non-hydraulic lime mortars. When the mortar was tested for water vapour permeability over the 3 different driving pressures it was clear that it was performing in a similar manner to Galbraiths'

samples, exhibiting an increase in water vapour permeability with an increase in relative humidity.

The Shap non-hydraulic lime mortars are very pure, that is to say have virtually no hydraulic components present within the binder. The hydraulicity of the material is therefore deemed to be zero. This was reflected in the crystallography of the samples exhibiting mass calcite development with a relatively cavernous pore structure.

The Shap non-hydraulic mortar type followed the hypothesis in so much as, with zero hydraulicity of the binder; high water vapour permeability values were attained.

5.5.3 Binary Isle of Man non-hydraulic lime mortar samples

When assessing the average water vapour permeability for the Isle of Man mortar samples it was evident that this mortar type had the third highest capability to transmit water vapour from the sample range (8 in all). The average water vapour permeability was $2.54x10^{-11}Kgm/m^{2}{\cdot}s{\cdot}Pa$. The Isle of Man samples were not tested for hydraulicity as they were thought to be non-hydraulic. However, from ESEM analysis it was evident that very low levels of C-S-H were seen interdispersed between the mass of calcite agglomerates. The pore structure was unimpeded by smaller C-S-H formation and retained a relatively cavernous pore structure. This information should be taken into consideration when looking at the water vapour permeability results. When the mortar was tested for water vapour permeability over the 3 different driving pressures it was clear that it was performing in a similar manner to Galbraiths' samples, exhibiting an increase in water vapour permeability with an increase in relative humidity.

The Isle of Man non-hydraulic mortar type followed the hypothesis in so much as, with low level hydraulicity of the binder; relatively high water vapour permeability was attained.

5.5.4 Binary NHL2 lime mortar samples

When assessing the average water vapour permeability for the NHL2 mortar samples it was evident that this mortar type had the fourth highest capability to transmit water vapour from the sample range (8 in all) with an average of $2.38x10^{-11}Kgm/m^{2}{\cdot}s{\cdot}Pa$. This would be expected when looking at traditional information [27] upon water vapour

permeability of mortars. The samples ability to transmit water vapour permeability increased with a rise in relative humidity as was common to the other samples tested.

The NHL2 mortars are feebly hydraulic, that is to say they have low levels of hydraulic components present within the binder. This is reflected in the crystallography seen under ESEM, with C-S-H / C-A-S-(H) acicular crystals being seen interdispersed across the material. It must be emphasised that the majority of the binding matrix was calcite and only low levels of C-S-H could be seen to bridge the pore structure. The material is deemed to be feebly hydraulic, and followed the hypothesis in so much as, with low level hydraulicity of the binder; relatively high water vapour permeability was attained.

5.5.5 Binary Blair-Athol non-hydraulic lime mortar samples

When assessing the average water vapour permeability for the mortar samples it was evident that this mortar type had the fifth highest capability to transmit water vapour from the sample range (8 in all) with an average value of $1.84x10^{-11}Kgm/m^{2}{\cdot}s{\cdot}Pa$. The Blair Athol samples were not tested for hydraulicity as they were thought to be non-hydraulic. However, from ESEM analysis it was evident that low levels of C-S-H were seen. This information should be taken into consideration when looking at the water vapour permeability results, as a certain amount of acicular C-S-H / C-A-S-(H) could be seen to be bridging the pore structure. When the mortar was tested for water vapour permeability over the 3 different driving pressures it was clear that it was generally performing in a similar manner to Galbraiths' samples, exhibiting an increase in water vapour permeability with an increase in relative humidity.

The Blair-Athol hydraulic lime mortars have therefore been deemed to be feebly hydraulic, that is to say they have low levels of hydraulic components present within the binder.

The Blair-Athol feebly hydraulic mortar type followed the hypothesis in so much as, with low level hydraulicity of the binder; relatively high water vapour permeability was attained.

5.5.6 Binary NHL3.5 lime mortar samples

When assessing the average water vapour permeability of the NHL3.5 mortar samples it was evident that this mortar type had the sixth highest capability to transmit water

vapour from the sample range (8 in all) with a value of $1.56x10^{-11}$Kgm/m^2·s·Pa. This would be expected when looking at traditional information (St Astier) upon water vapour permeability of mortars. The level of acicular C-S-H / C-A-S-(H) was greater than those seen in previous samples and this reflected in the level of impedance of the pore structure. The samples ability to increase water vapour permeability transmission increased with a rise in relative humidity as was common to the other samples tested.

The NHL3.5 mortars are moderately hydraulic that is to say they have moderate levels of hydraulic components present within the binder. The NHL 3.5 mortar type followed the hypothesis in so much as, with moderate level hydraulicity of the binder; moderate levels of water vapour permeability were attained.

5.5.7 Binary NHL5 lime mortar samples

When assessing the average water vapour permeability of the NHL5 mortar samples it was evident that this mortar type had the second lowest capability to transmit water vapour from the sample range (8 in all) with an average value of $1.25x10^{-11}$Kgm/m^2·s·Pa. This would be expected when looking at traditional information [27] upon water vapour permeability of mortars. This was reflected in the crystallography seen in the sample and the higher levels of acicular C-S-H / C-A-H-(H) distributed through the mortar and bridging the pore structure. When the mortar was tested for water vapour permeability over the 3 different driving pressures it was clear that it was performing in a similar manner to the other samples, exhibiting an increase in water vapour permeability with an increase in relative humidity.

The NHL5 mortars are eminently hydraulic, that is to say they have high levels of hydraulic components present within the binder. The NHL 5 mortar type followed the hypothesis in so much as, with high level hydraulicity of the binder; low levels of water vapour permeability were attained.

5.5.8 Binary O.P.C. mortar samples

When assessing the average water vapour permeability of the OPC mortar samples it was evident that this mortar type had the lowest capability to transmit water vapour from the sample range (8 in all) with an average value $1.21x10^{-11}$Kgm/m^2·s·Pa. This would be expected, as it is well understood that OPC is considered to be a relatively

impermeable material. However, as with the other materials the samples ability to transfer water vapour increased with a rise in relative humidity.

The OPC mortars have the highest levels of hydraulic components present within the binder and would be expected to have a denser pore structure than the other materials. This was reflected in the dense nature of C_3S hydrated forms that led to high levels of densification within the structure of the C-S-H.

The OPC mortar type followed the hypothesis in so much as, with the highest levels of hydraulicity of any of the binder, the lowest levels of water vapour permeability were seen.

5.5.9 Ternary Shap non-hydraulic lime & NHL5 mortar samples

The NHL5 samples exhibited the highest levels of water vapour permeability of the ternary mortar samples with an average value of $8.57x10^{-11}Kgm/m^2{\cdot}s{\cdot}Pa$. This would not be expected when assessing the levels of hydraulicity. However, it must be emphasised that the affects of gauging a mix are little understood in terms of performance.

The results were higher than any of those seen in the ternary range of mortars, and the material would not be expected to perform better than those mortars with no or very low hydraulic activity.

5.5.10 Ternary Shap non-hydraulic lime & NHL3.5 mortar samples

The Shap non-hydraulic lime and NHL3.5 samples performed well with respect to the water vapour permeability and was the second highest of the ternary range of samples $4.33x10^{-11}Kgm/m^2{\cdot}s{\cdot}Pa$. The samples ability to transmit water vapour increased with a rise in relative humidity as with the other materials.

The results were higher than any of those seen in the binary range of mortars, and the material would not be expected to perform better than those binary mortars with no or very low hydraulic activity.

5.5.11 Ternary Shap non hydraulic lime & OPC mortar samples

The Shap non-hydraulic lime and O.P.C samples were performing with a moderate level of water vapour transfer with an average value of $3.46x10^{-11}Kgm/m^2{\cdot}s{\cdot}Pa$, when

compared with the other ternary samples. It would not be expected that ternary mixes adopting NHL2 and Jura-Kalk would exhibit lower water vapour permeability than the OPC.

The samples ability to transmit water vapour increases with a rise in relative humidity as with the other materials.

The effectiveness of OPC in gauged mixes has been questioned in the results of research undertaken by English Heritage. They found that when small proportions of OPC were added to lime-sand mortars the effect was detrimental, believing 'the addition of small quantities of cement to lime: sand mortars has a negative effect on the strength and durability of the mortars' [51]. It was believed that proportions of OPC must equal at least half the lime content of a mortar before positive effects in strength are seen.

The addition of small quantities of OPC to lime-sand mortars are also believed to be counter-productive due to theoretical occurrence of cement particle flocculation. The grouping of OPC particles would theoretically have an effect upon the particle distribution, hydration and therefore, ultimately long term performance. It must be emphasised that the aforementioned have not been independently verified and may be questionable.

5.5.12 Ternary Shap non-hydraulic lime & NHL2 mortar samples

When the Shap non-hydraulic lime and NHL2 samples were assessed against the other materials it had the 2nd lowest average water vapour permeability value of 2.91×10^{-11} Kgm/m^2·s·Pa, with Jura-Kalk being the only material with a lower water vapour permeability value. This would not be expected when looking at traditional information upon water vapour permeability of mortars for non-hydraulic / feebly hydraulic lime mortars, however, the affects of gauging a mix is little understood. It must be emphasised that the water vapour permeability of this mortar is high when compared to the binary samples.

The samples ability to transmit water vapour increased with a rise in relative humidity as with the other materials.

5.5.13 Ternary Shap non-hydraulic lime & Jura-Kalk mortar samples

The Jura-Kalk ternary samples exhibited the lowest water vapour permeability of all the ternary materials with a value of $1.57x10^{-11}$Kgm/m^2·s·Pa. It would not be expected that a gauged mortar sample adopting Jura-Kalk would have a lower water vapour permeability than OPC. However, as previously stated, gauged mixes are little understood in scientific or practical terms. It must be emphasised that the samples ability to transmit water vapour increased with a rise in relative humidity as with the other materials.

5.6 Summary of water vapour permeability

The binary mortar samples tended to follow the expected water vapour permeability performance with the exception of Jura-Kalk that exhibited higher levels of water vapour permeability than would have been expected for its level of hydraulicity.

The water vapour permeability values are reinforced by tests undertaken by St Astier. These may be seen in table 48, in which a range of materials were tested. It must be emphasised that test procedure, materials adopted and units could not be ascertained and therefore these values should be viewed with caution.

Table 48: Binary Mortar samples (Author after St Astier)

Mortar type	Concrete (OPC)	OPC mortars	Hydrated lime (CL) mortars	NHL5 mortars	NHL3.5 mortars	NHL2 mortars
Vapour exchange	0.15	0.23-0.25	0.46-0.51	0.55	0.65	0.71

When assessing the water vapour permeability results it was apparent that the higher the driving pressure across the sample (generated by alternate desiccants) then the lower the rate of water vapour permeability that was seen. Conversely, the lower the driving pressure across the sample lead to higher water vapour permeabilities.

It would be realistic to expect the opposite of this phenomenon to occur. One tentative explanation of this phenomenon may be hypothesised as follows: at low pressures water vapour transfers at a relatively steady rate. No significant pressure differentials are established within the micro pore system. When higher pressures within the pore system are exhibited the likelihood of pore condensation may be increased due to pressure differentials between the main pore and the pore neck. This may lead to condensation

occurring through an alteration of the volume of the pore system and therefore an alteration in both pressure and temperature. This phenomenon may be seen diagrammatically represented in figure 85.

If condensation of water vapour within the pore lining occurs then theoretical alteration of the moisture flow characteristics may have taken place: from water vapour into liquid phase. This may ultimately lead to the slower transfer rates through the material. In addition once condensation has occurred the liberation of liquid water into water vapour may also be affected by the nature of the composite material with some of components being hydrophilic and others being hydrophobic depending upon the wettability of the material in question (i.e: calcite, silica or other elemental components within the mortar). This has been shown by Buckman [36] and Torraca [35] to alter the moisture transfer characteristics within the material, and may be partially associated with differences between the contact angles of the water and the surface of the material (see figure 31 and Plate 11 in chapter 2).

Figure 85: Pore condensation in idealised pore system

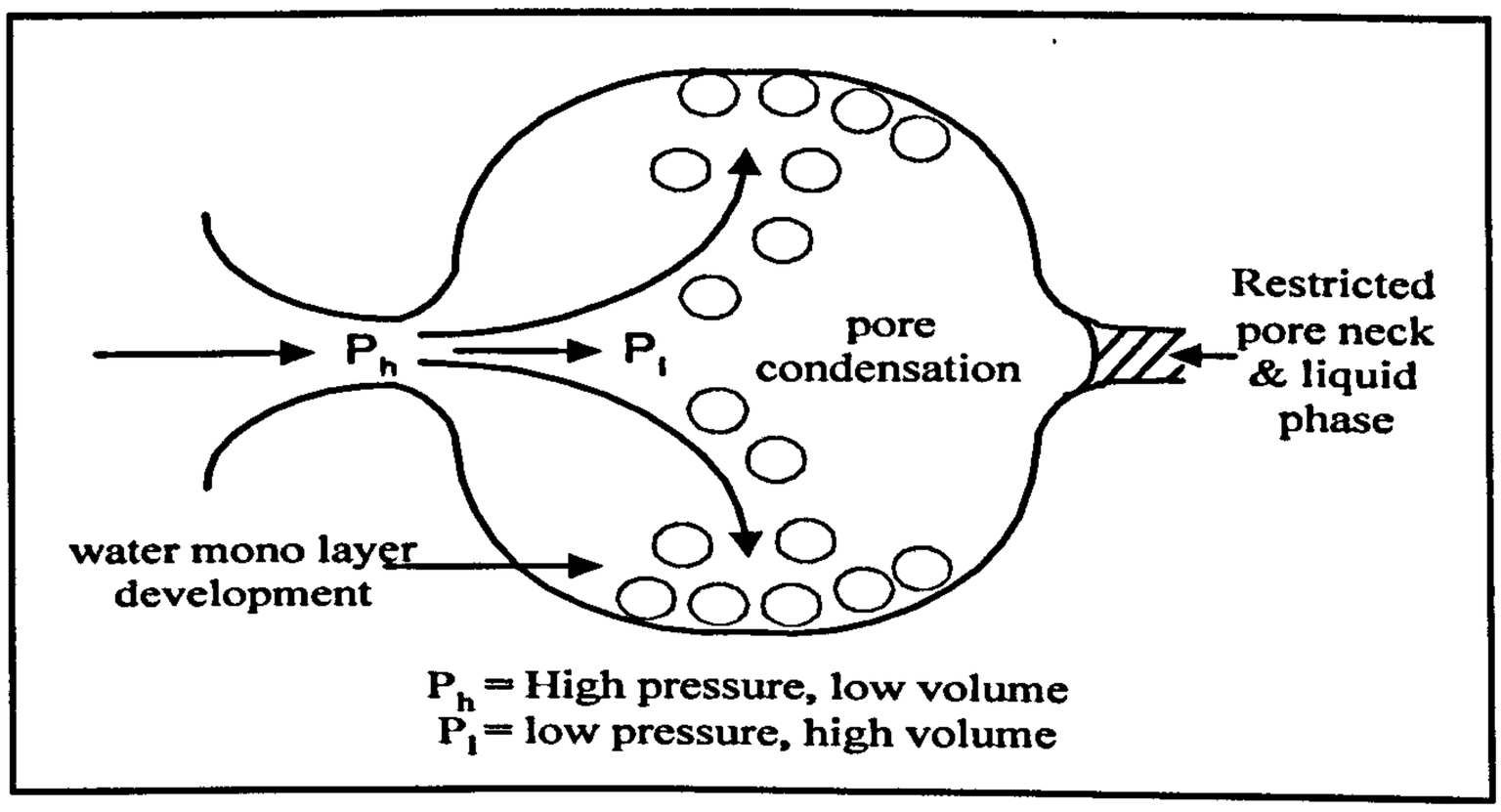

In addition to the pore condensation, distillation and alteration of moisture flow characteristics another explanation of altered permeability at high driving pressures may also be hypothesised. This pertains of the concept of boundary effects and viscous drag. When the water vapour molecules move through the pore system at low pressures very little resistance is generated between the molecules and the material. However, when this is reversed a high level of resistance may be encountered. A simple analogy is to consider 2 car journeys, one travelling slowly and the other fast. When the passenger places their arm out of the window at a slow speed no real effect is noted, however,

when the same occurs at high speed the passengers arm will be 'buffeted' rather excessively. The increase in speed had lead to increased resistance.

Generally, those mortars with high levels of non-hydraulic component (namely calcite / portlandite) exhibited a higher water vapour permeability, conversely those with a higher level of C-S-H like components appeared to have a reduced water vapour permeability. The non-hydraulic limes had a rather coarse structure with pore sizes in excess of 1μm. This value is considered by Bazant and Najjar [40] to be the critical size for allowing water vapour transfer to occur. However, it must be emphasised that they believe that in high relative humidity systems (95%+) then pore diameters of 3.5mm and below will sustain a meniscus.

The development of C-S-H across the natural hydraulic lime mortars pore structure was evident, however, densification of the pore structure as seen in OPC did not appear to occur possibly due to the predominance of a chunky calcite substrate in all the hydraulic limes. This may act as quasi 'spacers' allowing a coarse pore structure to develop. This in turn will allow relatively free development of the C-S-H like components to occur within the coarse structure and therefore no densification will be exhibited in low level hydraulic limes.

The level of pore interconnectivity appeared high for those mortars with lesser hydraulicity. It is generally accepted that the greater the degree of hydraulic activity then the higher the pore segmentation. This is reinforced by Cabera and Claisse [40] who believe that certain hydraulic components will lead to total impermeability to oxygen and water (based upon OPC studies). This phenomenon occurs when the mean size of a water molecule at room temperature is greater than the continuous OPC pore structure. This will have a major effect upon the moisture flow characteristics.

Although densification may not occur in non-hydraulic and to a lesser degree hydraulic limes the moisture transfer mechanisms may also be affected by numerous physical factors. These include the nature of the composite material and its wettability characteristics, hence, whether hydrophillic or hydrophobic in nature. Buckman [36] has indicated that the effects of moisture flow whether in liquid, vapour or in a state of flux between the 2 may be aided or hindered by this phenomenon. This has been emphasised by Torraca [35] who believes that evaporation is difficult in porous materials as the

media will readily attract moisture, however, the liberation of water into water vapour is difficult. Liberation or suppression of liquid from a pore structure will be ultimately affected by these characteristics i.e.: Torraca [35] believes that lime is electro-negative which aids in the repulsion of water at the surface of the material and readily aids flow characteristics. This is opposed to silica that is hydrophobic and therefore 'traps' moisture upon its surfaces. This will theoretically resist the liberation of moisture accordingly. It is reasonable to assume that C-S-H will have a combined effect being composed of both of these elements. This increases the difficulty of studying the moisture flow, and when twinned with the issues of binder / aggregate interface the analysis is further complicated.

In reality the quantity of water within a porous body will also vary across the sample in a non-uniform manner, being affected by the changes in pore diameter throughout the material. It is believed by Bomberg [39] that the water content within a pore structure will vary, with ramifications for not only saturated flow but also all other forms of moisture transfer mechanisms. He continues to emphasise that under normal conditions the critical water content equates to all the small pores being saturated and the large pores being covered in a mono-layer of water or above.

The flow characteristics are ultimately affected by the pore interconnectivity, pore geometry and size. The processes in action within this system will vary but may include a combination of the following:

- Condensation within micro regions of the pore structure
- Distillation and evaporation processes especially important at the neck of the pore
- Boundary effects between the water and material and or matrix and aggregate

Saidani-Scott [31] believes that non-uniform flow in porous materials very rarely achieves moisture transfer characteristics above level 2, hence, all the small pores are filled with water but the larger pores have a mono-layer covering. These characteristics have been reinforced by Maekawa [40] in which he believes that moisture loss of this nature is hindered by a necking effect within the small pores. He compares this with an 'ink bottle' which exhibits reduced amounts of evaporation occurring at the restricted neck region. This is of major significance as it must be considered as one of the primary factors in reducing the moisture transfer mechanisms of the samples.

In this research the average water vapour permeability values for the binary mortar samples all fell within a very small range. The values were between $2.69x10^{-11}Kgm/m^{2}.s.pa$ for Shap non-hydraulic to $1.21x10^{-11}Kgm/m^{2}.s.Pa$ for OPC.

The ternary mortar samples did not appear to follow the expected water vapour permeability performance. The array of data appears to follow a somewhat random distribution.

The average water vapour permeability values for the ternary samples fell within a range of between $8.57x10^{-11}$ for NHL5 through to $1.57x10^{-11}Kgm/m^{2}.s.Pa$ for Jura-Kalk. However, the samples all saw an increase in the water vapour permeability with an increase in relative humidity. Comparative values for the ternary mortars is rare and therefore makes any assessment difficult, however, when comparing the water vapour permeability values available from St Astier [27] lime manufacturers, their mortar samples exhibited low vapour exchange in OPC's and higher vapour exchange with NHL5. See table 49.

Table 49: Ternary Mortar samples (Author after St Astier)

Mortar type	OPC / CL / sand mortars (1:1:6)	OPC / CL / sand mortars (1:2:9)	NHL5 / CL mortars (0.9:0.1:3)	NHL5 / CL / sand mortars (0.7:0.3:3)	NHL5 / CL / sand mortars (0.5:0.5:3)
Vapour exchange	0.23	0.25	0.60	0.59	0.63

The data is difficult to compare due to the varying gauging proportions and the use of only one hydraulic lime type, namely NHL5. As aforementioned it must be emphasised that test procedure and materials adopted could not be ascertained and therefore these values should be viewed with caution.

5.7 General ESEM Analysis

The hydration products associated with the samples varied greatly within the material depending upon the quantity of hydraulically reactive components and or carbonate products. The full sample range will be discussed with an examination of the hydration products and their respective effect upon the crystallography and pore structure of the material being undertaken for each type of binder.

5.7.1 Binary Shap Non-hydraulic lime mortar samples

ESEM analysis of the binary Shap non-hydraulic lime mortar samples showed tiny (approximately 1-2μm) mass calcite agglomerations, which were only partially fused together. At low magnification the samples appeared to be well consolidated, however, at higher magnification it was evident that a relatively cavernous pore structure was present.

No evidence of any type of C-S-H could be seen at any magnification, as would be expected from a non-hydraulic lime. This has a significant effect upon the binding characteristics of the mortar that are consequently relatively friable and exhibit low compressive strengths. The low affinity lime has for aggregate was reinforced in plate 18 in which a relatively bare piece of aggregate could be seen with calcite deposition occuring sporadically across the surface. This phenomenon was also encountered by Lewins; with his samples also exhibiting low adhesion to 'siliceous substrates' [49]. In addition non-hydraulic limes have a limited inter-particle fusion between the developing calcite-calcite surfaces, hence the relative contact area is low. When this is twinned with the aforementioned low affinity for quartz surfaces a material with relatively low mechanical strength will always be derived.

The macro pore structure of the Shap non-hydraulic lime appeared to be relatively large and showed no signs of bridging and or interference due to smaller crystal types. This would be expected in a non-hydraulic lime that is deemed to have zero hydraulicity. In addition the lack of C-S-H type crystal morphology within the Shap non-hydraulic mortar samples correlates with the mortars high level of water vapour permeability. It would appear that the relatively large calcite crystals allow a greater degree of water vapour permeability to occur.

5.7.2 Binary Blair-Athol non-hydraulic lime mortar samples

Despite the Blair-Athol lime being referred to as non-hydraulic, when assessing the ESEM plates 19-20 the presence of very small acicular crystal types (approximately 1μm in length and 0.5μm in diameter) were noted. This correlated with slight traces of silica and alumina within the EDX analysis. Hence, it may be necessary to reclassify the lime as a feebly hydraulic. The primary crystal topography is associated with rather chunky calcite crystals with approximate dimensions of between 1-4μm. As with the Shap samples the majority of the calcite is formed into tiny masses of agglomerates.

The macro pore structure is also relatively large when compared with the Shap samples and very little bridging of the apparently interconnected pore structure appeared to occur.

The Blair-Athol hydraulic lime samples had water vapour permeability values that fell within the mid-range for the binary mortars. This would be expected as the mortar was in reality a feebly hydraulic lime and therefore exhibited low levels of C-S-H within the matrix. This could possibly be attributed with the materials reduced ability to transmit water vapour.

5.7.3 Binary Isle of Man non-hydraulic lime mortar samples

The binary Isle of Man ESEM samples was closely related to the previous limes samples in terms of macro pore structure, crystallography and consequent binding characteristics. The principal difference with the Isle of Man samples was the greater level of visible acicular rod-like crystals. Charola [48] believes that these acicular crystal types have been attributed with alumino-silcate C-A-S-(H) formation. However it must be emphasised that these are not widespread.

Chunky calcite crystals, approximately 1-2μm in width, were widespread (see plate 21) and as a result the generation of a large interconnected macro pore structure had developed, with little or no impedance to the pore structure being seen due to C-S-H or C-A-S-(H).

The large chunky calcite crystals have a relatively large open texture that lends itself to a rather cavernous pore structure. The presence of very small quantities of C-S-H acicular crystals that are sporadically distributed throughout the sample may be correlated with the mortars' ability to transmit relatively high levels of water vapour. An increase in the quantity of C-S-H would tend to lead to a reduced ability to generate a material that can freely allow water vapour permeability to occur. This is reflected in the materials extremely high levels of water vapour permeability, only been out performed by the very pure Shap non-hydraulic lime.

5.7.4 Binary NHL2 lime mortar samples

The primary set characteristics within the feebly hydraulic NHL2 mortar types are associated with carbonation of portlandite crystallites which form calcite crystals. The

concentration of $Ca(OH)_2$ within the lime is approximately 43% and is the highest within the NHL range. This is reflected in the hydration products seen within ESEM plates 23-24 with high levels of calcite been seen. The calcite crystallography is rather chunky (1-2μm) and is widespread throughout the mortar in tiny mass agglomerations. This tended to derive a relatively large interconnected macro pore structure with relatively low binding characteristics.

The portlandite crystallites are essential for the formation of the 'strategic components' [20], that is to say those products that yield hydraulic components. This is reflected in the small yet significant C-S-H / C-A-S-(H) rod like products seen in ESEM plates 23 and 24. These acicular C-A-S-(H) crystal types are formed from the portlandite and appear to grow in bundles. They are approximately 0.5μm in cross section and 5-6μm in length. The formation of these crystal types are thought to be 'side reactions' [20] and are therefore hydraulic in nature. This means that the primary set characteristics occurring in NHL2 develop through carbonation processes. This has an effect upon the binding characteristics of the material and therefore, non-hydraulic limes are considered to be more friable than those more relatively dense NHL mortars with higher proportions of hydraulic components. The C-S-H bundles are relatively tightly packed however, they are rather sporadically located throughout the sample when compared with the higher NHL types. This is reflected in the concentration of silica within NHL2 being only approximately 6%.

The material has a relatively high water vapour permeability and this would appear to be reflected in the predominance of calcite as the primary binding material. The increased presence of C-S-H / C-A-S-(H) acicular rods would appear to be indicative of higher levels of hydraulicity when compared with non-hydraulic limes. The occurrence of C-S-H / C-A-S-(H) is reflected in the conduction calorimetry hydraulicity tests in which low levels of heat of hydration was seen within the NHL2 samples. The quantity and distribution of these C-S-H / C-A-S-(H) forms are associated with the decrease in the materials ability to transmit water vapour, relative to non-hydraulic limes. The C-S-H appears to be bridging the pore structure of the material and is therefore theoretically of greater impedance to the flow of water vapour than non-hydraulic lime mortars.

5.7.5 Binary NHL3.5 lime mortar samples

Natural hydraulic lime 3.5 (NHL3.5) is classified as a moderately hydraulic lime. The set characteristics of the mortar is derived from a dual carbonation / hydration process, ultimately yielding both calcite, C-S-H / C-A-S-(H) and other hydraulically formed crystallites. The concentration of $Ca(OH)_2$ within the lime is less than that seen in the NHL2, with some 28%, and this is reflected in the crystallography within the ESEM plates namely, 25, 26 and 27. The calcite concentration is lower due to free lime consumption that is required for the formation of C-S-H and other hydraulic components.

The tiny mass agglomerates of calcite are widespread across the mortar sample and can be clearly seen adhering to the surface of the aggregates in plate 25. However, a reduced quantity of calcite is noted with an increased quantity of C-S-H replacing the primary binder. Due to this an increase in the binding characteristics of the mortar is seen with obvious effects upon the strength of the mortar. The C-S-H and / C-A-S-(H) type components are relatively widespread throughout the sample and can be clearly seen bridging the macro pore structure of the material, binding it together. The rods are approximately 0.5μm and less in cross section and 5-10μm in length. These can be clearly seen in plate 27. An increase in the proportion of the strategic components is to be expected due to the higher level of reactive silicates and aluminates within the material. The C-S-H / C-A-S-(H) bundles are relatively tightly packed, and more widespread than in the NHL2 binary mortar samples.

The level of C-S-H / C-A-S-(H) exhibited within the NHL3.5 mortars are significant and their distribution is formed into what Charola [48] previously called a hyphae mat. This mat would appear to have an effect upon the pore structure by bridging the material. The reduction of calcite as the primary component in the binding matrix would appear to have affected the materials water vapour permeability characteristics and with the increase in C-S-H and other hydraulically reactive components, a decrease in permeability would have appeared to occur. In terms of water vapour permeability the NHL3.5 mortars were within the final 3 in the test range of materials (8 in all) with only NHL5 and OPC exhibiting lower values. This would be expected and generally follows the hypothesis.

5.7.6 Binary NHL5 lime mortar samples

Natural Hydraulic Lime 5 (NHL5) is classified as eminently hydraulic with dual set propagation occurring from both carbonation and hydration. The primary set is derived from the development of strategic components, namely, C-S-H and portlandite with a lesser reliance upon carbonation, which must be deemed in this material as the side reaction. This reduced reliance upon carbonation is reflected in the smaller quantity of calcite concentration seen within the mortar. This is countered by an increase in the C-S-H and other hydraulically reactive components that can clearly be seen within ESEM plates 28, 29 and 30. As aforementioned the concentration of tiny calcite agglomerates (approximately 2μm in diameter) have reduced and have become more sporadically dispersed. This has a significant effect upon the binding characteristics of the mortar, with a considerable increase in the strength noted with the increase in the strategic components. The average size of C-S-H / C-A-S-(H) ranges from 5-20μm in length and can clearly be seen bridging the macro pore structure and aggregate / lime interface.

Although difficult to assess, the presence of tabular crystal types may also be seen in ESEM plate 28 and are most likely to be associated aluminate phases. At higher magnification the dense nature of the C-S-H / C-A-S-(H) can be seen (plate 30), however, it is evident that the random pore structure is relatively unimpeded.

The level of C-S-H exhibited within the NHL5 mortars is significant and its distribution is formed into what has previously been called a hyphae mat. This mat appears to have a bridging effect upon the pore structure. The reduction of calcite as the primary component in the binding matrix would appear to have affected the materials water vapour permeability characteristics and with the increase in C-S-H / C-A-S-(H) a decrease in permeability would have appeared to occur. In terms of water vapour permeability the NHL5 mortars were second last in the range of materials with only OPC exhibiting a lower value. It would be expected that the degree of hydraulicity within the NHL5 mortars would result in the aforementioned decrease in water vapour permeability.

5.7.7 Binary Jura-Kalk (NHL5) lime mortar samples

Jura-Kalk is classified as an eminently hydraulic lime. However, Hughes and Swann [21] have emphasised that it should be reclassified as an 'imperfectly burned natural cement'. The Jura-Kalk samples are the strongest of the range of hydraulic limes in

terms of hydraulicity (measured via conduction calorimetry). The primary set characteristic of the material is not carbonation but hydration and therefore the formation of strategic components prevails. The formation and widespread distribution of portlandite / calcite is seen at low magnification (2000x) with approximate crystal dimensions of 1-2μm. Inter-dispersed and forming from the $Ca(OH)_2$ are tiny C-S-H type components which are common across the sample. At higher magnification C-S-H / C-A-H and C-A-S-(H) crystalline forms can be clearly seen growing from the calcite substrate. The macro pore structure is clearly bridged by the growth of the aforementioned C-S-H. In the relatively small pores micro-crystalline matrices may be seen and may cause an impedance to the macro pore structure.

The binary Jura-kalk samples have a water vapour permeability that falls within the mid range of values. This was the exception to the general rule, with C-S-H / C-A-S-(H) being seen throughout the sample and therefore it would be expected that a lower level of water vapour permeability would be exhibited. In addition in terms of measured levels of hydraulicity from the calorimeter it would be expected that lower levels of water vapour permeability would be seen. Further research to explain this anomaly must be sort.

5.7.8 Binary O.P.C. mortar samples

The OPC binary mixes rely purely upon hydration for the materials set characteristics and hence no (or very little) carbonation occurs. When comparing the subsequent hydraulic crystalline components within OPC mortars, differences do occur as would be expected when compared with lime. The most significant of these differences is the presence of alite (C_3S), which should not theoretically be found within hydraulic limes. In the case of plate 34 several crystal types are clearly seen including calcium aluminate phases and what appears to be type III and IV C-S-H that is associated with relatively mature hydrated alite (C_3S). It would also appear that densification of the C-S-H has also occurred and is correlated with a compaction of the matrix. Tiny portlandite agglomerates can clearly be seen adhering to the surface of the aggregate. The larger tabular crystal types follow calcium aluminate morphology. The acicular (rod like) / prismatic crystal types may be associated with Aft and compare favorably with those assessed by Jawed, Skalny and Young [18]. At high magnification these C-S-H crystallites are densely packed and will theoretically impede moisture transmission.

The C-S-H morphology seen in ESEM plate 34 appears to be exhibiting similar formations to those noted by Taylor [17] and Jawed, Skalny and Young [18]. As expected no calcite was present within the ESEM plates for OPC and it would appear that the higher levels of hydraulicity lead to the relative impermeability of the OPC mortars. The water vapour permeability within the OPC mortars were consistently low when compared with the other mortar samples. This is reflected in the level of dense type III and IV alite (C_3S) C-S-H seen within the ESEM plates.

5.7.9 Ternary Shap non-hydraulic lime & NHL2 mortar samples

The ternary gauged Shap non-hydraulic lime and NHL2 showed mass calcite agglomeration adhering to the aggregates. At high magnification (plate 37) the calcite appears to be amorphous rather than the regular, 2μm chunky well-formed calcite crystals. It is known that the conversion of portlandite [$Ca(OH)_2$] into mineral calcite via carbonation may be retarded when hydraulic components are introduced into primarily non-hydraulic lime mortars. This occurs due to the relatively rapid growth of hydraulic components that develop into the pore structure, thereby impeding the flow of CO_2 reaching the $Ca(OH)_2$.

C-S-H's and C-A-S-(H) are seen randomly distributed throughout the mortar sample, and are generally clumped together. However, a small quantity of hyphae formed acicular like crystals associated with C-A-S-(H) can be seen distributed across the predominately calcite substrate. At high magnification (approximately 10000x) the C-S-H / C-A-S-(H) appear to form into well developed agglomerates, with acicular crystals being tightly packed, knitting into each other. They are approximately 2μm in length and 0.5μm or less in width. It is difficult to assess the cross section of the crystals. Randomly dispersed within the needles appear to be very small particles of unconverted calcium hydroxide that are approximately 0.5μm or less in width. This is similar to the crystal formation seen in work by Lewins [49]. The rather tight grouping of C-S-H / C-A-S-(H) could possibly be associated with flocculation of the anhydrous particles within the ternary gauged mortar samples.

Several C-S-H like crystallites can be seen to bridge the pore structure, however it must be emphasised that this is at low level formation only. The acicular crystal types appear to be grouped into a mass of dense, relatively impenetrable formation rather than distributed throughout the whole sample. The acicular crystal types are similar to those

seen in work by Blanco-Varela et al, [55] who attributed them to calcium aluminate (aft phases). Blanco-Varela et al believes that the crystals are ettringite, but this is unlikely since gypsum is not present in high enough quantities in hydraulic limes for the ettringite development. It is more likely that the C-A-S-(H) and or di-calcium phases are responsible for the acicular crystals. It is known that the composition of NHL contains both alumina and iron at about 0.5%. However, even with the low concentration of iron and alumina it would still be expected to lead to the formation of low level C_2A_3 and other associated hydration products.

As aforementioned the pore structure of the ternary NHL2 samples was only slightly abridged by acicular C-S-H / C-A-S-(H) crystals. At higher magnification the acicular crystals were interlocked and this may have had an effect upon the water vapour permeability characteristics of the mortar. This is reflected in the NHL2 ternary samples having a low water vapour permeability (second from last), and does not correlate with the binary samples.

5.7.10 Ternary Shap non-hydraulic lime & NHL3.5 mortar samples

The ternary Shap and natural hydraulic lime 3.5 samples (NHL3.5) exhibited mass calcite agglomeration forming the substrate of the mortar. The C-S-H / C-A-S-(H) acicular crystal types appear to be more evenly distributed than those seen in NHL2 and Shap ternary mortar samples, and are clearly seen bridging calcite agglomerates and the macro pore structure alike. The C-S-H / C-A-S-(H) crystallites are approximately 2-3μm in length and approximately 0.5μm in width. The determination of the crystal cross section is difficult to assess.

In plate 41 the origin of the acicular crystals can be seen in what appears to be a reactive particle with crystals radiating from the origin. These crystals can also be seen to be bridging the pore structure. At high magnification the C-S-H / C-A-S-(H) components do not appear to be as tightly packed as the ternary NHL2 samples although this could be simply a micro-regional variation.

The ternary NHL3.5 samples exhibited relatively high water vapour permeability values (second highest in the range of ternary mortars) and these may be associated with the rather sporadic distribution of C-S-H and other hydraulically components throughout

the mortar. Low level pore impedance was exhibited as with the NHL3.5 samples and may also be associated with higher levels of water vapour permeability.

5.7.11 Ternary Shap non-hydraulic lime & NHL5 mortar samples

The ternary Shap and NHL5 mortar samples appeared to have a substrate primarily composed of relatively large portlandite (calcium hydroxide) crystals and smaller calcite agglomerates. The portlandite plate like crystal types appear to be laminar and form sheets overlaying each other in an almost stack effect. As aforementioned tiny calcite agglomerates appear to be adhered to the $Ca(OH)_2$ plates and have widespread development across the surface. At higher magnification C-S-H / C-A-S-(H) acicular type crystals can be seen dispersed and integrated into the surface calcite crystals. In addition the rod like C-S-H / C-A-S-(H) crystals can be seen to bridge the pore structure (see plate 43)

The ternary NHL5 samples exhibited high water vapour permeability values (highest in the range of ternary mortars) and these may be associated with the rather sporadic distribution of C-S-H and other hydraulically reactive components throughout the mortar. Low level pore impedance was exhibited as with the NHL5 samples and may also be associated with levels of water vapour permeability.

5.7.12 Ternary Shap non-hydraulic lime & Jura-Kalk mortar samples

The ternary Shap and Jura-Kalk samples have widespread calcite distribution across the sample with crystal sizes ranging from approximately 0.5-2μm. Larger tabular crystals are also seen and may be associated with C-A-H phases. The formation of C-S-H / C-A-S-(H) acicular crystals are dispersed throughout the sample. These appear to be present in higher proportions than those seen in the ternary NHL5 samples as would be expected for the degree of hydraulicity associated with Jura-Kalk. The profusion of acicular crystals are extremely small with a width of approximately 0.5μm in width and approximately 2-5μm in length. These hydration products can be clearly seen bridging the macro pore structure. The regional agglomeration in C-S-H and C-A-S-(H) type crystals seen in the ternary NHL3.5 sample are not noted in either the NHL5 or Jura-Kalk samples.

The ternary Jura-Kalk samples exhibited a greater level of C-S-H and other hydrates distributed throughout the mortar. The C-S-H was also more evenly distributed

throughout the sample. The water vapour permeability was the lowest of all the samples and may have been directly effected by the quantity and distribution of the C-S-H / C-A-S-(H) and C-A-H.

5.7.13 Ternary Shap non-hydraulic lime & OPC mortar samples

The ternary Shap and O.P.C. mortar samples exhibit widespread tiny calcite and portlandite crystals. In the case of plate 47, calcite crystals appear to have formed agglomerated sheets (see left and right side of plate). Aggregate may be seen with what appears to be radiating crystal types that have smaller sub-crystalline calcite particles deposited in between the radial forms. This phenomenon has been reported by Radonjic, [20] who believes that the radiating crystals form due to dissipated heat to the relatively cold aggregate surface, causing a 4 stage reaction process in which the sub-crystalline particles form due to dissolution, evaporation, saturation and finally, precipitation.

The ternary OPC samples exhibited a greater level of C-S-H distribution throughout the mortar than the other samples. The C-S-H was also more evenly distributed throughout the sample. The water vapour permeability was in the mid-range of all the samples. The water vapour permeability value for the ternary OPC samples may have been directly affected by the distribution and quantity of the C-S-H throughout the mortar.

5.8 Summary of ESEM

Generally the set characteristics of the material reflects upon the final physical properties and performance of the mortar. The micro-structural development of the material allows holistic durability and strength to be derived within historic mortars with the pore size and pore distribution playing a fundamental role in the performance of the material.

5.8.1 Binary mortar samples

When assessing the binary mortar samples it was evident that an increase in hydraulicity of the material saw a reduction in the reliance upon calcite for its binding characteristics, and saw an increase in the quantity of C-S-H and other hydraulically reactive components.

The Shap non-hydraulic lime reflects this and is bound together by rather chunky calcite crystallites (approximately 1-2μm) with no evidence of C-S-H, C-A-H or C-A-S-(H)

being seen throughout the sample. The Blair-Athol lime (feebly hydraulic) had a very small quantity of acicular crystal types associated with C-A-S-(H) and C-S-H, however, the majority of the binder was calcite (approximately 1-2μm). The Isle of Man lime mortars exhibited similarities in terms of crystallography to those seen in the Blair-Athol lime mortars, except for an increased quantity of acicular C-A-S-(H) and C-S-H types.

NHL2 had a substrate that was primarily composed of calcite, with an inter-dispersion of acicular crystals. NHL3.5 had a greater level of acicular C-S-H / C-A-S-(H) crystals, some being tightly packed and bundled, and this had an affect upon the quantity of chunky calcite crystals exhibited. The NHL5 mortar samples saw the lowest quantity of calcite and the highest amount of acicular C-S-H / C-A-S-(H). This was indicative of the increased strength associated with these mortar samples.

Jura-Kalk, which is traditionally classified as an eminently hydraulic lime had a much greater level of acicular C-S-H and C-A-S-(H) than the NHL5 lime mortar samples. This work suggests that Jura-Kalk should be reclassified as a natural cement.

It was interesting to note that the acicular crystal types were similar in width (0.5μm) throughout the NHL range, however, they tended to be different in length with the shortest being seen in the NHL 2 (5-6μm) and the longest seen in the NHL5 (6-10μm). The O.P.C mortar samples had a very low degree of portlandite and obviously the highest levels of C-S-H. The latter was extremely densely packed and small in comparison with the other mortars samples.

Generally, the degree of C-S-H and other hydraulically reactive components associated with the hydraulic materials increased from being rather slightly and sporadically distributed in the in the feebly hydraulic mortars through to more evenly distributed in the moderately and eminently hydraulic limes. The acicular C-S-H and C-A-S-(H) crystals were seen to bridge the pore structure in those materials with higher levels of hydraulicity, and it has been correlated that a relationship between the hydraulicity and water vapour permeability of the material exists.

5.8.2 Ternary mortar samples

Just as with the binary mortars, an increase in hydraulicity of the material in ternary mortars saw a reduction in the reliance upon portlandite / calcite for binding, and saw an increase in the quantity of C-S-H and other hydraulically reactive components. However, the addition of the Shap non-hydraulic lime within the mortar increased the overall quantity of calcite crystalline formation.

The ternary NHL2 mortar samples exhibited agglomerations of calcite and random C-S-H, C-A-S-(H) acicular crystal formation protruding from the substrate. These crystals were generally in a flocculated form rather than freely dispersed throughout the sample. At higher magnification the acicular crystals appeared tightly packed, although it must be emphasised that they may also be seen sporadically distributed throughout the sample. The general length of the acicular crystals was approximately 0.5 x 2μm.

The ternary NHL3.5 mortar samples exhibited agglomerations of calcite and a more even distribution of C-S-H / C-A-S-(H) acicular crystal formation protruding from the substrate. Evidence of acicular crystals bridging the pore structure was also noted in greater number than the NHL2 samples. The general length of the acicular crystals was approximately 0.5 x 3μm.

The ternary NHL5 mortar samples exhibited agglomerations of calcite and a more even distribution of C-S-H / C-A-S-(H) acicular crystal formation protruding from the substrate. Evidence of acicular crystals bridging the pore structure was also noted in greater number than the NHL3.5 samples. The general length of the acicular crystals was approximately 0.5 x 3μm.

The ternary Jura-Kalk mortar samples exhibited agglomerations of calcite and a more even distribution of C-S-H / C-A-S-(H) acicular crystal formation protruding from the substrate. The addition of tabular crystal types were also noted and were associated with C-A-H. Evidence of acicular crystals bridging the pore structure was also noted in greater numbers than the previous NHL samples. The general length of the acicular crystals was approximately 0.5 x 5μm.

The O.P.C samples exhibited mass calcite and sub-crystalline calcite agglomerations. Thus, as with the binary mortars, it appeared that the C-S-H and other hydraulically

reactive components seen throughout the materials increased in quantity as the hydraulicity increased. The acicular crystals appeared to be slightly smaller than those seen in the binary mortar samples, ranging from 2-5μm.

5.9 General discussion

Generally the results discussed within this chapter tend to confirm the relationship between the hydraulicity and water vapour permeability. However, it has been shown through the water vapour permeability experiments that all mortars, whether lime based or cementitious have permeability's' that fall within a very small range. It is true that those mortars that are manufactured with OPC perform worse than any of the lime based materials, however, it must be emphasised that the OPC mortars water vapour permeability is only approximately 30% of that of the best performing lime mortars. This begs us to ask does this approximate 70% increase in the ability of lime mortars to transfer water vapour constitute 'breathing'? Alternatively, the OPC mortars have only one third of the capacity of non-hydraulic limes to transfer water vapour and therefore, if breathing is associated with this then breathing must fall within an extremely narrow spectrum. This will be discussed in the following chapter.

Chapter 6: Conclusions

The hypothesis under test was that there is a correlation between hydraulicity and water vapour permeability in mortars. In general this was confirmed for binary mortar samples but not ternary mortars. The hypothesis was visually verified by the profusion of C-S-H / C-A-S-(H) and other hydraulicity reactive components or lack of them within the mortars.

6.1 Binary mortars

In binary mortars the higher hydraulicities saw an increase in the degree of C-S-H / C-A-S-(H). When this was seen the reliance upon calcite acting as the primary binding component was reduced with a subsequent increase in the strength of the mortars.

An increase in calcite as the primary binder saw an increase in the water vapour transmission of the mortars. Conversely, an increase in acicular crystals and forms of C-S-H / C-A-S-(H) within the mortar saw a decrease in the mortars' ability transmit water vapour. This was confirmed visually by ESEM for all the hydraulic mortar types, with it becoming evident that the tight knitting effect of acicular crystals and C-S-H / C-A-S-(H) forms could impede water vapour transfer as they bridge pore structures. In addition the degree of C-S-H densification associated with the OPC mortars was considerably greater than any of the hydraulic lime samples and was reflected by the reduced ability of the OPC samples to pass water vapour.

Densification of the belite (β-C_2S) within hydraulic lime does not appear to occur as it does within the alite (C_3S) forming C-S-H of the same age. The densification of OPCs C-S-H occurs due to a reduced level of space in the pore structure. Therefore, it would be expected that limes pore structure would lead to reduced levels of densification as it is relatively cavernous. This is based upon the premise that belite (C_2S) and alite (C_3S) hydration in OPC have similar formation characteristics, with alite (C_3S) having a higher rate of densification due to increased C-S-H level and crystallography. This concept is reinforced by Odler [5] when discussing low water / cement ratios in Portland Cement, indicating that they tend to generate an environment which lacks sufficient space for C-S-H growth and $Ca(OH)_2$ precipitation with consequent reductions in holistic cementitious formations. In addition Charola [48] believes that the hydration products in OPC share great similarities to those found in hydraulic limes.

The results for both hydraulicity and water vapour permeability may be seen in table 50.

Table 50: Hydraulicity / water vapour permeability of binary mortar types

Binary mortar type	Ave. Water vapour permeability in $Kgm/m^2.s.Pa$ (alternatively $KgmN^{-1}s^{-1}$)	Hydraulicity via conduction calorimetry Kj/Kg (ΣH)
1) Jura Kalk	$3.87x10^{-11}$	3041
2) Shap non hydraulic lime: putty	$2.69x10^{-11}$	-
3) Isle of Man: putty	$2.54x10^{-11}$	-
4) NHL 2	$2.38x10^{-11}$	2067
5) Blair Athol: putty	$1.84x10^{-11}$	-
6) NHL 3.5	$1.56x10^{-11}$	1517
7) NHL 5	$1.25x10^{-11}$	2909
8) OPC	$1.21x10^{-11}$	13149

The experiments for assessing the hydraulicity and water vapour permeability of the binary mortars have derived the following:

- All of the hydraulic materials with the exception of NHL3.5 followed expected performance with respect to heat evolution (initial 72 hours tests only). However, it must be emphasised that the NHL3.5 may be being affected by 'doping' of the silicates and would therefore see a postponement of the hydration of the calcium silicate and other hydraulically reactive phases within the material. An increase or reactivation of the aforementioned post 72 hours may occur, allowing for a better indication of the medium - long term hydraulicity of the material. Alternatively, the NHL2 samples may be exhibiting higher than expected heat of hydration up to 72 hours) and may be less realistic of longer-term hydration.

- The water vapour permeability tests upon the range of binary mortar samples all followed the hypothesis, with the exception of the Jura-Kalk. This anomaly cannot be fully explained, however, it may be as a result of the water binder ratio and / or a complex relationship between the level of combined CaO and SiO_2 formed upon calcination or the aluminate phases yielding alternative hydration products to those exhibited in the other hydraulic limes.

- The JAF conduction calorimeter has the potential to deliver a more reliable classification system for hydraulic limes. The advantages of the system include the ability to not only assess the total heat of hydration but to also identify individual

hydration products that develop at different stages. This is extremely useful for the identification of 'rogue' components, such as that seen in the Jura-Kalk samples (see figure 51 in chapter 4), with their high levels of gypsum and aluminium, generating heat peak 'B'. The system also eliminates the problems associated with the traditional methods of hydraulicity assessment, such as hydraulic index, cementitious index, compressive strength, and soluble silica concentration. Although the last is commercially used as a reasonable assessment of hydraulicity it is fundamentally flawed as it does not consider those components such as the aluminate phases that may add to hydraulicity in the material.

6.2 Ternary Mortars

On the other hand the assessment of the hydraulicity and water vapour permeability of the ternary mortars was inconclusive and no relationship could be obtained for these relatively complex mortars. They may be performing differently from the binary mortar because flocculation of anhydrous binders that were introduced into lime putty mortar matrix may have occurred. This is reflected in the agglomeration of C-S-H / C-A-S-(H) products seen in several of the ESEM plates (see plate 37). The phenomenon did not occur in the binary mortars and if this were to be true it would yield a mortar with only limited binding characteristics. This opinion has been reinforced by work by English Heritage in which they believe the gauging of small proportions of a hydraulic component into a mix may have a detrimental effect, however, it is more likely to be the batching technique than the actual proportions that cause this phenomenon.

Table 51: Hydraulicity / water vapour permeability of ternary mortar types

Ternary mortar type	Ave. Water vapour permeability in $Kgm/m^2.s.Pa$ (alternatively $KgmN^{-1}s^{-1}$)	Hydraulicity via conduction calorimetry Kj/Kg
1) Shap non-hydraulic lime & NHL5	$8.57x10^{-11}$	Proportion 2909 kj/Kg
2) Shap non-hydraulic lime & NHL3.5	$4.33x10^{-11}$	Proportion 1517 kj/Kg
3) Shap non-hydraulic lime & OPC	$3.46x10^{-11}$	Proportion 13149 kj/Kg
4) Shap non-hydraulic lime & NHL2	$2.91x10^{-11}$	Proportion 2067 kj/Kg
5) Shap non-hydraulic lime & Jura-Kalk	$1.57x10^{-11}$	Proportion 3041 kj/Kg

6.3 General comments

The concept of breathing does not appear to be as straight-forward as professionals in the industry would lead us to believe. It is true that non-hydraulic limes and hydraulic limes have a greater ability to transmit water vapour than OPC, however, the largest increase over OPC observed here was only about 70%.

This may be seen in figure 86 below in the water vapour permeability / hydraulicity scale. It must be emphasised that a scale of this nature is a first attempt to express the relationship between the two factors and it is the authors view that this should be used as a stage for subsequent researchers to elaborate upon allowing a more rigid model to develop.

Figure 86: Relationship between water vapour permeability and hydraulicity

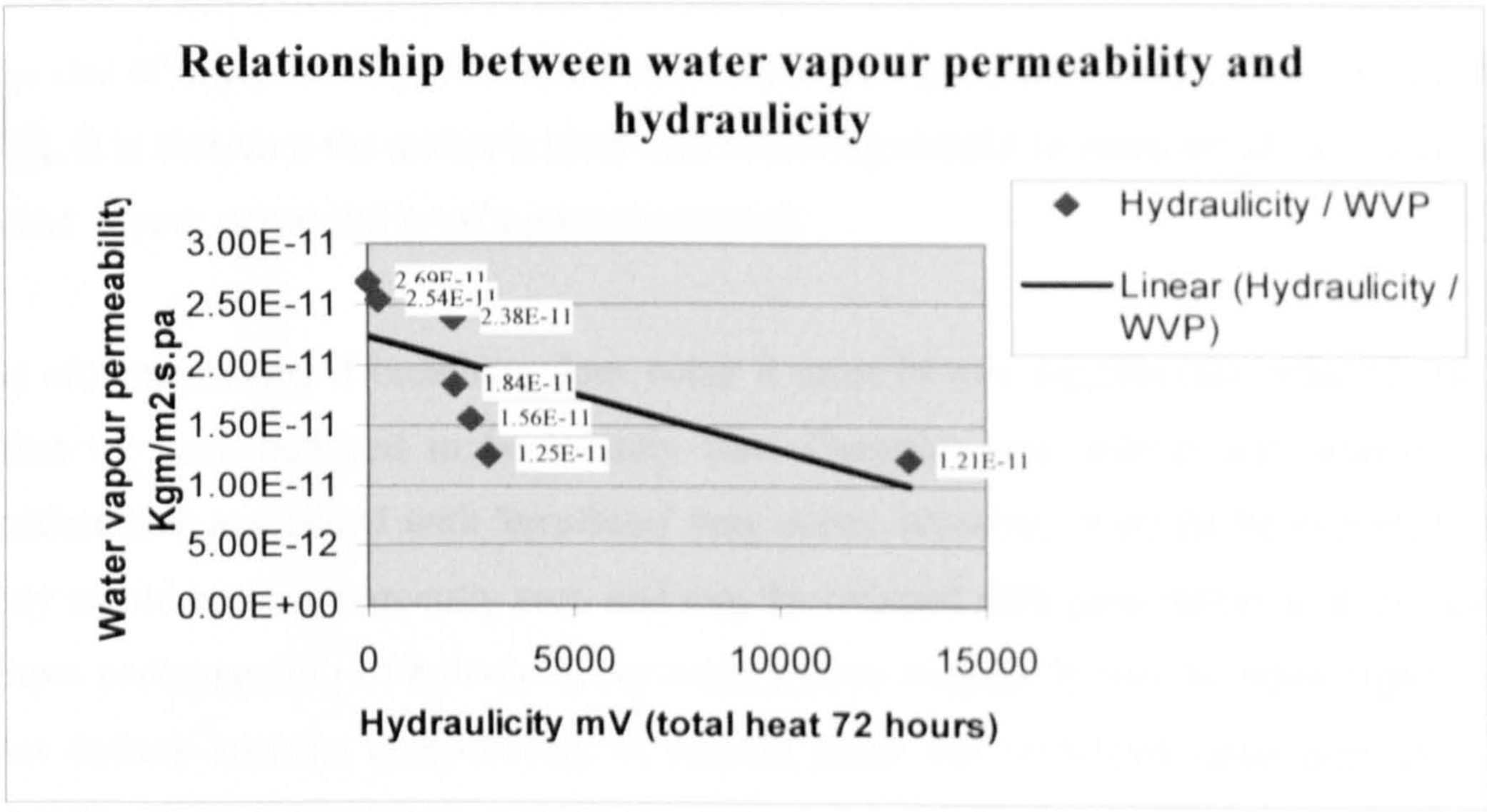

The data shown in figure 86 reflects the water vapour permeability characteristics of the binary mortar samples. 3 sets of data have been manipulated to give a more realistic indication of hydraulicity and values for Isle of Man and Blair-Athol have been estimated based upon the visual identification of C-S-H like components rather than conduction calorimetry results. In addition NHL3.5 exhibited lower than expected heat of hydration over the first 72 hours. It has therefore been altered to reflect the longer-term hydraulic activity within the material and also by assessing the profusion of C-S-H products exhibited under ESEM analysis.

Jura-Kalk was omitted from the figure as anomalies in the water vapour permeability data were seen, these have been discussed previously.

If 'breathing' is a materials ability to transmit water vapour, then it has been shown that both OPC and the range of lime based materials do possess this ability. However, a rather flippant analogy may be that OPC mortar 'breathes' with a respirator, hydraulic limes have a normal lung capacity and non-hydraulic limes have a high lung capacity.

In addition choice of terminology to describe water or gas transfer in porous materials must be used with caution rather than the blanket coverage that occurs. The term 'breathing' is defined in the dictionary of science as the 'activity of animals etc, resulting in the rapid movement of the environment - air or water' and does not necessarily seem to be an apt description for the performance of building materials. Permeability is however a better description of the movement of moisture in materials and is defined as 'the rate of diffusion of gas or liquid under a pressure gradient through a porous material [33]. It is therefore the author's view that breathing should be measure of the water and water vapour permeability of a porous material.

As aforementioned if breathing does occur it must be at a significantly reduced rate to what we have believed to be initially true. Therefore, the defects and deterioration mechanisms associated with 'breathing' may occur, however, it would be expected that they would be less frequently seen and may be twinned with poor defect analysis and a lesser understanding of holistic decay mechanisms in play. It may be more significant that defects such as deterioration of natural stone and soft-fired brick may also be partially attributed to OPC's inability to move and its high stiffness when compared with relatively flexible lime based materials. This effect may lead to tensile forces being established in the deteriorating areas of the material and lead to a visually similar type of failure.

Unfortunately, studying the water vapour permeability of porous materials is rather difficult and the attainment of steady state conditions is unreliable if not virtually impossible to achieve. Hence, to discuss breathing in terms of water vapour permeability would be unwise as the transfer of water vapour through the liquid phase may be in a constant state of change and must therefore be considered as non-uniform in nature.

'Breathing' must therefore be a measure of a combination of moisture transfer mechanisms and not only the water vapour permeability. For example it would be wise to measure additional factors such as water permeability and those physical factors that affect this such as sorption and capillarity. This would aid in the holistic understanding of the performance and mechanisms of 'breathing'.

The study is further complicated as the material is not homogenous and has many different materials incorporated, such as silica and calcium components. These will greatly affect the attraction / repulsion to moisture transfer and is reinforced by Buckman's [36] work on wetting in which it is believed that an appreciable range of material properties will be seen within the same specimen.

A rather apt quotation taken from works by Saidani-Scott [31] seems to penultimately conclude the study of moisture movement in porous materials *'This study does not pretend to be the final work. There is no question of an exact description of what really happens; it must be considered as one out of many steps along this hard-going road which, as we earnestly hope, will bring us to a good understanding of what is going on in moist materials'.*

In conclusion the hypothesis under test namely; *'There is a correlation between the hydraulicity and permeability of lime mortars for use within the historic building and conservation industry'* was provisionally confirmed. This was seen in the assessment of the binary mortars, however, the ternary system had too many variables to allow attainment of satisfactory data to be achieved.

Chapter 7: Recommendations for further research

Certain limitations in the work have been highlighted within chapter 6, and in addition throughout the document there have been many topics that have been little researched. The following areas require study in an attempt to reduce the level of ambiguity of the subject area.

- A medium - long term (post 72 hour) detailed study of the hydraulicity of hydraulic limes is required adopting conduction calorimetry. The study should attempt to develop a true system of classification for natural hydraulic limes.

- The rather random nature of the water vapour permeability results associated with the ternary mortar batches is plausibly due to flocculation of the anhydrous particles within the matrix. It is therefore suggested that this phenomenon should be assessed to measure the distribution of the particles throughout the material.

- It has been suggested that 'doping' of silicates may occur in a Ca rich solutions during hydration, leading to periods of relative dormancy. This is believed to occur in C_3S particles in cement, however, it is not yet fully understood how the phenomena affects individual hydration products in natural hydraulic limes. This area should therefore be fully tested.

- The initial water binder ratio is crucial in determining the ensuing pore structure development [Whether, micro (<2nm), meso (2-50nm) or macro (>50nm) pore structure] of the mortar. Those materials that adopt a high w/c or w/l ratio will attain a higher degree of pore interconnectivity as opposed to the highly segmented materials generated with low w/l or w/c ratios. At first, total connectivity of the pore structure will be seen but over time isolation of initially connected pores will occur as hydration products develop. This relationship is little understood or documented in natural hydraulic limes and should be assessed.

- The difficulty in assessing pore structure development is further complicated when additional components are added such as aggregate type. The modelling of the mortars is therefore, further complicated by an increase in the number of variables associated with the samples, and further work would be better concentrated on pastes.

- As expressed in the conclusions the measurement of 'breathing' must be combined with other parameters such as capillarity, water permeability, sorption and wettability studies of the homogenous materials. These must be integrated into a new holistic test regime to develop a model of greater accuracy.

- Although the basic BS EN1015-19 calculation was adopted it seems to be of limited value in assessing the water vapour permeability of materials in realistic situations. A better understanding of moisture transfer in porous media may be attained by mathematical modelling, which is beyond the scope of this work and it is therefore suggested that further research in this area is undertaken.

References

1- Bonen. D, Tasdemir. M, & Sarkar. S, (1995) 'The evolution of cementitious materials through history', Mat. Res. Symp. Proc. Vol 370

2- L.G. Mallinson, (1986), 'A Historical Examination of Concrete', Taylor Woodrow Ltd

3- Morgan, M.H, (1960) 'Vitruvius: Ten Books On Architecture', Dover Publications

4- Alberti, L.B, (1992) 'On the art of building in ten books', 4th edition, MIT Press

5- Hewlett, P.C, (1998), 'The chemistry of cement and concrete', 4th Edition, Arnold

6- Neville. A.M. & Brooks. J.J, (1990), 'Concrete Technology', 2nd Edition, Longman Publications

7- Meek, T, (1996), 'Case studies of traditional lime harling: a discussion document', Kall Kwik publications

8- Earl, J, (1997), 'Building conservation philosophy' College of estate management

9- Knight, J, (1995), 'The repair of historic buildings in Scotland', Historic Scotland Publication

10- Hughes, P, (1992), 'The need for old buildings to breathe' S.P.A.B News Vol. 18

11- Townsend, A, (1990), 'repairs to historic rough cast' Society for the Protection of Historic Buildings (SPAB), Technical advice sheet No.11

12- Holmes, S, & Wingate, M, (1997), 'Building with lime' Intermediated Technology Publications

13- Pasley, C.W, (1838), 'Observations on limes', Donhead Publications

14- Vicat, L.J, (1837), 'Mortars and Cements', Donhead Publications

15- Eckels, E. C, (1980), 'Cement, Limes & Plasters', 2nd Edition, John willey & Sons Ltd

16- Bergoin, P, (1998), 'Lime after Vicat – Considerations', Building limes forum

17- Taylor, H.F.W, (1990), 'The Chemistry of Cements' Academic Press Ltd

18- Barnes et al, (1983), 'Structure and performance of cements' Applied Science Publishers

19- Verbeck & Foster, (1952), 'Cement hydration at ordinary temperatures', Proceedings of the 3rd International Symposium on the Chemistry of Cement, Cement and Concrete Association

20- Radonjic M, Hallam K.R, Allen G.C, & Hayward R.J, (2001), 'The characterisation of ancient mortars', Journal of the building limes forum, Vol 8

21- Hughes, D, & Swann, S, (1998), 'Hydraulic limes- a preliminary investigation', The journal of the building limes forum, Vol 6, Privately Published

22- Young et al, (1977), 'Journal of the American ceramic society' Vol 60:193

23- Boynton, R, (1980), 'Chemistry & technology of lime & limestone', 2nd Edition, John Wiley & Sons

24- Livesey, P, (2001), 'Hydraulic lime chemistry & performance', The journal of the building limes forum, Vol 8, Privately Published

25- Tian, M, (1920), 'Utilisation de la Methode Calorimetrique en Dynamique Chimique: Emploi d'un Micro-Calorimetre a Compensation' Bulletin societe Chemique de France, Vol 33

26- Forrester, J.A, (1970), 'a conduction calorimeter for the study of cement hydration', Cement technology, Cement and concrete research, Vol. 1

27- Johnson, D, & Spano, U, (2001), 'hydraulicity and properties of hydraulic lime', http://StAstier.co.uk (Accessed August 2002)

28- Bentz, Z.D, & Stutzman, P.E, (1999), 'SEM/X-ray imaging of cement based materials', National Institute of Standards & Technology, http//:ciks.nist.gov/~bentz/eurosem/semcolor.html (Accessed August 2002)

29- Garboczi, E.J, & Bentz, D.P, (1992), 'Effects of pore space percolation and diffusivity' National Institute of Standards & Technology, http://ciks.nist.gov/~garbocz/paper26/node5.html (Accessed January 2000)

30- J. A. Clarke, Yaneske, P.P, & Pinney, A.A, (1990), 'The harmonisation of thermal properties of building materials' BEPAC Research Report

31- Saidani-Scott, H. (1992) 'Analysis of moisture transfer in porous media: application to building materials', PhD thesis, University of Bristol

32- Walker, E. & Morgan, S, (1975), 'Construction Science 1'. Huthcinson Press

33- Wordsworth Reference (1995) 'Dictionary of science and technology' Wordsworth pub

34- Teutonico, J, (1998), 'A laboratory manual for architectural conservators', ICCROM

35- Torraca, G, (1988), 'Porous Building Materials'. 3rd Edition ICCROM

36- Buckman, J.O, (2000), 'Wettability studies of petroleum reservior rocks' FEI Electron optics

37- Rose, D.A, (1965), 'Water movement in unsaturated porous material'. RILEM Bulletin, No.29

38- Powers, T.C, (1960), 'Physical properties of cement paste and concrete'. Washington D.C.

39- Bomberg, M, (1974), 'Moisture flow through porous building materials', Report 52, Division of building technology, Lund Institute of technology

40- Maekawa, K, (1999), 'Practical thermodynamics of young concrete development' Spon

41- Oxley,T.A, & Gobert, E.G, (1994), 'the professional & home owners guide to dampness in buildings' 2nd Edition, Butterworth / Heinemann

42- Schofield. J, (1995), 'Lime in building: a practical guide' 2nd Edition, Black dog press

43- Carrington, D, & Swallow, P, (1996), 'Lime and lime mortars - part 2' Journal of Architectural Conservation, Donhead Publications

44- Gordon, J.E, (1991), 'The new science of strong materials', Penguin books

45- Philibert, J, (1978), 'Microanalysis Scanning Electron Microscopy', Les editions de physique'

46- Chandler, J.A, (1978), 'X-ray Microanalysis in the Electron Microscope' North-Holland

47- Piccoli, P, (2002), 'Environmental Scanning Electron Microscopy', Centre for microanalysis, University of Maryland, USA
http://inform.umd.edu/microanalysis/esem.html (Accessed August 2002)

48- Charola A.E, & Henriques A.M.F, (1999), 'Hydraulicity in lime mortars revisited', RILEM, Pro12

49- Lewin. S.Z, (1986), 'Mortars, cements and grouts used in the conservation of historic buildings', ICCROM

50- Boxhall, J & Trotman, P.M, (1996) 'lime wash water vapour permeability testing' Society for the Protection of Ancient Buildings, SPAB news, Vol 18 No3

51- Teutonico, J.M, McCaig, I, Burns, C, Ashurst, J, (1999), 'The Smeaton Project: Factors affecting the properties of lime-based mortars' ICCROM

52- Anderson et al (1985) 'Material science' 3rd edition. VNR publication

53- Batty W.J, (1982), 'Vapour diffusion and condensation' Cranfield school of mechanical engineering

54- Maclean, R.C, & Galbraith, G.H, (1988), 'Interstitial condensation: applicability of conventional vapour permeabilitity values', Institution of Building Services Engineering

55- Blanco-Varela, M.T et al, (1999), 'Environmental effects of SO_2 on hydraulic mortars', 12th Proc, RILEM